

Disposal Systems Evaluations and Tool Development - Engineered Barrier System (EBS) Evaluation

(FCRD-USED-2011-000132)

Fuel Cycle Research & Development

Prepared for
**U.S. Department of Energy
Used Fuel Disposition Campaign**
Carlos F. Jové Colón (SNL)
Florie A. Caporuscio, Schön S. Levy (LANL)
Mark Sutton, James A. Blink, Harris R. Greenberg,
Massimiliano Fratoni, William G. Halsey, Thomas J. Wolery (LLNL)
Jonny Rutqvist, Carl I. Steefel, Juan Galindez,
Jens Birkholzer, Hui-Hai Liu, (LBNL)
June 15th, 2011



SAND2011-4335 P

DISCLAIMER

This information was prepared as an account of work sponsored by an agency of the U.S. Government. Neither the U.S. Government nor any agency thereof, nor any of their employees, makes any warranty, expressed or implied, or assumes any legal liability or responsibility for the accuracy, completeness, or usefulness, of any information, apparatus, product, or process disclosed, or represents that its use would not infringe privately owned rights. References herein to any specific commercial product, process, or service by trade name, trade mark, manufacturer, or otherwise, does not necessarily constitute or imply its endorsement, recommendation, or favoring by the U.S. Government or any agency thereof. The views and opinions of authors expressed herein do not necessarily state or reflect those of the U.S. Government or any agency thereof.

Prepared by:
Sandia National Laboratories
Albuquerque, New Mexico 87185

Sandia National Laboratories is a multi-program laboratory managed and operated by Sandia Corporation, a wholly owned subsidiary of Lockheed Martin Corporation, for the U.S. Department of Energy's National Nuclear Security Administration under contract DE-AC04-94AL85000.

ACKNOWLEDGEMENTS

The authors acknowledge the contributions of Randall T. Cygan (SNL) on the molecular dynamics work on clay. We also express our gratitude to Yifeng Wang (SNL), Ernest Hardin (SNL), Mark. Nutt (ANL), William Spezialetti (DOE NE-53), Prasad Nair (DOE NE-53), and Robert Howard (ORNL) for their helpful discussions on topics covered in this report.

SUMMARY

The engineered barrier system (EBS) plays a key role in the long-term isolation of nuclear waste in geological repository environments. This report focuses on the progress made in the evaluation of EBS design concepts, assessment of clay phase stability at repository-relevant conditions, thermodynamic database development for cement and clay phases, and THMC coupled phenomena along with the development of tools and methods to examine these processes. This report also documents the advancements of the Disposal System Evaluation Framework (DSEF) for the development of repository design concepts and potential variants according to waste form and disposal environment characteristics. A set of idealized multi-barrier EBS design concepts with various levels of complexity has been described only with the purpose of exemplifying a conceptual basis of flexible EBS options while retaining the overall geometry consistent with current waste package configurations. A key characteristic of EBS design concepts is the ability to be flexible in order to accommodate various waste types and satisfy performance requirements in the process of design optimization.

The organization of this report can be summarized as follows:

- Overview and examples of backfilled multi-barrier EBS design concepts and recommended international collaborations (Section 1);
- Characterization of clay stability and clay-metal barrier interactions at repository conditions (Section 2);
- Thermodynamic database development and modeling tools for clay and cement phases (Section 3);
- THMC processes in EBS focusing on the implementation of the double-structure constitutive model for bentonite. Also, progress in the model development for reactive diffusion in clay (Section 4);
- Disposal System Evaluation Framework (DSEF Version 1.0) and thermal analysis (Section 5).

CONTENTS

AKNOWLEDGEMENTS	4
SUMMARY	5
ACRONYMS	12
1. Overview of Engineered Barrier System (EBS) Concept Evaluation	16
1.1 Introduction	16
1.2 Historical Overview of Backfilled EBS Design Concepts	21
1.2.1 Early EBS Performance Analysis of Design Concepts	21
1.3 Recommended Areas of International Collaboration	31
1.3.1 Opportunities and considerations	31
1.3.2 DECOVALEX Project	34
1.3.3 HE-E Heater Test at Mont Terri URL, Switzerland	36
1.3.4 SEALEX Experiment at the Tournemire URL, France	36
1.3.5 Mont Terri Project	38
1.3.6 Colloid Formation and Migration (CFM) Project	40
1.3.7 Other active collaboration opportunities	42
1.3.8 Recommendations and path forward	45
1.4 Summary and Planned Work for FY12	45
1.4.1 Planned Work for FY12	45
1.5 References	46
2. Clay Stability in Natural and Synthetic Systems	50
2.1 Mineral Evolution in the Yucca Mountain Drift-Scale Thermal Test	50
2.1.1 Overview of the Drift-Scale Test	51
2.1.2 Sample Collection for the Drift-Scale Test	54
2.1.3 Bulk Mineralogy and Chemistry of Study Materials	55
2.2 Summary of Clay Recovery from the DST Study	58
2.3 Engineered Barrier System Components – Experimental Studies Review	58
2.4 Clay Studies	58
2.4.1 Summary of Clay Studies	62
2.5 Iron – Clay Interaction	62
2.5.1 Summary of of Iron Clay interaction	65
2.5.2 Copper Corrosion	66
2.5.3 Japanese URL Water Chemistry	66
2.5.4 Path Forward – Experimental Program 2011-2012	67
2.6 References	69
3. Thermodynamic Data and Modeling of Cement and Clay Phases	74
3.1.1 Thermodynamic Data and Modeling of Cementitious Materials	74
3.1.2 Thermodynamic Data and Modeling of Clay Minerals	76
3.2 References	93
4. THMC Processes in EBS	99
4.1 THM Modeling of EBS Including Buffer-Rock Interaction	99
4.1.1 Base-Case Simulation Results	99

4.2	Thermal management study and peak temperature	105
4.2.1	Buffer Saturation and Thermal Conductivity	106
4.2.2	Tunnel and Canister Spacing	107
4.2.3	Rock thermal conductivity	107
4.2.4	Extreme case of high peak temperature	107
4.3	Resaturation Time and Buffer Swelling.....	108
4.4	Rock failure for layered rock.....	109
4.5	Model Development and Code Implementation of Double-Structure Constitutive Model for Bentonite.....	112
4.6	Reactive Diffusion in Bentonite.....	113
4.6.1	Experimental Investigation of Diffusion Through Compacted Bentonite	114
4.6.2	Single Type Pore Model	117
4.6.3	Double Type Pore Model.....	122
4.6.4	Analytical Solution.....	127
4.7	Future Work.....	131
4.7.1	THM Modeling	132
4.7.2	Reactive-Diffusive Transport	132
4.8	References	132
5.	Disposal System Evaluation Framework (DSEF) and Thermal Analysis	136
5.1	DSEF Conceptual Abstraction.....	136
5.2	DSEF Implementation	137
5.2.1	Excel File Architecture	138
5.2.2	Architecture	138
5.2.3	Revision Control	141
5.2.4	Configuration Management.....	142
5.3	Inputs and Results	143
5.4	Interface Parameters	145
5.4.1	Internal Interfaces.....	145
5.4.2	External Interfaces.....	149
5.5	Waste Forms	150
5.6	Disposal System Environment.....	155
5.7	Design Constraints	156
5.8	Thermal.....	158
5.8.1	Analytic Models.....	159
5.8.2	Finite Element Models.....	166
5.8.3	Model Testing.....	171
5.8.4	Decay Heat	176
5.9	Material Properties	180
5.9.1	Example Structure and Data Included in the Thermal and Transport Property Worksheets.....	180
5.9.2	Data Evaluation and Selection of Input Values to Use as Representative Data for Analysis	182
5.9.3	Materials Longevity.....	182
5.10	Performance Assessment	183
5.11	Cost.....	184
5.12	Knowledge Management	184

5.12.1	Levels of Knowledge Management	185
5.12.2	LLNL DSEF-Specific Knowledge Management	185
5.13	Fuel Cycle System Impacts	187
5.14	Summary of Current Status and Look Ahead	189
5.14.1	Current Status	189
5.14.2	Looking Ahead in FY11 and FY12	189
5.15	Recommended Areas of International Collaboration and Participation	190
5.16	References	190

FIGURES

Figure 1-1.	Generalized depiction of a generic EBS plus important interactions/processes at EBS components and interfaces.	18
Figure 1-2.	Radial and axial cross-sectional view of the supercontainer concept.....	25
Figure 1-3.	Schematic setup of HE-E heater test at Mont Terri and photo of micro-tunnel	36
Figure 1-4.	Schematic setup of mini-tunnel with seal core and instrumentation	37
Figure 1-5.	Planned experiments and schedule.	37
Figure 1-6.	Geological cross-section of the Tournemire site, South France	38
Figure 1-7.	Summary schematic of the Mont Terri URL with side galleries and drifts for testing.....	39
Figure 1-8.	Plan and side view of experiment setup and observation borehole layout	40
Figure 1-9.	Schematic setup of bentonite plug and colloid transport experiment	42
Figure 1-10.	Layout of the PRACLAY In-Situ Experiment which is constituted of the the Seal Test, and the actual Heater Test	43
Figure 1-11.	Schematic picture of repository seal design for GAST experiment.	43
Figure 1-12.	LASGIT experiment at Äspö.	44
Figure 2-1.	Schematic depiction of Drift Scale Test (DST) at Yucca Mountain, Nevada, USA.	52
Figure 2-2.	Average monthly temperature profiles in the vicinity of the boiling zone in borehole ESF-HD-137-TEMP-5 for October 2000 and October 2001.	53
Figure 2-3.	X-ray diffraction (XRD) pattern of ESF-HD-TEMP-2 121.3 ft oriented clay separate.....	58
Figure 3-1.	Comparison of logK values for the solubility of hydrogarnet and monosulphate.	77
Figure 3-2.	Snapshot of an equilibrated molecular dynamics simulation of sodium montmorillonite.....	91
Figure 4-1.	Model domain for an assumed bentonite back-filled horizontal emplacement drift at 500 m depth in clay host rock.	100
Figure 4-2.	Simulated evolution of THM processes in buffer: (a) temperature, (b) liquid saturation, (c) fluid pressure, and (d) total radial stress (σ_x). See Figure 4-1 for locations of V1, V2, V3, and V6.	104

Figure 4-3. Calculated evolution of stresses: (a) stress evolution a point V3 located at the tunnel wall, and (b) stress evolution at point V6 located 10 m away from the tunnel. See Figure 4-1 for locations of V3 and V6.	105
Figure 4-4. Calculated principal stress path at point V3 located at the tunnel wall.	105
Figure 4-5. Calculated evolution of (a) liquid saturation and (b) temperature in the case of a buffer consisting of granular bentonite with 1% initial saturation.	107
Figure 4-6. Calculated temperature evolution for the extreme case densely spaced waste canisters (reduced canister and tunnel spacing) and a buffer consisting of granular bentonite with 1% initial saturation, as well as a low thermal conductivity of the rock.	108
Figure 4-7. Time to 99% saturation for different values of rock-mass permeability.	109
Figure 4-8. (a) Volumetric strain and (b) shear strain in the rock at 100,000 years for the case of anisotropic strength properties	111
Figure 4-9. Calculated stress path for the case of anisotropic strength properties of the host rock.	112
Figure 4-10. Microstructural and macrostrural elastoplastic responses in a double-structure model equivalent to the Barcelona Expansive Model.	113
Figure 4-11. Schematic view of the experimental setup used in the through-diffusion experiment.	114
Figure 4-12. Logarithmic representation of the dependence of cD and Rd for ${}^{22}Na^+$ and ${}^{85}Sr^{2+}$ on the cation concentration in the external water phase [A].	117
Figure 4-13. Tracer concentration profile at steady state for chloride through-diffusion..	117
Figure 4-14. Spatial distribution of concentration of chloride as modeled by Birgersson and Karnland (2009).	118
Figure 4-15. Fit of experimental data reported by Van Loon et al. (2007) obtained by the single type pore model: (a) 1300 kg/m ³ , (b) 1600 kg/m ³ , (c) 1900 kg/m ³	122
Figure 4-16. Spatial distribution of concentration of chloride as modeled in CrunchFlow.	125
Figure 4-17. Fit of experimental data reported by Van Loon et al. (2007) obtained by the single type pore model: (a) 1300 kg/m ³ , (b) 1600 kg/m ³ , (c) 1900 kg/m ³	127
Figure 4-18. Normalized profiles of concentration of chloride obtained with varying ionic strength for a range of dry density values (a) 1300 kg/m ³ ; (b) 1600 kg/m ³ ; (c) 1900 kg/m ³	129
Figure 4-19. Fit of experimental data reported by Van Loon at al. (2007) obtained by the analytical solution of the simplified form of the Poisson-Boltzmann equation for the case of a binary solution between two parallel plates: (a) 1300 kg/m ³ ; (b) 1600 kg/m ³ ; (c) 1900 kg/m ³	131
Figure 5-1. DSEF architecture schematic diagram.	139
Figure 5-2. Information flow through DSEF Excel workbook.	145
Figure 5-3. Interface Parameters – thermal worksheet input-process-output example.	146
Figure 5-4. Once Through Fuel Cycle Waste Stream.	150
Figure 5-5. Modified Open Cycle Waste Streams.	150
Figure 5-6. Closed Fuel Cycle Waste Streams.	151

Figure 5-7. Thermal decay curves from the six heat-producing waste forms (OC, MOC, CFC).....	154
Figure 5-8. Application of the Method of Images for a Single Isothermal Surface.	164
Figure 5-9. Application of the method of images to two isothermal surfaces (the ground and water table surfaces).	165
Figure 5-10. Example of a configuration with three parallel layers.	167
Figure 5-12. Example of a configuration with two concentric cylinders.	169
Figure 5-13. Example of a configuration with two concentric cylinders and cylindrical mesh.	170
Figure 5-14. Mesh structure generated using the block (left) and the cylinder (right) structure.	170
Figure 5-15. Mathcad model reproduction of Carslaw and Jaeger (1959, figure 11).	172
Figure 5-16. Mathcad model reproduction of Carslaw and Jaeger (1959, figure 12).	173
Figure 5-17. Comparison of the temperature at sample centerline as a function of time obtained with TOPAZ3D and dimensionless analysis.	174
Figure 5-18. Fuel temperature distribution (K) for a central cross section of a 2 x 2 x 8 cm parallelepiped at selected time steps (x and z axis dimensions in meters).	175
Figure 5-19. Long-term waste form decay heat for each base case fuel cycle per canister assembly or canister.....	178
Figure 5-20. Short-term waste form decay heat for each base case fuel cycle per canister assembly or canister.....	179
Figure 5-21. The DSEF addresses combinations of waste form, geologic setting, and repository design.	186
Figure 5-22. The relationship between DSEF and the SA, SE, and UFD campaigns.	187
Figure 5-23. Hierarchy of nuclear fuel cycle models.....	188
Figure 5-24. Systems Engineering Catalog - Fuel Cycle O-T/R.1 PWR UOX – Once-through.	188

TABLES

Table 1-1. Synopsis of the Results of the Priority Ranking for the Engineered Barrier System (Nutt et al., 2011).....	19
Table 1-2. Summary of HLW/SF Disposal Concepts for the UK Nuclear Decommissioning Authority after Baldwin et al. (2008).	22
Table 1-3. EBS design concepts for backfilled disposal environments – modified after Stula et al. (1980).	28
Table 1-4. Summary of UNF and HLW Management Programs in Other Countries.....	32
Table 1-5. Planned UFD Generic EBS work for FY12.....	46
Table 2-1. Chemical Compositions of Bentonites and Smectite (weight %).....	55

Table 2-2. Mineral Abundances of Yucca Mountain Tuff and Bentonitic Products (weight %)	56
Table 3-1. Sources of Data for Common Cementitious Phases (after Wolery and Jové- Colón, 2007 and this report)	78
Table 3-2. Thermodynamic Properties of Cement Phases from the YMP and Other Thermodynamic Databases.....	80
Table 3-3. LogK values at 25°C of Cement Phases from the YMP and Other Thermodynamic Databases.....	84
Table 3-4. Complex clay minerals included in the last YMP thermodynamic database.....	89
Table 4-1. Thermal and hydraulic properties of the bentonite buffer.....	101
Table 4-2. BBM material parameter for the bentonite buffer	102
Table 4-3. THM rock properties for the clay stone host rock.....	103
Table 4-4. Material properties of the ubiquitous joint model.....	110
Table 4-5. Effective diffusion coefficients reported by Van Loon et al. (2007) as a function of dry density of clay and sodium chloride concentration in the pore water.....	116
Table 4-6. Values of electrical potential at the shear plane and of semispacing between clay layers as a function of dry density obtained by fitting procedures of experimental data reported by Van Loon et al. (2007).	129
Table 5-1 Revision History.....	142
Table 5-2 Base case waste forms for once-through, modified open and closed fuel cycles.....	153
Table 5-3 FEPs-identified waste forms.....	155
Table 5-4 FEPs-identified disposal system environments.....	156
Table 5-5 Fuel cycle, disposal environment, and aging time for 24 base case combinations.....	157
Table 5-6 Engineered Barrier System (EBS) concepts and components.....	180

ACRONYMS

AFCI	Advanced Fuel Cycle Initiative
ANDRA	Agence Nationale pour la gestion des Déchets RAdioactifs
ANL	Argonne National Laboratory
BBM	Barcelona Basic Model
BRIE	Bentonite Rock Interaction Experiment
CFC	Closed Fuel Cycle
CFM	Colloid Formation and Migration
CEA	Commissariat à l'Énergie Atomique
CEC	Cation Exchange Capacity
CSNF	Commercial Spent Nuclear Fuel (CSNF)
COEX	Co-Extraction
COTS	Commercially available Off-The-Shelf
DECOVALEX	DEvelopment of COupled Models and their VALidation against EXperiments
DOE	Department of Energy
DSEF	Disposal Systems Evaluation Framework
DST	Drift Scale Test
DSNF	DOE Spent Nuclear Fuel
EBR-II	Experimental Breeder Reactor II
EBS	Engineered Barrier System
EC	European Community
EC, Echem	Electrochemical processing
EDZ	Excavated Disturbed Zone
EGTS	Engineered Gas Transport System
ESDRED	Engineering Studies and Demonstrations of Repository Designs
FC-R&D	Fuel Cycle Research and Development
FCT	Fuel Cycle Technology
FEBEX	Full-scale Engineered Barriers Experiment
FEP	Features, Events, and Processes
FORGE	Fate of Repository Gases
GAST	Gas-Permeable Seal Test
GDSE	Generic Disposal System Environment

GTCC	Greater Than Class C
GWd	Gigawatt days
GWd/MT	Gigawatt (thermal) - days per Metric Ton
GWe	Gigawatts electric
GWt	Gigawatts thermal
HADES	High Activity Disposal Experimental Site
HLW	High-Level nuclear Waste
HM	Heavy Metal
HTGR	High Temperature Gas Reactor
IAEA	International Atomic Energy Agency
IED	Information Exchange Document
INL	Idaho National Laboratory
IGSC	Integration Group for the Safety Case
LAMMPS	Large-scale Atomic/Molecular Massively Parallel Simulator
LANL	Los Alamos National Laboratory
LBNL	Lawrence Berkeley National Laboratory
LLNL	Lawrence Livermore National Laboratory
LLW	Low Level Waste
LTHLW	Lower Than High Level Waste
LWR	Light Water Reactor
MD	Molecular Dynamics
MOC	Modified Open Cycle
MOX	Mixed OXide fuel
MT	Metric Ton
MTHM	Metric Tons of Heavy Metal
MTIHM	Metric Tons of Initial Heavy Metal
MTU	Metric Tons of Uranium
MWd	Megawatt days
NAGRA	National Cooperative for the Disposal of Radioactive Waste
NBS	Natural Barrier System
NE	DOE-Nuclear Energy
NEA	Nuclear Energy Agency
NUEX	New Extraction

NUMO	Nuclear Waste Management Organization of Japan
NW	Nuclear Waste
OC	Open Cycle
OECD	Organization for Economic Co-operation and Development
PA	Performance Assessment
PNNL	Pacific Northwest National Laboratory
PWR	Pressurized Water Reactor
R&D	Research and Development
SCM	Supplementary Cementitious Materials
SEM	Scanning Electron Microscopy
SF	Spent Fuel
SFHP	Spent Fuel Handling and Packaging
SFR	Sodium Fast Reactor
SNF	Spent Nuclear Fuel
SNL	Sandia National Laboratories
SRNL	Savannah River National Laboratory
SURF	Spent UnReprocessed Fuel
SZ	Saturated Zone
TALSPEAK	Trivalent Actinide Lanthanide Separation by Phosphorus-based Aqueous Komplexes [sic.]
TEM	Transmission Electron Microscopy
THM	Thermal-Hydrological-Mechanical
TM	Thermal-Mechanical
THMC	Thermal-Hydrological-Mechanical-Chemical
TRISO	Tristructural-isotropic (fuel)
TRU	Transuranic
TSX	Tunnel Sealing Experiment
UDS	Undissolved Solids
UFD(C)	Used Fuel Disposition (Campaign)
UK	United Kingdom
UNF	Used Nuclear Fuel
UOX	Uranium Oxide Fuel
UREX	Uranium Extraction
URL	Underground Research Laboratory

UZ	Unsaturated Zone
WAC	Waste Acceptance Criteria
WIPP	Waste Isolation Pilot Plant
XRD	X-ray Diffraction
YMP	Yucca Mountain Project

USED FUEL DISPOSITION CAMPAIGN/DISPOSAL SYSTEMS EVALUATIONS AND TOOL DEVELOPMENT

1. Overview of Engineered Barrier System (EBS) Concept Evaluation

1.1 Introduction

In a previous report (Jové Colón et al., 2010), key components of the nuclear fuel cycle related to engineered barriers in long-term disposal of nuclear waste were discussed in light of current R&D needs and/or priorities. This study served as an input to the Used Fuel Disposition campaign (UFDC) R&D Roadmap report (Nutt et al., 2011) where important aspects of this campaign mission are “*To identify alternatives and conduct scientific research and technology to enable storage, transportation, and disposal of used nuclear fuels and wastes.....*”. The disposal of UNF entails the immobilization of radioactive waste streams produced by various phases of the nuclear fuel cycle. This definition extends to the realm of EBS design concepts for the permanent disposition of nuclear waste forms (e.g. UNF, vitrified) safely contained and emplaced in subsurface geological repository environments far from the biosphere (Bennett et al., 2006). The current report is a continuation and expansion of work started in Jové Colón et al. (2010) but focused towards the development of EBS design concepts and applications of THMC modeling tools and approaches to assess barrier responses to changes in temperature. This report also describes progress made in the development of thermodynamic databases (cement and clay) and interactions between barrier materials.

The development and evaluation of EBS design concepts and their potential interactions with the natural barrier or with other EBS interfaces are inherently important to the long-term (i.e., in the order of thousands of years) safety and performance assessment of the safety case. In order to build the safety case for EBS disposal concepts along with the necessary system requirements (safety and/or performance) in the decision-making process requires a multi-faceted integration of knowledge and evidence gathering to demonstrate the confidence level of a geological disposal site (Bennett et al., 2006). It's worth to note the distinction in the European programs between safety assessment and performance assessment where the former is defined as the evaluation of the disposal system in its totality on the basis of radiological impact or dose exposure as a performance indicator. The latter mainly refers to parts of the system where radiological impact is not necessarily used as a gauge for performance (Bennett, 2010). It has been recognize that in nuclear waste repository programs, these definitions have been used interchangeably but we will restrict to the one consistent performance assessment for the EBS part without considering radiological impacts.

The definition of the EBS based on the consensus of several international repository research programs and given by the Nuclear Energy Agency (NEA) Integration Group for the Safety Case (IGSC) EBS project is given as:

“The “engineered barrier system” represents the man-made, engineered materials placed within a repository, including the waste form, waste canisters, buffer materials, backfill and seals. The “near-field” includes the EBS and those parts of the host rock in contact with or near the EBS, whose properties have been affected by the presence of the

repository. The “far-field” represents the geosphere (and biosphere) beyond the near-field” (NEA OECD State-Of-The-Art Report, 2003).”

The Joint EC/NEA Engineered Barrier System Project final report (Bennett, 2010) summarizes the EC and OECD NEA EBS project which has been conducting collaborative work for several years. In this report, various key points with regard to the study and importance of EBS design concepts and their assessment have been discussed:

- Continuous iteration between comprehensive research activities and process modeling exercises (e.g. safety assessment) are needed in the development, evaluation, and “optimization” of EBS design concepts. Dynamic integration of various types of information ranging from EBS performance requirements to process model and material details as a result of safety and performance assessment. The Disposal System Evaluation Framework (DSEF) could very well fit here as a tool in providing the necessary iterations between various levels of system evaluations and related performance requirements.
- EBS safety performance is defined as a functional assembly of components rather than on independent parts of the system. This is important to the evaluation of EBS design concepts particular in coupled thermal-hydrological-mechanical-chemical (THMC) processes in the near-field and interactions far-field or host rock domain. Performance requirements are to be examined considering the EBS as a whole functional system according to specific types of wastes and host-rock media.
- The role of the EBS is key to the safety case even when the natural barrier or host-rock is considered sufficiently adequate as to provide the expected level of disposal safety performance. As stated in the previous bullet, the goal of the EBS is to perform its function in concert with adjacent barriers (e.g., the natural barrier) so collectively these can maximize their barrier capability.

The focus of this section of the report is to provide an overview of EBS design concepts based on previous evaluations and/or adopted forms in international repository programs. Many of these topics evolved from continued work presented in the FY10 milestone report by Jové Colón et al. (2010). The current report content is organized as follows:

- Synopsis of backfilled EBS design concepts and a description of opportunities for international collaboration on EBS and nuclear waste disposal (this section);
- Clay-Mineral Evolution in the Yucca Mountain Drift-Scale Thermal Test and Engineered Barrier System Components – Experimental Studies (LANL, SNL);
- Thermodynamic database and model development for cement and clay phases;
- Continued development of modeling approaches for reactive transport and coupled thermal-hydrological-mechanical-Chemical (THMC) processes in clay-based barriers (LBNL);
- Continued Development of a Disposal Systems Evaluation Framework (DSEF; Version 1.0) and Thermal analysis with preliminary results (LLNL)

The evaluation of knowledge gaps and R&D prioritization in EBS is already documented and discussed in Sections 4.5.9 to 4.5.15 of the UFDC Disposal R&D Roadmap (Nutt et al., 2011). There are various aspects of EBS physical and chemical processes such as chemical evolution of the barrier and related barrier material degradation that are

prioritized for generic R&D. Table 1-1 list the EBS items along with the assigned priority rankings for R&D. The priority scoring procedure is described in Section 3.2 of Nutt et al. (2011). This ranking exercise is a way of establishing relative priorities for various issues necessitating generic R&D. In general, issues with high scores are those where there is an information gap and R&D is therefore needed. Issues where currently available information and state of the art are considered adequate have a ‘Low’ score given the absence of an information gap. Priority scores in between high and low during the assessments of importance of the issue have a medium ranking.

Notice the EBS issues that consistently ranked with a ‘HIGH’ score in all categories are those for waste form, waste container, radionuclide speciation and solubility, and buffer/backfill material (in particular, clay host-rock media). Such high prioritization is exemplified by the importance of THMC processes and interactions at EBS interfaces as shown in Figure 1-1. These EBS interfaces are the loci for important degradation processes in the near-field and at the boundary with far-field region that can indeed affect radionuclide transport beyond the confines of EBS and thus barrier performance. Given the inherent complexity of THMC processes and their feedbacks in response to changing repository conditions with time (e.g., temperature), it is necessary to accurately represent and capture the properties of the EBS in models with a high level of confidence and adequacy. Moreover, THMC models must assess the generic aspects of EBS design concepts and therefore these need to be flexible and agile in accommodating the important characteristics of the considered disposal concepts in various host-rock media. Section 3 of this report provides a description of the current advances in THMC model development in this UFD activity and applications to EBS performance. It also provides key aspects for future work to address the needs in the improvement of THMC models. Landolt et al. (2009) also emphasize the importance of the local corrosion environments at the canister/bentonite and bentonite/steel supports interfaces for different relative humidities and temperatures at different time periods upon waste emplacement.

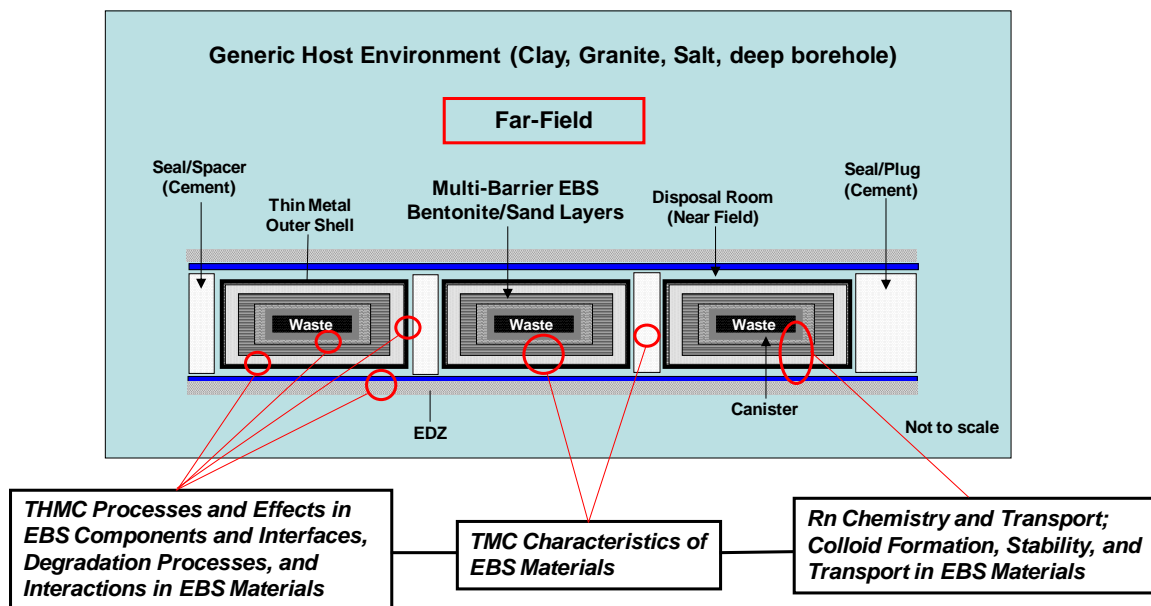


Figure 1-1. Generalized depiction of a generic EBS plus important interactions/processes at EBS components and interfaces.

Table 1-1. Synopsis of the Results of the Priority Ranking for the Engineered Barrier System (Nutt et al., 2011).

WASTE MATERIALS →	SNF	Glass	Ceramic	Metal
2.1.01.01, .03, .04: INVENTORY	Low	Low	Low	Low
2.1.02.01, .06, .03, .05: WASTE FORM	High	High	High	High
WASTE PACKAGE MATERIALS →	Steel	Copper	Other Alloys	Novel Materials
2.1.03.01, .02, .03, .04, .05, .08: WASTE CONTAINER	High	High	High	High
2.1.07.03, .05, .06, .09: MECHANICAL PROCESSES	Medium	Medium	Medium	Medium
2.1.08.02, .07, .08: HYDROLOGIC PROCESSES	Low	Low	Low	Low
2.1.09.01, .02, .09, .13: CHEMICAL PROCESSES - CHEMISTRY	Medium	Medium	Medium	Medium
- Radionuclide speciation/solubility	High	High	High	High
2.1.09.51, .52, .53, .54, .55, .56, .57, .58, .59: CHEMICAL PROCESSES - TRANSPORT	Low	Low	Low	Low
- Advection, diffusion, and sorption	Medium	Medium	Medium	Medium
2.1.10.x: BIOLOGICAL PROCESSES (no FEPs were scored in this category)	Low	Low	Low	Low
2.1.11.01, .02, .04: THERMAL PROCESSES	Medium	Medium	Medium	Medium
2.1.12.01: GAS SOURCES AND EFFECTS	Low	Low	Low	Low
2.1.13.02: RADIATION EFFECTS	Low	Low	Low	Low
2.1.14.01: NUCLEAR CRITICALITY	Low	Low	Low	Low
BUFFER / BACKFILL (media type) →	Clay	Salt	Crystalline	Mixed Materials
2.1.04.01: BUFFER/BACKFILL	High	Medium	Medium	Medium
2.1.07.02, .03, .04, .09: MECHANICAL PROCESSES	Medium	Medium	Medium	Medium
2.1.08.03, .07, .08: HYDROLOGIC PROCESSES	Medium	Medium	Medium	Medium
2.1.09.01, .03, .07, .09, .13: CHEMICAL PROCESSES - CHEMISTRY	Medium	Medium	Medium	Medium
- Radionuclide speciation/solubility	High	High	High	High
2.1.09.51, .52, .53, .54, .55, .56, .57, .58, .59, .61: CHEMICAL PROCESSES – TRANSPORT	Medium	Medium	Medium	Medium
- Colloid facilitated transport	Low	Low	Low	Low
2.1.10.x: BIOLOGICAL PROCESSES (no FEPs were scored in this category)	Low	Low	Low	Low
2.1.11.04: THERMAL PROCESSES	Medium	Medium	Medium	Medium
2.1.12.01, .02, .03: GAS SOURCES AND EFFECTS	Medium	Medium	Low	Low
2.1.13.02: RADIATION EFFECTS	Low	Low	Low	Low
2.1.14.02: NUCLEAR CRITICALITY	Low	Low	Low	Low

Table 1-1. Synopsis of the Results of the Priority Ranking for the Engineered Barrier System (Nutt et al., 2011) (continued)

SEAL / LINER MATERIALS →	Cement	Asphalt	Metal	Polymer
2.1.05.01: SEALS	Medium	Medium	Medium	Medium
2.1.06.01: OTHER EBS MATERIALS	Medium	Medium	Medium	Medium
2.1.07.02, .08, .09: MECHANICAL PROCESSES	Medium	Medium	Medium	Medium
2.1.08.04, .05, .07, .08, .09: HYDROLOGIC PROCESSES	Low	Low	Low	Low
- Flow through seals	Medium	Medium	Medium	Medium
2.1.09.01, .04, .07, .09, .13: CHEMICAL PROCESSES – CHEMISTRY	Medium	Medium	Medium	Medium
- Radionuclide speciation/solubility	High	High	High	High
2.1.09.51, .52, .53, .54, .55, .56, .57, .58, .59: CHEMICAL PROCESSES - TRANSPORT	Low	Low	Low	Low
- Advection, diffusion, and sorption	Medium	Medium	Medium	Medium
2.1.10.x: BIOLOGICAL PROCESSES (no FEPs were scored in this category)	Low	Low	Low	Low
2.1.11.04: THERMAL PROCESSES	Medium	Medium	Medium	Medium
2.1.12.02, .03: GAS SOURCES AND EFFECTS	Low	Low	Low	Low
2.1.13.02: RADIATION EFFECTS	Low	Low	Low	Low
2.1.14.02: NUCLEAR CRITICALITY	Low	Low	Low	Low
OTHER MATERIALS →	Low pH Cements	Salt-Sat. Cements	Geo-polymers	Barrier Additives
2.1.06.01: OTHER EBS MATERIALS	Medium	Medium	Medium	Medium
2.1.07.08, .09: MECHANICAL PROCESSES	Medium	Medium	Medium	Medium
2.1.08.04, .05: HYDROLOGIC PROCESSES	Medium	Medium	Medium	Medium
2.1.09.04, .07, .09, .13: CHEMICAL PROCESSES - CHEMISTRY	Medium	Medium	Medium	Medium
- Radionuclide speciation/solubility	High	High	High	High
2.1.09.51, .52, .53, .54, .55, .56, .57, .58, .59: CHEMICAL PROCESSES – TRANSPORT	Low	Low	Low	Low
- Advection, diffusion, and sorption	Medium	Medium	Medium	Medium
2.1.10.x: BIOLOGICAL PROCESSES (no FEPs were scored in this category)	Low	Low	Low	Low
2.1.11.04 THERMAL PROCESSES	Medium	Medium	Medium	Medium
2.1.12.02, .03: GAS SOURCES AND EFFECTS	Low	Low	Low	Low
2.1.13.02: RADIATION EFFECTS	Low	Low	Low	Low
2.1.14.02: NUCLEAR CRITICALITY	Low	Low	Low	Low

Notes:

1. Shading for an entry indicates that research in that area has been undertaken in other geologic disposal programs
2. FEP number lists delimited by commas show only the change in the fourth field of the FEP

1.2 Historical Overview of Backfilled EBS Design Concepts

1.2.1 Early EBS Performance Analysis of Design Concepts

Early efforts to evaluate performance of EBS design concepts dates back to the late 1970's and early 1980's. The work of Stula et al. (1980) appears to be one of the earliest efforts in the performance analysis of various backfilled EBS design concepts. The analyses given by these authors included a sensitivity assessment of EBS performance according to design parameters specific to various types of waste packages. Further, assessment of radionuclide transport and associated releases beyond the confines of the EBS were also part of this study. This work was restricted to a limited set of EBS designs concepts but with a sufficiently wide range of specified parameters to capture sensitivities in barrier performance (Stula et al., 1980). Such activity signifies the early introduction of the generic evaluation of EBS design concepts. That is, given the multiple options that include host-rock media, nuclear waste types, and thus a range of barrier performance requirements necessitates the flexibility of generic analysis to treat a range of EBS design concepts. These EBS concepts have a strong tie to the larger scale of disposal concepts at a site. The work by Baldwin et al. (2008) provides a synthesis of disposal concepts considered by various NW (SF/SNF/HLW) repository programs and these are described below.

1.2.1.1 EBS Design Concepts and Materials

Baldwin et al. (2008) evaluated many generic disposal concepts for the UK Nuclear Decommissioning Authority for HLW and SF in deep subsurface geological repository environments. These authors analyzed various concepts by systematically synthesizing the large body of existing information from various NW repository programs using a set of evaluation criteria to capture important attributes such as safety, environmental impact, flexibility, and cost. Among these attributes, safety is mainly captured within the EBS and related components to provide long-term isolation of the waste. The evaluation of Baldwin et al. (2008) describes this synthesis on the basis of 12 concepts and their key attributes are summarize in Table 1-2. Their assessment of disposal concepts in geological media is fairly encompassing and provides an excellent summary of the advantages and disadvantages of each based on many years of NW repository R&D.

There are various levels of maturity between these concepts as well as similarities. Some of these concepts (e.g., 3, 4, 5, 6, and 7 in Table 1-2) have been adopted for development in some form by various European and USA nuclear waste repository programs. In envisioning potential EBS design concepts, the current report will focus on disposal concepts that are consistent with in-tunnel axial emplacement having corrosion-resistant canister/overpack and backfilled configurations (e.g., concepts 3 – 7 in Table 1-2). There are other concepts such as 1 and 2 that could be modified for HLW/SF disposal in salt host media and therefore deserve some attention. Concept 2 is somewhat similar to that adopted for TRU waste disposal at WIPP but with different disposal room configurations. In this case the comparison is very general but provides a concept similarity of a workable example of a mined repository in salt host media. Figure 1-2 shows a schematic example of the supercontainer disposal concept (ESDRED, 2009).

Table 1-2. Summary of HLW/SF Disposal Concepts for the UK Nuclear Decommissioning Authority after Baldwin et al. (2008).

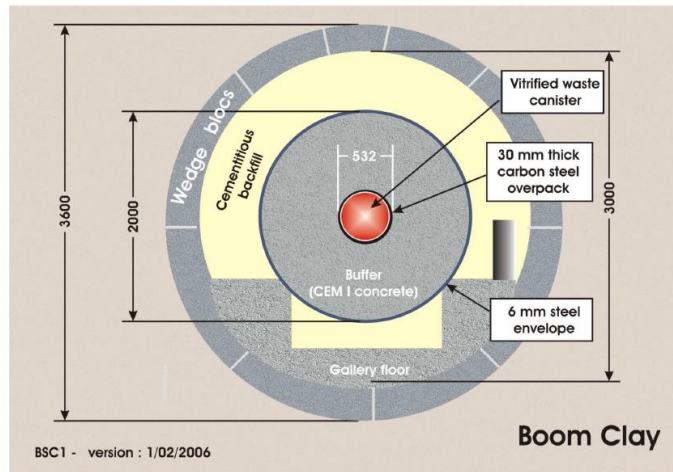
Concept	Emplacement Characteristics	Options	Key Features
1 2	In-tunnel emplacement within boreholes	(1) Vertical (2) Horizontal	<p>Vertical or horizontal emplacement of waste canisters with annulus regions backfilled with clay or crushed salt (salt host media)</p> <p>Borehole length: 6 – 8 m. Borehole diameter: 0.6 – 1.5 m</p> <p>Corrosion-resistant canister/overpack (copper or stainless steel)</p> <p>Barrier/buffer materials: clay, cement, crushed salt (in salt media disposal)</p> <p>Concepts is flexible in accepting HLW/SF waste</p> <p>Concept (1) considered by SKB (Sweden), e.g., KBS-3V</p> <p>Concept (2) considered by SKB (Sweden) (e.g.,KBS-3H); ANDRA (France) for disposal at the Callovo-Oxfordian clay host rock</p>
3 4	In-tunnel axial emplacement	(3) Short-lived canister (4) Long-lived canister	<p>Waste canister is emplaced axially within tunnel encircled by annulus of bentonite clay backfill/buffer material</p> <p>Tunnel diameter: 2 – 3.7 m</p> <p>Concepts considered by: NAGRA (Switzerland), SAFIR 2 (Belgium), NUMO (Japan)</p> <p>Considered to be matured and flexible by various repository programs</p>

Table 1-2 (cont.). Summary of HLW/SF Disposal Concepts for the UK Nuclear Decommissioning Authority after Baldwin et al. (2008).

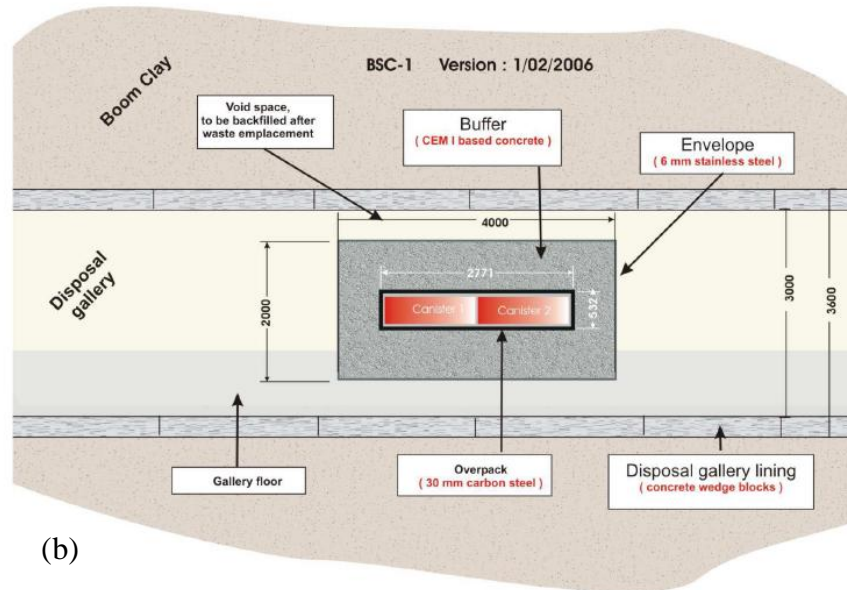
Concept	Emplacement Characteristics	Options	Key Features
5 6 7	In-tunnel axial emplacement with Supercontainer	(5) Small annulus (6) Small annulus + concrete buffer (7) Large annulus	<p>(5) Supercontainer (pre-assembled multi-component corrosion-resistant waste package and buffer surrounded by perforated steel sleeve) axially emplaced in small tunnels. No additional backfill material is used. The KBS-3H concept adheres to this description. Translates is less excavated volume. Drift diameter is ~1.85 m (POSIVA, 2008).</p> <p>(6) Supercontainer (assembly of waste canister/overpack encased in a steel sleeve) axially emplaced in tunnels with larger diameters than the container assembly (e.g., up to ~3 m). These are backfilled with cementitious material. The SAFIR 2 concept adheres to this description.</p> <p>(7) Supercontainer (assembly of waste canister/overpack encased in a steel sleeve) axially emplaced in tunnels with diameters of ~3 m that are backfilled with bentonite clay or crushed rock material. Very similar to Concept (5) except for the presence of backfill.</p> <p>Concept (5) is considered by SKB (Sweden) and POSIVA (Finland). Concept (6) is considered by ONDRAF/NIRAS (Belgium). Concept (7) is considered as an alternative concept by NUMO (Japan).</p> <p>All these concepts are considered to be flexible and robust</p>
8 9	Caverns with cooling, delayed backfilling	(8) Cavern structure hosting steel multi-purpose containers (MPCs) plus bentonite clay backfill (9) Cavern structure hosting steel multi-purpose containers (MPCs) plus cement backfill	<p>(8) Multi-purpose sealed/metallic containers (MPCs) of large capacity are emplaced in a vertical position within an excavated cavern storing multiple SF assemblies or HLW. MPCs are designed for storage, transport, and disposal. These units require long-term cooling before bentonite clay backfilling of the cavern. The concept is ideal for disposal in salt host media with crushed-salt backfill.</p> <p>(9) MPCs or concrete disposal casks are emplaced in a vertical position within an excavated cavern storing multiple SF assemblies or HLW. Cementitious backfill is used upon cooling.</p> <p>These concepts provide for flexibility and a smaller footprint at the site. Although these concepts have been considered, these have never been developed for HLW or SF disposal.</p>

Table 1-2 (cont.). Summary of HLW/SF Disposal Concepts for the UK Nuclear Decommissioning Authority after Baldwin et al. (2008).

Concept	Emplacement Characteristics	Options	Key Features
10	Mined deep borehole (cavern disposal gallery)		<p>A large number of waste canisters (either as supercontainers or waste canisters/overpack with clay backfilled annulus) are emplaced in vertical stacks within boreholes having diameters of 1.5 – 2 m. This concept has been envisioned for boreholes excavated at a depth of ~300 m in salt host media.</p> <p>This concept is considered to be flexible and provides for a smaller footprint at the site. However, there are concerns about the technology for buffer emplacement in long vertical boreholes, thermal convection, and package-bearing weight onto seals.</p> <p>Concept considered by DBE Technology (Germany) for HLW (vertical) and SF (horizontal) disposal in salt (Bollingerfehr et al., 2010).</p>
11	Hydraulic cage	Cavern repository	<p>The concept of a hydraulic cage refers to the emplacement of coarse-grained high porosity backfill material surrounding disposal units in caverns. The purpose of the coarse-grained material is to divert potential water flow away from the disposal units or waste containment domain. This concept is consistent with the emplacement of a capillary or Richards barrier.</p> <p>This concept has been considered for ILW but not for HLW or SF disposal. However, a Richards barrier has been considered in other concepts such as those for multi-component or multi-layer barriers in axially-emplaced containers.</p>
12	Deep borehole (depth 2 – 5 km)		<p>Waste package canisters are emplaced in borehole drilled at depths between 2 and 5 km with minimal barrier components except for the metal borehole casing and a robust system of seals.</p> <p>Consideration of this concept is built on the expected high level of isolation in a deep and stable geological environment, and flexibility in terms of host rock media. Further R&D is needed to assess potential issues with borehole drilling, waste canister emplacement, uncertainties about retrievability, and operational/monitoring activities.</p>



(a)



(b)

Figure 1-2. Radial (a) and axial (b) cross-sectional view of the supercontainer concept (ESDRED, 2009).

The EBS design concepts evaluated by Stula et al. (1980) are consistent with recently-advanced multi-component or multi-layered barrier configurations envisioned for backfilled disposal environments. Although variants of these EBS design concepts were initially conceived in the mid-to-late 1970's as part of the Spent UnReprocessed Fuel (SURF) and Spent Fuel Handling and Packaging (SFHP) programs (Westerman, 1979), these were adopted and slightly modified by Stula et al. (1980); but also subsequently embraced by others in the advancement of tailored multi-barrier concepts (Apted, 1998; McKinley et al., 2006) as described in Jové Colón (2010). The goal of Stula et al. (1980) is to evaluate generic EBS design concepts that are representative of various levels of intricacy ranging from basic to complex. This approach provides the basis for design optimization to assess the need for ensuring adequacy and compliance with performance and/or functional requirements of generic EBS design concepts. Table 1-3 shows a series of EBS design concepts starting from a relatively simple one-domain barrier to a more complex three-domain barrier EBS concept with additions of metal sleeves to enhance

barrier stability and overall barrier performance. Although, the basis for these EBS design concepts is based on the work of Stula et al. (1980), these were modified in accord with more recent ideas on waste package/canister geometries, barrier materials, and disposal configurations. This allows for the advancement of EBS design concepts based on a number of combinations of barrier materials and dimensional constraints. For example, granular backfill barrier material can be tailored to have quartz and bentonite mixed in various proportions to achieve the desired permeo-porous properties as well as levels of compaction during barrier emplacement. Further, the emplacement of coarser material as a single domain adjacent to the canister surface may act as a capillary or Richards barrier to divert potential flow (at elevated liquid saturations) that could reach the waste package canister assembly. Also, peak waste temperatures increase with increasing backfill/buffer thickness as well as with the use of low conductivity barrier materials (Stula et al., 1980). Therefore, the combined optimization of barrier thicknesses and materials can be used to produce long-term scenarios for thermal management that can drive important chemical, mechanical, and hydrological processes in the EBS. The set of barrier materials considered by Stula et al. (1980) is relatively simple but similar to those considered in other repository programs:

- Non-metallic:(Bentonite clay, silica-rich sand, clinoptilolite)
- Metallic (mild-steel, zircaloy-2, inconel-600, 304 stainless steel, copper, lead, cast iron)

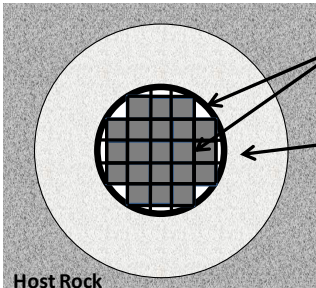
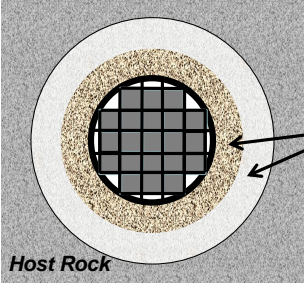
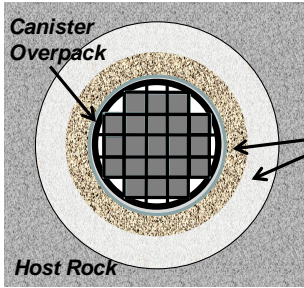
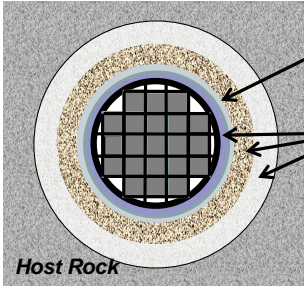
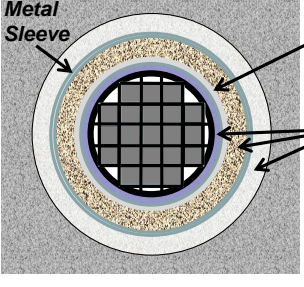
The cases studied by Westerman (1979) and Stula et al. (1980) involve a combination of these materials for the canister/barrier ensemble along with barrier dimensions to evaluate EBS performance through design optimization. The behavior of these materials has been studied extensively under conditions relevant to disposal environments and many of their properties can be reliably predicted. For example, the mechanical and chemical properties of clay material (e.g., MX-80, Fo-Ca) have been investigated for many years with regards to their barrier capability for fluid transport and related sealing properties. The rationale for the choice of these materials has to do with the current knowledge on their properties and behavior when subjected to conditions typical of repository environments, demonstrated barrier longevity, and performance. Still, further investigations are needed to narrow knowledge gaps, for example, on the behavior of these materials at elevated temperatures in relation to their barrier properties.

There has been a wide range of candidate materials for EBS concepts along with various proposed modes of barrier emplacement. The main candidates for metallic phases considered for canister and related overpack materials are various types of steels (carbon, stainless steel), copper, and cast iron (Bennett and Gens, 2008). For example, Bennett and Gens (2008) describes some of the general characteristics of the metallic waste barrier and buffer materials for various European disposal concepts and waste types. A large body of work has been published in the last two decades on the material characteristics of metallic barriers and their expected performance under various environments (Bennett and Gens, 2008). Emplacement of clay barrier/buffer material have also being discussed in these studies whether the choice is compacted clay blocks or dry granular material. Granular material offers certain advantages in terms of facilitating emplacement around the canister. However, thermal conductivity of dry granular material is low and temperature across the barrier can exceed 100°C (Johnson and King, 2003). Barrier additives such as carbon-based materials like graphite and quartz mixed

with the predominant clay phase have been considered for enhancement of the backfill/buffer thermal conductivity (Beziat et al., 1992; Geneste et al., 1990; Jobmann and Buntebarth, 2009; Westerman, 1979). The graphite component in clay-quartz mixtures is responsible for significantly enhancing the thermal conductivity in the backfill mix but it is also attractive for its impervious (in some forms), mechanical, and inert properties; in addition to its low cost (Beziat et al., 1992; Geneste et al., 1990). Section 1.2.1.2 provides a general overview of some important highlights with respect to performance requirement and criteria of the EBS.

The considered set of EBS design concepts (Table 1-3) should be viewed as a starting point to develop a conceptual basis that allows for flexible options in terms of material types and dimensions while retaining the overall geometry consistent with current waste package configurations whether is HLW or SF disposal. Concept A represents what could be considered the simplest EBS configuration with a single-domain backfill/buffer annulus surrounding the waste/canister; it has been adopted and tested by the FEBEX program for the Spanish EBS concept. A flexible multi-barrier concept (e.g., concepts A1 through D) is able to better accommodate near-field performance requirements with increased complexity in the EBS. No recommendations are made here since the consideration of a design concept depends on many factors such as performance and safety criteria, site characteristics, concept feasibility, and cost.

Table 1-3. EBS design concepts for backfilled disposal environments – modified after Stula et al. (1980).

EBS Concept	Description	Generalized Geometric Depiction (Not To Scale)
Concept A	Simplest EBS Design Concept with one-domain backfill/buffer barrier. The annulus barrier domain can be composed of single phase bentonite clay or bentonite-sand mixture. Candidates for barrier additive are graphite or radionuclide sorption getter. EBS concept consistent with the FEBEX (Spain) EBS design adopted in mock-up and site-scale experiments (GRIMSEL URL site, Switzerland).	 <p>Waste Container and SF Assembly (arbitrary)</p> <p>One-Domain Backfill/Buffer</p> <p>Host Rock</p>
Concept A1	EBS concept A1 is very similar to A but with a two-domain (two-layer) backfill/buffer barrier. The inner annulus barrier domain has a coarser grain size than the outer barrier annulus. Barrier candidate materials for the inner- and outer-barrier annulus are sand-bentonite mixtures of specific proportions (e.g., sand-rich inner domain). Outer-barrier annulus domain can be composed of single phase bentonite. Candidate additives are graphite or radionuclide getter.	 <p>Two-Domain Backfill/Buffer Barrier Material</p> <p>Host Rock</p>
Concept B	Similar to EBS concept A1 but with added canister overpack as a metallic barrier.	 <p>Canister Overpack</p> <p>Two-Domain Backfill/Buffer Barrier Material</p> <p>Host Rock</p>
Concept C	Similar to EBS concept B but with backfill/buffer material included within the waste canister/overpack assembly. In principle, the concept is consistent with the Supercontainer design and the disposal concept adopted by NIRAS/ONDRAS, Belgium.	 <p>Canister Overpack</p> <p>Three-Domain Backfill/Buffer Barrier Material</p> <p>Host Rock</p>
Concept D	Similar to EBS concept C but with added metal sleeve between outer and inner annular backfill/buffer domains. The addition of a metal sleeve enhances barrier capabilities and could result in easing emplacement of multi-layered backfill/buffer material.	 <p>Canister Overpack</p> <p>Three-Domain Backfill/Buffer Barrier Material</p> <p>Metal Sleeve</p>

Increase in Complexity

1.2.1.2 EBS Performance Requirements

The choice of design concepts and their optimization strongly depends on the performance requirements established for the EBS that includes the expected time period for the barrier to perform under specific physico-chemical conditions and long-term barrier integrity and longevity.

Westerman (1979), Balady (1996), and Bennett (2010) presented a set of criteria or requirements in the development and performance evaluation of EBS design concepts that can be summarized as follows:

1. Time period required for optimal EBS integrity and longevity after waste emplacement to ensure long-term containment of radioactive material in waste canisters. Most repository programs consider time periods in the order of thousands of years (e.g., 1000 to 10,000 years, or more). This is viewed in terms of the waste canister resisting water percolation through the required length of time.
2. Flexibility to accommodate changes in barrier design, materials, and site conditions at the various stages of the disposal system evaluation, and also during construction, monitoring and testing. The need to adjust in response to operational conditions during disposal activities, stakeholder and site requirements, safety, and cost are key to the multiple criteria considered in building options for EBS design concepts.
3. Maximum permissible temperatures of the fuel and resulting thermal history. Optimization of generic EBS designs can be driven by thermal loadings of the radioactive material as to maintain temperatures below 100°C or boiling, and thus minimize the inducement of flow depending on the barrier and host-rock media. One notable exception is the NAGRA Swiss repository concept where temperatures of the waste canister surface exceed 100°C (see text below). Other key processes affected by temperature are the generation of chemical gradients and degradation of barrier materials.
4. Consider design concepts that keep retrievability as a feasible option. Some repository programs consider waste retrievability for up to ~50 years after disposal.
5. Accurate understanding of the EBS chemical environment and its consequences to long-term barrier degradation, particularly at EBS interfaces. For example, eventual disruption of the EBS due to slow-rate mechanical deformation modes such as creep in clay and salt disposal environments.
6. Design concepts along with fuel assemblies need to be constrained as to prevent criticality.
7. Consideration of fuel components as barriers such as fuel cladding.

This list is focused on EBS performance requirements and obviously it should not be considered as complete. Many other requirements can factor in such as those from stakeholder demands, regulatory entities, and site criteria where these becomes important in making decisions about which design concept satisfy the margins of compliance and adequacy. For this reason, one of the main purposes for evaluation and analysis of EBS

design concepts is to communicate key information and attributes of the potential choices to be considered in the process of decision making.

As described by Bennett and Gens (2008), most European disposal concepts have stipulated peak temperatures on the waste package or outer overpack surface ranging from ~75 to ~95 °C (i.e., <100°C). However, as indicated above in item 3, the exception is the Swiss disposal concept where peak temperatures of up to ~125°C at the waste canister surface have been considered, exceeding the 100°C limit for the barrier domain. As described by Johnson and King (2003), there is no stringent requirement on the peak temperatures in the EBS and/or near-field domain in the Swiss disposal concept except to alleviate the potential for deleterious effects on the chemical and mechanical properties of the barrier material. At temperatures above 100°C, the barrier performance of the waste canister metallic components is expected to resist pervasive corrosion in the long-term, assuming dry conditions. However, clay buffer/backfill material exposed to temperatures exceeding 100°C is susceptible to significant chemical changes and mineralogical phase transformations as a result of hydrothermal alteration (Pusch et al., 2010; Wersin et al., 2007). It should be noted that Bel and Bernier (2001) defined a temperature criterion of <100°C for radioactive waste disposal in clay host-rock (Boom Clay) and clay-bearing backfill/buffer barriers. This criterion is mainly based on some of the aforementioned effects of temperature on clay backfill/buffer materials. For example, reduction of the following: (1) steam generation, (2) phase mineral transformation (smectite to illite), (3) effects from coupled processes, (4) corrosion rate, (5) uncertainty in model predictions (e.g., radionuclide solubility), and (6) problems with high-temperature material characterization. Although these are valid considerations, there is still uncertainty and lack of knowledge on the key barrier properties (chemical, mineralogical, hydrological, and mechanical) of clay at temperatures exceeding 100°C (Wersin et al., 2007) as to stringently establish a peak temperature limit to the backfill/buffer domain in the EBS.

Wersin et al. (2007) describes the long-term effects of clay exposure to temperatures above 100°C and the irreversible changes that could incur in the properties of the clay materials such as mineralogical, swelling, and deformation. The two main resulting effects of this exposure to elevated temperatures are silica cementation and phase transformation of smectite to illite. This resulting alteration yields a reduction in clay swelling and stiffening of the clay phase (Pusch et al., 2010) that can affect the transport properties of the clay barrier domain (Wersin et al., 2007). Stiffening or strengthening of the clay phase as a result of this alteration could translate in the compromise of the self-sealing properties of the clay (Pusch et al., 2010). According to Wersin et al. (2007), the process of illitization releases silica in solution that could in turn precipitate as silica cement. This type of alteration is expected to be localized and adjacent to the hot waste package surface. In the Swiss disposal concept, at least half of the clay-ring outer domain should not exceed a temperature of ~125°C as to preserve the peak swelling properties of the clay (Johnson and King, 2003). It is therefore considered that the extent of clay alteration is expected to be of low consequence at temperatures of ~125°C and could exceed this value in regions close to the waste canister then loosening the peak temperature constraint for the clay backfill/barrier phase. Moreover, relaxing the temperature constraint could translate in cost-effective options for waste emplacement since it would not require large distances between waste canisters within the disposal galleries and thus minimizing spatial requirements at the site (Wersin et al., 2007). This could be essential for the need in flexibility of thermal requirements for various

emplacement configurations of various types of HLW and UF having a wide range of burnup rates and heat loads in the considered host-rock media. Such a better understanding of the response to high temperature phenomena for barrier materials is important to disposal environments such as deep borehole environments where waste packages placement are expected to be closer to each other relative to shallower disposal concepts.

Contrary to the view of low consequence for the consideration of temperatures above 100°C, there are other important aspects of the clay barrier performance that should not be compromise, for example:

- Ion exchange properties of clay materials;
- Mechanical and related swelling properties that could affect sealing behavior;
- Permeability and porosity.

The relative importance of these properties versus the need to adopt an elevated temperature criterion in the near-field environment needs to be weighted from the standpoint of performance requirements for any adopted EBS concept.

1.3 Recommended Areas of International Collaboration

1.3.1 Opportunities and considerations

For the UFD Campaign (UFDC), international collaboration is a very beneficial and cost-effective strategy for advancing disposal science in multiple disposal options and different geologic environments. While the United States disposal program had focused solely on Yucca Mountain tuff as the host rock, several international programs have made significant progress over the past decades in the characterization and performance evaluation of other geologic repository options, most of which very different from the Yucca Mountain site in design and host rock characteristics. Because Yucca Mountain was so unique (e.g., no backfill, unsaturated densely fractured tuff), areas of direct collaboration with international disposal programs were quite limited during that time. The decision by the U.S. Department of Energy to no longer pursue the disposal of UNF at Yucca Mountain has shifted UFDC's interest to disposal options and geologic environments more in line with many international disposal programs; much can be learned in close collaboration with these programs to get access to valuable experience and data gained over decades. LBNL and researchers from other U.S. national laboratories are actively pursuing opportunities for such collaboration. Dr. Jens Birkholzer from LBNL has recently assumed the role of UFDC's Technical Lead for International Activities, and as such, will advise the campaign on international activities with potential for significant technical advances. He will also interact with international organizations and programs to help advance specific collaborations, in particular those that would provide *active* collaboration of UFDC researchers within international R&D projects.

International geologic disposal programs are at different maturation states, ranging from essentially “no progress” to selected sites and pending license applications to regulators. Table 1-4 summarizes the status of UNF and HLW management programs in several countries. The opportunity certainly exists to collaborate at different levels ranging from

providing expertise to those countries “behind” the U.S. to obtaining access to information and expertise from those countries with mature programs (*Used Fuel Disposition Campaign International Activities Implementation Plan, FCR&D-USED-2011-000016 REV 0, November 2010 [Nutt, 2011]*).

Table 1-4. Summary of UNF and HLW Management Programs in Other Countries.

Country	Material to be Disposed	Centralized Storage	Geologic Environments	URL	Site-Selection	Anticipated Start of Repository Operations
Finland	SNF		Granite, Gneiss, Grandiorite, Migmatite	ONKALO (Granite)	Site at Olkiluoto Selected	2020
Sweden	SNF	CLAB - Oskarshamn	Granite	Aspo (Granite)	Site at Osthhammar Selected	2023
France	HLW and ILW		Argillite and Granite	Bure (Argillite)	Site near Bure Selected	2025
Belgium	HLW		Clay/Shale	Mol (clay)	Not Initiated	~2040
China	HLW		Granite		Preliminary Investigations Underway - Beishan in Gobi Desert	~2050
Switzerland	HLW	Wulenlingen (ZWILAG)	Clay and Granite	Mont Terri (Clay) Grimsel (Clay)	Initiated	No sooner than 2040
Japan	HLW		Granite and Sedimentary	Mizunami (Granite) Homonobe (Sedimentary)	Initiated	No Decision Made
Canada	SNF		Granite and Sedimentary	Pinawa (Granite) - being decommissioned	Initiated	No Decision Made
United Kingdom	HLW and ILW		Undecided		Initiated	No Decision Made
Germany	HLW, SNF, heat generating ILW	Gorleben and Ahaus	Salt	Gorleben (Salt)	On Hold	No Decision Made
Republic of Korea	SNF	Envisioned	Granite	Korea Underground Research Tunnel (Granite, Shallow)	Not Initiated	No Decision Made
Spain	No Decision Made	Siting Process Initiated	Granite, Clay, Salt		Not Initiated	No Decision Made

Source: Nuclear Waste Technical Review Board, 2009. Survey of National Programs for Managing High-Level Radioactive Waste and Spent Nuclear Fuel

As to the possible types of international involvement, one may distinguish between two broad categories. The first category comprises participation in multi-national or bilateral organizations, working groups, or committees, and typically involves high-level information exchanges, expert panels, review functions, training and education, etc. Recent or ongoing UFDC (or NE-53) activities in this area have been summarized in *Used Fuel Disposition Campaign International Activities Implementation Plan (FCR&D-USED-2011-000016 REV 0, November 2010 [Nutt, 2011]*). A few selected examples include multi-national activities such as under IAEA (e.g., review activities, conference participation, education within the International training Center, ITC, ...), OECD/NEA (e.g., participation in annual meetings, Integration Group for the Safety Case membership, R&D on NEA Thermodynamic Database,...), EDRAM (International Association for Environmentally Safe Disposal of Radioactive Waste), or bilateral agreements such as PUNT (U.S. – China Peaceful Uses of Nuclear Energy) and NEAP (U.S. – Japan Nuclear Energy Action Plan. UFDC will continue participation and/or support of many of the international activities discussed above, and may need to expand on certain activities, but will need to be selective in its choices to further those opportunities that are of most benefit to the campaign.

The second category involves *active* R&D collaboration of UFDC researchers within international projects or programs in close collaboration with multi-national scientists. With active R&D, we mean here that UFDC scientists work together closely with international scientists on concrete research projects relevant to both sides. Such active collaboration would provide direct access to information, data, and expertise on various disposal options and geologic environments that has been collected over the past decades. Many international programs have operating Underground Research Laboratories (URLs)

in clay/shale, granite, and salt environments, in which relevant field experiments have been and are being conducted. Depending on the type of collaboration, UFDC researchers may be able to participate in planning, conducting, and interpreting these experiments, and thereby get early access to field studies without having *in situ* research facilities in the U.S. We consider such active R&D activities to be most beneficial to UFDC, to help efficiently achieve its long-term goals of conducting “experiments to fill data needs and confirm advanced modeling approaches” (by 2015) and of having a “robust modeling and experimental basis for evaluation of multiple disposal system options” (by 2020). Most efforts to date are focused in exploring opportunities of active international collaboration, both at LBNL and within the UFDC as a whole. Advancing such opportunities will be the primary focus of UFDC’s international activities in the next few years. (Obviously, the first category of international involvement discussed above is important in helping identify and facilitate avenues of active R&D collaboration; it is thus important that UFDC or NE-53 continue participation in multi-national or bilateral organizations such as IAEA, or OECD/NEA.)

Active collaboration can be achieved under different working models. One first straightforward option is informal peer-to-peer interaction with international R&D organizations. Several UFDC scientists, most of which are associated with DOE’s national laboratories, have close relationships with their international counterparts, resulting from workshops and symposia meetings, or from active R&D collaboration outside of UFDC’s scope. Continued UFDC support for participation of UFDC researchers in relevant international meetings will help to foster and expand such relationships.

Other working models for active collaboration may require formal agreement and sometimes long-term (financial) commitment before R&D collaboration can take place. It is advisable that such agreements with international organizations/partners should be exercised by DOE, rather than by the UFDC or individual DOE national laboratories. Examples of valuable multi-national and multi-partner initiatives that promote active R&D in nuclear waste disposal science and that require DOE “membership” are the DECOVALEX Project, the Mont Terri Project and the Colloid Formation and Migration Project, all of which are further discussed below. Instead of multi-partner initiatives, there may also be direct participation of DOE national laboratories in specific projects run by individual international disposal programs. The latter may or may not require formal bilateral agreements.

The following sections describe in more detail opportunities for active research with international disposal programs. The focus here is on such opportunities that provide access to field data (and respective interpretation/modeling) or may even allow participation in ongoing field experiments. Of these opportunities, we describe in this report near-term options related to the engineered barrier system (EBS) work package of the UFDC, with focus on buffer/backfill and seal behavior, and on the interaction of these materials with other EBS components and the surrounding host rock. (It should be noted, however, that the opportunities discussed here and the recommendations made are also be applicable to other related work packages, in particular to the natural barrier system (NBS), as most of the field experiments include both the EBS and the NBS.) Open R&D issues with respect to EBS have been discussed in previous progress reports (e.g., Steefel et al., 2010), and have been evaluated in consideration of their importance to the safety

case in a recently conducted roadmap exercise (*Used Fuel Disposition Campaign Disposal Research and Development Roadmap, FCRD-USED-2011-000065 Rev 0, March 2011; Tables 7 and 8; [Nutt, 2011]*).

1.3.2 DECOVALEX Project

The DECOVALEX Project is a unique international research collaboration, initiated in 1992, for advancing the understanding and mathematical modeling of coupled thermo-hydro-mechanical (THM) and thermo-hydro-mechanical-chemical (THMC) processes in geological systems—subjects of importance for performance assessment of radioactive waste repositories in geological formations. DECOVALEX is an acronym for “Development of Coupled Models and their Validation against Experiments”. Starting in 1992, the project has made important progress and played a key role in the development of numerical modeling of coupled processes in fractured rocks and buffer/backfill materials. The project has been conducted by research teams supported by a large number of radioactive-waste-management organizations and regulatory authorities, including those of Canada, China, Finland, France, Japan, Germany, Spain, Sweden, UK, South Korea, Czech Republic, and the USA. Through this project, in-depth knowledge has been gained of coupled THM and THMC processes associated with nuclear waste repositories, as well as numerical simulation models for their quantitative analysis. The knowledge accumulated from this project, in the form of a large number of research reports and international journal and conference papers in the open literature, has been applied effectively in the implementation and review of national radioactive-waste-management programs in the participating countries. A good overview of the project is given in Tsang et al. (2009).

The DECOVALEX Project is typically conducted in separate 3-4 year project phases. Each phase features a small number (typically three to five) modeling test cases of importance to radioactive waste disposal. Many test cases are laboratory and field experiments that have been conducted by one of the project partners and are then collectively studied and modeled by DECOVALEX participants. Numerical modeling of these test cases can assist both to interpret the test results and to test the models used. Over the years, a number of large-scale, multiyear field experiments have been studied within the project (e.g. the Kamaishi THM Experiment, FEBEX, and the Yucca Mountain drift scale heater test). Thus the project provides access to valuable technical data and expertise to DECOVALEX partner organizations; this is particularly useful in disposal programs that are starting their research on certain disposal or repository environments and have no URLs. DECOVALEX has a modeling focus, but tight connection to experimental data.

In order to participate in a given DECOVALEX phase, interested parties—such as waste management organizations or regulatory authorities—need to formally join the project and pay a small annual fee that covers administrative and technical matters. In addition to this fee, participating organizations provide funding to their own research teams to work on some or all of the problems defined in the project phase. Representatives from the funding organizations form a Steering Committee that collectively directs all project activities.

DOE was a DECOVALEX partner for several project phases, but decided to drop out in 2007 with the increasing focus on the license application for Yucca Mountain. Now that the U.S. has shifted to other disposal options and geologic environments, a renewed

engagement of DOE with DECOVALEX would provide UFDC researchers access to relevant field data from international programs and allow them to work collaboratively with international scientists on analyzing and modeling these data. The next DECOVALEX phase, referred to as DECOVALEX-2015, will start in early 2012. A planning session for this next DECOVALEX phase was held in a recent workshop in Helsinki, and several modeling test cases involving field data were proposed by prospective funding organizations.

- **HE-E Heater Test:** Studies of bentonite/rock interaction to evaluate sealing and clay barrier performance, in a micro-tunnel at the Mont Terri URL, proposed by ENRESA (Spain).
- **SEALEX Experiment:** A long term test of the hydraulic (sealing) performance of a swelling bentonite core (5 m long) in a mini tunnel (60 cm diameter) at the Tournemire URL in France, proposed by ISRN (France).
- **MB Test:** Mine-by test studying pore pressure and stress evolution during excavation, at the Mont Terri URL, proposed by NAGRA (Switzerland).
- **Bedrichov Tunnel Experiment:** Interpretation of inflow patterns and tracer transport behavior in a fractured granite, proposed by NAWRA (Czech Republic)
- **THMC Processes in Single Fractures:** Modeling of laboratory experiments on mechano-chemical impacts on fracture flow, tentatively proposed by KAERI/LBNL (South Korea/USA).
- Possible revisits of past **DECOVALEX** phases for the purpose of identifying potential tasks containing unsolved but important issues, tentatively proposed by CEA (France).

Of the five experimental data sets, the first two are highly relevant to the EBS work package of UFDC, as both target the behavior of backfill and sealing materials in interaction with clay host rock. More details on these two experiments, the HE-E Heater Test and the SEALEX Experiment, are given below. (The other proposed test cases are more relevant to the NBS work package of UFDC.) The DECOVALEX secretariat will soon distribute short summaries of each suggested test case.

One issue to resolve soon is the question as to how to handle the cost of international commitments such as the DECOVALEX project. A possible solution is that the "membership fee" for DOE participation would come out of some centralized international fund, while the staff support for active R&D would be covered out of the relevant UFDC work packages (e.g., EBS, NBS). The expected "membership fee" for DECOVALEX 2015 is about \$42,000, somewhat dependent on the final number of participating organizations as well as the currency exchange rate. In the case of the DECOVALEX project, DOE membership ensures that any national laboratory associated with DOE would be allowed to participate.

1.3.3 HE-E Heater Test at Mont Terri URL, Switzerland

The HE-E Heater Test at the Mont Terri URL, shown in Figure 1-3, focuses on the THM behavior of bentonite barriers in the early non-isothermal resaturation stage and their THM interaction with Opalinus Clay (see Section 5.3 for more information on the Mont Terri URL). The objective is to better understand the evolution of a disposal system of high level waste in the early post-closure period with emphasis on the thermal evolution, buffer resaturation (in situ determination of the thermal conductivity of bentonite and its dependency on saturation), pore water pressure in the near field, and the evolution of swelling pressures in the buffer. Because the test is conducted in a micro-tunnel (at 1:2 scale), it is considered a validation, not a demonstration experiment. The heating test involves two types of bentonite buffer materials. The heater-buffer interface will be heated to a maximum of 135°C and a temperature of 60-70°C is expected at the buffer-rock interface. A dense instrumentation network is already in place in the host rock surrounding the micro-tunnel (from a previous experiment testing the impact of ventilation on the clay host rock) and will be improved (up to 40 piezometers in total); various sensors will also be placed in the buffer material. Heating is expected to start in late summer of 2011 and will be continued for at least three years.

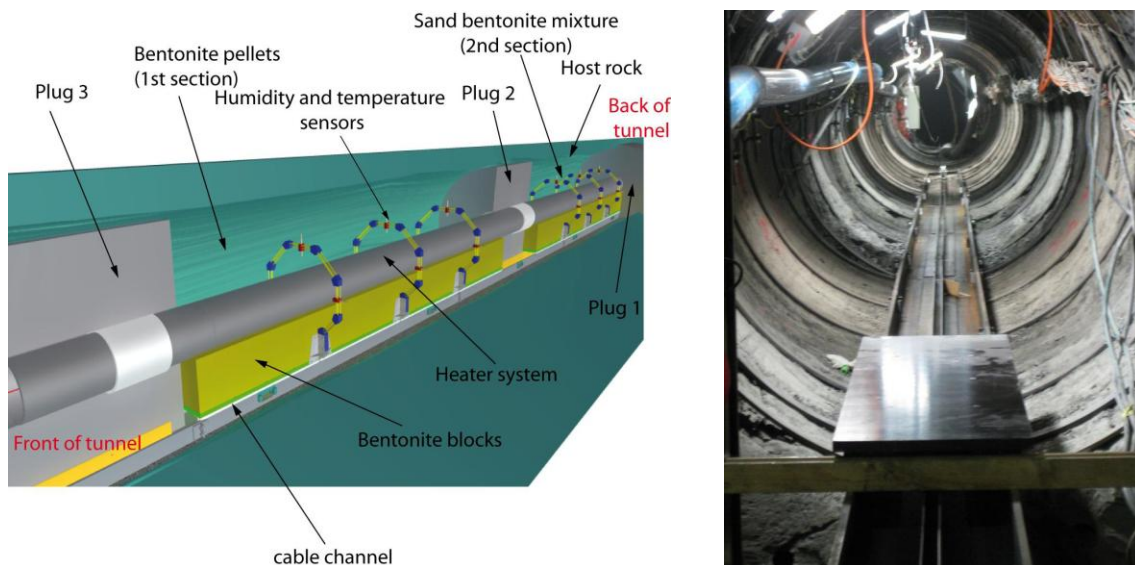


Figure 1-3. Schematic setup of HE-E heater test at Mont Terri and photo of micro-tunnel (from Garitte et al, 2011).

1.3.4 SEALEX Experiment at the Tournemire URL, France

The SEALEX experiment aims at investigating the long-term HM behavior and hydraulic performance of swelling clay-based seals (Figure 1-4). A suite of experiments will be conducted in several 60-cm diameter mini-tunnels (5 m long) that are exposed to nominal conditions, different technological choices for seal mixtures and emplacement, and altered situations (e.g., forced resaturation or not; loss of mechanical confinement or not) (Figure 1-5). Forced resaturation can lead to heterogeneous saturation and porosity/permeability fields within the bentonite core, and hence the possibility of clay-core erosion due to flow channeling. The experiments will test these hydraulic parameters and their spatial distribution via state-of-the-art measurement technology (e.g., wireless

sensors installed within the core to limit preferential flow along cables). Hydraulic tests (pulse tests + constant load tests) will eventually be conducted to determine the overall hydraulic properties (permeability, leaks) of the seals, for different representative conditions. While not decided yet, IRSN considers adding one particular test to the experimental plan that would evaluate HMC behavior with concrete/steel and concrete/bentonite interaction.

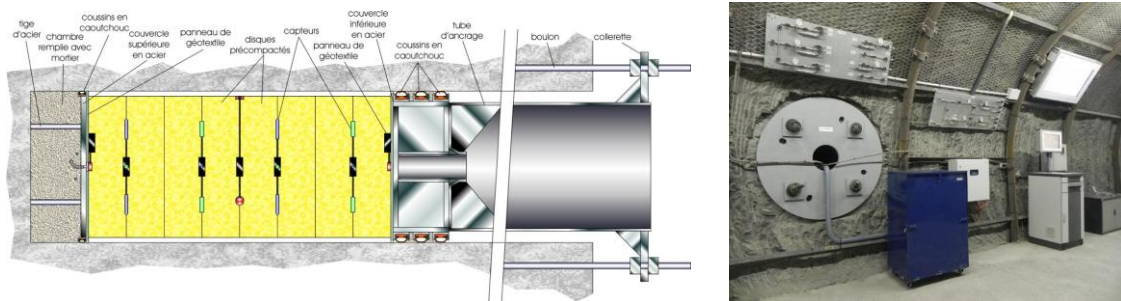


Figure 1-4. Schematic setup of mini-tunnel with seal core and instrumentation (left); view from gallery after core emplacement (right) (from Barnichon, 2011).

	Reference Tests	Performance Tests	Intra-core geometry Core conditioning Composition (MX80/sand)	Core view	Altered conditions	Emplacement date
Base case	RT-1	PT-N1	Monolithic disks Precompacted (70/30)		No	12/2010 06/2011
Variations / Base case	-	PT-A1	Monolithic disks Precompacted (70/30)		Confinement loss	06/2012
	-	PT-N2	Disks + internal joints (4/4) Precompacted (70/30)		No	12/2011
	RT-2	PT-N3	Pellets/powder In situ compacted (100/0)		No	12/2012 06/2013
	-	PT-N4	Monolithic disks Precompacted (20/80)		No	12/2013

Figure 1-5. Planned experiments and schedule (from Barnichon, 2011).

The SEALEX experiments are conducted at the Tournemire URL in the south of France. This site is characterized by a sub-horizontal indurated argillaceous claystone layer 250 m thick. A railway tunnel, constructed in 1881 through the argillaceous formation, is 2 km long, 6 m high and 4.7 m wide, and was excavated using a pneumatic tool. In 1996 and 2003, additional research tunnels were excavated off the main railway tunnel. Thus, this facility allows study of near field rock behavior in indurated clay with different time periods of exposure to the atmosphere, namely 130, 15 and 8 years, respectively (Rejeb and Cabrera, 2006) (Figure 1-6).

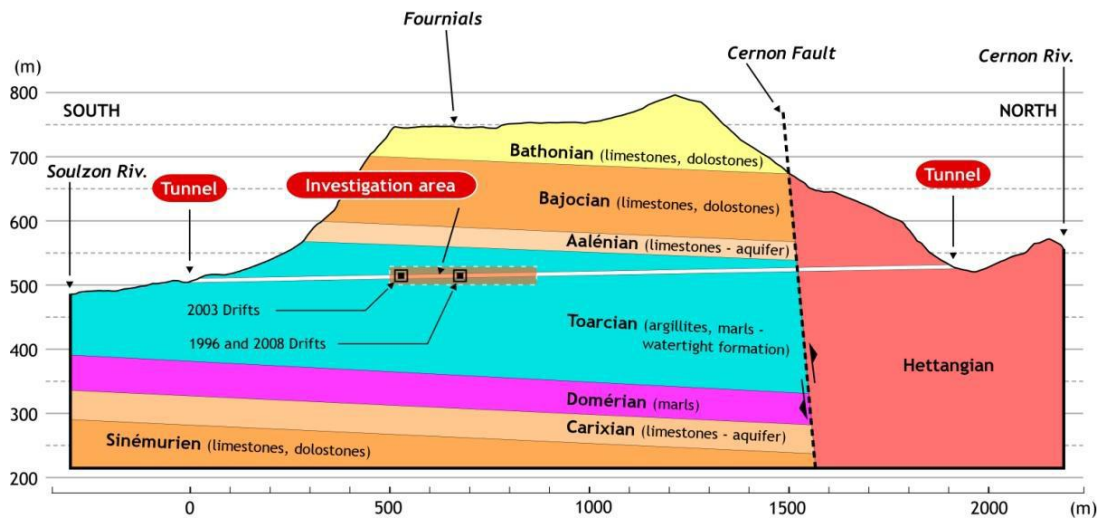


Figure 1-6. Geological cross-section of the Tournemire site, South France (from Rejeb and Cabrera, 2006) (from Barnichon, 2011).

1.3.5 Mont Terri Project

The Mont Terri Project is an international research project for the hydrogeological, geochemical and geotechnical characterisation of a clay/shale Formation suitable for geologic disposal of radioactive waste (Zuidema, 2007). The project utilizes an underground rock laboratory, which lies north of the town of St-Ursanne in Northeastern Switzerland and is located at a depth of around 300 meters below the surface in argillaceous claystone (Opalinus Clay). Construction of the facility in conjunction with a motorway tunnel started in 1987, and the Mont Terri Project was officially initiated in 1996 (Figure 1-7). (<http://www.mont-terri.ch/ids/default.asp?TopicID=72>).

Often using co-sponsorship from European Community funds, the project essentially operates as a collaborative program providing open access to an existing URL. Mont Terri partner organizations may select and conduct experiments, and they have access to all project results from past and ongoing efforts. Larger field experiments are often conducted by more than one organization. Current project partners are from Switzerland (swisstopo/SGS, ENSI, NAGRA), Belgium (SCK/CEN), France (ANDRA, IRSN), Germany (BGR, GRS), Japan (OBAYASHI, JAEA, CRIEPI), Spain (ENRESA, Empresa), Canada (NWMO), and USA (CHEVRON).

Participation of DOE as a partner in the Mont Terri Project would provide UFDC researchers access to relevant field data and project results from past efforts. Mont Terri has been in operation for a long time, and a wide range of experimental studies on clay/shale behavior (including backfill/buffer behavior) have already been conducted. More importantly, UFDC researchers could work collaboratively with international scientists on *ongoing and future* experimental studies, which would include all design, characterization, modeling, and interpretation aspects related to field experiments and. In the long term, UFDC researchers would also be able to propose and eventually conduct their own experiments at the Mont Terri URL. This type of international collaboration goes beyond the mostly modeling focus of DECOVALEX, and may arguably be the most

fruitful approach to active international R&D. Three prominent experiments are currently being conducted or are in preparation stages, two of which are also proposed as DECOVALEX modeling test cases (e.g., the HE-E Heater Test and the MB Mine-By Test). The third one, referred to as FE Heater Test (described below in more detail), is a long-term (> 10 years), full-scale test that will serve as an ultimate validation and demonstration test for emplacement of heat-producing waste in Opalinus Clay, at realistic temporal and spatial scales. Validation will include THM coupling effects with focus on both the EBS components and the host rock behavior.

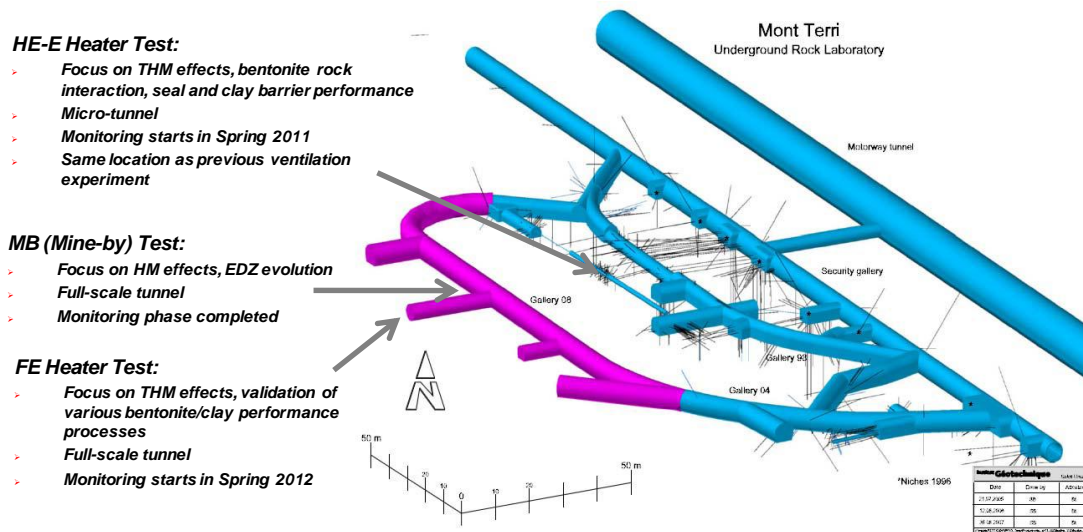


Figure 1-7. Summary schematic of the Mont Terri URL with side galleries and drifts for testing (based on Garitte, 2010)

In order for DOE to become a formal Mont Terri partner, there are two main rules: (1) The present Mont Terri Project partners have to unanimously accept new partner organizations, and (2) As a buy-in, new partners have to invest an amount of about 500K Swiss Francs (about \$500K), which can be spread over a period of 3 years. The buy-in fee can partially be provided in kind (i.e., by having UFDC researchers conduct work). The fraction of in-kind contributions can be negotiated with the Mont Terri partners, but is expected to be somewhere between 30 to 50% of the total. In addition to the "membership fee" for DOE participation, staff support for active R&D would have to be covered out of the relevant UFDC work packages (e.g., EBS, NBS).

Because of its potential relevance to UFDC's EBS and NBS areas, we provide here some further detail on the FE Heater Test, one of the largest and longest-duration heater tests worldwide. As mentioned before, this heater experiment is undertaken by NAGRA and other European partners as an ultimate test for the performance of geologic disposal in Opalinus Clay, with focus on both the EBS components and the host rock behavior. The experiment will provide data useful for the validation of THM coupling effects regarding the processes in the host rock while correctly accounting for (and examining) the conditions in the emplacement tunnel (temperature, saturation, and swelling pressure). Due to the 1:1 scale of the experiment, it will be possible to achieve realistic temperature, saturation, and stress gradients. It will also be possible to test backfilling technology with

granular bentonite as well as lining technology with shotcrete, anchors and steel ribs. Processes examined in the test cover many aspects of repository evolution, such as EDZ creation and desaturation of the EDZ during tunnel excavation and operation (including ventilation for about one year), as well as reconsolidation of the EDZ, resaturation, thermal effects, thermal stresses, and thermal pore pressure increase after backfilling and heating (heating and monitoring period > 10 years).

As shown in Figure 1-8, the FE Heater Test will be conducted in a side tunnel at Mont Terri, excavated along the claystone bedding plane for this purpose, with 50 m length and about 2.8 m diameter. Heating from emplaced waste will be simulated by three heat-producing canisters of 1500 W maximum power. A sophisticated monitoring program is planned, including dense pre-instrumentation of the site for in-situ characterization, dense instrumentation of bentonite buffer and host rock, and extensive geophysical monitoring (seismic and electric “tomography”). A THM modeling program will be conducted in parallel with the testing and monitoring activities.

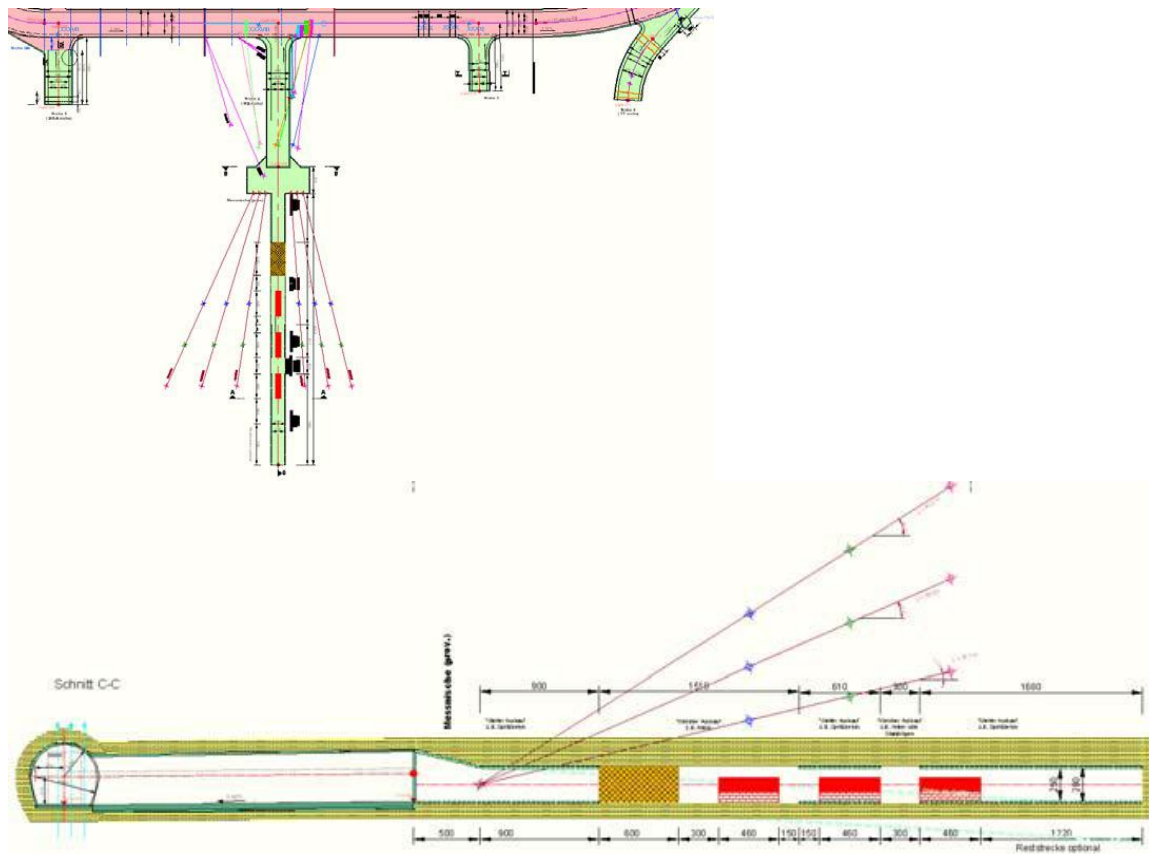


Figure 1-8. Plan (top) and side view (bottom) of experiment setup and observation borehole layout (from Garitte, 2010).

1.3.6 Colloid Formation and Migration (CFM) Project

The Colloid Formation and Migration Project is an international research project for the investigation of colloid formation/bentonite erosion, colloid migration, and colloid-

associated radionuclide transport, relevant to both EBS and NBS areas of UFDC. This collaborative project is associated with the Grimsel Test Site (GTS) in the Swiss Alps, a URL situated in sparsely fractured crystalline host rock (<http://www.grimsel.com/>). Colloid-related R&D comprises *in situ* field work, but also laboratory and modeling studies. Current project partners are from Germany (BMWi), Japan (JAEA, CRIEPI), Sweden (SKB), South Korea (KAERI), Finland (POSIVA), and Switzerland (NAGRA). The main R&D objectives, relevant to both EBS and NBS issues, are as follows:

- To examine colloid generation rates and mechanisms at the Engineered Barrier System (EBS) - host rock boundary under in situ conditions,
- To evaluate the long-distance migration behavior of EBS-derived colloids in a water-conducting feature in a repository relevant flow system (i.e. with a very low flow rate/water flux),
- To study the long-term geochemical behavior (mobility, mineralization, colloid formation, etc) of radionuclides at the EBS-host rock boundary,
- To examine reversibility of radionuclide uptake onto colloids,
- To gain experience in long-term monitoring of radionuclide/colloid propagation near a repository

A series of colloid-facilitated radionuclide field transport experiments have been conducted at the Grimsel Test Site, and more of these CFM field tests are planned for future years. With respect to EBS-related issues, a new field experiment is planned to start in late 2011; it will involve the emplacement of a radionuclide-doped bentonite plug into a Grimsel borehole followed by long-term monitoring (over many years) for both colloids and radionuclides (Figure 1-9). The bentonite emplacement borehole supplies the access for the colloid source to a water conducting feature in the crystalline host rock, outside the influence of the GTS tunnel system. The formation and transport of colloids and colloid-associated radionuclides is then monitored utilizing an array of down-gradient boreholes drilled at various travel distances into the shear zone. In order to evaluate the transport under near-natural flow conditions, the shear zone is hydraulically isolated by installing a sophisticated mega-packer system, counteracting the natural gradient towards the tunnel surface.

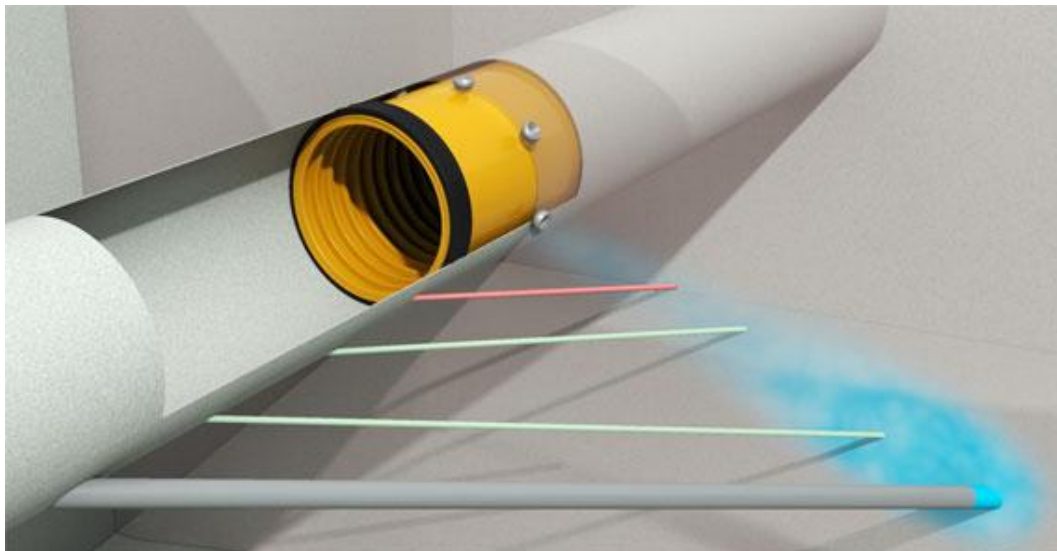


Figure 1-9. Schematic setup of bentonite plug and colloid transport experiment (from <http://www.grimse.com/gts-phase-vi/cfm-section/cfm-concept>).

Similar to the Mont Terri Project discussed above, DOE may consider becoming a formal partner of the Colloid Formation and Migration Project (CFM). Formal partnership would give DOE and affiliated national laboratories access to CFM data from past and ongoing experiments, would allow for UFDC researchers to work collaboratively with international scientists on *ongoing* experimental studies, and would involve them in the planning of new experimental studies to be conducted in the future. DOE partnership would require a “membership contribution” of approximately \$95K per year based on the current participation level of 85K Swiss Francs per year by the other partners. It is likely that a commitment of at least three years is required, but this has yet to be confirmed. In addition to the “membership fee” for DOE participation, staff support for active R&D would have to be covered out of the relevant UFDC work packages (e.g., EBS, NBS).

1.3.7 Other active collaboration opportunities

In some cases, access to data on international field experiments and participation of UFDC researchers in collaborative field studies may also be facilitated via informal or semi-formal agreements directly between national laboratories and international partners. Several UFDC scientists already have close relationships with their international counterparts, resulting from workshops and symposia meetings, or from collaboration outside of UFDC’s scope. International disposal programs are aware of the technical capabilities of UFDC scientists and are generally quite open to include them in their ongoing research teams. This may or may not require bilateral MoUs or other types of agreements.

Below is a short list of major (soon-to-start or planned) field experiments conducted by international disposal programs that may be open to national laboratory participation, without “membership fees” or other long-term commitments on behalf of DOE.

1.3.7.1 PRACLAY Test at HADES URL in Belgium

The PRACLAY Heater Test is a full-scale validation and confirmation experiment to be conducted at the HADES (High Activity Disposal Experimental Site) URL, excavated at 223 m depth in Boom Clay, a tertiary clay formation in Mol, Belgium. The heater test, which will begin in late 2011 or early 2012, will involve heating a 30 m gallery section for 10 years with many monitoring sensors, for the purpose of investigating the thermo-hydro-mechanical (THM) behavior of plastic clay under the most “penalizing” conditions that may occur around a repository (Van Marcke and Bastiaens, 2010) (Figure 1-10). These include THM behavior of plastic clay under undrained conditions. For this objective, a hydraulic seal will be installed at the intersection between the planned heated and unheated sections of the gallery. This installation makes up the Seal Test, which was initiated in 2010, and allows testing the functionality of the hydraulic seal under heated repository conditions. The Belgium organizations involved in conducting and interpreting these experiments (EIG Euridice, SCK CEN, ONDRAF/NIRAS) have long-standing relationships to scientists at Lawrence Berkeley National Laboratory (LBNL); they have already invited LBNL researchers to provide THM modeling expertise to the project team.

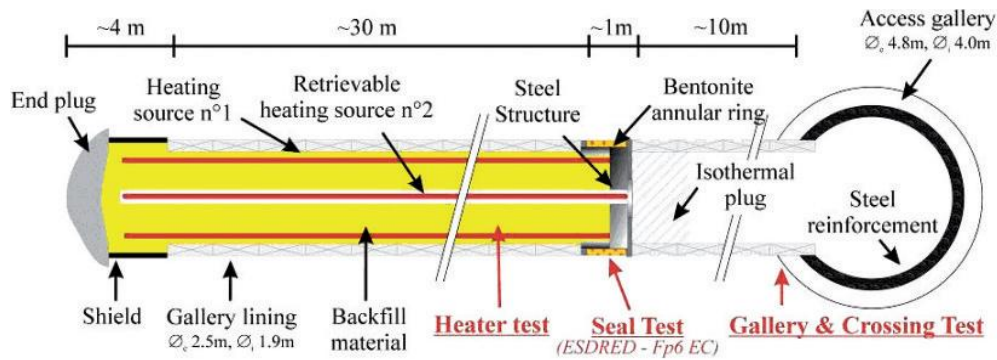


Figure 1-10. Layout of the PRACLAY In-Situ Experiment which is constituted of the the Seal Test, and the actual Heater Test (from Van Marcke and Bastiaens, 2010).

1.3.7.2 Gas-Permeable Seal Test (GAST) at Grimsel Test Site, Switzerland

The objective of the soon-to-start GAST experiments is to demonstrate the construction and performance of repository seals and plugs and to improve the understanding and the base datasets for reliably predicting water and gas transport through these sealing systems. The experiment will test a specific design option called "engineered gas transport system (EGTS)" (Figure 1-11), which involves specially designed backfill and sealing materials such as high porosity mortars or sand/bentonite (S/B) mixtures. The reason to develop these special designs is to allow for increased gas transport capacity (to mitigate pressure buildup from gas generation) of the backfilled underground structures without compromising the radionuclide retention capacity of the engineered barrier system. The managing organization for this experiment is NAGRA (Switzerland); a few other European partners are also involved. NAGRA has expressed that it would possibly be open for UFDC scientists to participate in aspects of the experiment.

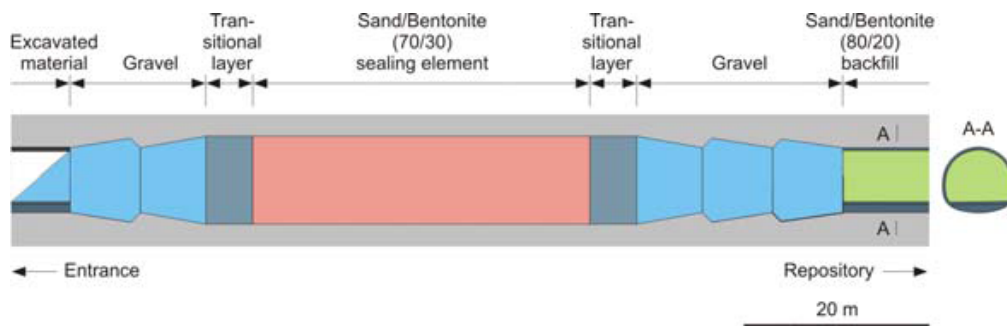


Figure 1-11. Schematic picture of repository seal design for GAST experiment (from Vomvoris, 2011).

1.3.7.3 Large-Scale Gas Injection Test (LASGIT) at Äspö URL, Sweden

This ongoing field experiment, which has been in operation for over five years, evaluates gas flow processes (related to the potential for gas generation from canister corrosion) in an unsaturated bentonite embedded in fractured crystalline rock. Current knowledge pertaining to gas flow in a compact saturated bentonite is based on small-scale laboratory studies; the LASGIT tests (Fig. 1-12) are designed to address specific issues relating to gas migration and its long-term effect on the hydro-mechanical performance of the buffer clay, the question of heterogeneity and tortuosity of flow paths and the possible

generation of new flow paths, and the complex coupling between gas, stress, and porewater pressure at different scales. The main organization conducting the experiment is SKB (Sweden), together with the British Geological Survey (BGS). The LASGIT experiment was initially proposed as a modeling test case for DECOVALEX-2015, but is not under consideration anymore. However, SKB and BGS may be open to collaboration or participation of UFDC scientists.



Figure 1-12. LASGIT experiment at Äspö (from Cuss, 2010).

1.3.7.4 Bentonite Rock Interaction Experiment (BRIE) at Äspö URL, Sweden

Another option for UFDC engagement may be the upcoming BRIE test to be conducted at the Äspö URL in Sweden. The main objective of this experiment is to enhance the understanding of the hydraulic interaction between the fractured crystalline rock at Äspö and unsaturated bentonite. The setup is aligned with the Swedish concept of emplacing canisters into vertical deposition holes that are subsequently backfilled. The main organization conducting the experiment is SKB (Sweden).

1.3.7.5 Other Participation Options for Mont Terri Project and CFM Experiments

Note that some benefits that the above-mentioned multi-national and multi-partner initiatives (such as the Mont Terri Project or the Colloid Formation and Migration Project) can provide to UFDC may also be achievable via less formal partnerships. For example, LBNL has been offered the opportunity to become one of NAGRA's modeling and analysis partners for the full-scale FE Heater experiment at Mont Terri. Similarly, scientists at Los Alamos National Laboratory (LANL) have been engaged in the Colloid Formation and Migration Project without DOE being a full partner, and could presumably continue to do so. However, in both cases, without formal agreement, LBNL's and LANL's role would be limited to ad-hoc contributors. Full partnership, on the other hand, would give *all* DOE national laboratories full access to *all* of the many

experiments that have been or will be conducted within the Mont Terri Project and CFM, respectively. Full partnership would also allow for DOE to be in a position to propose or conduct its own suite of experiments.

1.3.8 Recommendations and path forward

Active collaboration with international programs, initiatives, or projects is considered very beneficial to UFDC, providing access to the decades of experience that some international programs have in various disposal options and geologic environments. We postulate that increasing international engagement will help efficiently achieve UFDC's long-term goals of conducting "experiments to fill data needs and confirm advanced modeling approaches" (by 2015) and of having a "robust modeling and experimental basis for evaluation of multiple disposal system options" (by 2020). Above report section discusses different opportunities of active international collaboration, with focus on EBS aspects and those opportunities that provide access to field data (and respective interpretation/modeling) or allow participation in ongoing field experiments. Similar assessments are ongoing with focus on NBS aspects, and will be documented in an upcoming NBS status report.

The next step will be to develop a concise list of promising international opportunities, which documents their cost and benefits, the mode of participation, and the key research gaps addressed (with tight link to roadmap and FEPs importance ranking; using the *Used Fuel Disposition Campaign Disposal Research and Development Roadmap, FCRD-USED-2011-000065 Rev 0, March 2011 [Nutt, 2011]*). Based on this, potential activities will be ranked and recommendations will be made in time for the DOE/NE-53 and UFD planning process for FY12 and beyond. An early decision point is about DOE's possible participation in international agreements such as the DECOVALEX Project, the Mont Terri Project, and the Colloid Formations and Migration Project.

1.4 Summary and Planned Work for FY12

This section describes the continued and expanded work described in Jové Colón et al. (2010) focused on EBS design concepts for backfilled multi-layered EBS for use in NW isolation. A set of EBS design concepts has been presented with various levels of barrier complexity to demonstrate the need for flexibility to accommodate the anticipated levels of performance requirements. Sections 3 and 4 of this report provide development and implementation of various modeling tools and approaches to assess EBS performance. These tools and approaches will continue to expand and develop to attain the proper levels of confidence and adequacy in representing EBS processes.

1.4.1 Planned Work for FY12

Planned work for the remaining of FY11 will be focused on:

- Continuing buildup and evaluation of thermodynamic databases for cements and clay phases. This includes work on the development of solid solution models for these materials, and applications of thermodynamic modeling and chemical equilibria to represent their stability under various conditions.
- Experimental for the characterization of barrier phases interactions. This includes conducting initial experiments and characterization of reaction products. This

activity also includes characterization of clay phases in rock samples from the Yucca Mountain drift scale test (DST).

- Continue investigations of THMC processes models in clay barriers.
- Continue development of DSEF.

Planned work for FY12 is described in Table 1-5. This work will be integrated with other work packages such as thermal management, salt disposal investigations, and disposal concepts.

Table 1-5. Planned UFD Generic EBS work for FY12.

Barrier phase mineralogy (cement and clay): <ul style="list-style-type: none"> ○ Experimental and characterization studies on the stability at high temperatures ○ Thermodynamic properties, sorption, and ion exchange properties (thermodynamic models and databases) ○ Seal materials (e.g., cement) modeling tool development
Molecular dynamics (MD) evaluation of clay: <ul style="list-style-type: none"> ○ Characterization of volumetric and mechanical properties of clay at elevated temperatures and pressures using MD and High Performance Computing (HPC)
THCM coupled processes modeling for EBS NW (SF/SNF/HLW)salt disposal at elevated temperatures: <ul style="list-style-type: none"> ○ Focus on potential transport in crushed salt ○ Evaluation of Deaf Smith County site characterization data
THCM coupled processes modeling for EBS NW disposal in clay
Transport experiments in clay focusing on diffusion
Establishment of International collaborations and engagements on NW disposal
Continued development of the Disposal System Evaluation Framework (DSEF)

1.5 References

Apted, M.J., 1998, A modest proposal: A robust, cost-effective design for high-level waste packages: Scientific Basis for Nuclear Waste Management XXI, v. 506, p. 589-596.

Balady, M.A., 1996, Engineered Barrier System Performance Requirements Systems Study Report (BB0000000-01717-5705-00001 Rev. 01): Las Vegas, NV, Department of Energy.

Baldwin, T., Chapman, N., and Neall, F.B., 2008, Geological Disposal Options for High-Level Waste and Spent Fuel - Report for the UK Nuclear Decommissioning Authority, Prepared by Galson Sciences, UK, p. 118 pp.

Barnichon, J.D., IRSN proposal - the SEALEX In Situ Tests, Presentation given at 7th DECOVALEX 2011 workshop, April 2011, Helsinki.

- Bel, J., and Bernier, F., 2001, Temperature Criterion Related to Clay Based Backfill Materials in the Framework of a Geological Repository of Heat Producing Radioactive Waste (HLW), *in* Taboas, A., Vanbrabant, R., and Benda, G., eds., Proceedings 8th International Conference on Radioactive Waste Management & Environmental Remediation: Bruges, ASME, p. 1327-1331.
- Bennett, D.G., 2010, The Joint EC/NEA Engineered Barrier System Project : Synthesis Report (EBSSYN), Seventh Framework Programme, European Commission, p. 1-80.
- Bennett, D.G., and Gens, R., 2008, Overview of European concepts for high-level waste and spent fuel disposal with special reference waste container corrosion: *Journal of Nuclear Materials*, v. 379, p. 1-8.
- Bennett, D.G., Hooper, A.J., Voinis, S., and Umeki, H., 2006, The role of the engineered barrier system in safety cases for geological radioactive waste repositories: An NEA initiative in co-operation with the EC: *Scientific Basis for Nuclear Waste Management XXIX*, v. 932, p. 43-52.
- Beziat, A., Dardaine, M., and Mouche, E., 1992, Measurements of the thermal conductivity of clay-sand and clay-graphite mixtures used as engineered barriers for high-level radioactive waste disposal: *Applied Clay Science*, v. 6, p. 245-263.
- Bollingerfehr, W., Filbert, W., Graf, R., and Bammer, K.-J., 2010, State of the Art in Spent Fuel Disposal in Rock Salt in Germany, ENC Conference: Barcelona, Spain.
- ESDRED, 2009, Final Summary Report and Global Evaluation of the Project, *in* Project, Deliverable D6 of Module 6, WP4.
- Garitte, B., and others, HE-E experiment - In situ Heater Test, Presentation given at 7th DECOVALEX 2011 workshop, April 2011, Helsinki.
- Geneste, P., Raynal, M., Atabek, R., Dardaine, M., and Oliver, J., 1990, Characterization of a French Clay Barrier and Outline of the Experimental Program: *Engineering Geology*, v. 28, p. 443-454.
- Jobmann, M., and Buntebarth, G., 2009, Influence of graphite and quartz addition on the thermo-physical properties of bentonite for sealing heat-generating radioactive waste: *Applied Clay Science*, v. 44, p. 206-210.
- Johnson, L.H., and King, F., 2003, Technical Report 02-11: Canister Options for the Disposal of Spent Fuel, *in* NAGRA, ed.: Wettingen, Nagra, p. 57 pp.
- Jové Colón, C.F., Caporuscio, F.A., Levy, S.S., Xu, H., Blink, J.A., Halsey, W.G., Buscheck, T., Sutton, M., Serrano de Caro, M.A., Wolery, T.J., Liu, H.H., Birkholzer, J., Steefel, C.I., Rutqvist, J., Tsang, C.-F., and Sonnenthal, E., 2010, Disposal Systems Evaluations and Tool Development - Engineered Barrier System (EBS) Evaluation p. 1-200.
- Landolt, D., Davenport, A., Payer, J., and Shoesmith, D., 2009, A Review of Materials and Corrosion Issues Regarding Canisters for Disposal of Spent Fuel and High-level Waste in Opalinus Clay, Technical Report 09-02: Wettingen, Switzerland, National Cooperative for the Disposal of Radioactive Waste (NAGRA), 73 pp.
- McKinley, I.G., Neall, F.B., Kawamura, H., and Umeki, H., 2006, Geochemical optimisation of a disposal system for high-level radioactive waste: *Journal of Geochemical Exploration*, v. 90, p. 1-8.

- Moschner, G., Lothenbach, B., Rose, J., Ulrich, A., Figi, R., and Kretzschmar, R., 2008, Solubility of Fe-ettringite ($\text{Ca}_6[\text{Fe}(\text{OH})_6]_2(\text{SO}_4)_3 \cdot 26\text{H}_2\text{O}$): *Geochimica et Cosmochimica Acta*, v. 72, p. 1-18.
- Nutt, M., Voegele, M., Jové Colón, C. F., Wang, Y., Howard, R., Blink, J., Liu, H.-H., Hardin, E., and Jenni, K., 2011, *Used Fuel Disposition Campaign Disposal Research and Development Roadmap (Fuel Cycle Research and Development)*, p. 1-138.
- OECD (2003) “Engineered Barrier Systems and the Safety of Deep Geological Repositories State-of-the-Art Report”, Nuclear Energy Agency (NEA) Organization for Economic Co-operation and Development (OECD), 71 pp.
- POSIVA, 2008, Horizontal Deposition of Canisters for Spent Nuclear Fuel - Summary of the KBS-3H Project 2004 - 2007, *in* OY, P., ed.: Olkiluoto.
- Pusch, R., Drawite, A.B., Yong, R.N., and Nakano, M., 2010, Stiffening of smectite buffer clay by hydrothermal effects: *Engineering Geology*, v. 116, p. 21-31.
- Rejeb, A., J. Cabrera, Time-dependent evolution of the excavation damaged zone in the argillaceous Tournemire Site (France). Proceedings “GeoProc 2006,” Invited lecture in the 2nd International Conference on Coupled THMC Processes in Geosystems and Engineering, May 22-25 2006, Nanjing, China, pp. 65-74.
- Steeffel, C., J. Rutqvist, C.F. Tsang, H.H. Liu, E. Sonnenthal, J. Houseworth, J. T. Birkholzer, *Reactive Transport and Coupled THM Processes in Engineering Barrier Systems (EBS)*, Lawrence Berkeley National Laboratory (LBNL), Final Report of FY2010 Activities, Berkeley, August 2010.
- Stula, R.T., Albert, T.E., Kirstein, B.E., and Lester, D.H., 1980, *Systems Study on Engineered Barriers: Barrier Performance Analysis*, Technical Report ONWI-211, Office of Nuclear Waste Isolation (ONWI), p. 1-174.
- Tsang, C.-F., O. Stephansson, L. Jing, L., F. Kautsky, *DECOVALEX Project: from 1992 to 2007*, *Environmental Geology*, 57, 1221–1237, 2009
- Van Marcke, P., W. Bastiaens, *Construction of the Praclay Experimental Gallery at the Hades URF. Clay in Natural and Engineered Barriers for Radioactive Waste Confinement*, 4th International Meeting, March, 2010, Nantes, France.
- Vomvoris, S., Personal Communication. 2011.
- Wersin, P., Johnson, L.H., and McKinley, I.G., 2007, Performance of the bentonite barrier at temperatures beyond 100°C: A critical review: *Physics and Chemistry of the Earth*, v. 32, p. 780-788.
- Westerman, R.E., 1979, *Preliminary Conceptual Designs for Advanced Packages for the Geological Disposal of Spent Fuel: Richland, Washington, Pacific Northwest Laboratory*, 109 pp.

CLAY STABILITY AND CLAY – METAL INTERACTIONS

2. Clay Stability in Natural and Synthetic Systems

2.1 Mineral Evolution in the Yucca Mountain Drift-Scale Thermal Test

Clays will play an important role in used-nuclear-fuel disposition in geologic environments as potential backfill and/or buffers, and as potential host rock media. Bentonite clays in particular have properties such as water adsorption, cation exchange, swelling capacity, and self-sealing capability that are desirable for waste isolation. Clays and clay-rich rock in repository environments are not expected to be inert; they would likely experience changes in composition and swelling properties in response to altered physical and chemical conditions such as heating, dry-out, re-wetting, and evolving water composition and pH. Over the past few decades, extensive research has been devoted to studies of bentonite behavior as it relates to backfill/buffer performance.

Investigations of the thermal behavior of bentonites and clay-rich geologic formations relevant to their potential stability as repository components or host rocks fall into three general categories: natural analogues, laboratory-scale tests and reduced-scale field tests, and full-size field tests. Laine and Karttunen (2010) is an example of a literature study that summarizes properties and processes related to the long-term stability of bentonite and examine various natural analogues. Numerous laboratory-scale tests have been performed by all repository programs that plan for the use of bentonite backfill/buffer or clay-rich host rock. Examples of full-scale field thermal tests focused on bentonite in the engineered barrier include the FEBEX (Full-Scale HLW Engineered Barrier Experiment), FORGE (Fate of Repository Gases), and GAST (Gas-Permeable Seal Test) experiments at the Grimsel test site in Switzerland (Vomvoris et al., 2011). The Mont Terri Rock Laboratory in Switzerland is situated in shale (Opalinus Clay) and hosts numerous thermal experiments, some of which also involve bentonite backfill/buffer (Mont Terri Project, 2011).

In spite of their costs, field-scale tests have certain advantages for investigations of mineral stability. Perhaps the most important advantage is that mineralogic reaction rates tend to be slower than in laboratory tests and therefore are more representative of processes to be expected in an actual repository. The larger scale of a field test allows optimal integration with coupled-process modeling such as thermal-geochemical modeling that predicts temperature distributions, water compositions, and mineral reactions.

Given the variability in framework and exchangeable-cation chemistry of bentonites and the inevitable admixture of non-bentonite minerals, it is crucial to understand that there can be no single, definitive test of bentonite performance and stability under repository-relevant conditions. The variability of response for properties of interest will be best defined by combining results from multiple tests and recognizing that each test is unique. Field-scale tests are expensive, complex, and time-consuming, so that relatively few such tests have or will be performed. The range of clay-property responses ideally should be constructed from the results of as many tests and as many bentonite materials as possible. An economical way to maximize the available data would be to include analyses of changes in bentonite clays from thermal tests in rocks that contain the clay as a minor constituent.

The Yucca Mountain Project (YMP) was a multi-decade investigation of the Yucca Mountain site, Nevada, as a potential high-level nuclear-waste repository. An eight-year field-heating test in silicic devitrified tuff, the Drift Scale Test (DST), was conducted by the YMP to observe and measure changes in the natural geologic system due to thermal loading. Instrumental observations of temperature changes, water movement, and rock deformation were used to evaluate conceptual and numerical models of thermal effects in the host rock. Thermal-hydrologic-chemical effects, including mineralogic processes and changes in water chemistry, were identified by studies of pre-test and in-process rock-core and water samples collected from the test block. Test effects were not investigated for the bentonite clay that constitutes only a few weight percent of the rock because the clay was not expected to significantly affect any process of interest.

Clay-mineralogic effects of heating were considered to be of little or no significance for the Yucca Mountain repository concept in general and for the DST in particular. For example, the low clay content of devitrified tuff precluded measurable observation of macroscopic effects such as cracking or fracture sealing due to changes in bentonite clay hydration. This does not mean that the clays were inert during the heating test. At the crystal-lattice scale, clays would have experienced shrinkage due to heating and dry-out and interactions with pore fluids at elevated temperatures. Possible effects of long-term heating could include loss of swelling capacity, cation exchange, recrystallization, and neo-formation of new clay. All of these processes are relevant to the performance of bentonite in backfill/buffers and clay-rock repositories. The effects of these processes can be detected and quantified in clay separated from pre-test and post-test bulk rock. In summary, the conditions of the DST and mineralogic properties of the host rock can be examined as they apply to generic repository research.

This report presents an overview of the DST, with an emphasis on the thermal and chemical aspects relevant to clay-mineral reactions. Existing chemical and mineralogical data are used to explore how new data for clays from the thermal test might compare to the properties of bentonites commonly used in repository research. Early results of an exploratory study of clay extraction from DST core samples are also included. The goal is to determine whether sufficiently pure bentonite clay can be separated from whole-rock core to perform chemical and structural characterization of the clay. This is complemented by spatio-temporal information of the samples at the DST site along with thermal history. Swelling capacity is an example of an important bentonite attribute relevant to waste isolation, can be measured by X-ray diffraction (XRD).

2.1.1 Overview of the Drift-Scale Test

The DST at Yucca Mountain was an underground test in the unsaturated zone to investigate coupled thermal, mechanical, hydrologic, and geochemical processes similar to what would occur in a geologic repository heated by radioactive waste (Figure 2-1). The eight-year test consisted of a four-year heating phase followed by a four-year cooling phase. The heating phase began in December 1997, and ended in January 2002. Heaters in an excavated 47.5-m-long drift and in the adjacent rock raised the temperature at the drift walls to slightly above 200°C. Data and sample collection, including sampling of rock, water, and gas, were conducted from a series of boreholes drilled within the test block before heating commenced. As the rock was heated, the fluids naturally present in the rock migrated away from the heat sources. At the end of the heating phase, an

ellipsoidal boiling zone, separating the inner dryout zone from the outer condensation zone, existed at distances of about 9 to 22 m from the center of the drift.

The host rock for the DST is the crystal-poor, middle nonlithophysal zone (Ttptmn) of the Miocene Topopah Spring Tuff. This rock is a fractured, densely welded, devitrified silicic tuff. In the vicinity of the DST at Yucca Mountain, this zone is located about 222.5 m below the land surface and 350 m above the regional water table. The mean bulk porosity of dry-drilled core samples from the test block is 10.62 ± 1.14 percent, and the mean saturation is 83.85 ± 3.67 percent (CRWMS M&O 1997). These values yield an ambient volumetric water:rock ratio of $(0.8385)(10.62)/(100-10.62) = 0.1$. Given that most of the porosity resides in unsaturated fractures, the rock matrix is essentially saturated.

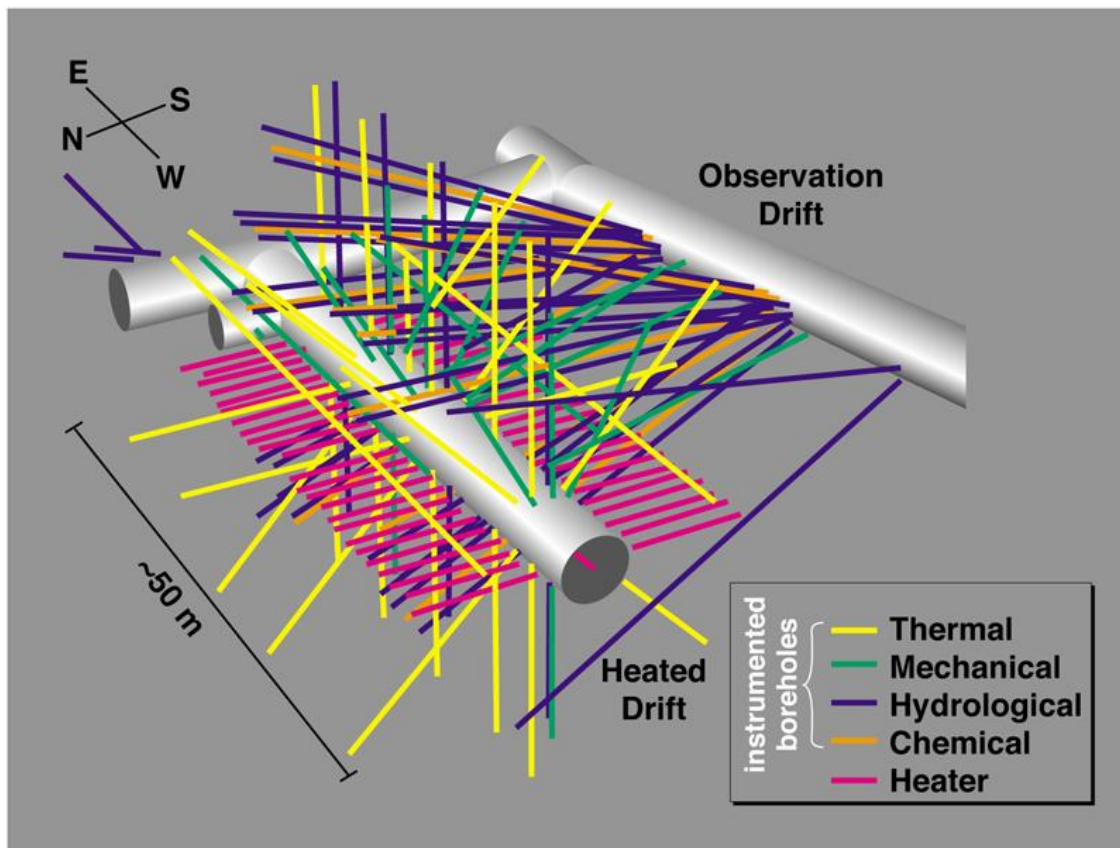


Figure 2-1. Schematic depiction of Drift Scale Test (DST) at Yucca Mountain, Nevada, USA.

The test block was an open system with respect to both heat and fluids. Thermal output of the heaters was monitored. Temperature measurements from borehole arrays of resistance temperature detectors were recorded every six hours. The spatial distribution and temporal variation of liquid water content in the rock mass were monitored by periodic neutron logging along boreholes, and by two-dimensional and three-dimensional imaging. The imaging was accomplished by electrical resistivity tomography and ground-penetrating radar (CRWMS M&O, 1998). Temperature and moisture content were monitored during the heating and cooling phases.

Both the conceptual model and numerical simulations of the test predicted the existence of a heat-pipe region within the outer margins of the boiling zone above the heaters

(Sonnenthal et al., 2005). In this region, water evaporated from the rock matrix into the fracture system, moved as vapor through fractures away from the boiling zone, then condensed and flowed back down through fractures to the boiling zone where the process was repeated. This was predicted to be the region of most active water-rock interaction, especially mineral dissolution and deposition.

Direct evidence of mineralogic alteration was obtained from sidewall samples drilled from the walls of pre-test boreholes about three years into the heating phase. A new cored hole, ESF-HD-CHEMSAMP-1 (abbreviated CHEMSAMP-1), whose trajectory angled upward from the access drift to intersect the heat-pipe zone, was drilled near the end of the heating phase. No thermal-history data were available for the location of the CHEMSAMP-1 borehole, but data from a nearby vertical borehole with temperature detectors indicated that the heat-pipe zone was about 1.5 m thick (in a vertical direction) at the time CHEMSAMP-1 was drilled (10/2001; Figure 2-2). The heat-pipe zone is recognizable on the temperature trace as an approximately isothermal interval representing the local boiling temperature, between 96° and 97°C. Figure 2-2 also includes a thermal trace for the same borehole from 10/2000 to document the onset of heat-pipe conditions at the location where the heat-pipe zone existed a year later. We infer from these data that the volume of rock existing under heat-pipe conditions and sampled by CHEMSAMP-1 had experienced those conditions for about one year at the time the hole was drilled. A second cored hole, CHEMSAMP-3, was angled downward from the access drift to intersect the heat-pipe zone below the heated drift in March 2003, fourteen months after the end of the heating phase in January 2002 (SNL, 2007).

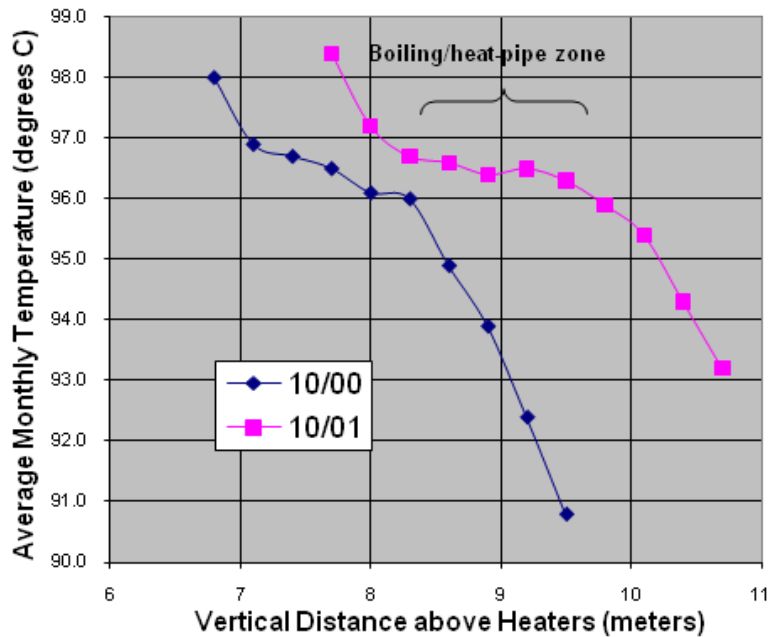


Figure 2-2. Average monthly temperature profiles in the vicinity of the boiling zone in borehole ESF-HD-137-TEMP-5 for October 2000 and October 2001, from Datta (2000) and Vogt (2002).

2.1.2 Sample Collection for the Drift-Scale Test

Core from the boreholes depicted in Figure 2-1 were collected and archived before the heating phase began. During the heating phase, small sidewall core samples (about one cubic centimeter of material per sample) were collected from monitoring boreholes. Two cored holes were drilled after almost four years of heating (CHEMSAMP-1) and after four years of heating, followed by fourteen months of cooling (CHEMSAMP-3). Upon completion of the cooling phase in early 2006, rock samples were collected from the surface of the heated drift. The planned drilling of new core holes at the end of the cooling phase was not carried out.

2.1.2.1 Specific Applicability of Test Conditions

Drill core and other rock samples that could be made available for study represent a range of thermohydrologic conditions. The test created a dynamic environment in which temperature gradually changed over time, increasing and then decreasing. The range of maximum temperature reached during the DST for most of the rock mass varied from ambient (about 25°C) to slightly over 200°C, with temperatures as high as 300°C adjacent to wall heaters (SNL, 2007). Figure 2-2 provides an example of how temperature was tracked over time at specific sensor locations.

Rock saturation gradually decreased to near-zero in the dry-out zone surrounding the heated drift (Figure 2-1). Toward the end of the heating phase, the moisture regimes consisted of the dry-out zone, the boiling/heat-pipe (reflux) zone, and the condensation zone at progressively greater distances outward from the heated drift. The thermohydrologic conditions experienced by the rock varied from higher temperature and low moisture content to lower temperature and high moisture content.

The host rock of the DST consists of low-porosity matrix and high-porosity fractures. The matrix and fractures differ in mineralogy, with secondary minerals such as stellerite (zeolite), calcite, opal, and manganese oxides largely restricted to fractures. Clay is present as a minor constituent in both the matrix and in fractures (Levy, 1999; Carlos, Chipera, and Bish, 1995). The sidewall coring technique restricted observations of mineralogic processes to the pre-test borehole surfaces and intersecting fractures. Substantial mineral deposition was observed on borehole surfaces because the boreholes provided preferential pathways for fluid migration. Dissolution of fracture-coating minerals was observed in natural fractures adjacent to boreholes. These observations suggest that rock alteration involving mineral dissolution and mineral deposition, including the possible neo-formation of Mg-bearing clays, was concentrated in fractures and fracture substitutes (boreholes). Evidence of mineral deposition was most common within the boiling/heat-pipe zone.

This preliminary study of clay alteration in the DST focuses on potential clay modification in the rock matrix rather than in the fracture fillings because much more rock-matrix material is available. Also, the mineral assemblage of the rock matrix poses fewer problems for clay-mineral separation. The low porosity of the rock matrix is a predictor of hydrologic behavior more akin to the hydrology of compacted bentonite.

2.1.2.2 Smectite/Bentonite Chemistry

In this discussion, the term “smectite” refers to the group of clay minerals responsible for the swelling properties of bentonite. Commercial suppliers of bentonite typically sell

products that contain mostly smectite clay along with other minerals. Some of the references cited here use the term “montmorillonite” either as a synonym for smectite or in reference to a specific clay mineral with swelling properties. The smectite clay mineral group encompasses a range of chemical compositions and variable swelling properties. Chemical variability is exhibited by both the sheet silicate framework and the interlayer cations. Multiple varieties of smectite are defined based on the chemical composition of the octahedral layer. Interlayered illite/smectites are defined by the variable presence of potassium in the interlayer.

Both clay-rich rock formations, which may be considered as repository host sites, and clay-rich mined products, that may be employed as backfill or buffers in repositories, are natural materials that vary in composition. The chemical and mineralogical properties of commercially available bentonites that have been used in repository-related research are described below.

Madsen (1998) conducted clay-mineralogical investigations of two commercial bentonites used by the Swiss authority for nuclear waste disposal (Nagra) and the Swedish program for nuclear-waste disposal (SKB). The two products are natural Na-bentonite MX-80 from Wyoming, USA, and natural Ca-bentonite Montigel (now called Calcigel) from Bavaria, Germany. The chemical analysis given by Madsen (1998) for MX-80 appears to contain errors; an analysis of Wyoming bentonite source clay SWy-2 (Mermut and Faz Cano, 2001) is given instead in Table 2-1. The clay-mineral chemical composition of DST smectite has not yet been determined. Table 1 includes an in situ electron-microprobe analysis of smectite from a clay-rich zone underlying the equivalent of the DST stratigraphic horizon (H-5 1666).

	SiO ₂	Al ₂ O ₃	Fe ₂ O ₃	FeO	MgO	CaO	Na ₂ O	K ₂ O	MnO	TiO ₂
SWy-2	61.46	22.05	4.37		2.94	1.18	1.47	0.20		0.09
Montigel	58.35	18.52	5.51	0.17	3.12	1.87	0.07	0.73	0.02	trace
H-5 1666	51.3	25.2	2.22		1.20	2.74	0.27	0.20	0.04	0.11

Sources: Mermut and Faz Cano (2001) for SWy-2; Madsen (1998) for Montigel <0.2 μm fraction; Levy (1984) for H-5 1666, with iron content recalculated to the ferric form.

2.1.3 Bulk Mineralogy and Chemistry of Study Materials

Bentonitic products to be used as buffers or backfill will be minimally processed natural materials rather than purified clays. Table 2-2 compares the mineralogy of MX-80, Montigel, and a drill-core sample (NRG-6 633.0) representing the host rock of the DST. The DST host rock contains substantially less bentonite than the two commercial products. It also contains two SiO₂ polymorphs – tridymite and cristobalite – that are potentially more reactive than quartz, the only silica polymorph detected in the commercial products.

	Illite/smectite	Tridymite	Cristobalite	Quartz	Feldspar	Carbonate	Mica	Other
NRG-6 633.0	3	6	21	16	54	1	trace	1
MX-80	75.5	—	—	15	5-8	1.4	<1	2.3
Montigel	66.3	—	—	8	2-4	3.8	12-15	2-3

"trace" signifies abundance < 0.5 wt %. Sources: Vaniman (1997) for NRG-6 633.0; Madsen (1998) for MX-80 and Montigel

The Opalinus Clay, an extensive shale formation present in France, Switzerland, and Germany, is under consideration as host rock for a used-fuel repository; it also is the host rock for the Mount Terri Underground Laboratory, a test facility for repository concepts. Mineralogic constituents of this formation include 20% quartz, 6% calcite, 2% K-feldspar, 38% illite, 21% kaolinite, 6% chlorite, 4.5% mixed illite/smectite, 1.5% albite, 1.6% pyrite, and 1.2% siderite (Wenk et al., 2008).

2.1.3.1 Clay Content of Test Materials

The montmorillonite (smectite) content of bulk MX-80 was determined to be 75.5 wt. %, and the montmorillonite content of bulk Montigel was 66.3 wt. %. For both materials, a large majority of the clay resides in the <0.2- μm fraction of the bulk sample (Madsen, 1998).

Tests of bentonite backfills commonly use mixtures of bentonite with non-clay materials such as quartz sand. Mixtures may be used due to economic reasons, to re-use granular material derived from excavation of repositories, or to minimize introduced changes in the natural geochemical environment (Mata Mena, 2003). A 70/30 mixture of crushed granite and bentonite has been selected for many SKB experiments, although mixtures with bentonite content as low as 10%, equivalent to a clay content of about 7.5%, also have been investigated.

Clay content of drill core equivalent to the DST host rock has been determined by quantitative XRD analysis. Smectite typically comprises about 1-3 wt % of the whole rock (Table 2.1.3-1; Bish and Chipera, 1989). This clay content is low compared to bentonite-containing mixtures investigated for use as backfill/buffers. However, the geochemical environment of a mixture that contains 70% crushed granite or quartz sand will be dominated by the non-clay component, and in this sense the DST host rock is comparable. From a mechanical perspective, intact tuff cannot be considered equivalent to any crushed-rock/bentonite mixture.

2.1.3.2 Separation of Drift-Scale Test Clay: Experimental Procedures

The purpose of this research is to document structural and compositional changes in smectites that may have occurred during the prolonged heating of the DST. Mineralogic change could have occurred as changes to existing smectites and/or as formation of new smectites.

The first step is to determine the feasibility of the investigation: whether enough smectite can be separated from available DST rock samples (cores) for structural and chemical characterization. At this stage of the investigation, available material is limited to samples on hand and an inventory was performed on these samples. Most of the samples,

including the largest samples, are pre-test core. This material would be suitable for separation of clay minerals representing ambient unheated pre-test conditions.

A core section from ESF-HD-TEMP-2 (121.3-122.0 ft), a pretest horizontal borehole that runs the length of the heated drift above the ceiling, was selected to test the feasibility of separating clay from the devitrified tuff. This is one of the largest available core sections, and contains no visible fractures. The ends of the core piece are natural fractures with mineral fillings: these were sawed off before the core was crushed. This core piece is representative of unfractured matrix, and the fracture fillings at the ends of the core were removed to prevent fracture minerals from complicating the separation of clay from the matrix.

The material was coarsely crushed and ground to powder. Care was taken in these processes to avoid heating the rock material. Approximately 18 g of rock powder was suspended in 500 ml of deionized water, sonicated for 20 min, and left to settle for at least 24 hr. After that time, the top 50 ml of suspension was pipetted into a collection beaker. This process was repeated until 500 ml of suspension was collected. The suspension was centrifuged for five minutes at 5000 rpm. Settled material representing approximately the 2.0- to 0.35- μ fraction was collected and archived. This centrifugation step was repeated twice. The final supernatant was collected and centrifuged at 8000 rpm for 40 min. The settled <0.35- μ material from this centrifugation was collected, and a portion of it used to produce an oriented-clay mount on an off-axis quartz slide (for low background). An XRD pattern for this sample, with tentative mineral identifications, is shown in Figure 2-3.

The XRD pattern documents a relatively successful clay separation with minor cristobalite (SiO_2 polymorph) as the only impurity. This material will be satisfactory for studies of clay-lattice expansion as a function of controlled humidity, the property that controls the macroscopic swelling capacity of bentonite. The expansion properties of this pre-test material will provide a baseline for comparison with the clay properties of post-test rock samples. Sufficient clay can be separated for chemical characterization so that the original composition and any chemical changes during the thermal test will be documented and can be compared with bentonite materials from other investigations.

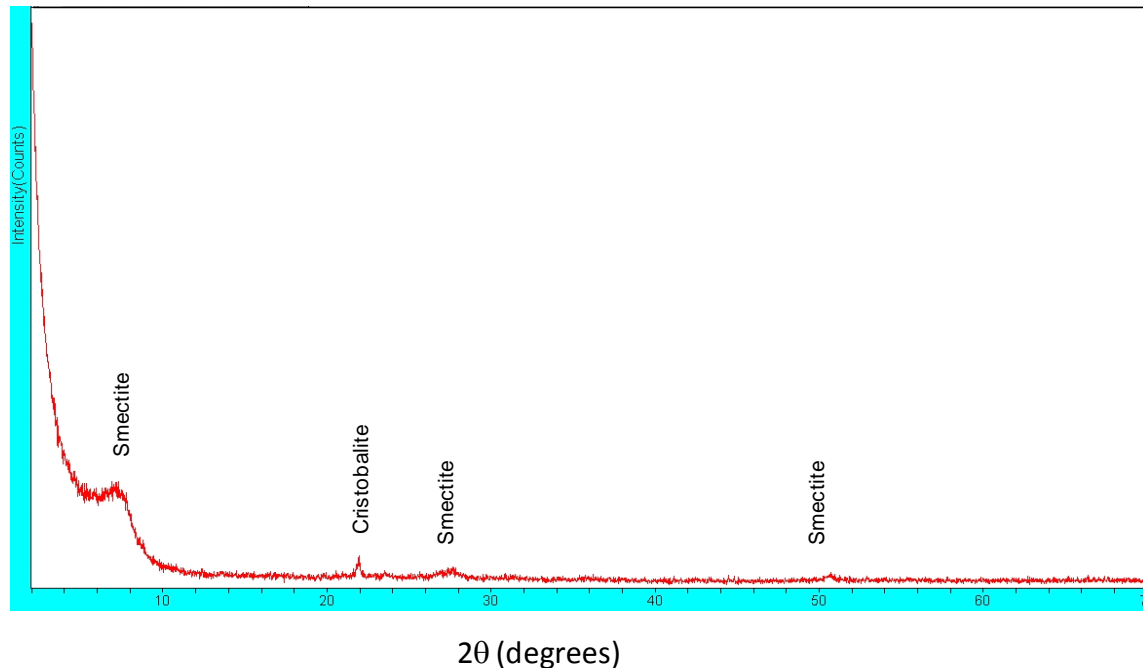


Figure 2-3. X-ray diffraction (XRD) pattern of ESF-HD-TEMP-2 121.3 ft oriented clay separate.

2.2 Summary of Clay Recovery from the DST Study

Experimental clay separation from Yucca Mountain DST pre-test core indicates that sufficient clay can be separated to perform XRD analyses, fine-scale electron microscopy, and chemical characterization. Minor cristobalite is the only impurity. Documentation of changes in composition and swelling properties of clay during the DST will enlarge the database of bentonite clay behavior in long-term, full-scale field thermal tests. One particular value of the DST data is the fact that the DST host rock is a common rock type with mineralogy similar but not identical to the compositions of natural bentonites, bentonite/crushed-rock mixtures, and potential silicic host rocks. Although compositional data are not yet available for the DST smectite, it probably is similar to the more calcium-rich varieties of bentonites under investigation as repository backfill/buffer.

2.3 Engineered Barrier System Components – Experimental Studies Review

2.4 Clay Studies

Clay minerals, either as backfill or buffer materials are critical to the performance of the EBS. This includes such factors as chemical interaction, radionuclide retention, physical and mechanical properties. This section of the report focuses primarily on chemical changes in clay at elevated temperature and/or pressures. The transformation of smectite to smectite / illite (I/S) is currently under discussion, with two main theories presently in vogue. The first is a solid state substitution of potassium (K) into the structure of the smectite, creating illite layers. The second concept for the transformation is a model called dissolution/crystallization. The merits of each are discussed below. Regardless, the availability of K should be viewed as the rate limiting factor in any reaction. A review

of the work by Tang and Cui (2010) looks at thermo-hydro-mechanical aspects of bentonite samples from Wyoming (MX80) and is of interest to physical aspects of clay in the EBS.

Wu et al. (1997) determined partial dehydration in Ca- and Mg-montmorillonite at pressures from the H₂O liquid-vapor boundary to about 10 kbars. This was due to the transformation from the 19 Å hydration state to the 15 Å hydration state. Mg-montmorillonite partially dehydrates at 200-250 °C, while the Ca-montmorillonite partially dehydrates in the range of 260-350 °C. Furthermore, the authors in this study were able to rehydrate the phases at the same temperature as dehydration. To summarize, there are two potential dehydration states for montmorillonite: (1) from the 19 Å to the 15 Å hydration state at lower temperatures, and (2) from the 15 Å to the 12.5 Å hydration state at higher temperatures. The conversion from the 19 Å to the 15 Å hydration state is totally reversible, while the conversion from the 12.5 Å to that of the 15 Å hydration state is only partially achievable.

Pusch and Madsen (1995) did early work to decide if the conversion of the original smectite of the Ordovician Kinnekulle K-bentonites into the present mixed layer illite/smectite took place through charge increase of the smectite with subsequent uptake and fixation of potassium. Their analyses show that the layer charge of the smectite component of the I/S is in fact low. The authors used Pytte's kinetic model which gave good agreement with the actual transformation rate for an activation energy of about 25 – 27 kcal/mole, according to adopted rate parameters, temperature history and assumed potassium source. In the Kinnekulle case, the rate-controlling factor appears to have been the source of potassium. Assuming that illitization took place in the heating period, it was found that the access to potassium must have been much greater than offered by diffusion of potassium in the pore water of the adjacent sediments.

McCarthy et al. (2009) characterized the illitization reaction in a thick K-bentonite bed located in an upper Cretaceous marine shale in Montana with the use of XRD, chemical analysis, and thermal gravimetric analysis. Modeling of the XRD patterns from oriented clay specimens in air-dried (AD) and glycolated (EG) states shows that at each location in the bentonite bed a mixture of random (R0) illite-smectite (I/S) and layered (R1) I/S coexist. The illite content in the random I-S and the layered I-S is equal to 30 and 62%, respectively. The main difference between the samples at different locations within the unit is the different weight concentrations of the coexisting I/S phases. The layered I/S content decreases progressively from the lower and upper contacts of the bed to its center. The reverse trend was observed for the random I/S.

Their analysis of both types of I/S shows that, in the middle of the bed, both phases are characterized by the lowest octahedral Mg and K contents and the highest tetrahedral Al contents. For McCarthy et al. (2009) to account for the crystal-chemical features of the coexisting I/S, they first assumed that the initial volcanic ash was altered into smectite having a constant Al composition throughout the bed. The process of illitization was controlled by the availability of Mg and K. Phase zonation of the K-bentonite is explained by the progressive migration of K from the margins toward the bed center with the associated decrease of K cations in the pore fluids. Because the mean K content in the pore fluids decreased toward the bed center, the period of relatively high K concentration was shorter further from the margins of the bed, and thus the content of the R1 I/S phase progressively decreased.

To summarize the paper of McCarthy et al. (2009), they developed a good modeling approach. The model covers both (1) relationship between weight concentrations of EG and AD I/S structures and (2) relationships between the probability parameters determined for the AD and EG R1 I/S structures. However, it is never clear in this paper whether the S to S/I transformation is solid state (i.e., cation exchange only with structure collapse), or dissolution/precipitation process, as discussed by Ferrage et al. (2011). The authors only assign variation due to availability of K and Mg in solution.

The article by Eberl et al. (2011) uses the samples of McCarthy et al. (2009) from a Montana metabentonite to promote USGS computer codes and describe a new nomenclature for the smectite/illite (I/S) series of minerals. This new method developed for modeling XRD patterns of I/S indicates that random and layered I/S in these samples are not separate phases, but that the samples are composed of illite crystals that have continuous distributions of crystal thicknesses, and of 1 nm thick smectite crystals. The patterns of these distributions indicate that the crystals were formed by simultaneous nucleation and growth. XRD patterns for random and layered I/S arises by interparticle diffraction from a random stacking of the crystals. Eberl et al. (2011) do not believe that Ostwald ripening is the controlling mechanism to generate I/S. The authors advocate initial simultaneous nucleation and growth of both illite and smectite phases, with stacking of the layered phases creating the fundamental particles.

Tang and Cui (2010) determined the thermal conductivity, water retention curve and swelling behavior of two MX80 bentonite samples. The two types of MX80 bentonites were provided by Cetco France Company (MX80a) and Cetco Europe Company (MX80b). The experiments were well thought out, and conducted properly. The authors were able to determine thermal conductivity of samples of MX80 as a function of dry density and observed significant differences. Their observations show that the thermal conductivity of the MX80a bentonite is higher than that of the MX80b bentonite. This difference probably results from the differing amounts of quartz. The quartz proportion varies from 2.8% (MX80b) to 15.2% (MX80a) in the two bentonite samples. As the thermal conductivity of this mineral is significantly higher than that of the others 8.8 W/(m·K) for quartz and 2.5 W/(m·K) for other minerals), the proportion of quartz may significantly affect the thermal properties.

The authors also recognized differences in the final swelling strain on these two bentonites. Montmorillonite is the main mineral that generates the swelling behavior and the water retention capacity of bentonite. The MX80a samples swelled by approximately 30 volume %, while the MX80b bentonite samples swelled by 50% volume. Since MX80a bentonite contains more quartz and less montmorillonite than the MX80b bentonite, all the observations on the thermal conductivity and swelling capacity were by variations in the quartz/montmorillonite ratios.

The benchmark paper (at present) for the mechanism of S to S/I transformation is by Ferrage et al. (2011). They have studied the hydrothermal reactivity of K-saturated Wyoming low-charge montmorillonite in the 250–400 °C temperature range with reactions lasting between 5 and 120 days. The authors provided very convincing experimental evidence depicting a dissolution – crystallization mechanism (DC), backed by thermodynamic calculations, XRD, TEM and modeling efforts. The authors claim it is a dissolution-precipitation process following the Ostwald step rule in which metastable smectite transforms into illite through a series of metastable illite-smectite phases.

Ferrage et al. (2011) use XRD, transmission electron microscopy (TEM) and chemical microanalysis results to describe the illitization process as a progressive replacement of expandable layers by layers with illitic behavior, in a single illite-smectite phase. The TEM and chemical analyses show several types of particle morphology with different interlayer K content and Al-for-Si substitution that seem to correspond to the phases detected by XRD. The actual illitization mechanism of smectite in the experiments of Ferrage et al. (2011) are not a progressive reaction but rather a dissolution-precipitation process following the Ostwald step rule in which metastable smectite transforms into illite through a series of metastable illite-smectite phases.

Ferrage et al. (2011) present TEM analyses that show the types of phyllosilicates created in the experiments. The initial smectite sample consists of flakes of irregular and undulated outlines. The samples analyzed after 30 days at 250 °C also consists of flakes, although most of them appeared to be thinner and with smaller lateral dimensions than in the initial sample. As temperature and time increased several morphologies were detected. They included smectite flakes and aggregates of very small flakes as for the previous samples and, there were round particles with clear outlines most often observed forming stacks. The round morphology was predominant in this sample. The most altered sample (120 days, 400 °C) displayed all the previous morphologies and a new type consisting of particles with polygonal shapes (3–4 sides, angles of 60, 90, and 120°), along with the highest K and tetrahedral Al contents. The polygonal and round particles, which have been already described for altered smectite in hydrothermal conditions by Whitney and Velde (1993), were predominant in their highest temperature sample.

The authors (Ferrage, et al, 2011) indicate that the process of illitization is a complex reaction for which multiple phenomena occurring at different temperatures which may lead to illitization of smectite layers. They calculated activation energies (6 kcal/mol) which are quite lower than Meunier et al. (1998) who calculated an activation energy of ~18 kcal/mol using the results obtained by Whitney and Northrop (1988). The latter value would be an acceptable activation energy for a DC mechanism. Ferrage et al. (2011) and Whitney and Northrop (1988) have similar experimental conditions and results, such as the changes in phyllosilicate phases, morphology and chemistry, all of which support a DC mechanism. Changes in particle morphology and chemistry appear to be more reliable evidence to support the DC reaction mechanism than the poorly defined activation energy derived by Ferrage et al. (2011).

The review paper by Meunier et al. (1998) is extremely useful in that the authors compare a large group of experimental data sets and put them into the perspective of two general geologic settings (diagenetic and hydrothermal). They have focused on the variables of time, chemical composition and temperature that have been varied in these experiments.

Essentially two sets of data were used from natural settings: those of geothermal areas such as the Saton Sea (Velde & Lanson, 1993), and those of burial diagenesis in the East Slovak Basin (Sucha et al.1993). The experimental reactions using bentonite clays as starting material do not produce an I-S sequence similar to that observed in diagenetic environments. In repository systems where bentonite smectite is used as barriers around nuclear waste, the experimental data on Wyoming bentonite can be used to predict the behavior of clays at high temperature. Therefore the hydrothermal systems are more pertinent than those of diagenesis. The authors (Meunier et al. 1998) summarized the bentonite reactions from the two environments:

1. Diagenesis in sedimentary environments: smectite → illite directly
2. Hydrothermal systems: smectite → illite + chlorite + quartz

It is apparent that the smectite in bentonites and the smectite formed in shales do not react to form similar mineral phases under the same thermal conditions. This can be due to the chemical processes (diffusion of K for the smectite / illite conversion) or fundamental mineralogical differences in the conversion process. In essence, bentonites and shales do not give the same kinetic response to thermal change. The authors believe this is one possible mechanism as temperature increases, however it is more probable that the end reactions are due to a combination of P, T trajectories, elemental composition of the bulk rocks involved, and differing water compositions.

A second review paper, by Wersin et al. (2007), characterized by experiments and natural analogues focused on bentonite properties above 100 °C. This is a valuable update to the article by Muenier, et al. (1998). Critical parameters include ambient rock temperature, heat output from the waste, initial moisture content of the bentonite, water and heat properties of the rock – all of which may vary with time. Major findings were that (1) no significant changes up to 110 °C, (2) SiO₂ precipitation occurs at 130 °C, (3) by 150 °C there are more significant changes due to increased SiO₂ precipitation and some phase transition to illite, and (4) chlorite may form when clay is in contact with Fe at elevated temperatures (Lantenois, 2005).

2.4.1 Summary of Clay Studies

Within the UFD campaign, there is the option for certain repository scenarios which have very high heat loads. The work by Meunier et al. (1998) and Wersin et al. (2007) summarize the fact that when smectite clays are heated above 100°C, various significant mineralogic changes may occur. For example, (1) SiO₂ precipitation at 130°C, (2) increased SiO₂ precipitation and inception of illite at ~150°C, and (3) chlorite formation in the presence of Fe at high temperatures. Because of these phase transformations, even if the repository cools below 100°C after the thermal pulse, the clays will not revert back to pure smectite. This is due in part to the extraction of SiO₂ from the clay structure, and potential deposition farther from the original clays. In fact, the high temperature transition of clay to illite and chlorite (high-charge mont. = illite + chlorite + quartz), is cited by Meunier et al. (1998) as irreversible. These chemical and structural changes to clays, either in the shale host rock or in backfill/buffer materials, may have significant affects on repository conditions. Therefore, the alteration of clay at higher temperatures may impact groundwater flow, transport pathways, and radionuclide sorption properties. Because clay alteration in a complex geologic system is still not well understood, there may be unforeseen changes to static structural properties and complex hydration dynamics. There is critical information still to be captured from high temperature, pressure experiments, especially by systematically increasing the components involved.

2.5 Iron – Clay Interaction

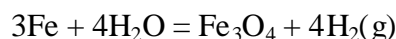
Most experimental studies consisting of metal – clay interaction as part of the EBS have taken place at temperatures below 100°C. Below are reviews of some of the pertinent studies. Even at low temperatures, iron may change its phase composition, depending on redox conditions. As temperatures increase, the likelihood that clays may transition to lower water content phyllosilicates (i.e., chlorite) also increases. Very commonly, free SiO₂ is often produced, and H₂ gas is generated from the breakdown of water in the

presence of iron. At present, the article by Mosser-Ruck et al. (2010) is most informative; however, their experiments were not specifically buffered to control redox conditions. Furthermore, none of the experiments were run at lithostatic pressures.

In the study of Schlegel et al. (2008), a set of microscopic and spectroscopic methods were used to characterize the chemistry and mineralogy of interfacial Fe–clay interactions at 90°C and 50 bar for a period of 8 months under saturated conditions. These experiments show the formation of two layers: (1) a corrosion layer made of magnetite with sub-layers of Fe-phyllsilicate, and (2) a clay conversion layer composed of Ca-rich FeCO₃. The paper by Schlegel et al. (2008), although using state of the art micro-analytical and spectroscopic techniques, fails on many levels. The authors did not characterize the metals/clays prior to the experiments. A major problem was that they did not solve the redox conditions they seem to have produced during the experiments, and have no explanation for the observed excess Fe which is important to the understanding of local redox conditions.

A second paper (Martin et al. 2008) by the same research group performed similar experiments (embedding metal bars in clay) and maintained the reactions at 90°C for 8 months. In addition to MX80 clay (Wyoming, USA), they also studied argillite from the Bure site in France. This time the focus was on in-situ electrochemistry using impedance spectra and chronopotentiometry. They also performed microanalyses of some of the reaction products. Reaction products indicate the tendency of pure Fe or the 1050 steel to passivate with time. They believe it was a two step process: generation of a corrosion layer, and then diffusion-limited corrosion kinetics. Reaction phase characterization showed the formation of layered magnetite (close to the metal interface), and calcium-rich siderite.

Xia et al. (2005) designed experiments to look at the corrosion of carbon steel in contact with bentonite. The experimental materials were carbon steel, corrosion products pre-formed under aerobic conditions, compacted bentonite, and buffer material. The experiments were run in a low-oxygen glove box. The experiments were well thought out in this article and will be useful in the design of any further experiments. Results indicate that even under anoxic conditions, the carbon steel oxidizes by scavenging oxygen from the water.



Experimental results demonstrated that carbon steel experienced anaerobic when in contact with bentonite. This resulted in H generation and therefore led to further reducing conditions (see reactions above). The corrosion rate was estimated to be ~0.1 $\mu\text{m}/\text{year}$. The presence of the bentonite and the corrosion products at the interface of carbon steel and bentonite caused a passivating surface.

Ishidera et al. (2008) performed long-term (10 year) experiments of montmorillonite in contact with carbon steel under reducing conditions at 80°C. The XRD analysis indicated that no phyllosilicates formed as a result of montmorillonite alteration. Therefore, montmorillonite alteration was not observed in this experiment that ran for ten years.

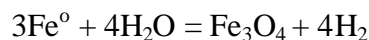
XRD analysis indicated the coexistence of some amount of green rust and lepidocrocite as corrosion products of carbon steel. To summarize, the investigation by Ishidera et al. (2008) carbon steel and bentonite reactions were run for 10 years at 80°C under reducing conditions. The experimental approach was very solid and simulated seawater was the fluid media. Four major conclusions were reached (1) montmorillonite was not altered, (2) Fe proceeded to Fe(OH)₂ by steps, (3) first green rust was produced, and then (4) lepidocrocite was generated.

Lantenois et al. (2005) described the interaction between metal Fe and a variety of natural and synthetic smectite samples with differing crystal chemistries. The experiments were conducted at 80°C for a typical time of 45 days. The phases were characterized by SEM and XRD. As background to their work, the authors point out that Fe-rich chlorite species are synthesized at high temperature (300°C, Guillaume et al., 2003) whereas Fe-rich serpentine species are obtained for temperatures near 80°C.

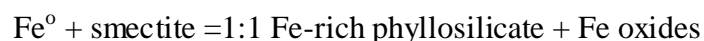
The experiments of Lantenois et al. (2005) demonstrate reaction differences as a function of smectite crystal chemistry. In mildly acidic to neutral pH conditions, metallic Fe is corroded to form magnetite without smectite destabilization. Under basic pH conditions, smectite and metallic Fe react to form magnetite and 1:1 phyllosilicate phases (odinite and crondstedtite). Of more interest, systematic alteration of both metal Fe and smectite is observed for dioctahedral smectites while trioctahedral smectites are essentially unaffected. Lantenois et al. (2005) determined that smectite reactivity is enhanced with Fe³⁺ content and the presence of Na⁺ cations in the smectite interlayers. A conceptual model for smectite destabilization was also proposed by Lantenois et al. (2005).

The reactions provided by Lantenois et al. (2005) can be summarized for the two pH realms (near neutral and basic) as follows:

pH 6 - In presence of smectite, metal Fe is oxidized to form magnetite according to the following reaction:



pH > 7- the reaction is dramatically different as dioctahedral smectites are involved in the reaction. (destabilization of dioctahedral smectite is common)



To summarize, the paper of Lantenois et al. (2005) the authors have provided a pivotal paper on Fe /clay interactions, especially for pH>7 conditions. Both the reaction products developed at neutral and basic pH will play a critical role in the use of concrete in repository setting. Their model of smectite destabilization will be very useful in further attempts to model bentonite stability.

Perronnet et al. (2007) conducted experiments with smectite and iron [Fe⁰] at 80°C to determine smectite degradation mechanisms. Three smectite samples were used: nontronite (Wards sample), montmorillonite from the Ordu region of Turkey, and montmorillonite from Kmiolos Island, Greece. Post experimental run analyses were done by XRD, Mossbauer, and CEC analyses. Perronnet et al. (2007) obtained a correlation between smectite reactivity and the energetic heterogeneity of its edge faces. The increase in the ‘‘energetic heterogeneity of edge faces’’ can be interpreted as the ability for Fe⁰ to find unstable sites on the smectite edges to transfer electrons and initiate

smectite destabilization. This mechanism at the edge faces of the smectites are believed to be the rate controlling steps in the reaction.

Mosser-Ruck et al. (2010) performed experiments to determine the conversion of smectite to Fe-rich clay phases in contact with Fe metal. Parameters that were varied include temperature, pH, and Fe/clay (Fe/C) and liquid/clay (L/C) ratios. All experiments were run under low oxygen fugacity ($<10^{-40}$), and temperatures ran up to 300°C. With the results of the mineral phase transformations listed below, Mosser-Ruck et al. (2010) were able to propose a conceptual model for the main mineralogical transformations which can be expected in clay formations surrounding high-level nuclear waste repositories. In the presence of Fe metal and with low redox conditions, Mosser-Ruck, et al. (2010) states that the main smectite mineralogy changes are as follows:

Neutral pH (6-7)

dioctahedral smectite = 7 A° Fe-rich phase (berthierine, odinite, or cronstedtite) (150°C, L/C > 5);

dioctahedral smectite = Fe-rich dioctahedral smectite + Fe-rich trioctahedral smectite (150°C, Fe/C ratios=0.1);

dioctahedral smectite = Fe-rich saponite = trioctahedral chlorite + feldspar + zeolite (300°C, L/C > 5. Fe/C ratio =0.1);

High pH (10-12)

dioctahedral smectite = Fe dioctahedral smectite (+/-palygorskite) (150°C, L/C > 5. Fe/C ratio =0.1);

dioctahedral smectite = Fe-rich vermiculite + mordenite (pH 10-12). (300°C, L/C > 5, Fe/C ratio =0.1);

At present, the work of Mosser-Ruck et al. (2010) is the benchmark research paper for experimental determinations of iron/clay iterations at temperatures up to 300°C. They did not however specifically buffer the redox conditions, nor did they perform experiments at elevated pressures. Because of the excellent work performed by this research team, their work must be considered the jump off point for further investigations of EBS materials at repository conditions.

2.5.1 Summary of of Iron Clay interaction

The predominance of experimental studies consisting of metal – clay interaction as part of the EBS have taken place at temperatures below 100°C. Reviews of some of the pertinent studies have been enlightening. Even at low temperatures, iron may change its phase composition, depending on redox conditions. As temperatures increase, the likelihood that clays may transition to lower water content phyllosilicates (i.e. chlorite) also increases. Free SiO₂ is often produced, and H₂ gas is generated from the breakdown of water in the presence of iron. One detracting issue encountered points to research that uses state of the art analytical facilities to characterize end run products, however the authors never characterized the initial experimental materials. Other authors may have very intriguing results, but never performed mass balance studies to confirm the reactions were realistic. Presently, the journal article by Mosser-Ruck et al. (2010) is the most

informative; however, their experiments were not specifically buffered to control redox conditions. Furthermore, none of the experiments reviewed were run at lithostatic pressures. Areas of further research would be to expand on the work of Mosser-Ruck et al. (2010), confirming their results and then working in buffered redox systems and elevated pressures. This research would also help to refine the smectite destabilization model of Lantenois et al. (2005).

2.5.2 Copper Corrosion

As both European and Japanese repositories are considering copper overpacks on waste containers, information on copper corrosion in sulfur-bearing groundwaters is important. The paper by Taniguchi and Kawasaki, (2008) provided very thoughtful work and experimental conditions. Immersion tests and slow strain rate tests (SSRT) on pure copper were carried out in synthetic seawater containing Na_2S and long-term predictions of corrosion due to presence of sulfide were performed based on the model of sulfide diffusion through buffer material. They have produced a strong model, and we will be able to use their corrosion rate values. Pure copper was attacked by uniform corrosion in the presence of sulfide under anaerobic conditions. The corrosion rate increased with sulfide concentration from less than 0.6 $\mu\text{m}/\text{y}$ for 0.001 M- Na_2S , 2–4 $\mu\text{m}/\text{y}$ for 0.005 M- Na_2S and 10–15 $\mu\text{m}/\text{y}$ for 0.1 M- Na_2S . The corrosion product in both cases (without Na_2S added) is cuprite. Once sulfur is added, the dominant corrosion product is chalcocite. It can be presumed that the corrosion rate of pure copper is self-limiting as corrosion propagates. One of the important factors controlling corrosion rate is assumed to be the formation of corrosion product film. Lower corrosion rates than those observed in previous studies are assumed to be due to the occurrence of protective corrosion product film in the simple solution cases. On the other hand, the state of surface corrosion products in bentonite–sand mixtures were obviously different from those in simple solution and seemed to be less protective. One possible factor could be the limitation of sulfide supply to the coupon surface through the bentonite–sand mixture.

2.5.3 Japanese URL Water Chemistry

Work has recently been performed to characterize the water geochemistry at Japanese Underground Research Laboratories (URLs) at Horonobe site (located in shale, Hama, et al, 2007) and the Mizunami site (located in granite, Iwatsuki, et al, 2005). It is extremely telling that both sites at depth seem to have chemical interaction (i.e. mixing) with fossil seawaters.

A hydrogeochemical investigation was carried out as part of the Horonobe URL project in Japan (Hama, et al, 2007). The main thrust was to investigate a geological environment in a sedimentary rock formation in Japan. The main rock formations were siliceous shales and diatomaceous shales, respectively. Aqueous geochemistry was developed at each sample location in the URL, with shallower groundwaters being fresh and having $\text{Na}-\text{HCO}_3$ dominated chemistry. With samples ranging in depths to 700 meters, there is a clear trend in each borehole to higher salinity associated with mixing from fossil seawaters. The deeper $\text{Na}-\text{Cl}$ dominated groundwater chemistry is explained as a dilution of fossil seawater, accompanied by diagenetic water–rock reactions.

Iwatsuki et al, (2005) have determined the hydrochemical conditions up to depths of 1000 m below ground level around the Mizunami URL. Groundwater chemistry in this area was classified as a $\text{Na}-\text{Ca}-\text{HCO}_3$ type of groundwater in the upper part of sedimentary

rock sequence and a Na–(Ca)–Cl type of groundwater in the deeper part of the sedimentary rock sequence and basement granite. The source of salinity in the deeper part of the granite was possibly fossil seawater that recharged in the Miocene, and has been subsequently modified by long-term water–rock interaction. The Cl-depth trend in granitic groundwater changes at a depth of 400 m below sea level. Note that the water chemistry at Mizunami is layered in a similar fashion to the URL at Horonobe in that both sites are influenced at depth by fossil seawater components.

2.5.4 Path Forward – Experimental Program 2011-2012

The Used Fuel Disposition (UFD) Campaign is presently engaged in looking at various generic options for disposal of used fuel. The focus of this experimental work is to characterize and bound EBS conditions in igneous rock based repositories. Previous research for the Yucca Mountain Project limited repository conditions to less than 100 °C and atmospheric conditions. The UFD now has the ability to look at multiple EBS, waste containers, rock types, heat loads, and high pressures (for deep boreholes). All of these variations have not been researched in the US and little has been done experimentally by the international community at high pressures and temperatures. The work thus far this year (included in the deliverable) has identified knowledge gaps that are now sufficiently clear to embark on new experiments. The defining work so far is that of Mosser-Ruck et al. (2010). Their experimental conditions did not consider (1) high pressures, (2) buffered redox conditions, (3) different metal types other than iron, (4) clay types from mined sites as those considered for backfill/buffer materials. LANL has the capability to provide these experiments with a full, operational high pressure/temperature laboratory (see Figure 2-4). As part of the UFD Campaign, we are planning experiments in the areas listed below:

UFD - Three General Experimental Research Arenas

- Water fate and transport in salt at intact/disturbed rock zone interface [should be funded by the Salt Disposition Initiative (SDI)];
- Clay Dehydration – Volume contraction and water evolution;
- Interactions and alteration mechanisms at EBS component interfaces.

Bounding test conditions (all of these could be modified if required)

Temperature – 100°C, 200°C, 300°C

Depths – 1.5 Km, 5 Km

Lithostatic pressure – approx. 0.39 Kb, 1.3 Kb

Water composition – saline Na-(Ca)-HCO₃ (?) also considering SO₄⁻. *deep seated shield composition*

Rock type – (1) granite (silicic), (2) amphibolites (mafic) – *These could be seen at as end member compositions.*

Clay – bentonite from Wyoming mine

Waste container – SS-316, mild steel, copper.

Time – 2 week, 1 month, 3 month, 6 month, 1 year?

Test Types

- A) Water – Clay
- B) Water – Clay – Metal(2)
- C) Water – Clay – Metal(2) – Rock(2)

Many scientists commonly refer to “granite” repositories as a future generic site, however they do not consider granite rock chemistry. The vision is to emplace NW in a more generic crystalline rock. Therefore, it is imperative to bound the igneous rock type chemistries by using both mafic (amphibolites) and silicic (granitic gneiss) end members. The experiments will run at repository conditions for both lithostatic pressures and potentially higher heat loads. This will therefore provide data for both mined repositories (similar to Swiss, Japanese and Swedish URLs) and potential deep borehole disposal sites. The experiments will systematically add components to capture discrete changes in both water and EBS component chemistries.

The **Type A experiments** will allow us to monitor changes in clay compositions and corresponding water chemistry changes. At higher temperatures, the clays may have a phase change to chlorite, thereby releasing water. **Type B experiments**, with the addition of waste canister metal chemistry (Alloy 22 and mild steel) will provide information on Fe buffering capabilities and the occurrence of micro redox conditions at material interfaces. We will be able to investigate how clay chemistry changes as mild steel is consumed. If sulfides are present in the clay mix or in the water, we will also see if metal degradation by H₂S occurs. **Type C experiments** (inclusive of EBS components, brine and wall rock) will allow us to delineate mineral reactions and interactions with EBS materials due to heat load, brine composition and oxygen fugacity buffering. The predicted mineral reactions would be laumontite-prehnite facies at the lower pressure (0.36 Kb), and lawsonite-albite facies at higher pressure (1.3 Kb). Expected results will include verification of waste container degradation rates and phase changes, changes in clay mineralogy with potential phase transformations, redox condition confirmation, brine chemistry evolution, and retrograde mineral changes in the host rocks. The experiments should yield a combination of kinetic and thermodynamic data to support EBS system modeling. Geochemical reaction-path modeling will be conducted to help interpret the experimental trends fluid chemistry.

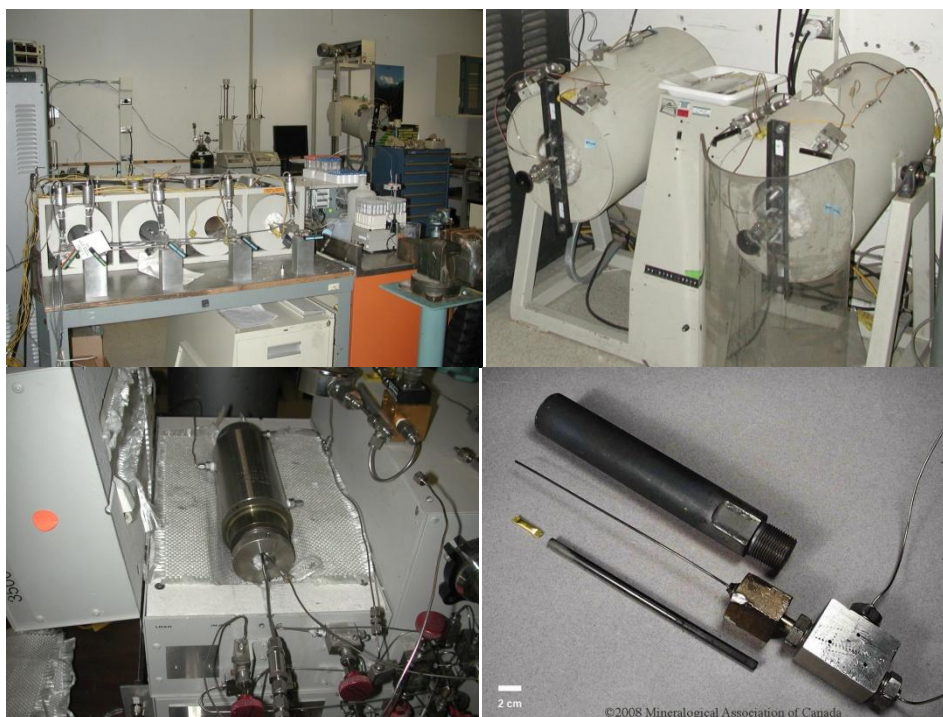


Figure 2-4. Experimental Hydrothermal Systems at LANL. Top left: Horizontal autoclave rack, each is 12” diameter (400°C, 600 bar max.). Top right: Rocking autoclave, 24” length (400°C, 600 bar max.). Lower left: Flow through autoclave (400°C, 600 bar max.). Lower right: Cold seal reaction vessel, disassembled (800°C, 2.5 kbar max.; from London 2008, Figure 14-1a).

2.6 References

- Bish, D.L., and Chipera, S.J., 1989, “Revised Mineralogic Summary of Yucca Mountain, Nevada,” Los Alamos National Laboratory report LA-11497-MS.
- Blanc, P., Bourbon, X., Lassin, A., and Gaucher, E.C., 2010a, Chemical model for Carlos, B.A., Chipera, S.J., and Bish, D.L., 1995, “Distribution and Chemistry of Fracture-Lining Minerals at Yucca Mountain, Nevada, Los Alamos National Laboratory report (LANL) LA-12977-MS.
- Civilian Radioactive Waste Management System Management & Operating Contractor (CRWMS M&O), 1997, “Ambient Characterization of the Drift Scale Test Block,” CRWMS M&O Report BADD00000-01717-5705-00001 REV 00, <http://www.lsnmet.gov>, LSN# DN2002293276.
- CRWMS M&O, 1998, “Drift Scale Test As-Built Report,” CRWMS M&O Report BAB000000-01717-5700-00003 REV 01, <http://www.lsnmet.gov>, LSN# DN2001008967.
- Datta, R., 2000, “Drift Scale Test (DST) Temperature, Power, Current, and Voltage Data for June 1, 2000 through November 30, 2000,” Yucca Mountain Project Data Submission MO0012SEPDSTPC.002.

- Eberl, D.D., Blum, A.E. And Sarravezza, M., 2011, Anatomy of a metabentonite: Nucleation and growth of illite crystals and their coalescence into mixed-layer illite/smectite. *Am. Min.*, Vol. 96, p. 586-593.
- Ferrage, E., Vidal, O., Mosser-Ruck, R., Cathelineau, M., and Cuadros, J., 2011, A reinvestigation of smectite illitization in experimental hydrothermal conditions: Results from X-ray diffraction and transmission electron microscopy. *Am. Min.*, Vol. 96, p. 207-223
- Guillaume, D., Neaman, A., Cathelineau, M., Mosser-Ruck, R., Peiffert, C., Abdelmoula, M., Dubessy, J., Villieras, F., Baronnet, A. and Michau, N., 2003. Experimental synthesis of chlorite from smectite at 300°C in the presence of metallic Fe. *Clay Min.*, Vol. 38, pp 281-302.
- Hama, K., Kunimaru, T., Metcalfe, R., and Martin, A.J., 2007. The hydrogeochemistry of argillaceous rock formations at the Horonobe URL site, Japan, *Phy Chem Earth*, Vol. 32, p.170-180
- Ishidera, T., Ueno, K., Kurosawa, S., and Suyama, T., 2008, Investigation of montmorillonite alteration and form of iron corrosion products in compacted bentonite in contact with carbon steel for ten years. *Phys. Chem. Earth*, Vol. 33, p. S269-S275.
- Iwatsuki, T., Furue, R., Mie, H., Ioka, S., and Mizuno, T., 2005. Hydrochemical baseline condition of groundwater at the Mizunami underground research laboratory (MIU). *Applied Geochem.*, Vol. 20, p. 2283-2302.
- Johnson, L.H., and King, F., 2003, Technical Report 02-11: Canister Options for the Disposal of Spent Fuel, *in* NAGRA, ed.: Wettingen, Nagra, p. 57 pp.
- Jové Colón, C.F., Caporuscio, F.A., Levy, S.S., Xu, H., Blink, J.A., Halsey, W.G., Buscheck, T., Sutton, M., Serrano de Caro, M.A., Wolery, T.J., Liu, H.H., Birkholzer, J., Steefel, C.I., Rutqvist, J., Tsang, C.-F., and Sonnenthal, E., 2010, Disposal Systems Evaluations and Tool Development - Engineered Barrier System (EBS) Evaluation p. 1-200.
- Laine, H. and Karttunen, P., 2010, "Long-Term Stability of Bentonite: A Literature Review," Posiva Working Report 2010-53, 132 pp.
- Lantenois, S., Lanson, B., Muller, F., Bauer, A., Jullian, M., and Plancon, A., 2005. Experimental Study of Smectite Interaction with Metal Fe at low Temperature: 1. Smectite Destabilization. *Clay and Clay Min.*, Vol. 53, No. 6, p. 597-612.
- Levy, S. S, 1984, "Petrology of Samples from Drill Holes USW H-3, H-4, and H-5, Yucca Mountain, Nevada," Los Alamos National Laboratory report LA-9706-MS.
- Levy, S., 1999, "Percent coverage by fracture-coating minerals in core ESF-HD-TEMP-2," Yucca Mountain Project Data Submission LA9912SL831151.002, <http://lsnnet.gov>, LSN# DEN000215369.
- London, D. 2008, Pegmatites. *Canadian Mineralogist*, Special Publication 10, Mineralogical Assoc. of Canada, Quebec, Canada. 347 pp.
- McCarty, D.K., Sakharov, B.A., Drits, V.A., 2009. New insights in smectite illitization: A zoned K-bentonite revisited. *Am. Min.*, Vol. 94, p. 1653-1671.

- Martin, F.A., Bataillon, C., and Schlegel, M.L., 2008, Corrosion of iron and low alloyed steel within a water saturated brick of clay under anaerobic deep geological disposal conditions: An integrated experiment. *Jour. Nuc. Materials*, Vol. 379, p. 80-90.
- Mata Mena, C., 2003, "Hydraulic Behaviour of Bentonite Based Mixtures in Engineered Barriers: The backfill and Plug Test at the Äspö HRL (Sweden), Ph.D. Thesis, Technical University of Catalonia, Department of Geotechnical Engineering and Geosciences, School of Civil Engineering, 253 pp.
- Mermut, A. R., and Faz Cano, A., 2001, "Baseline Studies of the Clay Minerals Society Clays: Chemical Analyses of Major Elements," *Clays and Clay Minerals* 49, 381-386.
- Meunier, A., Velde, B., and Griffault, L., 1998. The Reactivity of Bentonites: a Review. An Application to Clay Barrier Stability for Nuclear Waste Storage. *Clay Min.*, Vol. 33, p. 187-196.
- Mont Terri Project, 2011, <http://www.mont-terri.ch/ids/default.asp?TopicID=72>, last update 02.05.2011.
- Mosser-Ruck, R., Cathelineau, M., Guillaume, D., Charpentier, D., Rousset, D., Barres, O., and Michau, N., 2010. Effects of Temperature, pH, and Iron/Clay and Liquid/Clay Ratios on Experimental Conversion of Dioctahedral Smectite to Berthierine, Chlorite, Vermiculite, or Saponite. *Clay and Clay Min.*, Vol. 58, No. 2, p. 280-291.
- Perronnet, M., Villieras, F., Jullien, M., Razafitianamaharavo, A., Raynal, J., and Bonnin, D., 2007. Towards a link between the energetic heterogeneities of the edge faces of smectites and their stability in the context of metallic corrosion. *Geochim Cosmochim Acta*, V71, pp1463-1479.
- POSIVA, 2008, Horizontal Deposition of Canisters for Spent Nuclear Fuel - Summary of the KBS-3H Project 2004 - 2007, in OY, P., ed.: Olkiluoto.
- Pusch, R., and Madsen, F.T., 1995. Aspects on the Illitization of the Kinnekulle Bentonites. *Clay and Clay Min.*, Vol. 43, No. 3, p. 261-270.
- Sandia National Laboratories (SNL), 2007, "Thermal Testing Measurements Report," Report TDR-MGR-HS-000002 REV 01.
- Schlegel, M. L., Bataillon, C., Benhamida, K., Blanc, C., Menut, D., and Lacour, J. (2008) Metal corrosion and argillite transformation at the water-saturated, high-temperature iron-clay interface: A microscopic-scale study. *Applied Geochem*, Vol. 23, p. 2619-2633.
- Sucha V., Kraus I., Gerthofferova H., Petes J. and Serekova M., 1993, Smectite to illite conversion in bentonites and shales of the East Slovak basin. *Clay Min.*, Vol. 28, p. 243-253.
- Tang, A.M., and Cui, Y.J., 2010, Effects of mineralogy on thermo-hydro-mechanical parameters of MX80 bentonite. *Jour. Rock. Mech and Geotech Engin.*, Vol. 2, No. 1, p. 91-96.

- Taniguchi, N., and Kawasaki, M., 2008. Influence of sulfide concentration on the corrosion behavior of pure copper in synthetic seawater. *Jour. Nuc. Materials*, Vol. 379, p. 154-161.
- Vaniman, D., 1997, "Mineralogic Variation in Drill Holes, Yucca Mountain Project Data Submission LADV831321AQ97.001, <http://www.lsnnet.gov>, LSN# DEN000446464.
- Vaniman, D., Chipera, S., Lopez, R., Pannell, M., and Bish, D., 2005, "Dust and Wall-Rock Hazardous Mineral Distributions in the East-West Cross Drift, Yucca Mountain, Nevada," Yucca Mountain Project Milestone SP32P5M4 Report.
- Velde B. and Lanson B., 1993, Comparison of I-S transformation and maturity of organic matter at elevated temperature. *Clays Clay Min.* V41, p. 178 - 183.
- Vogt, T., 2002, "Drift Scale Test (DST) Temperature, Power, Current, and Voltage Data for June 1, 2001, through January 14, 2002," Yucca Mountain Project Data Submission MO0202SEPDSTTV.001.
- Vomvoris, S., Gaus, I., Rueedi, J., and Marschall, P., 2011, "Large-Scale Tests of the Behaviour of Bentonite-Based Barriers: FEBEX & GAST," Proceedings of the 13th International High-Level Radioactive Waste Management Conference, Albuquerque, New Mexico, April 10-14, 2011, 46-53.
- Wenk, H.-R., Voltolini, M., Kern, H., Popp, T., and Mazurek, M., 2008, "Anisotropy in shale from Mont Terri," *The Leading Edge*, June 2008, 742-748.
- Wersin, P., Johnson, L.H., and McKinley, I.G., 2007, Performance of the bentonite barrier at temperatures beyond 100°C: A critical review: *Physics and Chemistry of the Earth*, v. 32, p. 780-788.
- Whitney, G. and Northrop, H.R., 1988. Experimental investigation of the smectite to illite reaction: Dual reaction mechanisms and oxygen-isotope systematics. *Am Min.* Vol. 73, p. 77-90.
- Whitney, G. and Velde, B., 1993, Changes in particle morphology during illitization: an experimental study. *Clays and Clay Min.*, Vol. 41, p. 209-218.
- Wu, T.C., Bassett, W., Huang, W.L., Guggenheim, S., and Koster Van Groos, A.F. (1997) Montmorillonite under High H₂O pressures: Stability of Hydrate Phases, Rehydration Hysteresis, and the Effect of Interlayer Cations. *Am. Min.*, Vol. 82, p. 69-78.
- Xia, X., Idemitsu, K., Arima, T., Inagakia, Y., Ishiderab, T., Kurosawa, S., Iijima, K., and Sato, H. (2005) Corrosion of carbon steel in compacted bentonite and its effect on neptunium diffusion under reducing condition. *App. Clay Sci.*, Vol. 28, p. 89-100.

**THERMODYNAMIC DATABASE AND MODEL
DEVELOPMENT FOR CEMENTITIOUS AND CLAY
MATERIALS**

3. Thermodynamic Data and Modeling of Cement and Clay Phases

3.1.1 Thermodynamic Data and Modeling of Cementitious Materials

A description of existing thermodynamic data for cementitious phases was given in the UFD EBS milestone report for FY10 (Jové Colón et al., 2010). This section describes an expansion of that work to include new data, revise existing data, and provide comparisons between data sets. The thermodynamic database developed for the Yucca Mountain Project (YMP) contains 42 cementitious materials plus other associated phases (Wolery and Jové Colón, 2007). Additional data for cementitious materials has been identified and evaluated within the realm of recent modeling schemes for these materials.

Cementitious materials are a fundamental part of EBS design concepts whether these are used in the form of backfill/buffer (e.g., Belgian supercontainer concept), sealing material (WIPP salt repository), and construction material for plugs and linings in tunnels and disposal galleries. Given the ubiquitous presence of cementitious materials and their close interactions with other phases, these are inherently important to the EBS chemical environment. A general literature review on the assessment of thermodynamic data and chemical modeling of cementitious phases provides the basis for evaluating various types of data (e.g., solubility, thermodynamic) and to investigate the effects of solution composition on solubility (leaching) and interactions with other EBS materials and/or phases. Thermodynamic modeling and methods has been recognized as very powerful tools in the evaluation of chemical equilibrium between cement phases, aqueous solutions, and gases (Blanc et al., 2010b; Gartner and Jennings, 1987; Matschei et al., 2007; Reardon, 1990). Furthermore, thermodynamic relations have been widely used in the retrieval of thermodynamic data and parameter testing in the representation of stability relations for these phases. It should be noted that limitations on the applicability of these methods to evaluate and retrieve data have been indicated by various studies given the compositionally complexities of these phases and the overall scarcity of data. Jové-Colón et al. (2010) provided an example of a test case for modeling long-term Ordinary Portland Cement (OPC) leaching experiments reported by Kienzler et al. (2000) and Metz et al. (2004).

The cement phases and selected thermodynamic data in the YMP thermodynamic data compilation are given in Table 3-1. The sources reviewed in Wolery and Jové-Colón (2007), and in this report include the following: Taylor (1990); Reardon (1990); Bruton et al. (1993); Atkins et al. (1992); Neall (1996); Batchelor and Wu (1993); Sarkar et al. (1982); Atkins et al. (1993); Shaw et al. (2000); Glasser et al. (1987); Damidot et al. (1994); Bennett et al. (1992); Babushkin et al. (1985); Greenberg and Chang (1965); Fujii and Kondo (1983); Harvie et al. (1984); MacPhee et al. (1989); Berner (1987, 1990); Greenberg and Moller (1989); Perkins and Palmer (1999); Lothenbach et al. (2010a; 2008); Balonis et al. (2010); Matschei et al. (2007); Blanc et al. (2010a, b). Some of these sources also include previous modeling studies from U.S. and international nuclear waste research programs and emphasis is given to the most recent comprehensive efforts on the chemical and thermodynamic evaluation of cement phases, particularly those by Matschei et al. (2007), Moschner et al. (2008), Blanc et al. (2010a, b), and Lothenbach et al. (2010a; 2008; 2006). The combined efforts of these authors and others essentially comprise the CEMDATA07 thermodynamic database for cementitious phases by the

EMPA institute, ETH, Switzerland. See Table 3-2 footnote for a full list of sources of the CEMDATA07 thermodynamic database.

Additional consideration is given to the description and applications of supplementary cementitious materials (SCMs) in nuclear disposal (Lothenbach et al., 2010b). An example of such type of cement is the one adopted for WIPP in the form of salt-saturated cementitious materials (Poole et al., 1993; Wakeley et al., 1993). As described in Jové-Colón et al. (2010), cement interactions with saline solutions are vulnerable to degradation effects such as Ca loss and formation of Mg and sulfate-bearing phases affecting cement strength (Wakeley et al., 1993). Leaching behavior of salt-saturated cements in the presence of brines has been assessed in studies for the WIPP site (Poole et al., 1993). However, there is an important need for improving our understanding on the effects of brine interactions and sealing performance at elevated temperatures for this type of cementitious materials. Moreover, solubility and leaching data for these phases is scarce and limited to specific cement compositions. Work is planned to expand the existing literature and data (if available) to have a better understand the solubility behavior of these phases. The results of this preliminary work demonstrated the overall agreement in predicted compositional trends in relations to the experimental data.

Most current compilations of thermodynamic and solubility data for cements is limited to pure or nearly-pure end member phases. The main reason is the availability of well-constrained data for cementitious materials having end-member stoichiometric compositions. However, solid solutions in cement phases such as calcium silicate hydrate compounds or C-S-H are very important to leaching scenarios but data is scarce and limited to a few relatively number of studies. Moreover, in the case of C-S-H solids, their dissolution behavior is incongruent and dependent on the Ca/Si ratio of the phase (Berner, 1988, 1992; Greenberg and Chang, 1965; Greenberg et al., 1960; Soler and Mader, 2010). Theoretical treatment of solid solutions for cementitious materials is important in the accurate representation of cement leaching under various solution compositions (Borjesson et al., 1997; Carey and Lichtner, 2007; Kersten, 1996; Kulik and Kersten, 2001; Lichtner and Carey, 2006; Lothenbach et al., 2010a; Sugiyama and Fujita, 2006; Thomas and Jennings, 1998). These studies provide a comprehensive description of the two main types of theoretical approaches applied to the modeling of solid solutions of C-S-H phases: Gibbs energy minimization and mass action law equations (e.g., Lippmann functions; binary non-ideal solid solutions). Both approaches have proven very useful in describing the complex solid-solution behavior and solubility of these phases. Work is planned to implement a Gibbs energy minimization model of C-S-H using the Cantera suite of codes (Moffat and Jové Colón, 2009) to conduct this type of thermodynamic model coupled with equilibrium speciation and phase solubility. The cement phases listed in Table 3-1 are considered common to the hydration of Portland cements and are generally limited to the Ca-Al-Si-S-Mg-H₂O system. The combined compilations of thermodynamic data from various databases and/or literature sources are given in Table 3-2. Ancillary data for aqueous species in all cement reactions are taken from the "SPEQ06.dat" database developed for use with the code SUPCRT92 and described Wolery and Jové-Colón (2007). Data for the calcium silicate hydrate (C-S-H) cement phases are from Fujii and Kondo (1983) and Babushkin et al. (1985); the latter is also adopted as a source to the CEMDATA07 database.

Wolery and Jové-Colón (2007) describes the details of the development of the thermodynamic data for the cement phases in the YMP database “data0.ymp.R5”. To a large extent, the cement phase data is based on the thermodynamic compilation of Babushkin et al. (1985). A comparison logK values for various solubility reactions between the YMP thermodynamic database and CEMDATA07 plus other sources indicates a good level of agreement considering the inherent uncertainties present in this type of data. The listing of logK values for solubility reactions is given in Table 3-3. In some cases, the agreement is excellent as depicted by Figure 3-1a,b for the logK values for hydrogarnet (C_3AH_6) and monosulphate ($3CaO \cdot Al_2O_3 \cdot CaSO_4 \cdot 12H_2O$), respectively, as a function of temperature. The agreement is rather unsurprising given the potential similarities in the thermodynamic data sources used by Blanc et al. (2010a, b). The agreement in logK values also demonstrates the consistency with ancillary data adopted for the aqueous species in the solubility reactions in other database compilations. Note also the remarkable agreement with hydrogarnet and monosulphate solubility data reported to elevated temperatures; e.g., Peppler and Wells (1954), Glasser et al. (1998), Ghorab et al. (1998). However, there are still discrepancies between some logK values between the two databases, for example, for the phases afwillite and CAH_{10} . Still, the majority of these discrepancies are in reasonable agreement with the ranges identified by Blanc et al. (2010a, b) for many cement phases.

3.1.2 Thermodynamic Data and Modeling of Clay Minerals

Clay minerals play various roles in the geologic disposal of nuclear waste. They are nearly ubiquitous at some level in nearly all rock types, ranging from minor alteration components in igneous rocks to major components in sedimentary rocks, notably shales and claystones. Clays may be used as components in an engineered repository, usually in an attempt to limit the access of water to waste containers and/or waste forms. Clays may also form (or transform) in a repository, in response to water circulation and the thermal field that decaying waste may generate. Clay are sheet silicates that have a very wide range of chemical compositions and which exhibit complex behavior. Interpretation of experimental measurement of many clay properties is difficult because of the number of variables that can affect results is generally too high to permit full control. This is particularly true for those clays (smectites and their cousins the vermiculites) that contain exchange layers. These layers permit rapid exchange of cations with external aqueous solution. In addition to cations, they contain a variable amount of water. Various cation substitutions are also possible in the “non-exchange” layers, such as of Al for Si. Kinetically, such substitutions are very slow compared to substitutions in the exchange layers. Clays with no or negligible exchange layers also exist, notably illites and celadonites. These are fairly complex nonetheless. There are also a few simple clays, such as kaolinite, which has a fairly definite chemical composition ($Al_2Si_2O_5(OH)_4$). The thermodynamic properties of these are fairly well known.

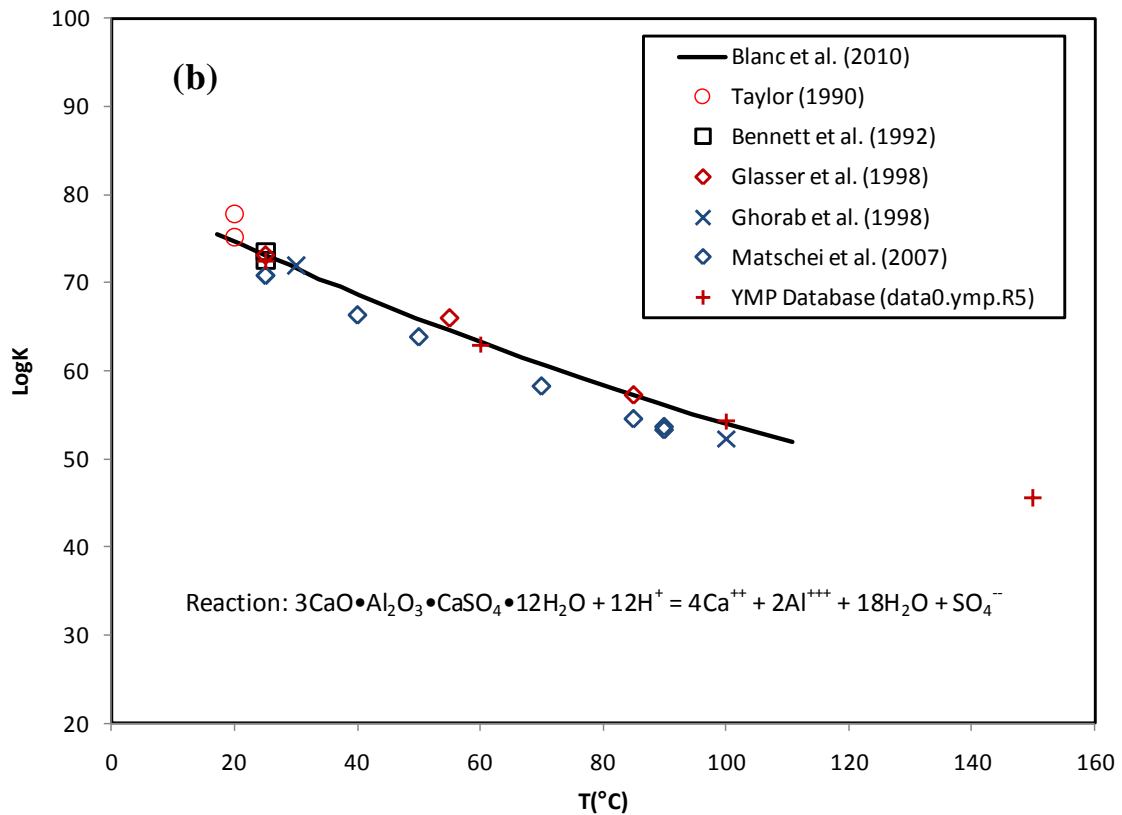
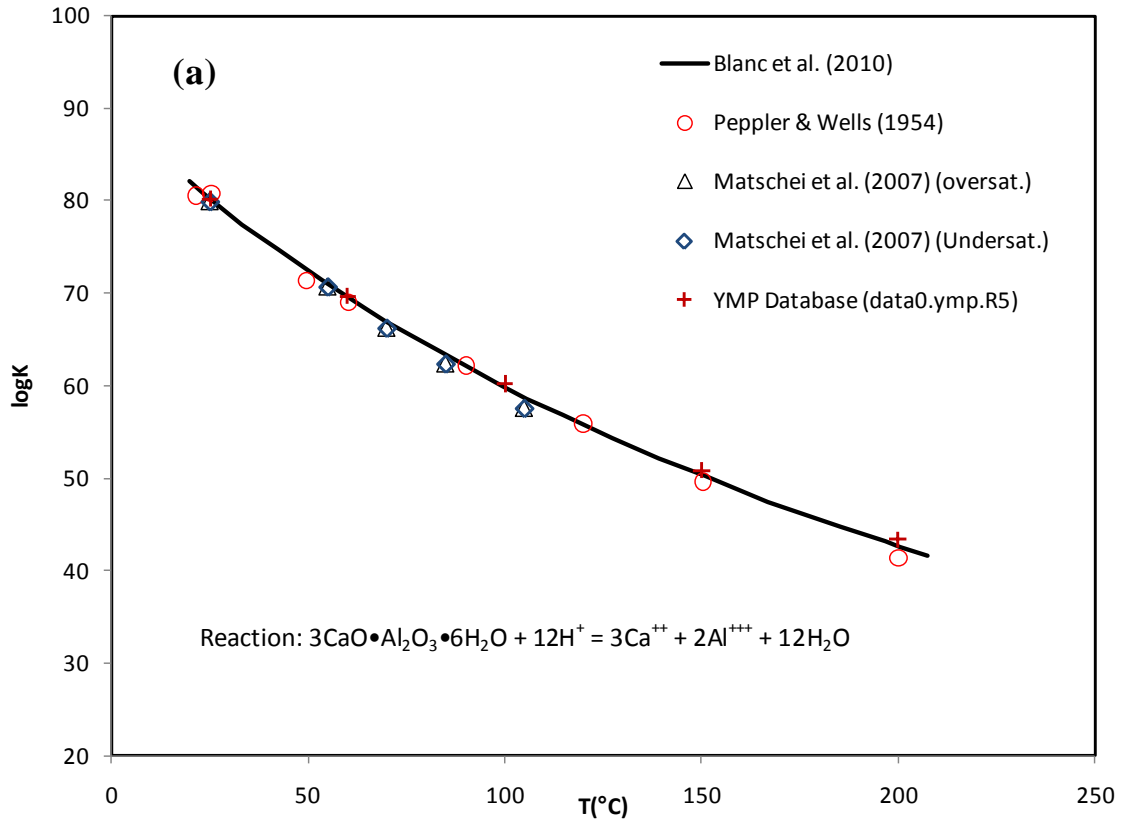


Figure 3-1. Comparison of logK values for the solubility of (a) hydrogarnet and (b) monosulphate.

Table 3-1. Sources of Data for Common Cementitious Phases (after Wolery and Jové-Colón, 2007 and this report)

Cement Phase	Taylor 1990	Reardon 1992	Bruton et al. 1993	Atkins et al. 1992	Neall 1996	Batchelor and Wu 1993	Sarkar et al. 1982	Atkins et al. 1993	Harvie et al. 1984	Bennett et al. 1992	CEMDATA07 ^j + other sources	Included in YMP Database ^d ?
Afwillite	X		X				X	X			X ^m	Y
Allite (C ₃ S)	X	X					X				X	Y
Anhydrite	X	X							X		X ^k	Y
Bellite (C ₂ S)	X	X					X				X	Y
Brucite	X	X		X					X			Y
C ₁₂ A ₇	X						X					Y
C ₂ AH ₈	X					X	X				X	Y
C ₃ A	X	X					X				X	Y
C ₃ AH ₆											X	N
C ₄ AF	X	X									X	Y
C ₄ AH ₁₃	X	X		X		X	X	X			X	Y
C ₄ AH ₁₉	X						X					Y
CA	X						X					Y
CA ₂	X						X					Y
CAH ₁₀	X						X				X	Y
C-S-H ^a	X	X		X	X	X	X	X		X	X	Y
Ettringite	X	X		X	X	X	X	X			X	Y
Ferrite-Ca	X						X					Y
Ferrite-Dicalcium	X						X					Y
Foshagite			X				X				X ^m	Y
Friedl Salt ^b	X					X	X	X				Y
Gehlenite Hydrate ^c	X			X				X		X		25 ^d
Gibbsite	X	X		X							X ^k	Y
Gismondine-Na								X				25 ^d
Gismondine-Ca								X				25 ^d
Gypsum	X			X					X		X ^k	Y
Gyrolite	X		X				X				X ^m	Y
Hillebrandite	X		X				X				X ^m	Y
Hydrogarnet	X	X		X	X		X	X		X	X ^k	Y
Hydrotalcite ^e	X	X		X	X			X		X		25 ^d
Jennite ^a	X							X			X	Y
Monocarboaluminate		X				X		X			X	25 ^d

Table 3-1. Sources of Data for Common Cementitious Phases (Wolery and Jové-Colón, 2007 and this report) (Cont.)

Cement Phase	Taylor 1990	Reardon 1992	Bruton et al. 1993	Atkins et al. 1992	Neill 1996	Batchelor and Wu 1993	Sarkar et al. 1982	Atkins et al. 1993	Harvie et al. 1984	Bennett et al. 1992	CEMDATA07 ^j + other sources	Included in YMP Database?
Monosulphate	X	X		X		X	X	X			X ^l	Y
Nekoite			X									N
Okenite			X				X				X ^m	Y
Periclase	X	X										Y
Plombierite ^f	X		X				X					Y
Portlandite	X	X		X	X				X		X ^k	Y
Reyerite			X									N
Riversideite ^g			X				X					Y
Syngenite	X	X				X			X			25 ^d
Thaumasite	X										X	N
Tobermorite-1.1nm ^h	X		X	X			X	X			X	Y
Truscottite	X		X								X ^m	N
Xonotlite	X		X				X				X ^m	Y
CaSO ₄ ·0.5H ₂ O (beta)												Y
Hemicarboaluminate											X	25 ^d
Tricarboaluminate ⁱ											X	N

^a C-S-H can be a solid solution. Note that Glasser et al. (1987, p. 338) indicates that Portland cement generally hydrates to give a C-S-H composition with a Ca/Si ratio close to 1.7. Matschei et al. (2007) provides data for two types of C-S-H phases: jennite-type (Ca/Si=1.67) and tobermorite-type (Ca/Si=0.83). The C-S-H phase included in the YMP database closely resembles the Ca/Si ration of a jennite-type cement.

^b Often listed as C₃AlCaCl₂·10H₂O or called calcium chloroaluminate hydrate (Taylor 1990). The reported name for this phase in the cement literature is “Friedel’s salt,” not “Friedl Salt.”

^c Also known as strätlingite (Taylor 1990; Matschei et al. (2007)).

^d The annotation “25” indicates 25°C data only. “Y” signifies “yes” and “N” corresponds to “no”.

^e Hydrotalcite referred to here is the formulation of Bennett et al. (1992), not the natural hydrotalcite mineral with a formula of (Mg_{0.75}Al_{0.25}[OH]₂)(CO₃)_{0.125}(H₂O)_{0.5}.

^f 1.4 nm tobermorite is also known as plombierite (Shaw et al. 2000, p. 143).

^g 9 nm tobermorite is known as riversideite (Shaw et al. 2000, p. 143).

^h This is commonly referred to as “normal” tobermorite or tobermorite 11Å.

ⁱ Never reported to occur in cement pastes exposed to intensive carbonation (Damidot et al. 1994, p. 563).

^j Sources for cement phases in CEMDATA07 are given in Table 3-2. CEMDATA07 contains several more phases than those listed in this table. See Table 3-2 for a list of cement phases considered in this database.

^k Considered by Matschei et al. (2007).

^l Reported in Matschei et al. (2007) as monosulfoaluminate.

^m Considered by Blanc et al. (2010a)

Note: Listing includes minerals used in modeling studies. For the cement phase nomenclature, the letter “A” stands for Al₂O₃, “C” for CaO, “S” for SiO₂, and “H” for H₂O components in the cement. The CEMDATA07 database and related data sources was not evaluated for cementitious phases included in the YMP thermodynamic database (Wolery and Jové-Colón, 2007).

Table 3-2. Thermodynamic Properties of Cement Phases from the YMP and Other Thermodynamic Databases.

Phase	Formula	$\Delta_f G^\circ$ (kJ/mol)	$\Delta_f H^\circ$ (kJ/mol)	S° (J/K mol)	C_p (J/K mol)	V° (cm ³ /mol)	Source
Ca-oxychloride hydrate	CaCl ₂ •3CaO•16H ₂ O	-7301.6802	-	-	-	-	[1a]
Friedel's Salt	Ca ₂ Al(OH) ₆ Cl•2H ₂ O	-147.1	-	-	-	-	[2]
	Ca ₄ Al ₂ (OH) _{12.05} Cl _{1.95} •4H ₂ O	-6814.6	-7625	731	829	-	[3]
Kuzen's Salt	Ca ₄ Al ₂ (SO ₄) _{0.5} Cl(OH) ₁₂ •6H ₂ O	-7533.3	-8587	820	929	-	[3]
Gyrolite	Ca ₂ Si ₃ O ₇ (OH) ₂ •1.5H ₂ O	-4542.36	-4919.7564	267.78	-	-	[4]
	Ca ₂ Si ₃ O ₇ (OH) ₂ •2H ₂ O	-4550.06	-4917.99	309.32	325.94	137.34	[5]
Tobermorite	5CaO•6SiO ₂ •5.5H ₂ O	-9880.31	-10695.56	611.49	-	-	[4]
Tobermorite-11	Ca ₅ Si ₆ (OH)O _{16.5} •5H ₂ O	-9889.25	-10680.92	692.55	764.91	-	[5]
Tobermorite-14	Ca ₅ Si ₆ (OH)O _{16.5} •10H ₂ O	-11090.12	-12175.15	874.57	973.53	-	[5]
Foshagite	Ca ₄ Si ₃ O ₉ (OH) ₂ •0.5H ₂ O	-5639.61	-6024.54	330.33	-	-	[4]
	Ca ₄ Si ₃ O ₉ (OH) ₂ •0.5H ₂ O	-5643.83	-6032.43	295.07	309.38	160.66	[5]
Afwillite	Ca ₃ Si ₂ O ₄ (OH) ₆	-4405.54	-4783.15	312.13	-	-	[4]
	Ca ₃ Si ₂ O ₄ (OH) ₆	-4469.06	-4853.82	289.7	303.55	129.53	[5]
Hillebrandite	Ca ₂ SiO ₃ (OH) ₂ •0.17H ₂ O	-2480.69	-2665.84	160.67	-	-	[4]
	Ca ₂ SiO ₃ (OH) ₂ •0.17H ₂ O	-2481.95	-2662.48	179.71	177.46	72.58	[5]
Plombierite	5CaO•6SiO ₂ •10.5H ₂ O	-11076.30	-12180.67	808.14	-	-	[4]
Riversideite	Ca ₅ H ₂ (SiO ₃) ₆ •2H ₂ O	-9267.56	-9937	513.1676	-	-	[4]
Xonotlite	Ca ₆ Si ₆ O ₁₇ (OH) ₂	-9453.33	-10027.79	507.52	-	-	[4]
	Ca ₆ Si ₆ O ₁₇ (OH) ₂	-9465.12	-10022.15	573.74	628.64	256.9	[5]
Okenite	CaSi ₂ O ₄ (OH) ₂ •H ₂ O	-2871.90	-3139.26	171.13	-	-	[4]
	CaSi ₂ O ₄ (OH) ₂ •H ₂ O	-2881.72	-3135.7	208.52	210.07	94.77	[5]

Table 3-2 (cont.) Thermodynamic Properties of Cement Phases from the YMP and Other Thermodynamic Databases.

Phase	Formula	$\Delta_f G^\circ$ (kJ/mol)	$\Delta_f H^\circ$ (kJ/mol)	S° (J/K mol)	C_p (J/K mol)	V° (cm ³ /mol)	Source
Al-Ettringite	Ca ₆ Al ₂ (SO ₄) ₃ (OH) ₁₂ •26H ₂ O	-15205.74	-17578.32	1747.24	-	-	[4]
	Ca ₆ Al ₂ (SO ₄) ₃ (OH) ₁₂ •26H ₂ O	-15205.94	-17535	1900	-	707	[6a,b]
	Ca ₆ Al ₂ (SO ₄) ₃ (OH) ₁₂ •26H ₂ O						[6a,b,c]
Fe-ettringite	Ca ₆ Al ₂ (SO ₄) ₃ (OH) ₁₂ •26H ₂ O	-14282.36	-16600	1937	-	717	[6a,g]
Cr-ettringite	Ca ₆ Al ₂ (CrO ₄) ₃ (OH) ₁₂ •26H ₂ O	-15131	-17330	-	-	-	[1b]
Monosulphate	3CaO•Al ₂ O ₃ •CaSO ₄ •12H ₂ O	-7778.64	-8771.50	747.26	-	-	[4]
	3CaO•Al ₂ O ₃ •CaSO ₄ •12H ₂ O	-7778.5	-8750	821	-	-	[6a,b]
	3CaO•Al ₂ O ₃ •CaSO ₄ •12H ₂ O				-	-	[6a,b,c]
Allite (C ₃ S)	3CaO•SiO ₂	-2784.33	-2930.60	168.62	-	-	[4]
	3CaO•SiO ₂	-2784.33	-2931	169	-	73	[6a,b,d]
Bellite (C ₂ S)	2CaO•SiO ₂	-2193.21	-2308.48	127.61	-	-	[4]
	2CaO•SiO ₂	-2193.21	-2308	128	-	52	[6a,b,d]
C ₁₂ A ₇	12CaO•7Al ₂ O ₃	-18451.44	-19414.43	1044.74	-	-	[4]
C ₂ AH ₈	2CaO•Al ₂ O ₃ •8H ₂ O	-4818.04	-5435.85	445.18	-	-	[4]
	2CaO•Al ₂ O ₃ •8H ₂ O	-4812.76	-5433.00	440.00	-	184	[6a,b]
	2CaO•Al ₂ O ₃ •8H ₂ O						[6a,b,c]
C ₃ A	3CaO•Al ₂ O ₂	-3382.35	-3561	205	-	89	[6a,b,d]
	3CaO•Al ₂ O ₃	-3382.35	-3560.58	205.43	-	-	[4]
C ₄ AF	4CaO•Al ₂ O ₃ •Fe ₂ O ₂	-4786.5	-5080	326	-	130	[6a,b,d]
	4CaO•Al ₂ O ₃ •Fe ₂ O ₃	-4786.5	-5080.21	326.35	-	-	[4]
C ₃ AH ₆ (Hydrogarnet)	3CaO•Al ₂ O ₃ •6H ₂ O	-5014.11	-5547.98	404.59	-	-	[4]
	3CaO•Al ₂ O ₃ •6H ₂ O	-5010.10	-5540.00	419	-	-	[6a,b]
	3CaO•Al ₂ O ₃ •6H ₂ O				-	-	[6a,b,c]

Table 3-2 (cont.) Thermodynamic Properties of Cement Phases from the YMP and Other Thermodynamic Databases.

Phase	Formula	$\Delta_f G^\circ$ (kJ/mol)	$\Delta_f H^\circ$ (kJ/mol)	S° (J/K mol)	C_p (J/K mol)	V° (cm ³ /mol)	Source
C ₄ AH ₁₃	4CaO•Al ₂ O ₃ •13H ₂ O	-7347.82	-8317.79	717.97	-	-	[4]
	4CaO•Al ₂ O ₃ •13H ₂ O	-7326.56	-8302.00	700.00	-	274	[6a,b]
	4CaO•Al ₂ O ₃ •13H ₂ O						[6a,b,c]
C ₄ AH ₁₉	4CaO•Al ₂ O ₃ •19H ₂ O	-8771.04	-10087.62	953.95	-	-	[4]
CA	CaO•Al ₂ O ₃	-2207.90	-2327.06	114.22	-	-	[4]
CA ₂	CaO•2Al ₂ O ₃	-3795.31	-4004.34	177.82	-	-	[4]
CAH ₁₀	CaO•Al ₂ O ₃ •10H ₂ O	-4617.88	-5319.54	485.76	-	-	[4]
	CaO•Al ₂ O ₃ •10H ₂ O	-4622.39	-5320	501	-	194	[6b]
	CaO•Al ₂ O ₃ •10H ₂ O						[6b,c]
C-S-H (1.7)	1.7Ca(OH) ₂ SiO ₂ •0.917H ₂ O	-2630	-2890	200	-	-	[1c]
C-S-H (1.6)	Ca _{1.6} (OH) _{1.54} SiO _{3.6} •1.81H ₂ O	-2550.86	-2819.79	154.42	190.1	84.68	[5]
C _{1.67} SH _{2.1} (Jennite-type)	Ca _{1.67} SiO ₂ (OH) _{3.33} •0.43H ₂ O	-2480.8	-2723	140	-	78	[6a]
C-S-H (1.2)	Ca _{1.2} (OH) _{1.08} SiO _{3.2} •1.52H ₂ O	-2161.23	-2384.34	129.14	162.13	71.95	[5]
C-S-H (0.8)	Ca _{0.8} (OH) _{0.6} SiO _{2.8} •1.24H ₂ O	-1769.03	-1945.13	107.85	138.38	59.29	[5]
Jennite	Ca ₉ Si ₆ O ₁₆ (OH) ₁₀ •6H ₂ O	-13886.77	-15189.04	839.25	933.21	456.4	[5]
C _{0.83} SH _{1.3} (tobermorite type)	0.8333CaO•SiO ₂ •1.3333H ₂ O	-1744.36	-1916	80	-	59	[6a]
Syngenite	K ₂ Ca(SO ₄) ₂ •H ₂ O	-2884.91	-3172	326	-	128	[6e]
	K ₂ Ca(SO ₄) ₂ •H ₂ O	-2886.33	-	-	-	-	[1a]
Truscottite	Ca ₇ Si ₁₂ O ₂₉ (OH) ₄ •H ₂ O	-15280.4	-16854.62	927.68	1034.1	478.73	[5]
Thaumasite	Ca ₆ (SiO ₃) ₂ (SO ₄) ₂ (CO ₃) ₂ •30H ₂ O	-15128.46	-17373	1883	-	663	[6h]
Jaffeite	Ca ₆ (Si ₂ O ₇)(OH) ₆	-6469.94	-6972.77	326.19	344.9	174.38	[5]
C ₂ SH _{1,α}	Ca ₂ (HSiO ₄)(OH)	-2449.12	-2634.92	122.38	111.88	71.12	[5]

Table 3-2 (cont.) Thermodynamic Properties of Cement Phases from the YMP and Other Thermodynamic Databases.

Phase	Formula	$\Delta_f G^\circ$ (kJ/mol)	$\Delta_f H^\circ$ (kJ/mol)	S° (J/K mol)	C_p (J/K mol)	V° (cm ³ /mol)	Source
M ₄ AH ₁₀	Mg ₄ Fe ₂ (OH) ₁₄ •3H ₂ O	-5498.84	-6289	586	-	232	[6a,e,f]
M ₄ A \bar{C} H	Mg ₄ Al ₂ (OH) ₁₂ CO ₃ •3H ₂ O	-6580.15	-7374	551	-	220	[6a,e,f]
M ₄ FH ₁₀	Mg ₄ Fe ₂ (OH) ₁₄ •3H ₂ O	-5498.84	-6289	586	-	232	[6a,f]
Tricarboaluminate	Ca ₆ Al ₂ (CO ₃) ₃ (OH) ₁₂ •26H ₂ O	-14565.64	-16792	1858	-	650	[6a,b]
C ₄ A \bar{C} H ₁₁ (mono-carboaluminate)	Ca ₄ Al ₂ (CO ₃)(OH) ₁₂ •5H ₂ O	-7337.46	-8250	657	-	262	[6a,b]
Mono-carboaluminate	3CaO•Al ₂ O ₃ •CaCO ₃ •10H ₂ O	-7118.89	-	-	-	-	[7]
C ₄ A \bar{C} _{0.5} H ₁₂ (hemi-carboaluminate)	Ca ₄ Al ₂ (CO ₃) _{0.5} (OH) ₁₃ •5.5H ₂ O	-7335.97	-8270	713	-	285	[6a,b]
Hemi-carboaluminate	3CaO•Al ₂ O ₃ •0.5CaCO ₃ •0.5Ca(OH) ₂ •10.5H ₂ O	-7127.193	-	-	-	-	[7]
C ₃ AS _{0.8} H _{4.4}	Ca ₃ Al ₂ (SiO ₄) _{0.8} (OH) _{8.8}	-5368.01	-5855	369	-	143	[6a,b]
C ₂ ASH ₈ (strätlingite)	Ca ₂ Al ₂ SiO ₂ (OH) ₁₀ •3H ₂ O	-5705.15	-6360	546	-	216	[6a,b]
C ₂ FSH ₈ (Fe-strätlingite)	Ca ₂ Fe ₂ SiO ₂ (OH) ₁₀ •3H ₂ O	-4809.53	-5453	583	-	227	[6a,f]
C ₂ FH ₈	Ca ₂ Fe ₂ (OH) ₁₀ •3H ₂ O	-3917.38	-4526	476	-	194	[6a,f]
C ₃ FH ₆	Ca ₃ Fe ₂ (OH) ₁₂	-4116.29	-4640	439	-	155	[6a,b]
C ₄ FH ₁₃	Ca ₄ Fe ₂ (OH) ₁₄ •6H ₂ O	-6430.94	-7395	737	-	286	[6a,f]
C ₄ FSH ₁₂ (Fe-monosulfate)	Ca ₄ Fe ₂ (SO ₄)(OH) ₁₂ •6H ₂ O	-6882.55	-7843	858	-	322	[6a,g]
C ₄ F \bar{C} H ₁₂ (Fe-monocarbonate)	Ca ₄ Fe ₂ (CO ₃)(OH) ₁₂ •5H ₂ O	-6679.2	-7637	737	-	290	[6a,g]
C ₄ F \bar{C} _{0.5} H ₁₂ (Fe-hemicarbonate)	Ca ₄ Fe ₂ (CO ₃) _{0.5} (OH) _{13.5} •5.5H ₂ O	-6440.19	-7363	749	-	296	[6a,f]

¹ data0.ymp.R5 thermodynamic database (Wolery and Jové Colón, 2007): (a) $\Delta_f G^\circ$ retrieved from Harvie et al. 1984 and YMP 'SPEQ06.dat' database; (b) $\Delta_f G^\circ$ obtained using data from Perkins et al. (2000); (c) $\Delta_f G^\circ$ retrieved using data from Fujii and Kondo (1983).

² Birnin-Yauri and Glasser (1998). Two logK values are provided in the source.

³ Balonis et al. (2010)

⁴ data0.ymp.R5 thermodynamic database (Wolery and Jové Colón, 2007). $\Delta_f G^\circ$ retrieved using data from Babushkin et al. (1985); Appendix I.

⁵ Blanc et al. (2010a)

⁶ CEMDATA07: (a) Lothenbach et al. (2008); (b) Matschei et al. (2007); (c) logK conversion made using the YMP 'SPEQ06.dat' database; (d) Babushkin et al. (1985); (e) Lothenbach and Winnefeld (2006); (f) described in the source as tentative values; (g) Möschner et al. (2008); (h) Schmidt et al. (2008).

⁷ data0.ymp.R5 thermodynamic database (Wolery and Jové Colón, 2007). Phase composition different from that in CEMDATA07. Composition after Damidot et al. (1994).

Table 3-3. LogK values at 25°C of Cement Phases from the YMP and Other Thermodynamic Databases.

Phase	Reaction	logK _(298 K)	Source ¹
Ca-oxychloride hydrate	$\text{CaCl}_2 \cdot 3\text{CaO} \cdot 16\text{H}_2\text{O} + 6\text{H}^+ = 4\text{Ca}^{++} + 2\text{Cl}^- + 19\text{H}_2\text{O}$	-56.32	[1a]
Friedel's Salt	$\text{Ca}_4\text{Al}_2(\text{OH})_{12}\text{Cl}_2 \cdot \text{H}_2\text{O} + 6\text{H}^+ = 4\text{Ca}^{++} + 2\text{Al}(\text{OH})_4^- + 2\text{Cl}^- + 4\text{OH}^- + 4\text{H}_2\text{O}$	-27.1 — -24.77	[2]
	$\text{Ca}_4\text{Al}_2(\text{OH})_{12.05}\text{Cl}_{1.95} \cdot 4\text{H}_2\text{O} = 4\text{Ca}^{++} + 2\text{AlO}_2^- + 1.95\text{Cl}^- + 4.05\text{OH}^- + 8\text{H}_2\text{O}$	-27.69	[3]
Kuzen's Salt	$\text{Ca}_4\text{Al}_2(\text{SO}_4)_{0.5}\text{Cl}(\text{OH})_{12} \cdot 6\text{H}_2\text{O} = 4\text{Ca}^{++} + 2\text{AlO}_2^- + \text{Cl}^- + 0.5\text{SO}_4^{--} + 4\text{OH}^- + 10\text{H}_2\text{O}$	-28.53	[3]
Gyrolite	$\text{Ca}_2\text{Si}_3\text{O}_7(\text{OH})_2 \cdot 1.5\text{H}_2\text{O} + 4\text{H}^+ = 2\text{Ca}^{++} + 3\text{SiO}_{2(\text{aq})} + 4.5\text{H}_2\text{O}$	23.68	[4]
	$\text{Ca}_2\text{Si}_3\text{O}_7(\text{OH})_2 \cdot 2\text{H}_2\text{O} + \text{H}_2\text{O} + 4\text{H}^+ = 2\text{Ca}^{++} + 3\text{H}_4\text{SiO}_{4(\text{aq})}$	22.34	[5]
Tobermorite	$5\text{CaO} \cdot 6\text{SiO}_2 \cdot 5.5\text{H}_2\text{O} + 10\text{H}^+ = 5\text{Ca}^{++} + 6\text{SiO}_{2(\text{aq})} + 10.5\text{H}_2\text{O}$	67.15	[4]
Tobermorite-11	$\text{Ca}_5\text{Si}_6(\text{OH})\text{O}_{16.5} \cdot 5\text{H}_2\text{O} + 10\text{H}^+ + 1.5\text{H}_2\text{O} = 5\text{Ca}^{++} + 6\text{H}_4\text{SiO}_{4(\text{aq})}$	65.58	[5]
Tobermorite-14	$\text{Ca}_5\text{Si}_6(\text{OH})\text{O}_{16.5} \cdot 10\text{H}_2\text{O} + 10\text{H}^+ = 5\text{Ca}^{++} + 3.5\text{H}_2\text{O} + 6\text{H}_4\text{SiO}_{4(\text{aq})}$	62.94	[5]
Foshagite	$\text{Ca}_4\text{Si}_3\text{O}_9(\text{OH})_2 \cdot 0.5\text{H}_2\text{O} + 8\text{H}^+ = 4\text{Ca}^{++} + 3\text{SiO}_{2(\text{aq})} + 5.5\text{H}_2\text{O}$	66.69	[4]
	$\text{Ca}_4\text{Si}_3\text{O}_9(\text{OH})_2 \cdot 0.5\text{H}_2\text{O} + 8\text{H}^+ + 0.5\text{H}_2\text{O} = 4\text{Ca}^{++} + 3\text{H}_4\text{SiO}_{4(\text{aq})}$	65.96	[5]
Afwillite	$\text{Ca}_3\text{Si}_2\text{O}_4(\text{OH})_6 + 6\text{H}^+ = 3\text{Ca}^{++} + 2\text{SiO}_{2(\text{aq})} + 6\text{H}_2\text{O}$	60.56	[4]
	$\text{Ca}_3\text{Si}_2\text{O}_4(\text{OH})_6 + 6\text{H}^+ = 3\text{Ca}^{++} + 2\text{H}_2\text{O} + 2\text{H}_4\text{SiO}_{4(\text{aq})}$	49.42	[5]
Hillebrandite	$\text{Ca}_2\text{SiO}_3(\text{OH})_2 \cdot 0.17\text{H}_2\text{O} + 4\text{H}^+ = 2\text{Ca}^{++} + \text{SiO}_{2(\text{aq})} + 3.17\text{H}_2\text{O}$	37.08	[4]
	$\text{Ca}_2\text{SiO}_3(\text{OH})_2 \cdot 0.17\text{H}_2\text{O} + 4\text{H}^+ = 2\text{Ca}^{++} + 1.17\text{H}_2\text{O} + \text{H}_4\text{SiO}_{4(\text{aq})}$	36.95	[5]
Plombierite	$5\text{CaO} \cdot 6\text{SiO}_2 \cdot 10.5\text{H}_2\text{O} + 10\text{H}^+ = 5\text{Ca}^{++} + 6\text{SiO}_{2(\text{aq})} + 15.5\text{H}_2\text{O}$	65.38	[4]
Riversideite	$\text{Ca}_5\text{H}_2(\text{SiO}_3)_6 \cdot 2\text{H}_2\text{O} + 10\text{H}^+ = 5\text{Ca}^{++} + 6\text{SiO}_{2(\text{aq})} + 8\text{H}_2\text{O}$	70.62	[4]
Xonotlite	$\text{Ca}_6\text{Si}_6\text{O}_{17}(\text{OH})_2 + 12\text{H}^+ = 6\text{Ca}^{++} + 6\text{SiO}_{2(\text{aq})} + 7\text{H}_2\text{O}$	93.37	[4]
	$\text{Ca}_6\text{Si}_6\text{O}_{17}(\text{OH})_2 + 12\text{H}^+ + 5\text{H}_2\text{O} = 6\text{Ca}^{++} + 6\text{H}_4\text{SiO}_{4(\text{aq})}$	91.34	[5]
Okenite	$\text{CaSi}_2\text{O}_4(\text{OH})_2 \cdot \text{H}_2\text{O} + 2\text{H}^+ = \text{Ca}^{++} + 2\text{SiO}_{2(\text{aq})} + 3\text{H}_2\text{O}$	10.89	[4]
	$\text{CaSi}_2\text{O}_4(\text{OH})_2 \cdot \text{H}_2\text{O} + 2\text{H}^+ + \text{H}_2\text{O} = \text{Ca}^{++} + 2\text{H}_4\text{SiO}_{4(\text{aq})}$	9.18	[5]
Al-Ettringite	$\text{Ca}_6\text{Al}_2(\text{SO}_4)_3(\text{OH})_{12} \cdot 26\text{H}_2\text{O} + 12\text{H}^+ = 6\text{Ca}^{++} + 2\text{Al}^{+++} + 3\text{SO}_4^{--} + 38\text{H}_2\text{O}$	56.88	[4]
	$\text{Ca}_6\text{Al}_2(\text{SO}_4)_3(\text{OH})_{12} \cdot 26\text{H}_2\text{O} = 6\text{Ca}^{++} + 2\text{Al}(\text{OH})_4^- + 3\text{SO}_4^{--} + 4\text{OH}^- + 26\text{H}_2\text{O}$	-44.9	[6a,b]
	$\text{Ca}_6\text{Al}_2(\text{SO}_4)_3(\text{OH})_{12} \cdot 26\text{H}_2\text{O} + 12\text{H}^+ = 6\text{Ca}^{++} + 2\text{Al}^{+++} + 3\text{SO}_4^{--} + 38\text{H}_2\text{O}$	55.49	[6a,b,c]

Table 3-3 (cont.) LogK values at 25°C of Cement Phases from the YMP and Other Thermodynamic Databases.

Phase	Reaction	logK _(298 K)	Source ¹
Fe-ettringite	$\text{Ca}_6\text{Fe}_2(\text{SO}_4)_3(\text{OH})_{12} \cdot 26\text{H}_2\text{O} = 6\text{Ca}^{++} + 2\text{Fe}(\text{OH})_4^- + 3\text{SO}_4^{--} + 4\text{OH}^- + 26\text{H}_2\text{O}$	-44	[6a,g]
Cr-ettringite	$\text{Ca}_6\text{Al}_2(\text{CrO}_4)_3(\text{OH})_{12} \cdot 26\text{H}_2\text{O} + 12\text{H}^+ = 6\text{Ca}^{++} + 2\text{Al}^{+++} + 3\text{CrO}_4^- + 38\text{H}_2\text{O}$	59	[1b]
Monosulphate	$3\text{CaO} \cdot \text{Al}_2\text{O}_3 \cdot \text{CaSO}_4 \cdot 12\text{H}_2\text{O} + 12\text{H}^+ = 4\text{Ca}^{++} + 2\text{Al}^{+++} + 18\text{H}_2\text{O} + \text{SO}_4^{--}$	72.47	[4]
	$3\text{CaO} \cdot \text{Al}_2\text{O}_3 \cdot \text{CaSO}_4 \cdot 12\text{H}_2\text{O} + 12\text{H}^+ = 4\text{Ca}^{++} + 2\text{Al}(\text{OH})_4^- + \text{SO}_4^{--} + 4\text{OH}^- + 6\text{H}_2\text{O}$	-29.26	[6a,b]
	$3\text{CaO} \cdot \text{Al}_2\text{O}_3 \cdot \text{CaSO}_4 \cdot 12\text{H}_2\text{O} + 12\text{H}^+ = 4\text{Ca}^{++} + 2\text{Al}^{+++} + 18\text{H}_2\text{O} + \text{SO}_4^{--}$	71.13	[6a,b,c]
Allite (C ₃ S)	$3\text{CaO} \cdot \text{SiO}_2 + 6\text{H}^+ = 3\text{Ca}^{++} + \text{SiO}_2 + 3\text{H}_2\text{O}$	73.66	[4]
	-	-	[6a,b,d]
Bellite (C ₂ S)	$2\text{CaO} \cdot \text{SiO}_2 + 4\text{H}^+ = 2\text{Ca}^{++} + \text{SiO}_2 + 2\text{H}_2\text{O}$	38.82	[4]
	-	-	[6a,b,d]
C ₁₂ A ₇	$12\text{CaO} \cdot 7\text{Al}_2\text{O}_3 + 66\text{H}^+ = 12\text{Ca}^{++} + 14\text{Al}^{+++} + 33\text{H}_2\text{O}$	-	[4]
C ₂ AH ₈	$2\text{CaO} \cdot \text{Al}_2\text{O}_3 \cdot 8\text{H}_2\text{O} + 10\text{H}^+ = 2\text{Ca}^{++} + 2\text{Al}^{+++} + 13\text{H}_2\text{O}$	59.27	[4]
	$2\text{CaO} \cdot \text{Al}_2\text{O}_3 \cdot 8\text{H}_2\text{O} = 2\text{Ca}^{++} + 2\text{Al}(\text{OH})_4^- + 2\text{OH}^- + 3\text{H}_2\text{O}$	-13.56	[6a,b]
	$2\text{CaO} \cdot \text{Al}_2\text{O}_3 \cdot 8\text{H}_2\text{O} + 10\text{H}^+ = 2\text{Ca}^{++} + 2\text{Al}^{+++} + 13\text{H}_2\text{O}$	58.84	[6a,b,c]
C ₃ A	-	-	[6a,b,d]
	$3\text{CaO} \cdot \text{Al}_2\text{O}_3 + 12\text{H}^+ = 3\text{Ca}^{++} + 2\text{Al}^{+++} + 6\text{H}_2\text{O}$	116.77	[4]
C ₄ AF	-	-	[6a,b,d]
	$4\text{CaO} \cdot \text{Al}_2\text{O}_3 \cdot \text{Fe}_2\text{O}_3 + 20\text{H}^+ = 4\text{Ca}^{++} + 2\text{Al}^{+++} + 2\text{Fe}^{+++} + 10\text{H}_2\text{O}$	139.87	[4]
C ₃ AH ₆ (Hydrogarnet)	$3\text{CaO} \cdot \text{Al}_2\text{O}_3 \cdot 6\text{H}_2\text{O} + 12\text{H}^+ = 3\text{Ca}^{++} + 2\text{Al}^{+++} + 12\text{H}_2\text{O}$	80.21	[4]
	$3\text{CaO} \cdot \text{Al}_2\text{O}_3 \cdot 6\text{H}_2\text{O} = 3\text{Ca}^{++} + 2\text{AlO}_2^- + 4\text{H}_2\text{O} + 4\text{OH}^-$	-20.84	[6a,b]
	$3\text{CaO} \cdot \text{Al}_2\text{O}_3 \cdot 6\text{H}_2\text{O} + 12\text{H}^+ = 3\text{Ca}^{++} + 2\text{Al}^{+++} + 12\text{H}_2\text{O}$	79.55	[6a,b,c]
C ₄ AH ₁₃	$4\text{CaO} \cdot \text{Al}_2\text{O}_3 \cdot 13\text{H}_2\text{O} + 14\text{H}^+ = 4\text{Ca}^{++} + 2\text{Al}^{+++} + 20\text{H}_2\text{O}$	100.63	[4]
	$\text{Ca}_4\text{Al}_2(\text{OH})_{14} \cdot 6\text{H}_2\text{O} = 4\text{Ca}^{++} + 2\text{Al}(\text{OH})_4^- + 6\text{OH}^- + 6\text{H}_2\text{O}$	-25.4	[6a,b]
	$\text{Ca}_4\text{Al}_2(\text{OH})_{14} \cdot 6\text{H}_2\text{O} + 6\text{H}^+ = 4\text{Ca}^{++} + 2\text{Al}^{+++} + 16\text{H}_2\text{O}$	102.98	[6a,b,c]

Table 3-3 (cont.) LogK values at 25°C of Cement Phases from the YMP and Other Thermodynamic Databases.

Phase	Reaction	logK _(298 K)	Source ¹
C ₄ AH ₁₉	4CaO•Al ₂ O ₃ •19H ₂ O + 14H ⁺ = 4Ca ⁺⁺ + 2Al ⁺⁺⁺ + 26H ₂ O	100.6	[4]
CA	CaO•Al ₂ O ₃ + 8H ⁺ = Ca ⁺⁺ + 2Al ⁺⁺⁺ + 4H ₂ O	45.73	[4]
CA ₂	CaO•2Al ₂ O ₃ + 14H ⁺ = Ca ⁺⁺ + 4Al ⁺⁺⁺ + 7H ₂ O	61.77	[4]
CAH ₁₀	CaO•Al ₂ O ₃ •10H ₂ O + 8H ⁺ = Ca ⁺⁺ + 2Al ⁺⁺⁺ + 14H ₂ O	39.04	[4]
	CaO•Al ₂ O ₃ •10H ₂ O = Ca ⁺⁺ + 2Al(OH) ₄ ⁻ + 6H ₂ O	-7.5	[6b]
	CaO•Al ₂ O ₃ •10H ₂ O + 8H ⁺ = Ca ⁺⁺ + 2Al ⁺⁺⁺ + 14H ₂ O	36.91	[6b,c]
C-S-H (1.7)	1.7Ca(OH) ₂ SiO ₂ •0.917H ₂ O + 3.4H ⁺ = 1.7Ca ⁺⁺ + SiO ₂ + 4.317H ₂ O	29.53	[1c]
C-S-H (1.6)	Ca _{1.6} (OH) _{1.54} SiO _{3.6} •1.81H ₂ O + 3.2H ⁺ = 1.6Ca ⁺⁺ + H ₄ SiO _{4(aq)} + 2.18H ₂ O	28.00	[5]
C _{1.67} SH _{2.1} (Jennite-type)	Ca _{1.67} (OH) _{3.33} SiO _{3.2} •0.43H ₂ O + 3.2H ⁺ = 1.67Ca ⁺⁺ + HSiO ₃ ⁻ + 2.33OH ⁻ + 0.43H ₂ O	-13.17	[6a]
C-S-H (1.2)	Ca _{1.2} (OH) _{1.08} SiO _{3.2} •1.52H ₂ O + 2.4H ⁺ = 1.2Ca ⁺⁺ + H ₄ SiO _{4(aq)} + 1.26H ₂ O	19.3	[5]
C-S-H (0.8)	Ca _{0.8} (OH) _{0.6} SiO _{2.8} •1.24H ₂ O + 2.4H ⁺ = 0.8Ca ⁺⁺ + H ₄ SiO _{4(aq)} + 0.34H ₂ O	11.05	[5]
Jennite	Ca ₉ Si ₆ O ₁₆ (OH) ₁₀ •6H ₂ O + 18H ⁺ = 9Ca ⁺⁺ + 6H ₄ SiO _{4(aq)} + 8H ₂ O	147.33	[5]
C _{0.83} SH _{1.3} (tobermorite type)	Ca _{0.8333} •SiO ₂ •1.3333H ₂ O + 0.5 H ₂ O = 0.8333Ca ⁺⁺ + H ₃ SiO ₄ ⁻ + 0.6667OH ⁻	-8	[6a]
Syngenite	K ₂ Ca(SO ₄) ₂ •H ₂ O = 2K ⁺ + Ca ⁺⁺ + SO ₄ ⁻ + H ₂ O	-7.2	[6e]
	K ₂ Ca(SO ₄) ₂ •H ₂ O = 2K ⁺ + Ca ⁺⁺ + SO ₄ ⁻ + H ₂ O	-7.45	[1a]
Truscottite	Ca ₇ Si ₁₂ O ₂₉ (OH) ₄ •H ₂ O + 14H ⁺ + 14H ₂ O = 7Ca ⁺⁺ + 12H ₄ SiO _{4(aq)}	77.08	[5]
Thaumasite	Ca ₆ (SiO ₃) ₂ (SO ₄) ₂ (CO ₃) ₂ •30H ₂ O = 6Ca ⁺⁺ + 2H ₃ SiO ₄ ⁻ + 2SO ₄ ⁻ + 2OH ⁻ + 2CO ₃ ⁻ + 26H ₂ O	-49.40	[6h]
Jaffeite	Ca ₆ (Si ₂ O ₇)(OH) ₆ + 12H ⁺ = 6Ca ⁺⁺ + 5H ₂ O + 2H ₄ SiO _{4(aq)}	114.06	[5]
C ₂ SH _α	Ca ₂ (HSiO ₄)(OH) + 4H ⁺ = 2Ca ⁺⁺ + H ₂ O + H ₄ SiO _{4(aq)}	35.54	[5]
M ₄ AH ₁₀	Mg ₄ Fe ₂ (OH) ₁₄ •3H ₂ O = 4Mg ⁺⁺ + 2Fe(OH) ₄ ⁻ + 6OH ⁻ + 3H ₂ O	-60	[6a,e,f]
M ₄ A \bar{C} H	Mg ₄ Al ₂ (OH) ₁₂ CO ₃ •3H ₂ O = 4Mg ⁺⁺ + 2Al(OH) ₄ ⁻ + CO ₃ ⁻ + 4OH ⁻ + 3H ₂ O	-51.14	[6a,e,f]
M ₄ FH ₁₀	Mg ₄ Fe ₂ (OH) ₁₄ •3H ₂ O = 4Mg ⁺⁺ + 2Fe(OH) ₄ ⁻ + 6OH ⁻ + 3H ₂ O	-60	[6a,f]

Table 3-3 (cont.) LogK values at 25°C of Cement Phases from the YMP and Other Thermodynamic Databases.

Phase	Reaction	logK _(298 K)	Source ¹
Tricarboaluminate	$\text{Ca}_6\text{Al}_2(\text{CO}_3)_3(\text{OH})_{12} \cdot 26\text{H}_2\text{O} = 6\text{Ca}^{++} + 2\text{Al}(\text{OH})_4^- + 3\text{CO}_3^{--} + 4\text{OH}^- + 26\text{H}_2\text{O}$	-46.5	[6a,b]
$\text{C}_4\text{A}\bar{\text{C}}\text{H}_{11}$ (mono-carboaluminate)	$\text{Ca}_4\text{Al}_2(\text{CO}_3)(\text{OH})_{12} \cdot 5\text{H}_2\text{O} = 4\text{Ca}^{++} + 2\text{Al}(\text{OH})_4^- + \text{CO}_3^{--} + 4\text{OH}^- + 5\text{H}_2\text{O}$	-31.47	[6a,b]
Mono-carboaluminate	$3\text{CaO} \cdot \text{Al}_2\text{O}_3 \cdot \text{CaCO}_3 \cdot 10\text{H}_2\text{O} + 13 \text{H}^+ = 4 \text{Ca}^{2+} + 2 \text{Al}^{3+} + \text{HCO}_3^- + 16 \text{H}_2\text{O}$	77.35	[7]
$\text{C}_4\text{A}\bar{\text{C}}_{0.5}\text{H}_{12}$ (hemi-carboaluminate)	$\text{Ca}_4\text{Al}_2(\text{CO}_3)_{0.5}(\text{OH})_{13} \cdot 5.5\text{H}_2\text{O} = 4\text{Ca}^{++} + 2\text{AlO}_2^- + 0.5\text{CO}_3^{--} + 5\text{OH}^- + 5.5\text{H}_2\text{O}$	-29.13	[6a,b]
Hemi-carboaluminate	Hemi-carboaluminate + 13.5 H ⁺ = 4Ca ⁺⁺ + 2Al ⁺⁺⁺ + 0.5HCO ₃ ⁻ + 17.5H ₂ O	88.32	[7]
$\text{C}_3\text{AS}_{0.8}\text{H}_{4.4}$	$\text{Ca}_3\text{Al}_2(\text{SiO}_4)_{0.8}(\text{OH})_{8.8} + 2.4\text{H}_2\text{O} = 2\text{Ca}^{++} + 2\text{Al}(\text{OH})_4^- + 0.8\text{H}_3\text{SiO}_4^- + 3.2\text{OH}^-$	-29.87	[6a,b]
C_2ASH_8 (strätlingite)	$\text{Ca}_2\text{Al}_2\text{SiO}_2(\text{OH})_{10} \cdot 3\text{H}_2\text{O} = 2\text{Ca}^{++} + 2\text{Al}(\text{OH})_4^- + \text{H}_3\text{SiO}_4^- + \text{OH}^- + 2\text{H}_2\text{O}$	-19.7	[6a,b]
C_2FSH_8 (Fe-strätlingite)	$\text{Ca}_2\text{Fe}_2\text{SiO}_2(\text{OH})_{10} \cdot 3\text{H}_2\text{O} = 2\text{Ca}^{++} + 2\text{Fe}(\text{OH})_4^- + \text{H}_3\text{SiO}_4^- + \text{OH}^- + 2\text{H}_2\text{O}$	-23.7	[6a,f]
C_2FH_8	$\text{Ca}_2\text{Fe}_2(\text{OH})_{10} \cdot 3\text{H}_2\text{O} = 2\text{Ca}^{++} + 2\text{Fe}(\text{OH})_4^- + 2\text{OH}^- + 3\text{H}_2\text{O}$	-17.6	[6a,f]
C_3FH_6	$\text{Ca}_3\text{Fe}_2(\text{OH})_{12} = 3\text{Ca}^{++} + 2\text{Fe}(\text{OH})_4^- + 4\text{OH}^-$	-25.16	[6a,b]
C_4FH_{13}	$\text{Ca}_4\text{Fe}_2(\text{OH})_{14} \cdot 6\text{H}_2\text{O} = 4\text{Ca}^{++} + 2\text{Fe}(\text{OH})_4^- + 6\text{OH}^- + 6\text{H}_2\text{O}$	-29.4	[6a,f]
$\text{C}_4\text{FSH}_{12}$ (Fe-monosulfate)	$\text{Ca}_4\text{Fe}_2(\text{SO}_4^-)(\text{OH})_{12} \cdot 6\text{H}_2\text{O} = 4\text{Ca}^{++} + 2\text{Fe}(\text{OH})_4^- + \text{SO}_4^{--} + 4\text{OH}^- + 6\text{H}_2\text{O}$	-33.2	[6a,g]
$\text{C}_4\text{F}\bar{\text{C}}\text{H}_{12}$ (Fe-monocarbonate)	$\text{Ca}_4\text{Fe}_2(\text{CO}_3)(\text{OH})_{12} \cdot 5\text{H}_2\text{O} = 4\text{Ca}^{++} + 2\text{Fe}(\text{OH})_4^- + \text{CO}_3^{--} + 4\text{OH}^- + 5\text{H}_2\text{O}$	-35.5	[6a,g]
$\text{C}_4\text{F}\bar{\text{C}}_{0.5}\text{H}_{12}$ (Fe-hemicarbonate)	$\text{Ca}_4\text{Fe}_2(\text{CO}_3)_{0.5}(\text{OH})_{13.5} \cdot 5.5\text{H}_2\text{O} = 4\text{Ca}^{++} + 2\text{Fe}(\text{OH})_4^- + 0.5\text{CO}_3^{--} + 5\text{OH}^- + 5.5\text{H}_2\text{O}$	-33.1	[6a,f]

Note: The listing of cement phases and solubility reactions map those listed in Table 3-2.

¹ Sources given in the Table 3-2 footnote.

Thermodynamic data and models for the complex clays (including the all-important smectites and illites) have always been problematic to geochemists. Typical experimental approaches such as solubility and calorimetry have been of limited value owing to the reactive nature of these phases and the difficulty in adequately characterizing them. Thus, models are generally used to estimate the relevant thermodynamic data from corresponding data for related phases, generally including kaolinite (which is a clay) and non-clay sheet silicates including various micas and chlorites. One of the best known of these is the model of Tardy and Garrels (1974), which derives data for the Gibbs energies of “silicate” oxide components from the known Gibbs energies of the related sheet silicates (kaolinite, micas, chlorites). A similar set of data for oxide components corresponding to exchangeable cations (e.g., $\text{Na}_2\text{O}_{(\text{ex})}$) is derived from ion exchange data. Estimated values for other thermodynamic properties (entropies, heat capacities, and molar volumes) can be estimated by a variety of similar “additive” or quasi-additive schemes (Helgeson et al., 1978; Ransom and Helgeson, 1994a, b). Using such schemes, one can estimate the properties of a complex clay mineral such as an idealized Ca-beidellite ($\text{Ca}_{0.165}\text{Al}_{2.33}\text{Si}_{3.67}\text{O}_{10}(\text{OH})_2$ (beidellites are a variety of smectite). For greater accuracy, such estimations may be made by using component oxide substitutions starting with a closely related phase for which real data exist, as opposed to using just component oxides. In the case of the beidellites, the closely related phase would be pyrophyllite ($\text{Al}_2\text{Si}_4\text{O}_{10}(\text{OH})_2$). Another twist is to account for mixing effects, using the basic estimation methods to define the properties of end-members, and assuming (usually) ideal mixing in the site-mixing sense to define the properties of phases of intermediate composition.

Geochemical modeling (including reactive transport modeling) generally uses such estimation methods to generate data for the complex clays. The last YMP thermodynamic database (data0.ymp.R5) contains data derived by such means for the complex clays shown below in Table 3-4. A detailed description of the methods and derivation of the corresponding thermodynamic data is given in the Analysis/Model Report ANL-WIS-GS-000003 (Rev. 01). Data were obtained for five idealized beidellites, five idealized montmorillonites, five idealized saponites, five idealized nontronites, three complex smectites, an illite, and three idealized celadonites. The beidellite, montmorillonite, saponite, and nontronite data were intended to be used in solid solution models in modeling software. Some data were also obtained by the same process for some chlorite and chlorite-related sheet silicates, though these will not be noted here.

Table 3-4. Complex clay minerals included in the last YMP thermodynamic database.

Phase	Formula
Na-Beidellite	$\text{Na}_{0.33}\text{Al}_{2.33}\text{Si}_{3.67}\text{O}_{10}(\text{OH})_2$
K-Beidellite	$\text{K}_{0.33}\text{Al}_{2.33}\text{Si}_{3.67}\text{O}_{10}(\text{OH})_2$
H-Beidellite	$\text{H}_{0.33}\text{Al}_{2.33}\text{Si}_{3.67}\text{O}_{10}(\text{OH})_2$
Ca-Beidellite	$\text{Ca}_{0.165}\text{Al}_{2.33}\text{Si}_{3.67}\text{O}_{10}(\text{OH})_2$
Mg-Beidellite	$\text{Mg}_{0.165}\text{Al}_{2.33}\text{Si}_{3.67}\text{O}_{10}(\text{OH})_2$
Na-Montmorillonite	$\text{Na}_{0.33}\text{Mg}_{0.33}\text{Al}_{1.67}\text{Si}_4\text{O}_{10}(\text{OH})_2$
K-Montmorillonite	$\text{K}_{0.33}\text{Mg}_{0.33}\text{Al}_{1.67}\text{Si}_4\text{O}_{10}(\text{OH})_2$
H-Montmorillonite	$\text{H}_{0.33}\text{Mg}_{0.33}\text{Al}_{1.67}\text{Si}_4\text{O}_{10}(\text{OH})_2$
Ca-Montmorillonite	$\text{Ca}_{0.165}\text{Mg}_{0.33}\text{Al}_{1.67}\text{Si}_4\text{O}_{10}(\text{OH})_2$
Mg-Montmorillonite	$\text{Mg}_{0.495}\text{Al}_{1.67}\text{Si}_4\text{O}_{10}(\text{OH})_2$
Na-Saponite	$\text{Na}_{0.33}\text{Mg}_3\text{Al}_{0.33}\text{Si}_{3.67}\text{O}_{10}(\text{OH})_2$
K-Saponite	$\text{K}_{0.33}\text{Mg}_3\text{Al}_{0.33}\text{Si}_{3.67}\text{O}_{10}(\text{OH})_2$
H-Saponite	$\text{H}_{0.33}\text{Mg}_3\text{Al}_{0.33}\text{Si}_{3.67}\text{O}_{10}(\text{OH})_2$
Ca-Saponite	$\text{Ca}_{0.165}\text{Mg}_3\text{Al}_{0.33}\text{Si}_{3.67}\text{O}_{10}(\text{OH})_2$
Mg-Saponite	$\text{Mg}_{3.165}\text{Al}_{0.33}\text{Si}_{3.67}\text{O}_{10}(\text{OH})_2$
Na-Nontronite	$\text{Na}_{0.33}\text{Fe}_2\text{Al}_{0.33}\text{Si}_{3.67}\text{O}_{10}(\text{OH})_2$
K-Nontronite	$\text{K}_{0.33}\text{Fe}_2\text{Al}_{0.33}\text{Si}_{3.67}\text{O}_{10}(\text{OH})_2$
H-Nontronite	$\text{H}_{0.33}\text{Fe}_2\text{Al}_{0.33}\text{Si}_{3.67}\text{O}_{10}(\text{OH})_2$
Ca-Nontronite	$\text{Ca}_{0.165}\text{Fe}_2\text{Al}_{0.33}\text{Si}_{3.67}\text{O}_{10}(\text{OH})_2$
Mg-Nontronite	$\text{Mg}_{0.165}\text{Fe}_2\text{Al}_{0.33}\text{Si}_{3.67}\text{O}_{10}(\text{OH})_2$
High Fe-Mg Smectite	$\text{Na}_{0.1}\text{K}_{0.2}\text{Ca}_{0.025}(\text{Mg}_{1.15}\text{Fe}^{3+}_{0.2}\text{Fe}^{2+}_{0.5}\text{Al}_{0.75})(\text{Al}_{0.5}\text{Si}_{3.5})\text{O}_{10}(\text{OH})_2$
Low Fe-Mg Smectite	$\text{Na}_{0.15}\text{K}_{0.2}\text{Ca}_{0.02}(\text{Mg}_{0.9}\text{Fe}^{3+}_{0.16}\text{Fe}^{2+}_{0.29}\text{Al})(\text{Al}_{0.25}\text{Si}_{3.75})\text{O}_{10}(\text{OH})_2$
Reykjanes Smectite	$\text{Na}_{0.33}\text{K}_{0.03}\text{Ca}_{0.66}(\text{Mg}_{1.29}\text{Fe}^{3+}_{0.35}\text{Fe}^{2+}_{0.33}\text{Mn}_{0.01}\text{Al}_{0.28})(\text{Al}_{0.83}\text{Si}_{3.17})\text{O}_{10}(\text{OH})_2$
Illite	$\text{K}_{0.6}\text{Mg}_{0.25}\text{Al}_{2.3}\text{Si}_{3.5}\text{O}_{10}(\text{OH})_2$
Celadonite	$\text{KMgAlSi}_4\text{O}_{10}(\text{OH})_2$
Ferroaluminoceladonite	$\text{KFeAlSi}_4\text{O}_{10}(\text{OH})_2$
Ferroceladonite	$\text{KFeFeSi}_4\text{O}_{10}(\text{OH})_2$

In the above derivations, the actual amount of water in the exchange layer of a smectite (beidellite, montmorillonite, saponite, nontronite, or “smectite”) was not taken into account (this water does not include the water that is structurally bound in the $(\text{OH})_2$ part of the formula). In deriving the data for the Na-beidellite, for example, the exchangeable sodium was represented by the $\text{Na}_2\text{O}_{(\text{ex})}$ component. The associated water can be thought of as being dealt with implicitly, although the argument for this is perhaps not strong. Interestingly, using the silicate Na_2O component instead would yield data for the dehydrated equivalent of this hydrated clay, which is something that we intend to do in future development. We note that data for exchangeable oxide components was based only on 25°C data, and that the temperature dependence of the properties of the

exchangeable components was assumed to be the same as those of the corresponding non-exchangeable components. This reduces the reliability of the estimated data at elevated temperature (in particular, the stabilities of affected clays with respect to other minerals becomes more uncertain). Also, because the water in the exchange layer is treated implicitly, dehydration cannot be properly accounted for.

We intend to improve the existing data/models for complex clays by:

- Explicitly accounting for water in the exchange layers of smectites and vermiculites;
- Accounting for a broader spectrum of physical measurements (e.g., basal spacing studies of clay dehydration, swelling pressure data, ion exchange data over a wide range of temperature);
- Including insights from molecular dynamics (MD) modeling regarding dehydration.

For example, for a fully hydrated smectite (100% relative humidity or unit water activity), the number of waters in the exchange layer appears to be about 4.5 per $O_{10}(OH)_2$ (Cuadros, 1997; Ransom and Helgeson, 1994a). This corresponds to two water layers in an exchange interlayer, in agreement with more recent MD modeling (Cygan, 2001) – see Section 3.1.2.1 on MD modeling of clays.

To carry out this work, we will:

- Conduct an extensive literature search;
- Collaborate with R. Cygan's MD modeling group at SNL;
- Test the new model against a broad spectrum of physical measurements (we note that some interesting new ideas in the literature that we may adopt need more testing);
- Compare the resulting model with alternative models;
- Conduct new experiments, both to check qualitative behavior and to compare with new quantitative results;
- Attempt to reconcile differences between clay, as mineral crystals, and clay, as an assemblage of such crystals with free water (and possibly other minerals).

Planned work on cement thermodynamic database and model development:

- Expand the number of solubility cases to further test the YMP thermodynamic database.
- Develop a solid solution model for the C-S-H system using a Margules parameterization – Gibbs energy minimization approach with the Cantera suite of codes. Make comparisons with existing solid solution models for this system.
- Consolidate the YMP and CEMDATA07 database plus others for use with the Cantera and EQ3/6 computer codes.
- Focus on the compilation of solubility and leaching data set for low-pH and salt-saturated cements. If the reliable data is available, conduct retrieval of thermodynamic properties for these two types of cement phases.

3.1.2.1 Clay Mineral Properties and Swelling Behavior through Molecular Simulation

A comprehensive performance assessment of the integrity of nuclear waste repositories requires knowledge of the chemical and physical properties for clay-based media. Often used as a backfill material for repository storage rooms and tunnels, clays and clay minerals, and details of their adsorptive behavior, are critical for ensuring the safe storage of nuclear waste. However, physical properties of clay minerals, especially under extreme environments associated with repositories, are difficult to ascertain compared to other geological materials.

Clay minerals are layered nano-crystalline multi-component phases exhibiting significant structural and atomic disorder. They possess low symmetry, significant defect structure, mixed disordered layering, and variable water content that ultimately affect cation exchange and other adsorptive properties. Consequently, analysis and characterization of clay minerals is difficult and often leads to ambiguous determinations. However, in recent years computational chemistry methods, especially advanced molecular simulation, have provided a supplemental approach for the characterization of clay minerals. Molecular dynamics simulations, in particular, have demonstrated accurate predictive models of clay mineral structure (e.g., *d*-spacing), hydration, adsorption, and many physical properties.

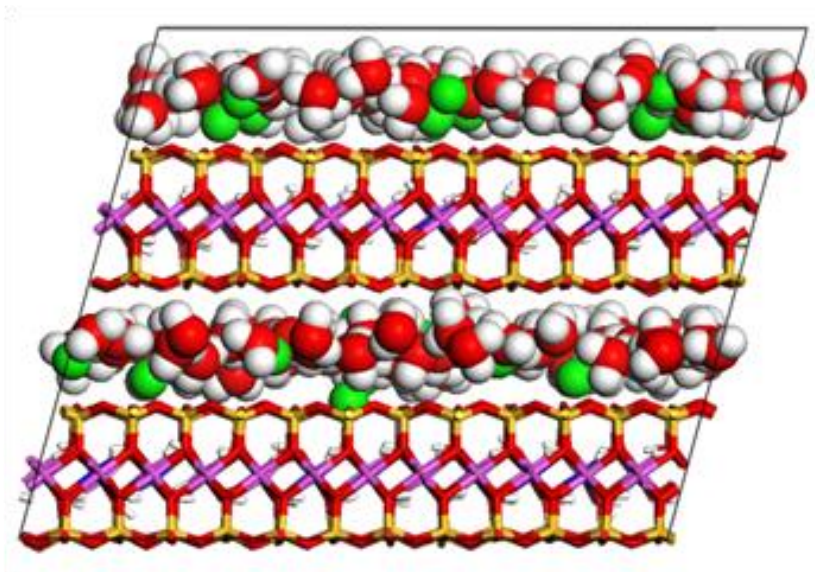


Figure 3-2. Snapshot of an equilibrated molecular dynamics simulation of sodium montmorillonite showing the Na^+ (green) and water (red/gray) molecules in the interlayer; projection view is along the *b*-axis.

Sodium montmorillonite is a common soil mineral that results from the weathering and alteration of basic rock types typically having low potassium contents under alkaline conditions. The nano-sized material is characterized by planar sheets of silica tetrahedra and alumina octahedra that coordinate to form a tetrahedron-octahedron-tetrahedron layer that is negatively charged by the aliovalent substitution of Mg^{+2} for Al^{3+} in the octahedral sheet. The negative charge is balanced by the incorporation of Na cations in the interlayer. Smectite clays, like montmorillonite, typically have a relatively low layer charge and therefore can be easily expanded by the insertion of water molecules into the interlayer to hydrate the Na^+ and internal surface of the tetrahedral sheet. The general chemical formula for sodium montmorillonite is given by $\text{Na}_x[\text{Mg}_x\text{Al}_{2-x}]\text{Si}_4\text{O}_{10}(\text{OH})_2 \cdot n\text{H}_2\text{O}$ where all of the layer charge resides on the octahedral sheet, although tetrahedral substitutions such as

Al^{3+} for Si^{4+} can also occur to augment the net negative layer charge. Figure 3-2 exhibits a model of Na-montmorillonite derived from the CLAYFF force field of Cygan et al. (2004) using the SNL code LAMMPS (Plimpton, 1995). Classical molecular dynamics simulations require interatomic potentials, like those provided by CLAYFF, to provide accurate descriptions of clay structure and behavior. CLAYFF was developed at SNL and has been widely accepted by international researchers for accurately simulating many hydrated environmental phases including clay minerals. Recent work on CLAYFF includes the enhancement of potentials to model clay edge sites that are important in acid-based reactions and adsorption phenomena.

Because of the nano-sized nature of clay materials and lack of suitable large single crystals for accurate structure determinations, molecular simulations have played a significant role in understanding clay structure and behavior. The swelling behavior of clay phases, in particular, has been examined to better evaluate the energy and hydration state of clay minerals (Cygan et al., 2004; Smith et al., 2006). Figure 3-3 presents results of a series of molecular dynamics simulations using an isothermal-isobaric ensemble to evaluate the expansion of the clay with increasing water content. This example, from Cygan et al. (2004), shows the expansion of montmorillonite with the development of a hydrogen bonded network of water molecules and the solvation of Na^+ to stabilize the interlayer and overcome the electrostatics that holds the layers together. Once expanded, the open interlayer region allows the backfill of water molecules to further stabilize the hydrogen bonding network until critical water content is reached and the clay interlayer swells to accommodate two water layers. The fine structure of the swelling curve is in very good agreement with experimental findings (Fu et al., 1990). The simulations also suggest the possibility of forming a third water layer that becomes somewhat diffuse at the higher water content, but which is not either observed or hard to resolve from the experimental data. Details of the swelling behavior of smectite clays, like montmorillonite, are important to understanding hydrolysis and volume changes associated with clays in repository environments.

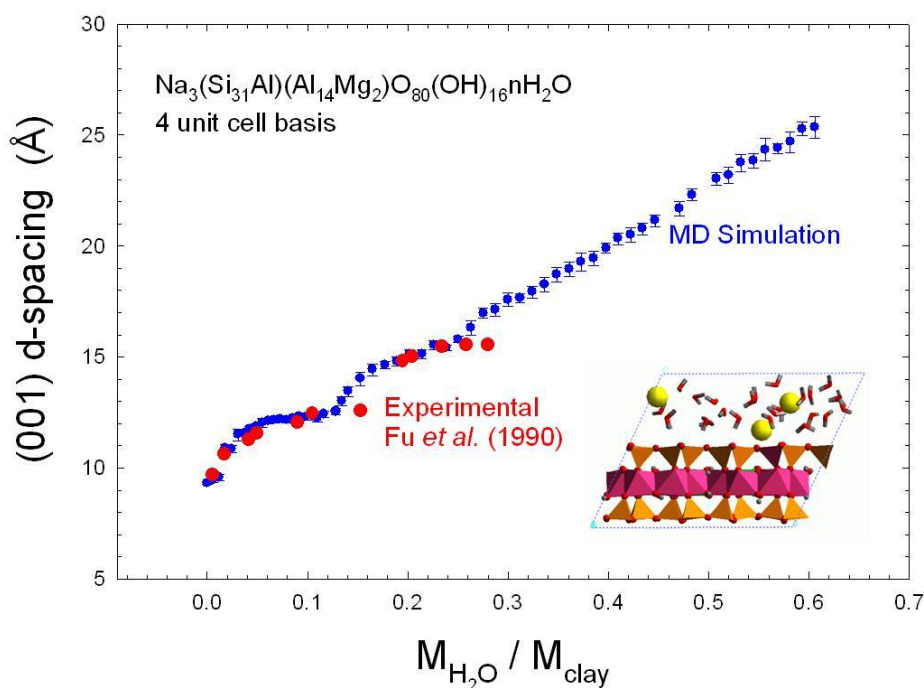


Figure 3-3. Swelling behavior of a montmorillonite clay based on constant-pressure (1 bar) molecular dynamics simulations – after Cygan et al. (2001).

3.2 References

- Apted, M.J., 1998, A modest proposal: A robust, cost-effective design for high-level waste packages: Scientific Basis for Nuclear Waste Management XXI, v. 506, p. 589-596.
- Atkins, M., Bennett, D.G., Dawes, A., Glasser, F., and Read, D., 1992, A thermodynamic model for blended cements: London, England, DoE/HMIP/RR/92/005, Department of the Environment.
- Atkins, M., Glasser, F.P., Moroni, L.P., and Jack, J.J., 1993, Thermodynamic modelling of blended cements at elevated temperatures (50-90°C), DoE/HMIP/RR/94/011: Aberdeen, United Kingdom, Aberdeen University.
- Babushkin, V.I., Matveyev, G.M., and Mchedlov-Petrosyan, O.P., 1985, Thermodynamics of silicates: Berlin, Germany, Springer-Verlag.
- Balady, M.A., 1996, Engineered Barrier System Performance Requirements Systems Study Report (BB0000000-01717-5705-00001 Rev. 01): Las Vegas, NV, Department of Energy.
- Baldwin, T., Chapman, N., and Neall, F.B., 2008, Geological Disposal Options for High-Level Waste and Spent Fuel - Report for the UK Nuclear Decommissioning Authority, Prepared by Galson Sciences, UK, p. 118 pp.
- Balonis, M., Lothenbach, B., Le Saout, G., and Glasser, F.P., 2010, Impact of chloride on the mineralogy of hydrated Portland cement systems: Cement and Concrete Research, v. 40, p. 1009-1022.
- Batchelor, B., and Wu, K., 1993, Effects of Equilibrium Chemistry on Leaching of Contaminants from Stabilized Solidified Wastes, *in* Spence, R.D., ed., Chemistry and Microstructure of Solidified Waste Forms: Boca Raton, Florida, Lewis Publishers.
- Bel, J., and Bernier, F., 2001, Temperature Criterion Related to Clay Based Backfill Materials in the Framework of a Geological Repository of Heat Producing Radioactive Waste (HLW), *in* Taboas, A., Vanbrabant, R., and Benda, G., eds., Proceedings 8th International Conference Radioactive Waste Management & Environmental Remediation: Bruges, ASME, p. 1327-1331.
- Bennett, D.G., 2010, The Joint EC/NEA Engineered Barrier System Project : Synthesis Report (EBSSYN), Seventh Framework Programme, European Commission, p. 1-80.
- Bennett, D.G., and Gens, R., 2008, Overview of European concepts for high-level waste and spent fuel disposal with special reference waste container corrosion: Journal of Nuclear Materials, v. 379, p. 1-8.
- Bennett, D.G., Hooper, A.J., Voinis, S., and Umeki, H., 2006, The role of the engineered barrier system in safety cases for geological radioactive waste repositories: An NEA initiative in co-operation with the EC: Scientific Basis for Nuclear Waste Management XXIX, v. 932, p. 43-52.
- Bennett, D.G., Read, D., Atkins, M., and Glasser, F.P., 1992, A thermodynamic model for blended cements. II: Cement hydrate phases; thermodynamic values and modelling studies: Journal of Nuclear Materials, v. 190, p. 315-325.
- Berner, U.R., 1987, Modeling porewater chemistry in hydrated Portland cement, *in* Bates, J.K., and Seefeldt, W.B., eds., Scientific Basis for Nuclear Waste Management X Symposium Volume 84: Boston, Massachusetts, Material Research Society, p. 319-330.
- Berner, U.R., 1988, Modelling the Incongruent Dissolution of Hydrated Cement Minerals: Radiochimica Acta, v. 44/45, p. 387-393.
- Berner, U.R., 1990, A Thermodynamic description of the evolution of pore water chemistry and uranium speciation during the degradation of cement, PSI-Bericht 62: Wurenlingen und Villigen, Switzerland, Paul Scherrer Institute.
- Berner, U.R., 1992, Evolution of Pore Water Chemistry During Degradation of Cement in a Radioactive Waste Repository Environment: Waste Management, v. 12, p. 201-219.
- Beziat, A., Dardaine, M., and Mouche, E., 1992, Measurements of the thermal conductivity of clay-sand and clay-graphite mixtures used as engineered barriers for high-level radioactive waste disposal: Applied Clay Science, v. 6, p. 245-263.
- Blanc, P., Bourbon, X., Lassin, A., and Gaucher, E.C., 2010a, Chemical model for cement-based materials: Temperature dependence of thermodynamic functions for nanocrystalline and crystalline C-S-H phases: Cement and Concrete Research, v. 40, p. 851-866.

- Blanc, P., Bourbon, X., Lassin, A., and Gaucher, E.C., 2010b, Chemical model for cement-based materials: Thermodynamic data assessment for phases other than C-S-H: *Cement and Concrete Research*, v. 40, p. 1360-1374.
- Bollingerfehr, W., Filbert, W., Graf, R., and Bammer, K.-J., 2010, State of the Art in Spent Fuel Disposal in Rock Salt in Germany, ENC Conference: Barcelona, Spain.
- Borjesson, S., Emren, A., and Ekberg, C., 1997, A thermodynamic model for the calcium silicate hydrate gel, modelled as a non-ideal binary solid solution: *Cement and Concrete Research*, v. 27, p. 1649-1657.
- Bruton, C.J., Meike, A., Viani, B.E., Martin, S., and Phillips, B.L., 1993, Thermodynamic and structural characteristics of cement minerals at elevated temperature, Topical Meeting on Site Characterization and Model Validation, FOCUS '93: Las Vegas, Nevada, p. 150-156.
- Carey, J.W., and Lichtner, P.C., 2007, Calcium silicate hydrate (C-S-H) solid solution model applied to cement degradation using the continuum reactive transport model FLOTRAN, in Mobasher, B., and Skalny, J., eds., *Transport Properties and Concrete Quality: Materials Science of Concrete*, John Wiley & Sons, Inc., p. 73-106.
- Cuadros, J., 1997, Interlayer cation effects on the hydration state of smectite: *American Journal of Science*, v. 297, p. 829-841.
- Cygan, R.T., 2001, Molecular Modeling in Mineralogy and Geochemistry in Rosso, J.J., ed., *Reviews in Mineralogy and Geochemistry*, Volume 42: Washington, D.C., Mineralogical Society of America, p. 1-35.
- Cygan, R.T., Liang, J.J., and Kalinichev, A.G., 2004, Molecular models of hydroxide, oxyhydroxide, and clay phases and the development of a general force field: *Journal of Physical Chemistry B*, v. 108, p. 1255-1266.
- Damidot, D., Stronach, S., Kindness, A., Atkins, M., and Glasser, F.P., 1994, Thermodynamic Investigation of the CaO-Al₂O₃-CaCO₃-H₂O Closed-System at 25°C and the Influence of Na₂O: *Cement and Concrete Research*, v. 24, p. 563-572.
- ESDRED, 2009, Final Summary Report and Global Evaluation of the Project, Engineering Studies and Demonstrations of Repository Designs (ESDRED) Integrated Project, Deliverable D6 of Module 6, WP4.
- Fu, M.H., Zhang, Z.Z., and Low, P.F., 1990, Changes in the Properties of a Montmorillonite-Water System during the Adsorption and Desorption of Water - Hysteresis: *Clays and Clay Minerals*, v. 38, p. 485-492.
- Fujii, K., and Kondo, W., 1983, Estimation of thermochemical data for calcium silicate hydrate (C-S-H): *Journal of the American Ceramic Society*, v. 66, p. C220-C221.
- Gartner, E.M., and Jennings, H.M., 1987, Thermodynamics of Calcium Silicate Hydrates and Their Solutions: *Journal of the American Ceramic Society*, v. 70, p. 743-749.
- Geneste, P., Raynal, M., Atabek, R., Dardaine, M., and Oliver, J., 1990, Characterization of a French Clay Barrier and Outline of the Experimental Program: *Engineering Geology*, v. 28, p. 443-454.
- Ghorab, H.Y., Kishar, E.A., and Elfetouh, S.H.A., 1998, Studies on the stability of the calcium sulfoaluminate hydrates. Part III: the monophases: *Cement and Concrete Research*, v. 28, p. 763-771.
- Glasser, F.P., Lachowski, E.E., and MacPhee, D.E., 1987, Compositional Model for Calcium Silicate Hydrate (C-S-H) Gels, Their Solubilities, and Free Energies of Formation: *Journal of the American Ceramic Society*, v. 70, p. 481-485.
- Glasser, F.P., Tyrer, M., Quillin, K., Ross, D., Pedersen, J., Goldthorpe, K., Bennett, D., and Atkins, M., 1998, The chemistry of blended cements and backfills intended for use in radioactive waste disposal, Research and Development Technical Report P98: UK, UK Environment Agency.
- Greenberg, J.P., and Moller, N., 1989, The prediction of mineral solubilities in natural waters: A chemical equilibrium model for the Na-K-Ca-Cl-SO₄-H₂O system to high concentration from 0 to 250°C: *Geochimica et Cosmochimica Acta*, v. 53, p. 2503-2518.

- Greenberg, S.A., and Chang, T.N., 1965, Investigation of the Colloidal Hydrated Calcium Silicates. II. Solubility Relationships in the Calcium Oxide-Silica-Water System at 25°C: *Journal of Physical Chemistry*, v. 69, p. 182-188.
- Greenberg, S.A., Chang, T.N., and Anderson, E., 1960, Investigation of Colloidal Hydrated Calcium Silicates: I. Solubility Products: *Journal of Physical Chemistry*, v. 64, p. 1151-1157.
- Harvie, C.E., Moller, N., and Weare, J.H., 1984, The Prediction of Mineral Solubilities in Natural Waters: The Na-K-Mg-Ca-H-Cl-SO₄-OH-HCO₃-CO₃-CO₂-H₂O System to High Ionic Strengths at 25°C: *Geochimica et Cosmochimica Acta*, v. 48, p. 723-751.
- Helgeson, H.C., Delany, J.M., Nesbitt, H.W., and Bird, D.K., 1978, Summary and Critique of the Thermodynamic Properties of Rock-Forming Minerals: *American Journal of Science*, v. 278, p. 1-229.
- Jobmann, M., and Buntebarth, G., 2009, Influence of graphite and quartz addition on the thermo-physical properties of bentonite for sealing heat-generating radioactive waste: *Applied Clay Science*, v. 44, p. 206-210.
- Johnson, L.H., and King, F., 2003, Technical Report 02-11: Canister Options for the Disposal of Spent Fuel, in NAGRA, ed.: Wettingen, Nagra, p. 57 pp.
- Jové Colón, C.F., Caporuscio, F.A., Levy, S.S., Xu, H., Blink, J.A., Halsey, W.G., Buscheck, T., Sutton, M., Serrano de Caro, M.A., Wolery, T.J., Liu, H.H., Birkholzer, J., Steefel, C.I., Rutqvist, J., Tsang, C.-F., and Sonnenthal, E., 2010, Disposal Systems Evaluations and Tool Development - Engineered Barrier System (EBS) Evaluation p. 1-200.
- Kersten, M., 1996, Aqueous solubility diagrams for cementitious waste stabilization systems .1. The C-S-H solid solution system: *Environmental Science & Technology*, v. 30, p. 2286-2293.
- Kienzler, B., Vejmelka, P., Herbert, H.J., Meyer, H., and Althenhein-Haese, C., 2000, Long-term leaching experiments of full-scale cemented waste forms: Experiments and modeling: *Nuclear Technology*, v. 129, p. 101-118.
- Kulik, D.A., and Kersten, M., 2001, Aqueous solubility diagrams for cementitious waste stabilization systems: II, end-member stoichiometries of ideal calcium silicate hydrate solid solutions: *Journal of the American Ceramic Society*, v. 84, p. 3017-3026.
- Landolt, D., Davenport, A., Payer, J., and Shoesmith, D., 2009, A Review of Materials and Corrosion Issues Regarding Canisters for Disposal of Spent Fuel and High-level Waste in Opalinus Clay, Technical Report 09-02: Wettingen, Switzerland, National Cooperative for the Disposal of Radioactive Waste (NAGRA), 73 pp.
- Lichtner, P.C., and Carey, J.W., 2006, Incorporating solid solutions in reactive transport equations using a kinetic discrete-composition approach: *Geochimica Et Cosmochimica Acta*, v. 70, p. 1356-1378.
- Lothenbach, B., Damidot, D., Matschei, T., and Marchand, J., 2010a, Thermodynamic modelling: state of knowledge and challenges: *Advances in Cement Research*, v. 22, p. 211-223.
- Lothenbach, B., Matschei, T., Moschner, G., and Glasser, F.P., 2008, Thermodynamic modelling of the effect of temperature on the hydration and porosity of Portland cement: *Cement and Concrete Research*, v. 38, p. 1-18.
- Lothenbach, B., Scrivener, K., and Hooton, R.D., 2010b, Supplementary cementitious materials: *Cement and Concrete Research*, v. *in press*.
- Lothenbach, B., and Winnefeld, F., 2006, Thermodynamic modelling of the hydration of Portland cement: *Cement and Concrete Research*, v. 36, p. 209-226.
- MacPhee, D.E., Luke, K., Glasser, F.P., and Lachowski, E.E., 1989, Solubility and aging of calcium silicate hydrates in alkaline solutions at 25°C: *Journal of the American Ceramic Society*, v. 74, p. 646-654.
- Matschei, T., Lothenbach, B., and Glasser, F.P., 2007, Thermodynamic properties of Portland cement hydrates in the system CaO-Al₂O₃-SiO₂-CaSO₄-CaCO₃-H₂O: *Cement and Concrete Research*, v. 37, p. 1379-1410.
- McKinley, I.G., Neall, F.B., Kawamura, H., and Umeki, H., 2006, Geochemical optimisation of a disposal system for high-level radioactive waste: *Journal of Geochemical Exploration*, v. 90, p. 1-8.

- Metz, V., Schussler, W., Kienzler, B., and Fanghanel, T., 2004, Geochemically derived non-gaseous radionuclide source term for the Asse salt mine – assessment for the use of a $Mg(OH)_2$ – based backfill material: *Radiochimica. Acta*, v. 92, p. 819-825.
- Moffat, H.K., and Jové Colón, C.F., 2009, Implementation of Equilibrium Aqueous Speciation and Solubility (EQ3 type) Calculations into Cantera for Electrolyte Solutions, SAND2009-3115: Albuquerque, N.M., Sandia National Laboratories, p. 146.
- Moschner, G., Lothenbach, B., Rose, J., Ulrich, A., Figi, R., and Kretzschmar, R., 2008, Solubility of Fe-ettringite ($Ca_6[Fe(OH)_6]_2(SO_4)_3 \cdot 26H_2O$): *Geochimica Et Cosmochimica Acta*, v. 72, p. 1-18.
- Neall, F.B., 1996, Modelling the long-term chemical evolution of cement-groundwater systems, *in* Murphy, W.M., and Knecht, D.A., eds., *Scientific Basis for Nuclear Waste Management XIX*, Symposium, Volume 412: Pittsburgh, Pennsylvania, Materials Research Society, p. 483-490.
- Nutt, M., Voegelé, M., Jové-Colón, C., Wang, Y., Howard, R., Blink, J., Liu, H.-H., Hardin, E., and Jenni, K., 2011, Used Fuel Disposition Campaign Disposal Research and Development Roadmap (Fuel Cycle Research and Development), p. 1-138.
- Peppler, R.B., and Wells, L.S., 1954, The system of lime, alumina, water from 50° to 250 °C: *Jour. Res. Natl. Bur. Stand.*, v. 52, p. 75-92.
- Perkins, R.B., and Palmer, C.D., 1999, Solubility of Ettringite ($Ca_6[Al(OH)_6]_2(SO_4)_3 \cdot 26H_2O$) at 5–75°C: *Geochimica et Cosmochimica Acta*, v. 63, p. 1969-1980.
- Plimpton, S., 1995, Fast Parallel Algorithms for Short-Range Molecular Dynamics: *J Comp Phys*, v. 117, p. 1-19.
- Poole, T.S., Wakeley, L.D., and Young, C.L., 1993, individual and Combined Effects of Chloride, Sulfate, and Magnesium Ions on Hydrated Portland-Cement Paste, SAND93-7040: Albuquerque, N.M., Sandia National Laboratories, p. 50.
- POSIVA, 2008, Horizontal Deposition of Canisters for Spent Nuclear Fuel - Summary of the KBS-3H Project 2004 - 2007, *in* OY, P., ed.: Olkiluoto.
- Pusch, R., Drawite, A.B., Yong, R.N., and Nakano, M., 2010, Stiffening of smectite buffer clay by hydrothermal effects: *Engineering Geology*, v. 116, p. 21-31.
- Ransom, B., and Helgeson, H.C., 1994a, A Chemical and Thermodynamic Model of Aluminous Dioctahedral-2/1 Layer Clay-Minerals in Diagenetic Processes - Regular Solution Representation of Interlayer Dehydration in Smectite: *American Journal of Science*, v. 294, p. 449-484.
- Ransom, B., and Helgeson, H.C., 1994b, Estimation of the Standard Molal Heat-Capacities, Entropies, and Volumes of 2/1-Clay-Minerals: *Geochimica Et Cosmochimica Acta*, v. 58, p. 4537-4547.
- Reardon, E.J., 1990, An Ion Interaction-Model for the Determination of Chemical-Equilibria in Cement Water-Systems: *Cement and Concrete Research*, v. 20, p. 175-192.
- Sarkar, A.K., Barnes, M.W., and Roy, D.M., 1982, Longevity of borehole and shaft sealing materials: Thermodynamic properties of cements and related phases applied to repository sealing, ONWI-201: Columbus, Ohio, Battelle Memorial Institute, Office of Nuclear Waste Isolation.
- Shaw, S., Henderson, C.M.B., and Komanshek, B.U., 2000, Dehydration/recrystallization mechanisms, energetics, and kinetics of hydrated calcium silicate minerals: An in situ TGA/DSC and Synchrotron Radiation SAXS/WAXS Study: *Chemical Geology*, v. 167, p. 141-159.
- Smith, D.E., Wang, Y., Chaturvedi, A., and Whitley, H.D., 2006, Molecular simulations of the pressure, temperature, and chemical potential dependencies of clay swelling: *Journal of Physical Chemistry B*, v. 110, p. 20046-20054.
- Soler, J.M., and Mader, U.K., 2010, Cement-rock interaction: Infiltration of a high-pH solution into a fractured granite core: *Geologica Acta*, v. 8, p. 221-233.
- Stula, R.T., Albert, T.E., Kirstein, B.E., and Lester, D.H., 1980, Systems Study on Engineered Barriers: Barrier Performance Analysis, Technical Report ONWI-211, Office of Nuclear Waste Isolation (ONWI), p. 1-174.
- Sugiyama, D., and Fujita, T., 2006, A thermodynamic model of dissolution and precipitation of calcium silicate hydrates: *Cement and Concrete Research*, v. 36, p. 227-237.
- Tardy, Y., and Garrels, R.M., 1974, Method of Estimating Gibbs Energies of Formation of Layer Silicates: *Geochimica Et Cosmochimica Acta*, v. 38, p. 1101-1116.

- Taylor, H.F.W., 1990, *Cement Chemistry*: San Diego, California, Academic Press Limited.
- Thomas, J.J., and Jennings, H.M., 1998, Free-energy-based model of chemical equilibria in the CaO-SiO₂-H₂O system: *Journal of the American Ceramic Society*, v. 81, p. 606-612.
- Wakeley, L.D., Poole, T.S., Ernzen, J.J., and Neeley, B.D., 1993, Salt Saturated Mass Concrete Under Chemical Attack, *in* Zia, P., ed., *High Performance Concrete in Severe Environments*, Volume SP-140: Detroit, MI, American Concrete Institute.
- Wersin, P., Johnson, L.H., and McKinley, I.G., 2007, Performance of the bentonite barrier at temperatures beyond 100°C: A critical review: *Physics and Chemistry of the Earth*, v. 32, p. 780-788.
- Westerman, R.E., 1979, *Preliminary Conceptual Designs for Advanced Packages for the Geological Disposal of Spent Fuel*: Richland, Washington, Pacific Northwest Laboratory, 109 pp.
- Wolery, T.J., and Jové Colón, C.F., 2007, *Qualification of Thermodynamic Data for Geochemical Modeling of Mineral–Water Interactions in Dilute Systems (ANL-WIS-GS-000003 REV 01)*: Las Vegas, Nevada, Sandia National Laboratories; OCRWM Lead Laboratory for Repository Systems, p. 412 pp.

**MODELING COUPLED THM PROCESSES AND REACTIVE
DIFFUSIVE TRANSPORT IN ENGINEERED BARRIER SYSTEMS (EBS)**

4. THMC Processes in EBS

The ensemble of multi-barrier systems essentially consists of the natural barrier system (e.g., repository host-rock) and the engineering barrier system (EBS). During the lifespan of a geologic repository, the performance of the EBS is affected by a combination of thermal, hydrogeological, mechanical, chemical and biological processes that are driven by heat release from radionuclide decay, multiphase flow and diffusive transport (e.g., gas generation as a result of metal corrosion), and waste degradation. Given the complex nature of these processes and their equally intricate feedbacks to the barrier system, an accurate understanding of these coupled processes is crucial for the EBS performance assessment (PA). Within the EBS work package of the Used Fuel Disposition (UFD) Campaign, LBNL's research is focused on two relevant issues, namely the (1) thermal-hydraulic-mechanical-chemical (THMC) processes in backfill/buffer materials (bentonite), and (2) the diffusive transport in clay within the EBS, with the long-term goal of developing a comprehensive understanding of (and verified modeling capabilities to simulate) the effects of coupled processes on radionuclide transport in the EBS, as well as the interaction between the near-field host rock (e.g., clay/shale) and EBS components.

LBNL's focus areas address key Features, Events and Processes (FEPs), which have been ranked in importance from medium to high as listed in Tables 7 and 8 of the *Used Fuel Disposition Campaign Disposal Research and Development Roadmap* (FCR&D-USED-2011-000065 REV0) (Nutt, 2011). Specifically, they address FEP 2.2.01, Excavation Disturbed Zone (EDZ), for shale by investigating the effects of coupled processes on interactions between shale (clay) disposal formations and the EBS; FEPs 2.1.04.01, Buffer/Backfill; FEPs 2.1.07.02, 03, 04, 09, Mechanical Processes; FEPs 2.1.08.03, 07, 08, Hydrologic Processes; and FEP 2.1.11.04, Thermal Processes, by studying coupled processes in the EBS; and FEPs 2.1.09.52, 53, 54, Chemical Processes—Transport by investigating reactive-diffusive radionuclide transport in bentonite.

4.1 THM Modeling of EBS Including Buffer-Rock Interaction

As described in the FY10 report (Jové Colón et al. 2010), the LBNL team incorporated the Barcelona Basic Model (BBM) into the TOUGH-FLAC simulator. The BBM is the most advanced and accepted constitutive model used for modeling of bentonite-buffer behavior in the various European and Japanese nuclear waste programs. In FY11, so far we have focused on using this new capability to model THM processes within a bentonite-backfilled emplacement tunnel and its interactions with the natural system (clay host-rock) and simulate the sensitivities of a number of processes and interactions to a variety of parameters. First, we present results for a base-case scenario that we developed during FY10 (Section 4.1.1 below) and then present results for a variety of parameter ranges from modeling conducted in FY11.

4.1.1 Base-Case Simulation Results

In the base-case simulation scenario, we used clay host-rock properties derived from the Opalinus clay stone at Mont Terri, Switzerland (Gens et al., 2007). The EBS design featured waste emplacement in horizontal tunnels backfilled with bentonite-based swelling clays as the protective backfill/buffer material (Figure 4-1). We adopted the heat load developed for the Generic Disposal System Environment (GDSE) within the UFD for Pressurized Water Reactor (PWR) used nuclear

fuel. We adjusted tunnel and canister spacing to limit the maximum temperature to less than 100°C.

The basic material properties used for the base-case simulation scenario are presented in Tables 4-1 to 4-3. The bentonite properties, including the thermal and hydraulic properties (Table 4-1) and Barcelona Basic Model (BBM) properties (Table 4-2), were derived from laboratory experiments and *in situ* tests of FEBEX bentonite, whereas the rock properties correspond to that on Opalinus Clay (Table 4-3). The initial saturation of the bentonite buffer was set to 65%.

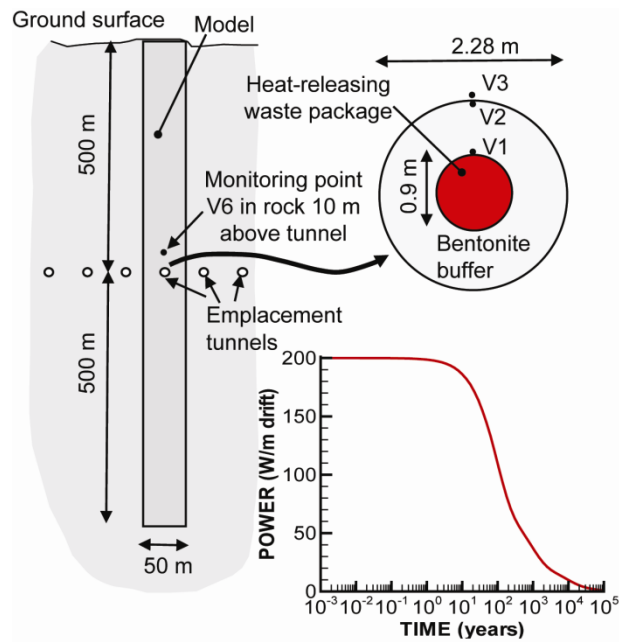


Figure 4-1. Model domain for an assumed bentonite back-filled horizontal emplacement drift at 500 m depth in clay host rock.

Table 4-1. Thermal and hydraulic properties of the bentonite buffer.

Parameter	Value/Function
Initial dry density, ρ_d [kg/m ³]	$1.6 \cdot 10^3$
Initial porosity, ϕ [-]	0.41
Saturated permeability, k [m ²]	$2.0 \cdot 10^{-21}$
Relative permeability, k_r [-]	$k_{rl} = S_t^3$
Van Genuchten's (1980) parameter, P_{VG} [MPa]	30
Van Genuchten's (1980) parameter, λ_{VG} [-]	0.32
Thermal expansion, β [1/°C]	$1.5 \cdot 10^{-4}$
Dry specific heat, C_s [J/kg·°C]	$c_s = 1.38T + 732.5$
Thermal conductivity, λ_m [W/m·°C]	$\lambda_m = 1.28 - \frac{0.71}{1 + e^{(S_t - 0.65)/0.1}}$
Effective vapor diffusion coefficient, D_v [m ² /s]	$D_v = 2.16e - 5 \times \tau \times \phi \times S_g \left(\frac{T_{abs}}{273.8} \right)^{1.8}$
Tortuosity factor, τ [-]	0.8

Table 4-2. BBM material parameter for the bentonite buffer

Parameter	Value
Compressibility parameter for stress-induced elastic strain, κ_{pSO} [-]	0.05
Compressibility parameter for suction-induced elastic strain, κ_{sPO} [-]	0.25
Shear modulus, G [MPa]	NA
Poisson's ratio, ν [-]	0.4
Parameter for suction induced elastic strain, α_{sS} [-]	0
Parameter for stress-induced strain α_{pS} [MPa ⁻¹]	-0.003
Parameter for stress-induced strain, α_{sP} [-]	-0.161
Reference stress state for relating elastic compressibility to suction, P_{ref} [MPa]	0.5
Parameters that relate elastic volumetric strain and temperature changes, α_0 [°C ⁻¹]	1.5e-4
Compressibility parameter in virgin soil states at zero suction, λ_{pSO} [-]	0.15
Parameter defining soil stiffness associated with loading collapse yield, r_λ [-]	0.925
Parameter for the increase of soil stiffness with suction, β_λ [MPa ⁻¹]	0.1
Parameter that relates cohesion to temperature, ρ_s [°C ⁻¹]	0
Parameter describing the increase of cohesion with suction, k_s [-]	0.1
Tensile strength at saturated conditions, P_{s0} [MPa]	0
A reference stress state for compressibility relation in virgin states, P^C [MPa]	0.5
Slope of the critical state line, M [-]	1
Non-associativity parameter in the plasticity flow rule, α_a [-]	0.53
Specific volume at reference stress states P^C in virgin states, v^c [-]	1.937
Net mean yield stress for saturated conditions at reference temperature, P_{OT}^* [MPa]	12.0

Table 4-3. THM rock properties for the clay stone host rock.

Parameter	Value
Bulk Density, [kg/m ³]	2400
Matrix Porosity [-]	0.15
Young's Modulus, [GPa]	5
Poisson's ratio, [-]	0.3
Specific heat, [J/kg·°C]	900
Thermal conductivity, [W/m·°C]	2.2
Thermal expansion coefficient, [°C ⁻¹]	1.0×10 ⁻⁵
Permeability, [m ²]	5.0×10 ⁻²⁰
Biot's effective stress parameter	1.0
Van Genuchten water retention parameter, <i>m</i>	0.41
Van Genuchten water retention parameter, <i>P₀</i> [MPa]	48

The coupled THM behavior of the bentonite clay was modeled TOUGH-FLAC simulator and a new implementation of the Barcelona Basic Model (BBM). The simulations were conducted in the following order: (1) pre-excavation, (2) excavation, (3) waste and buffer emplacement, (4) post-closure coupled processes modeling. The results (Figure 4-2) show strong THM-driven interactions between the bentonite clay buffer and the low permeability of the host rock. This is manifested in the delay in buffer resaturation as a result of the low rock permeability, and the fluid pressure in the host rock. This strong coupling with temperature changes results in a significant increase in pore pressure. This fluid pressure in excess of hydrostatic leads to an excess pressure gradient from the repository that lasts for up to 3,000 years.

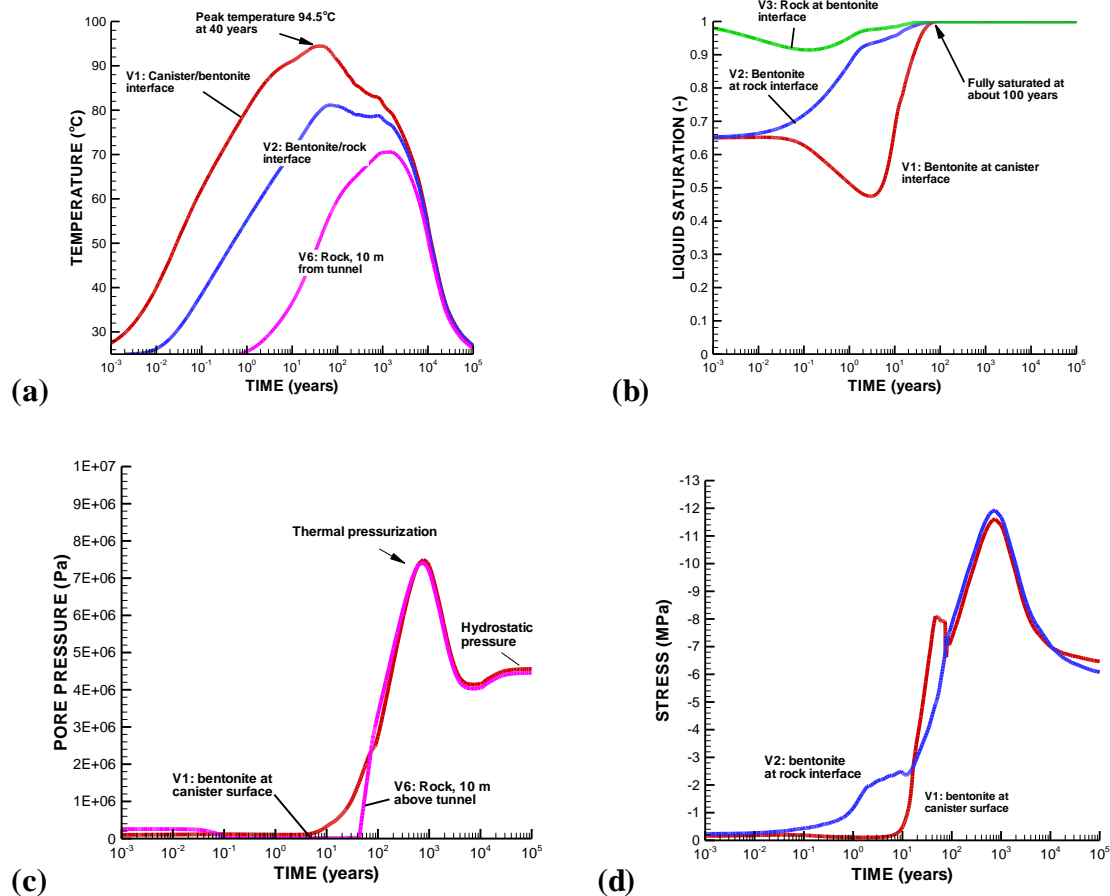


Figure 4-2. Simulated evolution of THM processes in buffer: (a) temperature, (b) liquid saturation, (c) fluid pressure, and (d) total radial stress (σ_x). See Figure 4-1 for locations of V1, V2, V3, and V6.

Figure 4-3 depicts the evolution of total and effective stresses near the tunnel wall (V3 in Figure 4-3a) and 10 m away from the tunnel (V6 in Figure 4-3b). Figure 4-4 shows the profound effect of pressurization on the effective stress evolution; it specifically shows the resulting effective stress path (σ'_1 versus σ'_3) at point V3. The result for the calculated elastic stress path is compared with strength values for the Opalinus clay stone. The range between low and high strength envelopes in Figure 4-4 corresponds to the estimated strength parallel and perpendicular to the bedding planes. This result indicates a high likelihood of failure for the lower strength, parallel to beddings. Such a failure would induce shearing along bedding planes that could lead to increased permeability adjacent to the tunnel, which could impact flow and radionuclide transport should the waste canister fail.

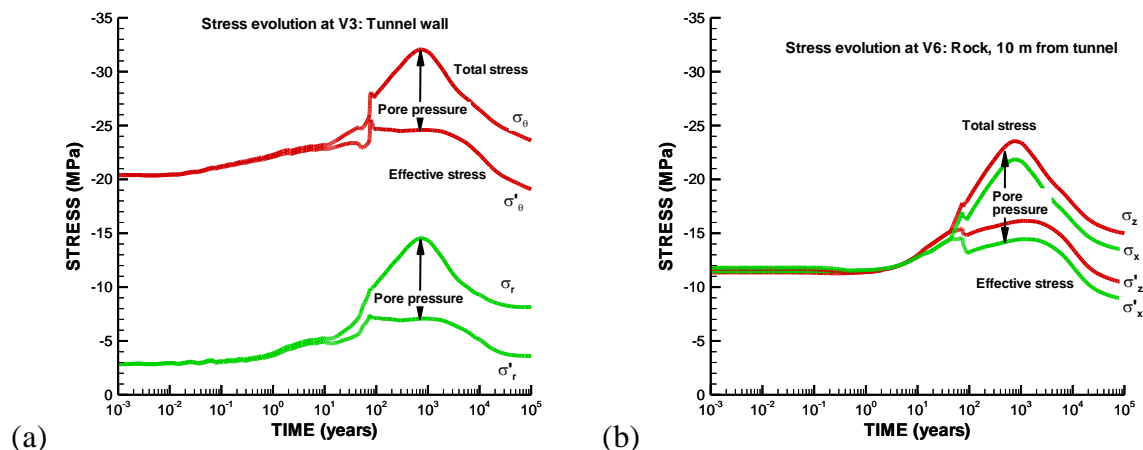


Figure 4-3. Calculated evolution of stresses: (a) stress evolution a point V3 located at the tunnel wall, and (b) stress evolution at point V6 located 10 m away from the tunnel. See Figure 4-1 for locations of V3 and V6.

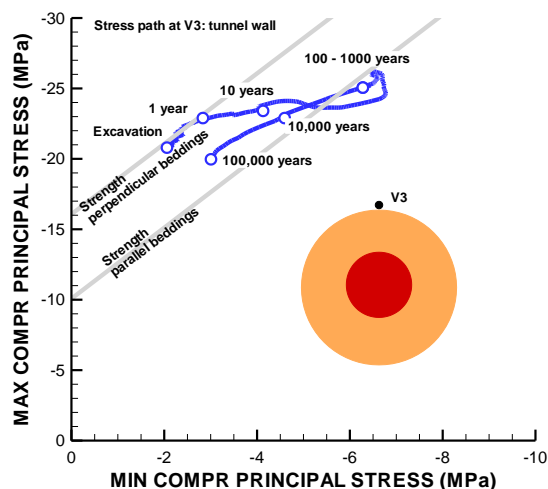


Figure 4-4. Calculated principal stress path at point V3 located at the tunnel wall.

4.2 Thermal management study and peak temperature

The maximum temperature and temperature-time behavior of the canisters are determined principally by the canister and areal thermal loading—which are controllable parameters—and the ambient temperature and thermal properties of the bentonite backfill and host rock. As described in Part 1 of this report, there is no stringent adherence to specific criteria in definitely set a maximum near-field temperature, for example, in the Swiss repository concept. However, it is generally considered that elevated temperatures in the near-field and long-term performance of the bentonite backfill/buffer can be an issue given the potential for barrier degradation; more so than those associated with corrosion performance of the canister (NAGRA, 2002). Specifically, the canister surface should be maintained at a sufficiently

low temperature that the desirable plasticity and hydraulic and diffusion properties of the buffer material are preserved (NAGRA, 2002). The most important potential degradation processes involve cementation as a result of silica dissolution and precipitation, and precipitation of sparingly soluble salts (e.g., calcite and anhydrite) at or near the canister surface. Several studies have proposed a design with a maximum canister surface temperature of 100°C, because of concerns about bentonite integrity at temperatures above 100°C and because of a lack of confidence in the coupled THM models describing the evolution of near-field conditions over the first few hundred years after emplacement (NAGRA, 2002).

In the Swiss concept for a repository in Opalinus Clay, the maximum surface temperatures for the canister are well above 100°C. Because of the low thermal conductivity of granular bentonite prior to resaturation and the relatively high ambient temperature (38°C) in Opalinus Clay at repository depth, it is difficult to keep temperatures below 125°C throughout the entire bentonite barrier (NAGRA, 2002). In fact, calculations of temperature evolution show that the maximum canister surface temperature will reach ~150°C, and at the point in the bentonite midway between the canister and the tunnel wall, it may reach ~110°C. However, it appears that the more recent studies indicated a maximum temperature of about 125 to 135°C near the canister, which are still substantially above 100°C.

In the previous simulation, we designed the repository in such a way that the peak temperature would be less than 100°C. To achieve this, we assumed a waste deposition after 60 years of interim storage (initial heat power per 1818 W per waste package), deposition at 500 m (initial temperature 25°C), a 50 m tunnel spacing, and canisters emplaced every 8th meter along the emplacement tunnels. Here, we present sensitivity-test results for the parameters related to peak temperature.

4.2.1 Buffer Saturation and Thermal Conductivity

A low buffer saturation and associated low thermal conductivity are mentioned as reasons for the high peak temperature in the Swiss repository concept in Opalinus clay. If buffer is emplaced using granular bentonite, the initial water content is low, leading to a low thermal conductivity (0.4 W/mK). In our simulation, we tried to vary initial saturation between 1% and 100%. A 1% buffer saturation corresponds to the current concept for the Swiss repository in Opalinus clay when using granular (pellets of) bentonite buffer. The results indicate that a change in initial saturation affects the temperature during the first 10 years, before any significant wetting of the buffer from the surrounding rock. As long as the initial saturation is higher than about 10%, the peak temperature is close to 94.5°C and occurs at about 40 years from waste emplacement. If initial saturation is less than 10%, an earlier temperature peak appears at about 2 years after waste emplacement. For the extreme case of a 1% initial saturation, the maximum temperature at the first peak is about 103.5°C, while the maximum temperature at the second peak remains at about 94.5°C (Figure 4-5).

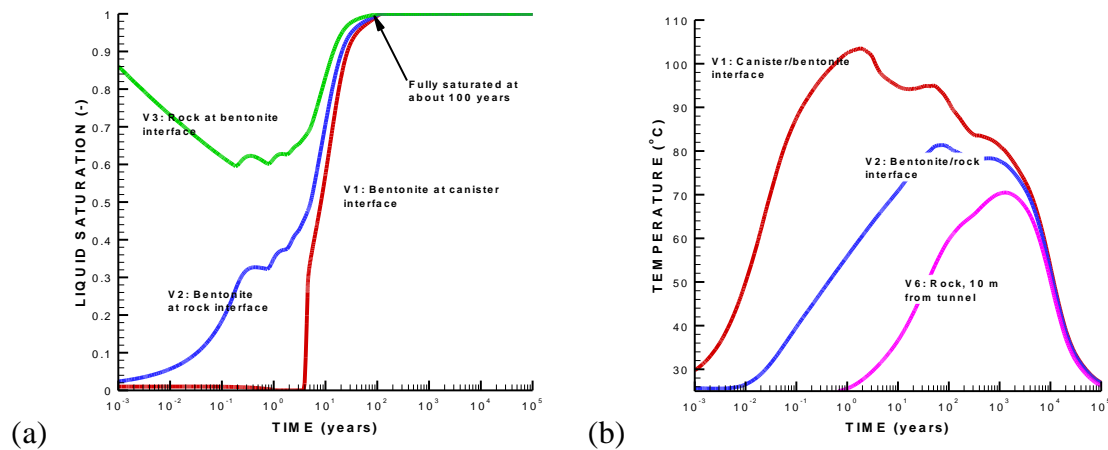


Figure 4-5. Calculated evolution of (a) liquid saturation and (b) temperature in the case of a buffer consisting of granular bentonite with 1% initial saturation.

4.2.2 Tunnel and Canister Spacing

Both tunnel and waste canister spacing will impact the temperature evolution. A change in waste canister spacing will affect the thermal line load along the axis of the emplacement tunnels. In the base case, the canisters containing four-PWR elements were assumed to be 4 m long and spaced 4 m apart. When we reduced the space between the canisters from 4 to 3 m (i.e., a canister every 7 m), the peak temperature increased to 104.2°C at 40 years. When reducing the distance between emplacement tunnels to 35 m, the temperature peaks at about 104.5°C at 60 years.

4.2.3 Rock thermal conductivity

In the base-case scenario, we assign an average thermal conductivity of 2.2 w/mK. This was the average value based on anisotropic thermal conductivity back-calculated from field experiments at Mont Terri, Switzerland. If we reduce the thermal conductivity to the lowest value of 1.6 W/mK, the calculated maximum temperature is about 108°C at 40 years.

4.2.4 Extreme case of high peak temperature

We present results for an extreme case with low initial buffer saturation, canisters placed every 6 m along the tunnels, and individual tunnels spaced 35 m apart (Figure 4-6). The low buffer saturation also results in a low thermal conductivity. Moreover, we used the lower limit thermal conductivity of rock (1.6 W/mK). The temperature evolution at the canister surface has two peaks: Peak 1 is caused by saturation dependent thermal conductivity of buffer, whereas peak 2 depends on host rock thermal conductivity and tunnel spacing etc. The peak temperature in this case is much too high.

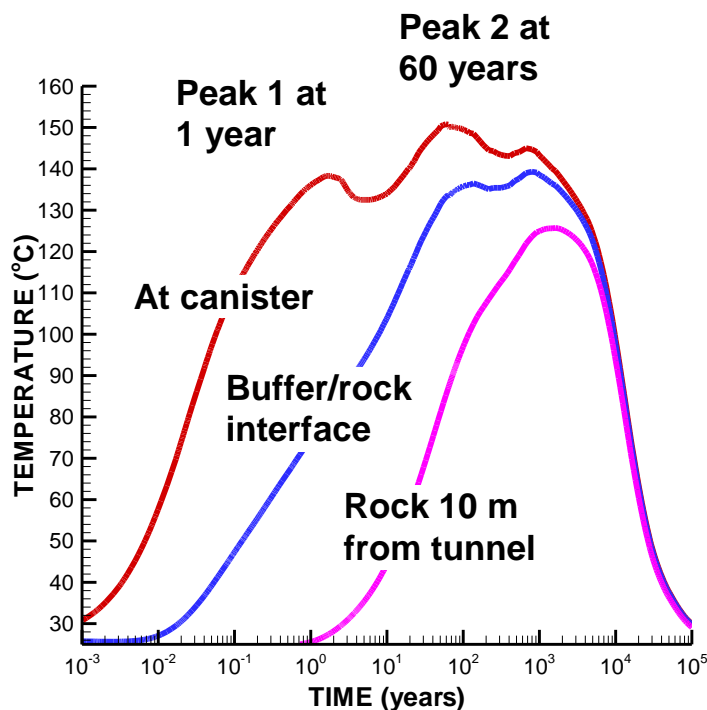


Figure 4-6. Calculated temperature evolution for the extreme case densely spaced waste canisters (reduced canister and tunnel spacing) and a buffer consisting of granular bentonite with 1% initial saturation, as well as a low thermal conductivity of the rock.

4.3 Resaturation Time and Buffer Swelling

The bentonite buffer will resaturate and swell with inflow from the surrounding rock mass. A certain swelling pressure will assure buffer homogeneity and tightness against the surrounding rock wall. The time to full resaturation and swelling depends on a number of parameters, most importantly the hydraulic properties of the rock and the bentonite. We found in our previous simulation that the resaturation time is about 100 years, assuming an average permeability of $5 \times 10^{-20} \text{ m}^2$. The 100-year resaturation time does not change significantly with the different options of heat load or initial saturation of the buffer.

We conducted a parameter study in which we varied the rock permeability and noted the time to reach 99% saturation at the canister surface. Figure 4-7 shows that for the base case, the exact time to 99% saturation is 55 years. If the permeability is one order of magnitude lower (i.e., $k = 5 \times 10^{-21} \text{ m}^2$), the resaturation time increased to 177 years. Increasing rock permeability by one order of magnitude results in a decrease in resaturation time of 26 years. Figure 4-7 also shows that if rock permeability were higher than about $1 \times 10^{-16} \text{ m}^2$, the resaturation time is 16.7 years and independent of the rock-mass permeability.

Next, we investigated the sensitivity of the rock water retention and relative permeability functions to the evolution of saturation. In the base case, van Genuchten water retention parameter $P_0 = 48 \text{ MPa}$. When decreasing P_0 from 48 to 4.8 MPa for the rock, we can see that the resaturation time increased slightly, from 55 to 65 years, and that there was a more substantial desaturation of the host rock. This desaturation results from high suction in the bentonite at its initial saturation of 65%. A change in the relative permeability function of the host rock had only a minor impact on

the resaturation time. Initially the rock is fully saturated while the buffer is 65% saturated at high suction. A strong pressure gradient from the host rock to the bentonite results in fluid flow from the host rock to the buffer. This results in desaturation of the host rock (See point V3 in Figure 4-2b). In the case of a lower P_0 for the host rock, the saturation is lower for a given suction.

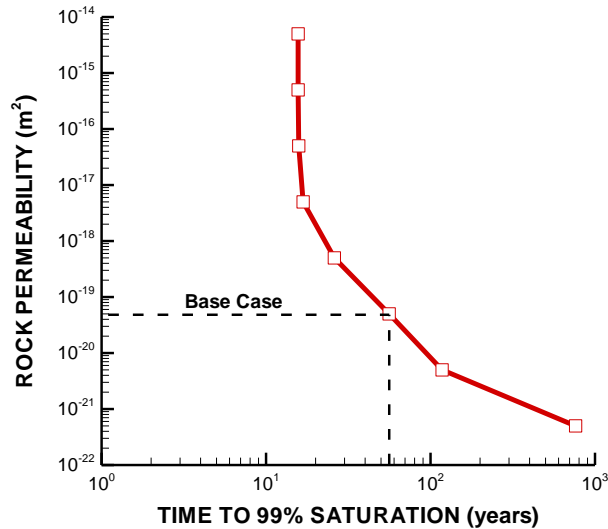


Figure 4-7. Time to 99% saturation for different values of rock-mass permeability.

4.4 Rock failure for layered rock

In this case, we introduced the anisotropic strength properties of the host rock. We used the ubiquitous joint model available in FLAC3D along with the properties shown in Table 4-4—the values used are taken from Gens et al. (2007). Here, we utilize the FLAC3D ubiquitous joint model, a model also used by Corkum and Martin (2007) when simulating previous *in situ* experiments in Opalinus clay at Mont Terri. We assumed that the bedding planes are parallel to the tunnel and slightly tilted (20°). We ran this simulation for base-case properties (except for rock mass).

The results of the simulation using the anisotropic strength properties are shown in Figures 4-8 and 4-9. Figure 4-8 shows volumetric and shear strain induced during the operation and post-closure periods of the repository until 100,000 years. We can observe the anisotropic strain pattern in which most strain occurs near the top and bottom of the tunnel. Actually, most of the rock mass failure around the tunnel occurs already during the excavation. As shown in Figure 4-9, the stress after excavation is already on the failure envelop for the assigned strength properties. During subsequent waste emplacement and heating of the rock mass, the stress path moves away from failure and the volumetric and shear stresses are quite small. The development of the swelling pressure in the buffer can prevent further rock failure from occurring. The stress path in Figure 4-9 looks similar to that in Figure 4-4, but the maximum compressive principal stress is shifted to a smaller level in Figure 4-9. Note that the simulation results presented in Figure 4-4 was for elastic stress in an elastic medium, whereas the results in Figure 4-9 includes full elasto-plastic analysis with stress response to failure.

Table 4-4. Material properties of the ubiquitous joint model.

Property	Value
Bulk modulus	4.17 GPa
Shear modulus	1.92 GPa
Cohesion	5 MPa
Friction angle	25°
Dilation angle	10°
Tensile strength	1.0 MPa
Joint cohesion	2.2 MPa
Joint friction	25°
Joint tensile strength	0.5 MPa

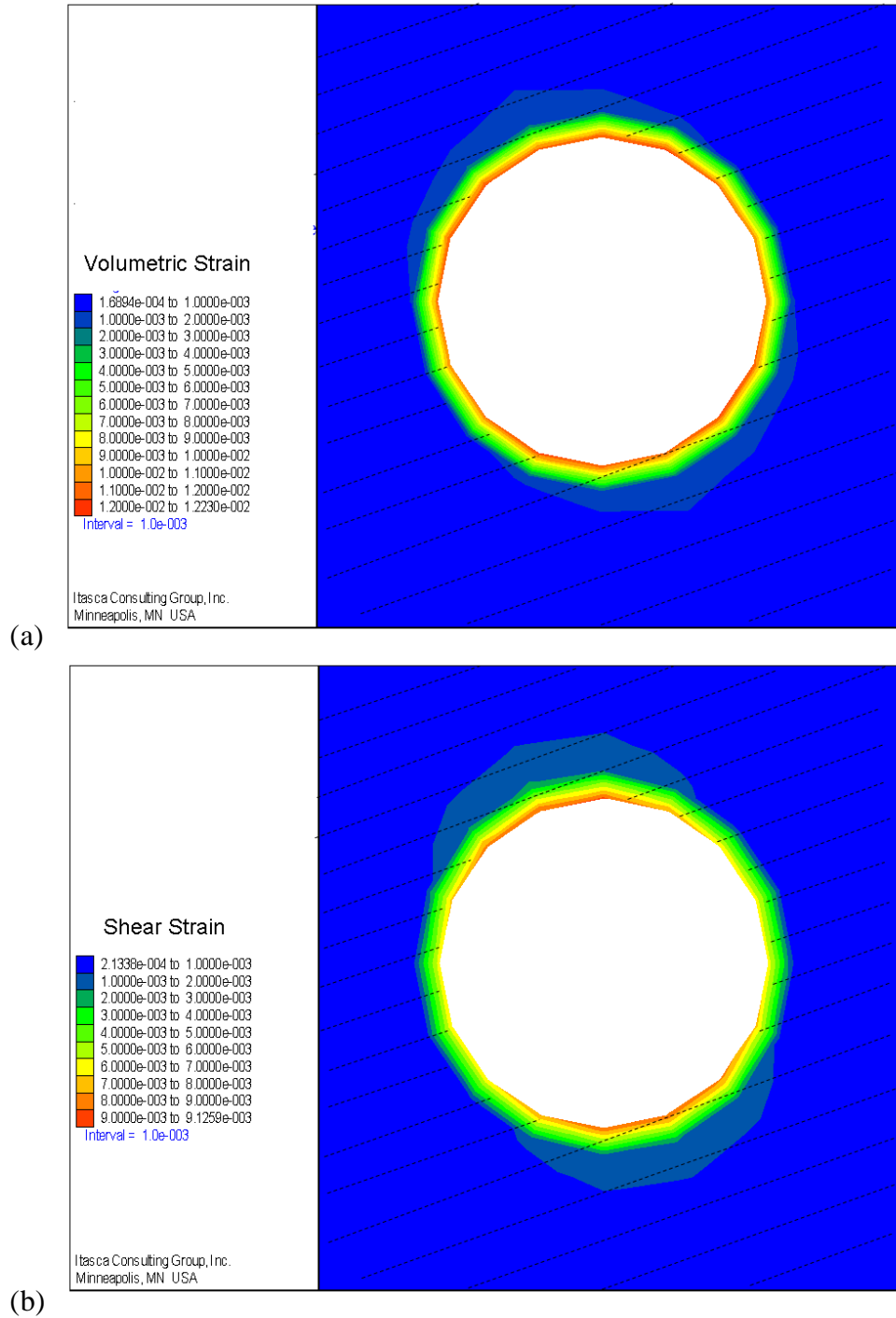


Figure 4-8. (a) Volumetric strain and (b) shear strain in the rock at 100,000 years for the case of anisotropic strength properties (the orientation of the bedding planes are indicated by dotted lines).

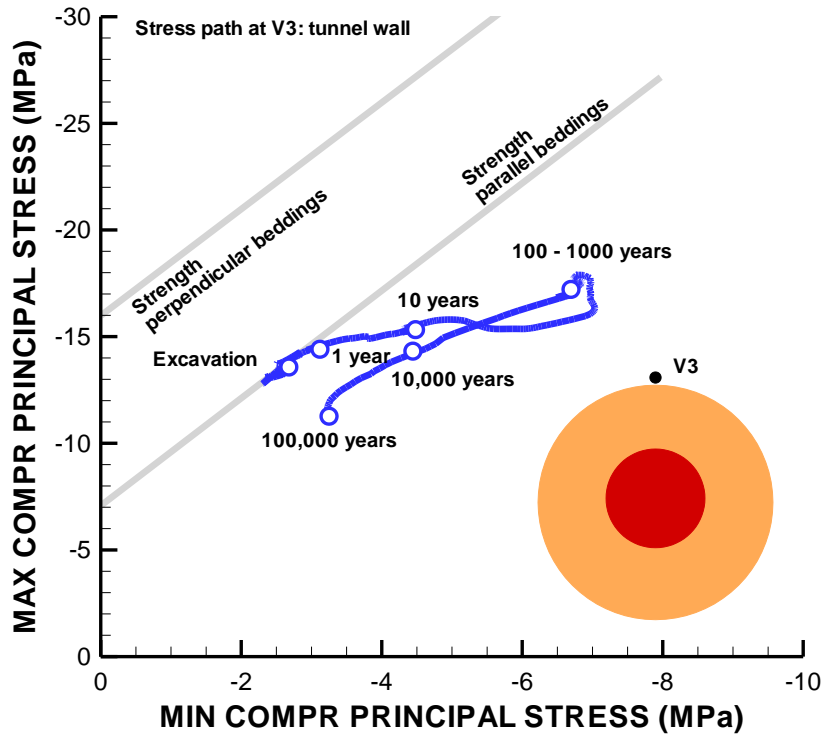


Figure 4-9. Calculated stress path for the case of anisotropic strength properties of the host rock.

4.5 Model Development and Code Implementation of Double-Structure Constitutive Model for Bentonite

We have identified an approach and suitable mathematical formulation (Alonso et al., 1999), equivalent to the Barcelona Expansive Model. The formulation is being implemented in C++ routines within the User Defined Model framework of the FLAC3D simulator. Once implemented, it will be verified and tested against published data. For example, Alonso et al. (1999) presents such experimental data and numerical tests. Using this model, we will be able to properly model both the micro- and macrostructure deformations and their interactions. Figure 2.10 shows the interaction between micro and macro-structure deformations in the suction, s , versus effective mean stress, p .

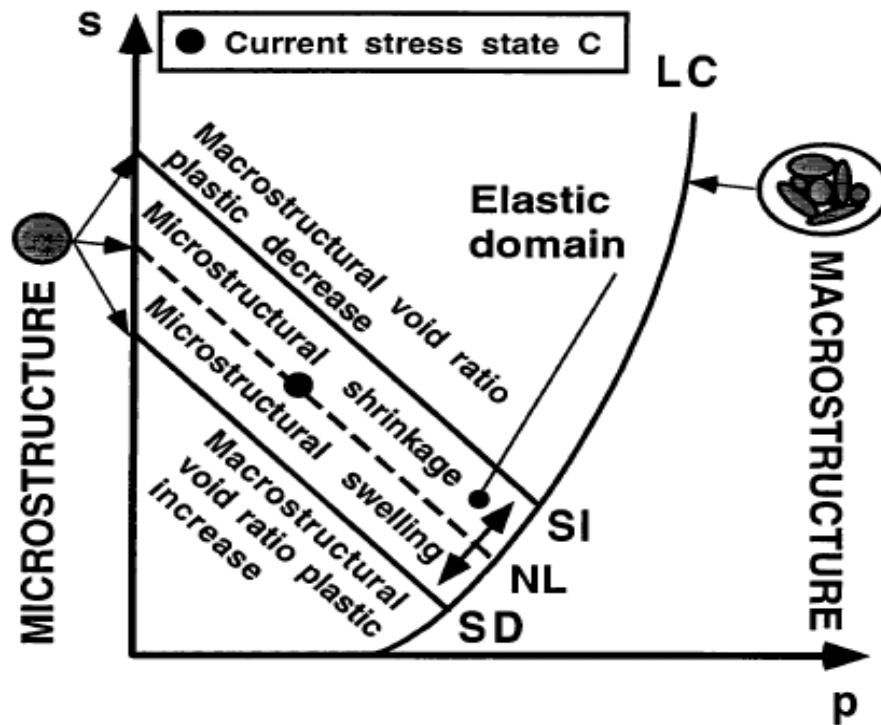


Figure 4-10. Microstructural and macrostructural elastoplastic responses in a double-structure model equivalent to the Barcelona Expansive Model.

4.6 Reactive Diffusion in Bentonite

Compacted bentonite has been proposed as backfill/buffer material in many of the European repositories due to its very low permeability (Kim et al., 1993; Muurinen, 1994; Pusch, 2001; Bourg et al., 2003) and its strong sorptive properties (Ochs et al., 2001), both of which will restrict radionuclide releases beyond the confines of the EBS. The low permeability of bentonite is due in large part to the high percentage of Na-montmorillonite, a clay that swells in the presence of water. Given the very low permeability of the compacted bentonite, the main mode of radionuclide transport beyond the waste form and waste package will be almost exclusively by molecular diffusion, with effective diffusivities far below that in water (Madsen, 1998; Ochs et al., 2001; Bourg et al., 2007). Very low effective diffusivities for the compacted bentonite are a result of its low porosity and nanosize pores. In compacted bentonite, the majority of pores are so small (<1 nanometer) that there is overlapping of electrical double layers balancing the charge of the bentonite (typically negative at circumneutral pH), thus potentially excluding anions altogether, or creating a deficiency in them with the diffuse double layer balancing the surface mineral charge (Bourg et al., 2003; Bourg et al., 2006; Leroy et al., 2006; Gonçalvès et al., 2007).

Three types of water presence are recognized in compacted bentonite (Bourg et al., 2003; Wersin et al., 2004):

1. Interlayer water (φ_{IL}) with only water and cations within the Tetrahedral-Octahedral-Tetrahedral (TOT) layers of the montmorillonite. Here, the cations balance the fixed charge of the TOT layers;

2. Diffuse double layer (φ_{DDL}) containing cations and anions, but with an excess of ions (normally cations) to balance the charge of the clay surface;
3. Bulk or free pore water (φ_B), which is charge balanced.

The relative proportions of each type of water in the clay material depend on the compaction of the bentonite, but also the solution ionic strength by affecting the width of the diffuse double layer. Moreover, the type of cation in solution affects the swelling behavior of the clay and therefore the interlayer spacing.

In this progress report, we focus on using the newly developed explicit diffuse double layer capability in the computer code CrunchFlow, along with analytical solutions that apply to the binary salt case, to attempt a predictive continuum model for diffusion through compacted bentonite. Also compared to our model is the “ion equilibrium” approach of Birgersson and Karnland (2009), which is based on a single porosity within the clay interlamellae.

4.6.1 Experimental Investigation of Diffusion Through Compacted Bentonite

Van Loon et al. (2007) performed a set of through-diffusion experiments in the experimental setup shown in Figure 4-11 using $^{36}\text{Cl}^-$ as a tracer and varying the dry density of bentonite and the ionic strength of the saturation solution.

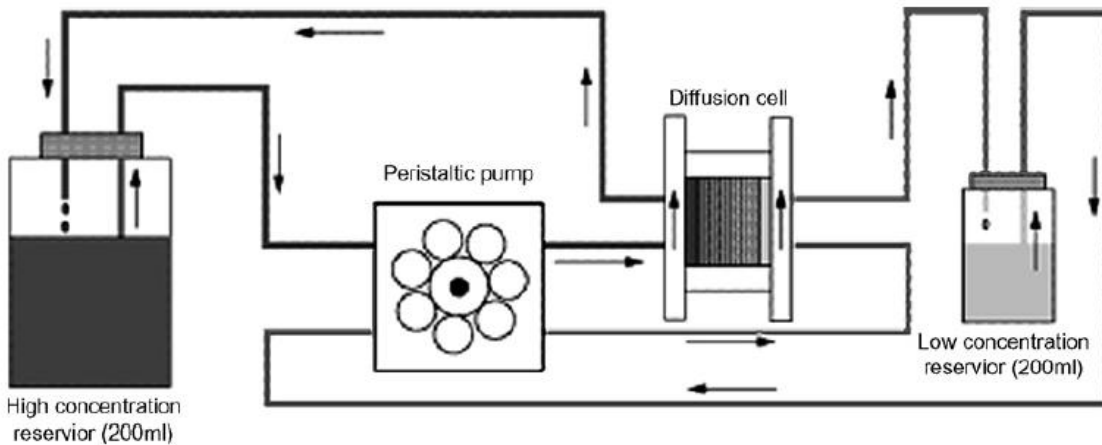


Figure 4-11. Schematic view of the experimental setup used in the through-diffusion experiment (from Van Loon et al., 2007).

The authors attempted to analyze through-diffusion experiments within the framework of the classical theory of molecular diffusion in porous media, using the well-known Fick’s law, as given by the following equation valid for one-dimensional cases:

$$\frac{\partial C}{\partial t} = D_e \frac{\partial^2 C}{\partial x^2} \quad (4.1)$$

where D_e represents the effective diffusion coefficient, C is the concentration of a given species and t and x are time and space, respectively.

Under steady-state conditions, the accumulated mass of the tracer is given by the following expression:

$$A(L,t) = SLC_0 \left(\frac{D_{eVL}t}{L^2} - \frac{\alpha}{6} \right) \quad (4.2)$$

where S is the cross-sectional area, L is the length of the sample, and C_0 is the concentration of the tracer in the high concentration reservoir. Here it is assumed that concentrations in the “low concentration” reservoir are equal to zero.

The values of D_{eVL} (the effective diffusion coefficient as defined by Van Loon et al., 2007) and α can be obtained graphically by plotting the measured values of $A(L,t)$ against time.

In turn, the rock capacity factor is defined as:

$$\alpha = \phi + \rho_b R_d \quad (4.3)$$

where ρ_b is the bulk dry density and R_d is the distribution coefficient of clay. If nonsorbing tracers are involved, then $R_d = 0$ and $\alpha = \phi$. In the identity above, the porosity ϕ refers to the pore space available to the tracer in question, and thus is strictly true whenever anion exclusion or, more generally, surface processes can be neglected. Otherwise, as is the case here, a distinction should be made between the total volume of pores and the smaller one that is effectively accessible to chloride. The obvious drawback of the so-defined chloride-accessible porosity, ε_{Cl^-} , is that its correspondence with a measurable physical entity is necessarily vaguer than is the case for the total porosity, ϕ . On the other hand, it is not entirely correct to assume that the measured chloride concentration at the outlet is uniformly distributed over the accessible porosity. Rather, it is strictly correct to state that a function of distribution of concentration with respect to space, $C(x, y, z)$, exists, such that:

$$\int_{\phi V_T} C(x, y, z) dV = [Cl^-] \varepsilon_{Cl^-} V_T \quad (4.4)$$

where V_T is the total volume of the sample.

In fact, the derivation of the actual form of the function $C(x, y, z)$ is one of the keys to the solution of the problem and will be dealt with in the following.

Furthermore, as a consequence of assuming that the concentration gradient should be calculated on the basis of the difference in tracer concentration between the upstream and downstream reservoirs, the effective diffusion coefficient was found to vary as a function of both the dry density of clay and the ionic strength of the solution. This is in conflict with the traditional Fickian formulation, according to which the effective diffusivity is a property of the porous medium only. Mathematically, this is explicitly accounted for by the traditional definition of the effective diffusion coefficient:

$$D_e = \tau D_0 \quad (4.5)$$

where the diffusion coefficient in pure water, D_0 , is corrected by the tortuosity of the porous network, τ .

As a matter of fact, the authors found that the effective diffusion coefficient defined using the two external reservoirs decreases at higher dry densities and at lower ionic strength values. Table 4-5 shows the values reported in Van Loon et al. (2007).

Table 4-5. Effective diffusion coefficients reported by Van Loon et al. (2007) as a function of dry density of clay and sodium chloride concentration in the pore water.

Dry density (kg/m ³)	NaCl (M)	Effective diffusion coefficient (m ² /s)
1300	0.01	2.60E-12
1300	0.05	7.50E-12
1300	0.10	1.60E-11
1300	0.40	2.50E-11
1300	1.00	4.90E-11
1600	0.01	3.90E-13
1600	0.05	1.10E-12
1600	0.10	2.30E-12
1600	0.40	4.60E-12
1600	1.00	1.00E-11
1900	0.01	3.30E-14
1900	0.05	1.20E-13
1900	0.10	2.40E-13
1900	0.40	5.00E-13
1900	1.00	1.20E-12

Glaus et al. (2007), on the basis of diffusion tests carried out in highly compacted clay columns with $^{22}\text{Na}^+$ and $^{85}\text{Sr}^{2+}$ as tracers, removed the ambiguity associated with a formulation based purely on the two (“upstream” and “downstream”) reservoirs by postulating that effective diffusion coefficients are independent of the composition of the external aqueous phase, if the concentration gradient in the interlayer water of the clay is considered. The internal concentration gradient should vary consistently as a function of the external salt concentration.

Figure 4-12 shows that the variation in the effective diffusion coefficient, as calculated from the concentration gradient in the external aqueous phase, does vary with the ionic strength of the saturation solution. That variation can nevertheless be evaluated using a function of the form:

$$D_{eVL} = f\left(D_e, CEC, [A]^{-z}\right) \quad (4.6)$$

where D_e is the actual effective diffusion coefficient of clay, CEC is its cation exchange capacity, $[A]$ is the cation concentration in the external water phase and z is the valence of the tracer. Plotted on a logarithmic scale, experimental points align along a line with slope $-z$, which is -1 for $^{22}\text{Na}^+$ and -2 for $^{85}\text{Sr}^{2+}$.

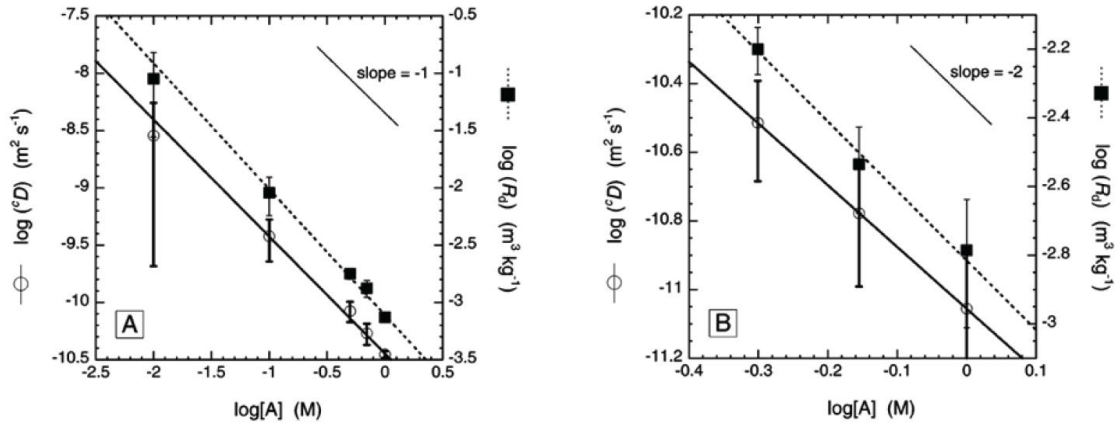


Figure 4-12. Logarithmic representation of the dependence of 6D and R_d for ${}^{22}\text{Na}^+$ (Plot A) and ${}^{85}\text{Sr}^{2+}$ (Plot B) on the cation concentration in the external water phase $[A]$. The data are mean values of results from through-diffusion experiments and profile analysis; 5 mm and 10 mm clay thickness (from Glaus et al., 2007).

4.6.2 Single Type Pore Model

It is then apparent that, just as diffusion through the interlayer water becomes the dominant pathway, surface reactions between the aqueous phase and the clay become an increasingly relevant factor to consider. As discussed above, all experiments were performed in highly compacted clays (dry density being $\sim 1950 \text{ kg/m}^3$) and therefore conclusions derived from that study could only be applied under similar conditions. These conditions motivated Birgersson and Karnland (2009) to develop their own model. In line with the notion that the effective diffusion coefficient should be independent of the external salt concentration, the authors explicitly account for the distortion of the concentration gradient in the interlayer (with respect to the gradient established between the inlet and outlet reservoirs) by assuming that Donnan equilibrium relationships hold when applied to the interface between the external and pore solutions. Indeed, anion concentration drops while cation concentration rises at the interfaces, as shown in Figure 4-13.

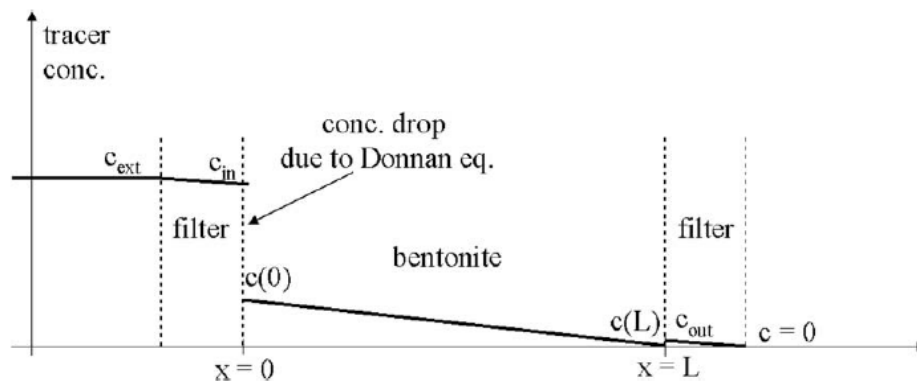


Figure 4-13. Tracer concentration profile at steady state for chloride through-diffusion. For typical experimental setups, the transport capacity of the filters is large enough to supply the clay with anions, and the full concentration drop occurs within the clay. Thus, filters do not need to be considered for evaluation of clay chloride diffusivity (from Birgersson and Karnland, 2009).

These effects can be quantified in terms of the ratio between the concentrations of the tracer in the pore solution and in the external solution (explicitly given for a case where chloride is used as a tracer):

$$\Xi_{Cl^-} = \frac{[Cl^-]^{MP}}{[Cl^-]} \quad (4.7)$$

where $[Cl^-]$ represents the concentration of chloride in the external solution and superscript MP stands for microporosity. This notation implies that, at such high levels of compaction, the entire volume of water in clay pores is affected by the surface charge, i.e., the thickness of the pores is such that the diffuse double layer fully occupies it (hence the term “single type pore model” often employed by the authors). In other words, the function of distribution of concentration over the pore space is $C(x, y, z) = [Cl^-]^{MP}$, for any point (x, y, z) lying in the pore space (Figure 4-14). This is a debatable assumption, and its consequences will be discussed later.

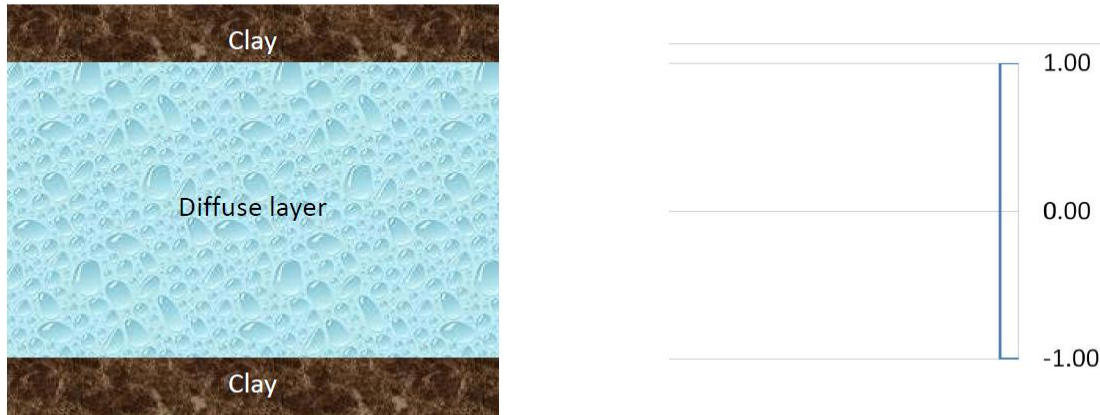


Figure 4-14. Spatial distribution of concentration of chloride as modeled by Birgersson and Karnland (2009).

In the following, the mathematical expression of Ξ_{Cl^-} will be derived on the basis of Birgersson and Karnland (2009) for a simple case involving a solution of sodium chloride. Moreover, it will be demonstrated that it corresponds to a special case of a more general problem that CrunchFlow is able to handle.

Let $[Na^+]^{MP}$ and $[Cl^-]^{MP}$ be the concentration of sodium and chloride in the microporosity; then the Donnan equilibrium constraint reduces to the following relationship:

$$\gamma_{Na^+} [Na^+] \gamma_{Cl^-} [Cl^-] = \gamma_{Na^+}^{MP} [Na^+]^{MP} \gamma_{Cl^-}^{MP} [Cl^-]^{MP} \quad (4.8)$$

where $[Na^+]$ and $[Cl^-]$ are the concentration of sodium and chloride in the external solution and γ_{X_i} is the activity coefficient of the species X_i .

So the problem revolves around the calculation of $[Na^+]^{MP}$ and $[Cl^-]^{MP}$ based on the equation above. In a 1:1 electrolyte, as in this case, $[Na^+] = [Cl^-]$, so:

$$[Cl^-]^{MP} = \frac{\gamma_{Na^+} \gamma_{Cl^-} [Cl^-]^2}{\gamma_{Na^+}^{MP} \gamma_{Cl^-}^{MP} [Na^+]^{MP}} = \Gamma_1 \frac{[Cl^-]^2}{[Na^+]^{MP}} \quad (4.9)$$

where,

$$\Gamma_1 = \frac{\gamma_{Na^+} \gamma_{Cl^-}}{\gamma_{Na^+}^{MP} \gamma_{Cl^-}^{MP}} \quad (4.10)$$

On the other hand, the mean concentration of sodium ions inside the clay is equal to the sum of the layer charge compensating part ($[Na^+]_0$) and the amount of ions which has entered from the external solution (the latter being equal to $[Cl^-]^{MP}$ due to electroneutrality), which is to say:

$$[Na^+]^{MP} = [Na^+]_0 + [Cl^-]^{MP} \quad (4.11)$$

Steeffel (2010) writes instead:

$$Q^{SL} = \phi^{MP} \sum_{i=1}^N z_i C_i^{MP} \quad (4.12)$$

which holds true for the pore solution in the microporosity (ϕ^{MP} represents the microporosity; Q^{SL} the total charge in the Stern layer, that can be calculated in CrunchFlow either dynamically through the surface complexation module, or introduced as a fixed charge in correspondence with the value of CEC ; and z_i is the valence of the ions of concentration C_i^{MP}). In the case analyzed, the above equation becomes:

$$Q^{SL} = \phi^{MP} \left([Na^+]^{MP} - [Cl^-]^{MP} \right) \quad (4.13)$$

which is equivalent to Equation (4.11), given that:

$$[Na^+]_0 = \frac{Q^{SL}}{\phi^{MP}} \quad (4.14)$$

So both formulations will provide identical results in those cases where it can be assumed that the entire porosity is made up of micropores, i.e., $\phi = \phi^{MP}$.

The charge of the Stern layer is provided by sodium counterions and counterbalances the surface charge of clay minerals. In terms of the cation exchange capacity CEC , that results in:

$$[Na^+]_0 = \left(\frac{CEC m_s}{z} \right) / \left(\frac{m_w}{\rho_w} \right) = \frac{CEC}{z} \rho_s \frac{(1 - \phi^{MP})}{\phi^{MP}} \quad (4.15)$$

where m_w and V_w are the water mass and volume, respectively; and ρ_w and ρ_s are the specific mass of water and the solid, respectively.

Alternatively, the foregoing equation could be expressed in terms of the surface site density and the specific surface area of clay minerals:

$$[Na^+]_0 = \frac{\rho_{site} A_{spec} MW_m \phi_m}{V_m} \quad (4.16)$$

where ρ_{site} represents the surface density (in mol/m²), A_{spec} is the specific surface area (in m²/g), MW_m is the molecular weight of the mineral (in g/mol) and ϕ_m and V_m are the volume fraction (per unit fluid volume, dimensionless) and the molar volume of the mineral (cm³/mol).

Therefore:

$$[Na^+]^{MP} = \frac{\rho_{site} A_{spec} MW_m \phi_m}{V_m} + [Cl^-]^{MP} \quad (4.17)$$

and later:

$$[Cl^-]^{MP2} + \frac{\rho_{site} A_{spec} MW_m \phi_m}{V_m} [Cl^-]^{MP} - \Gamma_1 [Cl^-]^2 = 0 \quad (4.18)$$

Writing

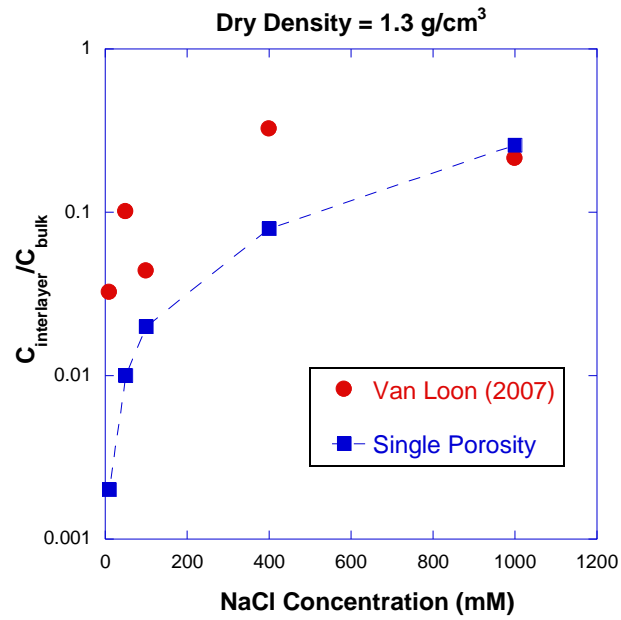
$$\Omega = \frac{\rho_{site} A_{spec} MW_m \phi_m}{V_m} \quad (4.19)$$

The only real solution of the equation is:

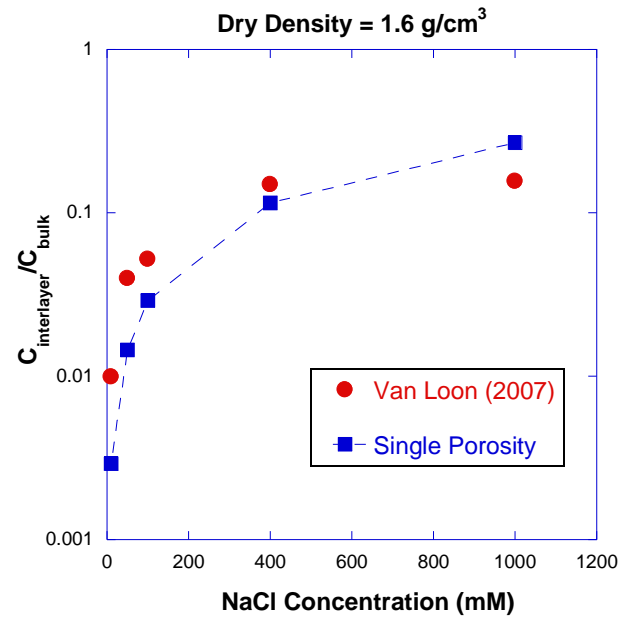
$$[Cl^-]^{MP} = \frac{-\Omega + \sqrt{\Omega^2 + 4\Gamma_1 [Cl^-]^2}}{2} \quad (4.20)$$

Finally:

$$\Xi_{Cl^-} = \frac{[Cl^-]^{MP}}{[Cl^-]} = \frac{-\Omega + \sqrt{\Omega^2 + 4\Gamma_1 [Cl^-]^2}}{2[Cl^-]} \quad (4.21)$$



(a)



(b)

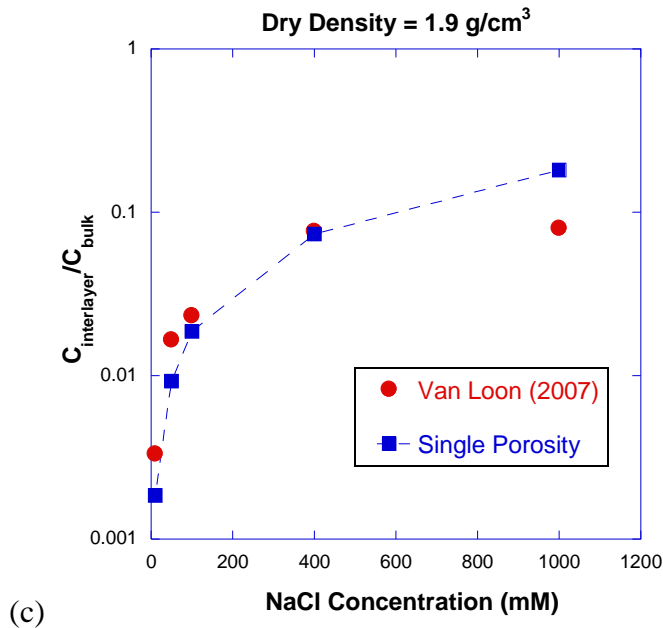


Figure 4-15. Fit of experimental data reported by Van Loon et al. (2007) obtained by the single type pore model: (a) 1300 kg/m³, (b) 1600 kg/m³, (c) 1900 kg/m³

In Figure 4-15, the results of the model are plotted against the values obtained from through-diffusion experiments carried out by Van Loon et al. (2007) for dry densities equal to 1300 kg/m³ (a), 1600 kg/m³ (b) and 1900 kg/m³ (c). As can be seen, the results of the model match accurately the trend of the ratio observed against both dry density of the clay and ionic strength of the solution. It is apparent, however, that the agreement between model simulations and experimental results is closer as dry density increases. Setting aside experimental errors (Van Loon et al., 2007) estimated the value of ε_{CT} by means of four different methods and some scatter is observable), divergences arising at lower dry densities appear to hint at a limit to the range of applicability of the Birgersson and Karland model. In other words, the hypothesis underlying the single type porosity model holds strictly true when the pore space is small enough (in correspondence with a high rate of compaction and dry density), while it becomes increasingly questionable as porosity increases, thus allowing for the coexistence of the double diffuse layer, on the one hand, and bulk water, where anion concentrations are much larger, on the other hand.

4.6.3 Double Type Pore Model

The new capabilities included in CrunchFlow and detailed in Steefel (2010), in line with analytical developments reported in Appelo et al. (2008), allow for the treatment of more complicated scenarios than those considered by the single porosity formulation of Birgersson and Karland (2009). Yet it remains to be seen how effective they are in simulating the response of clay as shown above.

It is clear that additional constraints had to be met in developing a more sophisticated and comprehensive model. Indeed, even for the very simple problem outlined above (a clay column saturated with a binary solution and subjected to a slight concentration gradient), the number of

unknowns doubles. For the problem to be solved, the unknown concentrations $[Na^+]^{MP}$, $[Cl^-]^{MP}$, $[Na^+]^P$ and $[Cl^-]^P$ (where the superscript P refer to macroporosity, as opposed to microporosity) have to be determined.

Let $[Na^+]$ and $[Cl^-]$ be the sodium and chloride concentration of the external solution. Then, the abovementioned constraints are:

1) Donnan equilibrium condition between external and micropore solutions:

$$\gamma_{Na^+} [Na^+] \gamma_{Cl^-} [Cl^-] = \gamma_{Na^{+MP}} [Na^+]^{MP} \gamma_{Cl^{-MP}} [Cl^-]^{MP} \quad (4.22)$$

2) Donnan equilibrium condition between micropore and macropore solutions:

$$\gamma_{Na^{+MP}} [Na^+]^{MP} \gamma_{Cl^{-MP}} [Cl^-]^{MP} = \gamma_{Na^{+P}} [Na^+]^P \gamma_{Cl^{-P}} [Cl^-]^P \quad (4.23)$$

3) Electroneutrality in the macroporosity:

$$[Na^+]^P = [Cl^-]^P \quad (4.24)$$

4) Charge balance in the microporosity:

$$[Na^+]_0 = [Na^+]^{MP} - [Cl^-]^{MP} \quad (4.25)$$

Note that imposing Donnan equilibrium between the external water and the macropore solution would be redundant.

The solution is then given by the following set of equations:

$$[Na^+]^{MP} = \frac{[Na^+]_0 + \sqrt{[Na^+]_0^2 + 4\Gamma_1 [Cl^-]^2}}{2} \quad (4.26)$$

$$[Cl^-]^{MP} = \frac{-[Na^+]_0 + \sqrt{[Na^+]_0^2 + 4\Gamma_1 [Cl^-]^2}}{2} \quad (4.27)$$

$$[Cl^-]^P = [Na^+]^P = \sqrt{\Gamma_1 \Gamma_2} [Cl^-] \quad (4.28)$$

$$\Gamma_2 = \frac{\gamma_{Na^{+MP}} \gamma_{Cl^{-MP}}}{\gamma_{Na^{+P}} \gamma_{Cl^{-P}}} \quad (4.29)$$

Let Γ_3 be defined as:

$$\Gamma_3 = \frac{\gamma_{Na^+} \gamma_{Cl^-}}{\gamma_{Na^{+P}} \gamma_{Cl^{-P}}} \quad (4.30)$$

Then:

$$[Cl^-]^P = [Na^+]^P = \sqrt{\Gamma_3} [Cl^-] \quad (4.31)$$

It is relevant here to point out that Equation (4.27) and Equation (4.20) are equivalent, in case the volume of reference for $[Na^+]_0$ is that of microporosity, which further confirms that the Birgersson and Karnland (2009) model represents a special case of a more general problem.

Then let the Debye length be defined as:

$$\lambda_D = \sqrt{\frac{\varepsilon RT}{2F^2 I_c}} \quad (4.32)$$

where ε is the permittivity of the medium, and I_c is the ionic strength of the solution. The Debye length (a function of the electrolyte solution) plays an important role in this context, as it gives a notion of the characteristic length over which the overpotential of the clay walls decays into the bulk. More generally, it can be assumed that a given constant K exists such that the double diffuse layer reaches a distance $\lambda'_D = K / \sqrt{I_c}$ from the clay walls. Beyond that distance, bulk water is found.

Let then the bulk surface area be calculated as:

$$S_{Bulk} = \rho_s A_{spec} \phi_m \quad (4.33)$$

The pore space occupied by the double diffuse layer is:

$$V^{MP} = S_{Bulk} \lambda'_D \quad (4.34)$$

if V^{MP} is less than ϕV_T

It follows that the microporosity is:

$$\phi^{MP} = \frac{V^{MP}}{V_T} \quad (4.35)$$

and the macroporosity becomes:

$$\phi^P = \phi - \phi^{MP} \quad (4.36)$$

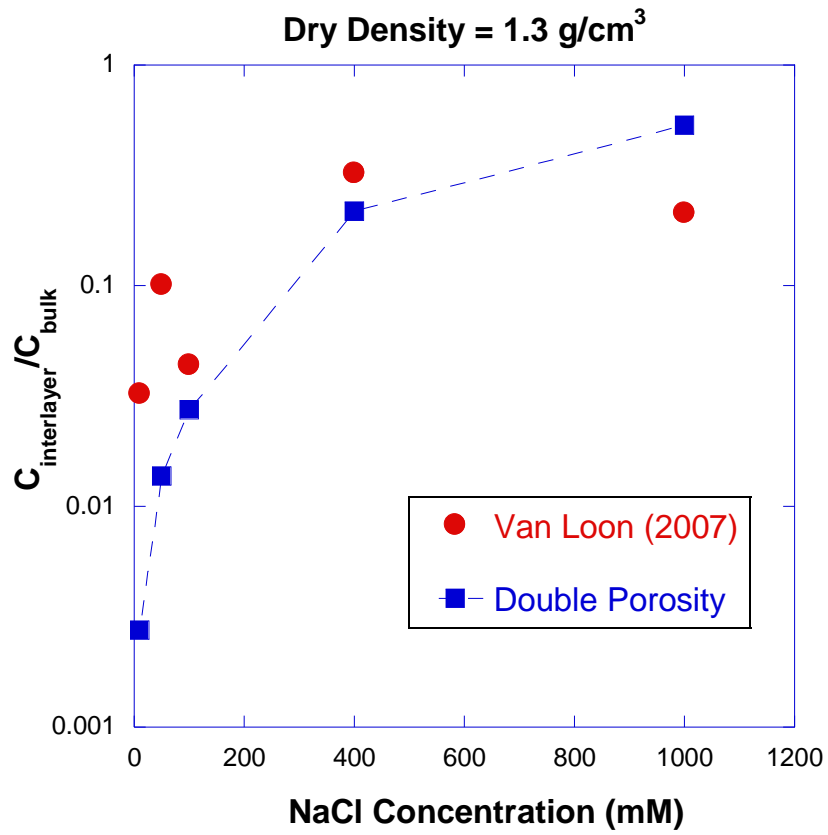
Therefore, the function of distribution of concentration becomes (Figure 4-16):

$$\begin{cases} C(x, y, z) = [Cl^-]^{MP}, & \forall (x, y, z) \in \phi^{MP} \\ C(x, y, z) = \sqrt{\Gamma_3} [Cl^-], & \forall (x, y, z) \in \phi^P \end{cases} \quad (4.37)$$

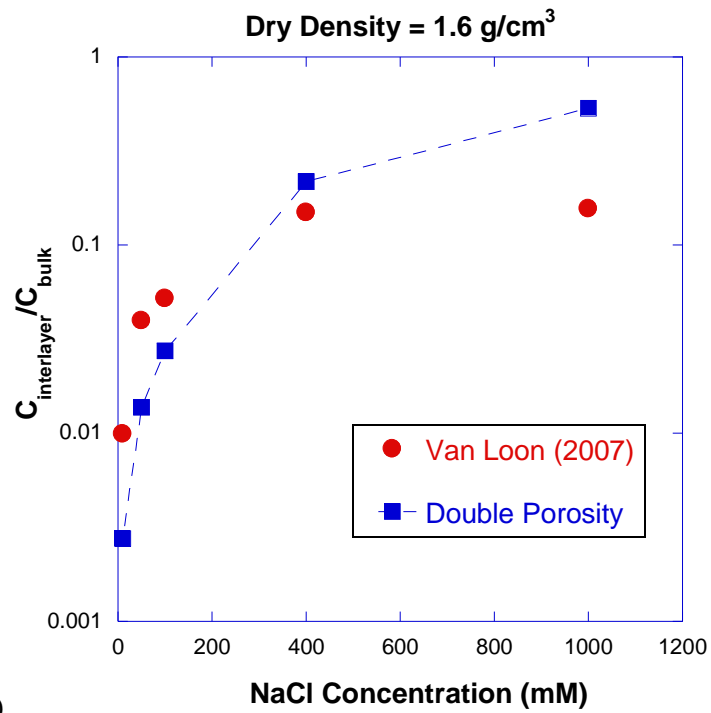


Figure 4-16. Spatial distribution of concentration of chloride as modeled in CrunchFlow.

Figure 4-17 shows the results obtained with those hypotheses for the cases considered in Van Loon et al. (2007). As can be seen, this approach does not really improve the fit with the Van Loon experimental data on the lower end of the spectrum (see Figure 4-17) of ionic strength values considered as compared to the Birgersson and Karnland model. In fact, as ionic strength decreases, the calculated thickness of the double diffuse layer becomes larger up to the point that it occupies the entire pore space, thus replicating the results of the single type pore model. On the higher end, the double type pore model consistently overestimates the actual chloride concentration in the pore water, as the concentration in the bulk water (orders of magnitude larger than that of the double diffuse layer) weighs decisively in the resulting average. All this suggests that, even though allowing for the fact that concentration varies over the pore space, the modeled dual distribution of concentration fails to reproduce the variation in diffusion rates and gradients properly.



(a)



(b)

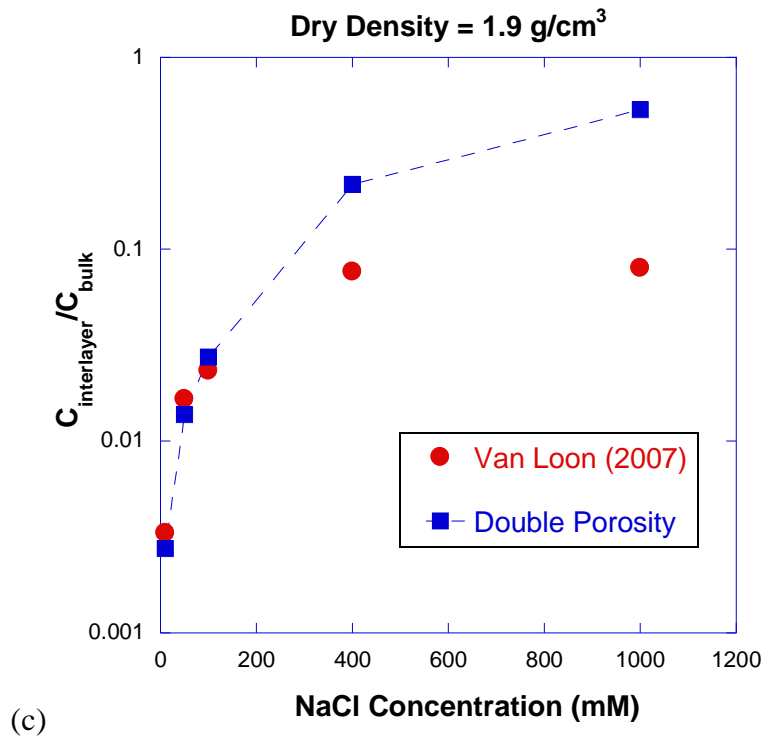


Figure 4-17. Fit of experimental data reported by Van Loon et al. (2007) obtained by the single type pore model: (a) 1300 kg/m³, (b) 1600 kg/m³, (c) 1900 kg/m³

4.6.4 Analytical Solution

In view of the conclusions reached thus far, a more sophisticated model is required to evaluate the actual distribution of concentration in the pore space. To that aim, it was deemed useful to approach the problem by attempting to solve the differential equations that describe the spatial distribution of electrical potential and its influence on the concentration of ionic species (Kirby, 2010).

Let the general form of the Poisson-Boltzmann equation be given by:

$$\nabla^2 \phi = -\frac{F}{\varepsilon} \sum_i^N c_{i,\infty} z_i \exp\left(-\frac{z_i F \phi}{RT}\right) \quad (4.38)$$

where $c_{i,\infty}$ represents the concentration of the i -th ionic species in the region of the pore unaffected by the electrical potential of clay walls.

For most practical cases, the Poisson-Boltzmann equation can only be solved numerically. Nevertheless, the problem simplifies significantly when dealing with a binary solution, as in this case. Moreover, if the product $z_i \phi$ is small enough with respect to unity, the exponential function could be linearized by truncating the Taylor expansion to the second term. Under such conditions, and assuming that clay particles are arranged according to a layered structure, so that the pores resemble the spaces between two parallel plates, the distribution of the electrical potential can be described by:

$$\varphi = \varphi_0 \frac{\cosh(y / \lambda_D)}{\cosh(d / \lambda_D)} \quad (4.39)$$

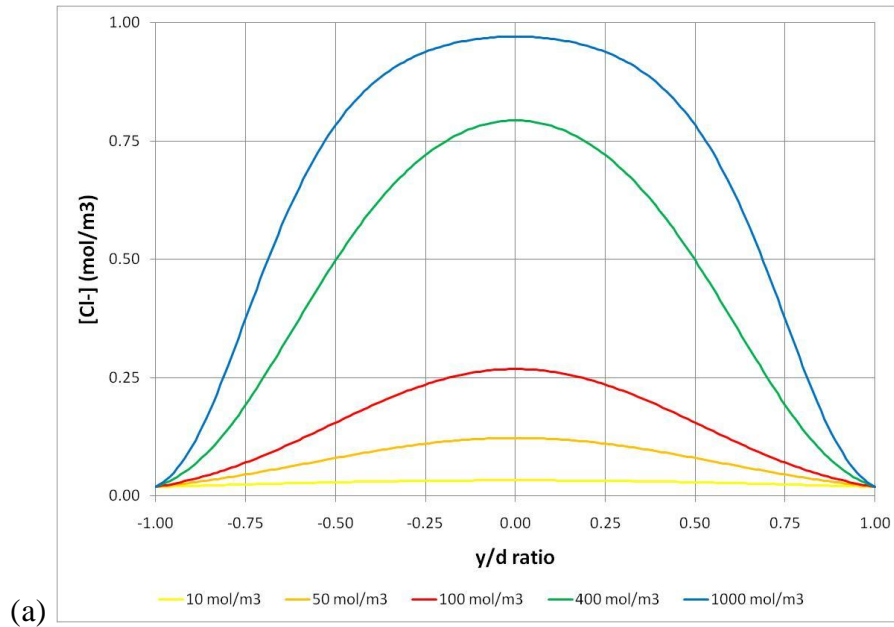
where φ_0 represents the electrical potential of the shear plane, d is the half-spacing between two layers of clays and y varies between $-d$ and d .

Then, the distribution of chloride concentration as a function over the pore space becomes:

$$C(x, y, z) = [Cl^-]^p \exp \left[-\frac{zF}{RT} \varphi_0 \frac{\cosh(y / \lambda_D)}{\cosh(d / \lambda_D)} \right] \quad (4.40)$$

where, for the sake of simplicity, the concentration of chloride in the bulk water $[Cl^-]^p$ was assumed to be equal to the concentration in the reservoir solution (thus neglecting any activity effects), and z (explicitly written here for more general cases) is its valence.

Trial and error was required in order to fit experimental values of Van Loon et al. (2007) by adjusting the variables φ_0 and d for all cases considered. Figure 4-18 shows the profiles obtained for dry densities equal to 1300 kg/m^3 (a), 1600 kg/m^3 (b) and 1900 kg/m^3 (c) with values listed in Table 4-6.



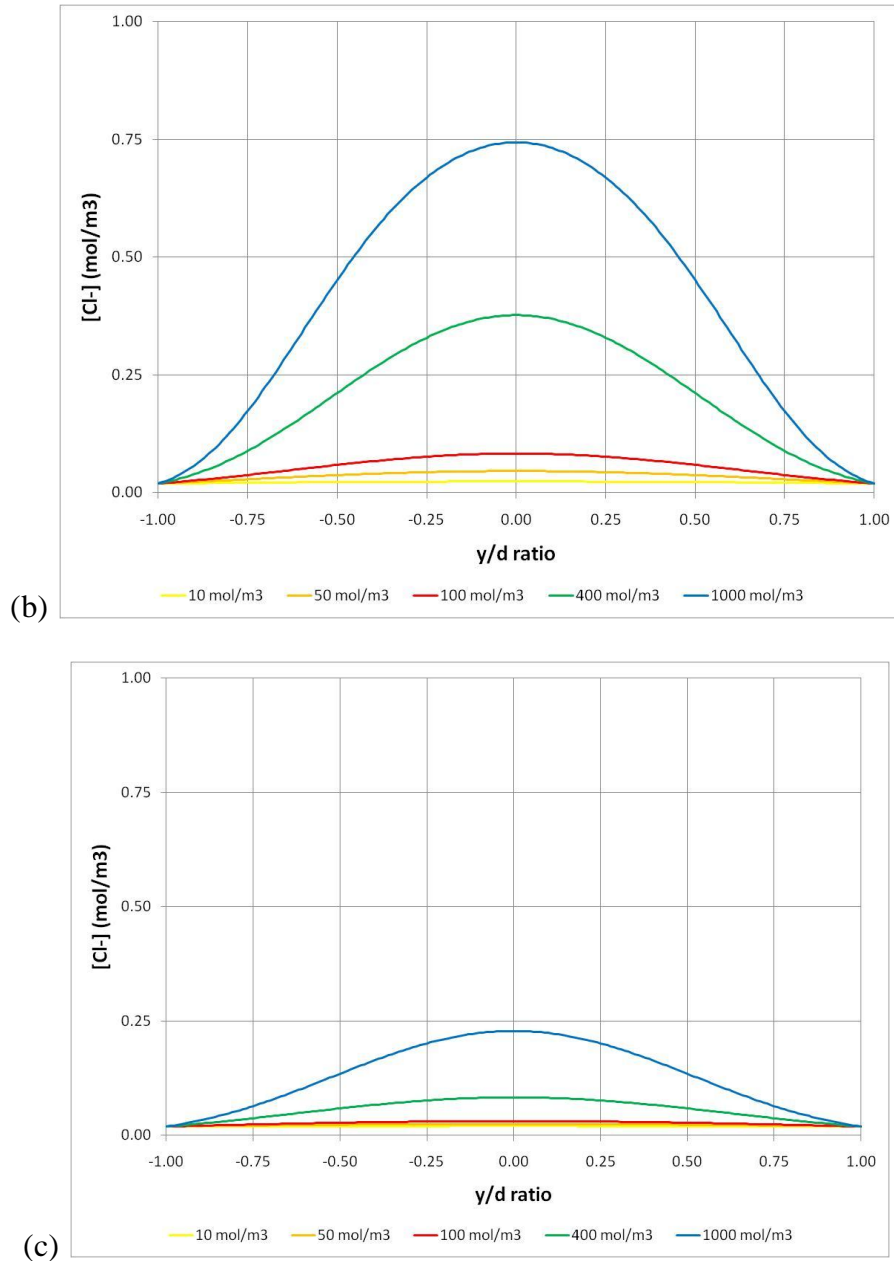
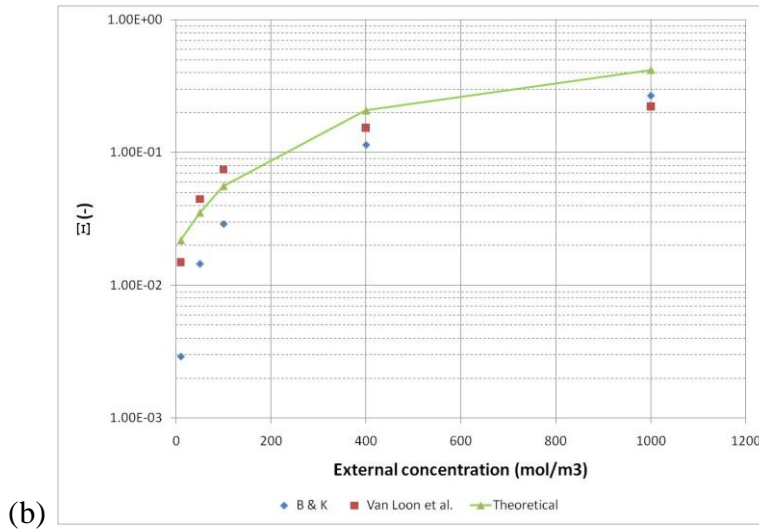
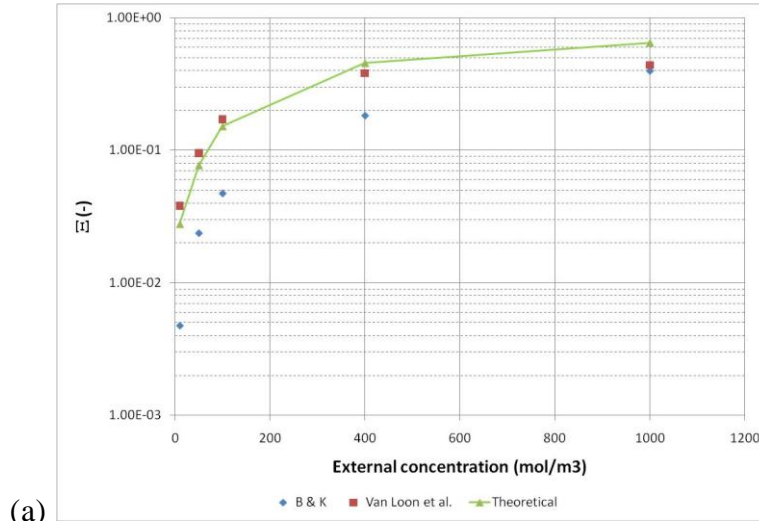


Figure 4-18. Normalized profiles of concentration of chloride obtained with varying ionic strength for a range of dry density values (a) 1300 kg/m³; (b) 1600 kg/m³; (c) 1900 kg/m³.

Table 4-6. Values of electrical potential at the shear plane and of semispacing between clay layers as a function of dry density obtained by fitting procedures of experimental data reported by Van Loon et al. (2007).

Dry density (kg/m ³)	ϕ_0 (V)	d (m)
1300	-0.10	1.70E-09
1600	-0.10	1.00E-09
1900	-0.10	5.00E-10

The electrical potential estimated by means of this procedure is significantly higher than that measured by Sondi et al. (1996), as cited in Leroy and Revil (2004), for smectites, which is $\varphi_0 = -0.03$ V for a wide range of pH values. Figure 4-19 shows the fit obtained of the experimental data.



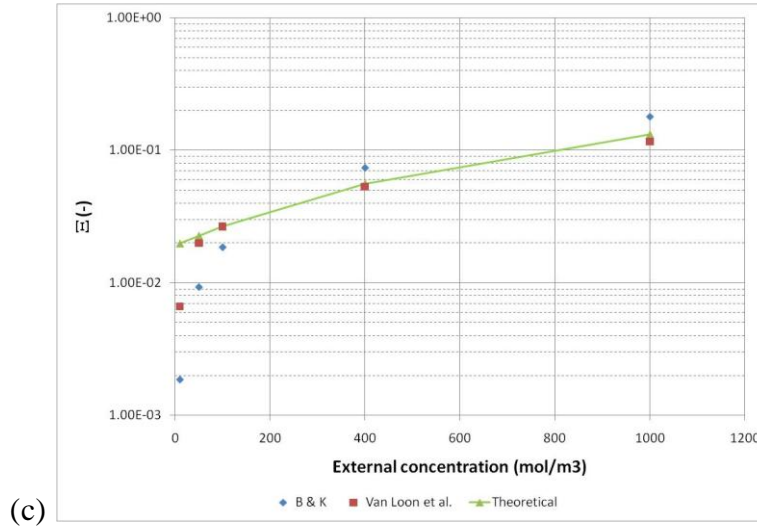


Figure 4-19. Fit of experimental data reported by Van Loon et al. (2007) obtained by the analytical solution of the simplified form of the Poisson-Boltzmann equation for the case of a binary solution between two parallel plates: (a) 1300 kg/m³; (b) 1600 kg/m³; (c) 1900 kg/m³.

For lower dry densities, there is acceptably good agreement between modeled and experimental values of Ξ_{Cl^-} at lower ionic strengths. For the same low dry densities, however, the model tends to overestimate the measured concentration at high ionic strength (Figure 4-19 (a) and (b)). In contrast, at a high dry density of 1900 kg/m³ (Figure 4-19 (c)) the analytical model fits the data reasonably well at high ionic strength, while overestimating the data at low ionic strength. One expects the closest agreement between a model based on a single type of porosity consisting of interlamellar spaces between clay sheets when the dry density is high and/or when the ionic strength is low, since in this case the electrical double layer should be wide and bulk water should not be present at all. The lack of agreement here may in fact be due to experimental artifacts associated with measurement of diffusive fluxes under these conditions, since the analytical solution for this simple binary system should be exact. Or the actual configuration of the pore space in the compacted bentonite is more complicated than can be represented with a single type of porosity with a single fixed interlamellar spacing and electrical double layer thickness. Despite these complexities, we plan to pursue the application of the analytical or semi-analytical solution in the context of multicomponent diffusion, since this appears to provide the closest match to the data over the range of conditions.

4.7 Future Work

The long-term R&D plans are to develop modeling capabilities and conduct laboratory experiments. Collaboration with international partners to address the technical issues is presented in Section 1.3. This subsection presents the work activities in the remaining months of FY11 and in FY12.

4.7.1 THM Modeling

- The double-structure model will be implemented into TOUGH-FLAC in the remaining months of FY11.
- The prototype of a fully coupled THMC simulator, TOUGHREACT-FLAC 3D, will be developed in the “Repository Science-THCM Near Field” work package. That development will be used in the EBS work activities in FY12.
- The double-structure model provides the link for incorporating the effects of chemical variables on the mechanical behavior of expansive clays. The linkage and its effects on THMC processes will be investigated.
- The BBM and double-structure capability development will be applied to conduct modeling of DECOVALEX cases, or of a major Mont Terri field experiment.

4.7.2 Reactive-Diffusive Transport

- Improvement of the mean electrostatic potential calculation based on Donnan equilibrium so that it captures the observed effective diffusivity over a wider range of conditions (bentonite compaction and ionic strength). This may involve an explicit integration over space, as in Figure 4-19a-c above, based on a semi-analytic approach for more general multicomponent systems.
- Calculation of the full Poisson-Boltzmann equation in the vicinity of the charged clay surfaces. This will likely be a nanometer scale version of the approach described above, with a focus on one or at most several clay grains, and will be used to provide guidance on possible approaches for treating the full continuum scale problem.
- Investigation of pore-network-scale modeling for modeling transport through clays.
- Collaboration with Dr. James Davis on a new set of radionuclide tracer experiments through clay (to be funded in part by the “Repository Science-THCM Near Field” work package).

4.8 References

- Alonso, E.E., J. Vaunat, A. Gens, 1999, Modelling the mechanical behaviour of expansive clays. *Engineering Geology* 54, p. 173–183.
- Appelo, C.A.J., A. Vinsot, S. Mettler, S. Wechner, 2008, Obtaining the porewater composition of a clay rock by modeling the in- and out-diffusion of anions and cations from an in-situ experiment, *Journal of Contaminant Hydrology* 101, p. 67–76.
- Birgersson, M., O. Karnland, 2009, Ion equilibrium between montmorillonite interlayer space and an external solution - Consequences for diffusional transport, *Geochimica et Cosmochimica Acta* 73, p.1908–1923.
- Barnichon, J.D., IRSN proposal - the SEALEX In Situ Tests, Presentation given at 7th DECOVALEX 2011 workshop, April 2011, Helsinki.
- Bourg, I.C., A.C.M. Bourg, G. Sposito, 2003, Modeling diffusion and adsorption in compacted bentonite: a critical review, *J. Contam. Hydrol.* **61**, p. 293–302.
- Bourg, I.C., G. Sposito, A.C.M. Bourg, 2006, Tracer diffusion in compacted, water-saturated bentonite, *Clays Clay Miner.* **54**, p. 363–374.

- Bourg, I.C., G. Sposito, A.C.M. Bourg, 2007, Modeling cation diffusion in compacted water-saturated sodium bentonite at low ionic strength. *Environ. Sci. Technol.* 41, 8118–8122.
- Corkum A.G., C. D. Martin, 2007, Modeling a mine-by test at the Mont Terri rock laboratory, Switzerland. *International Journal of Rock Mechanics & Mining Sciences* 44, p. 846-859.
- Cuss, R., Large scale gas injection test (Lasgit): Progress to May 2010, Presentation given at 6th DECOVALEX 2011 workshop, October 2010, Wuhan.
- Donat, R., A.Akdogan, E. Erdem, H. Cetisli, 2005, Thermodynamics of Pb^{2+} and Ni^{2+} Adsorption onto Natural Bentonite from Aqueous Solutions, *Journal of Colloid and Interface Science*, Vol. 286, p. 43-52.
- Garitte, B., New In Situ Experiments at Mt Terri, Presentation given at 6th DECOVALEX 2011 workshop, October 2010, Wuhan.
- Gaucher, E.C., P. Blanc, J.M. Matray, N. Michau, 2004, Modeling Diffusion of an Alkaline Plume in a Clay Barrier, *Applied Geochemistry* 19, p. 1505–1515.
- Gens, A., J. Vaunat, B. Garitte, B., Y.Wileveau, 2007, In situ behaviour of a stiff layered clay subject to thermal loading: observations and interpretation. *Geotechnique* 57, No. 2, 207–228.
- Glaus, M., B. Baeyens, M. Bradbury, A. Jakob, L. Van Loon, A. Yaroshchuk, 2007, Diffusion of ^{22}Na and ^{85}Sr in montmorillonite: evidence of interlayer diffusion being the dominant pathway at high compaction, *Environmental Science and Technology* 41, p. 478–485.
- Gonçalvès, I., P. Rousseau-Gueutin, A. Revil, 2007, Introducing interacting diffuse layers in TLM calculations: a reappraisal of the influence of the pore size on the swelling pressure and the osmotic efficiency of compacted bentonites, *J. Colloid Interface Sci.* **316**, p. 92–99.
- Houseworth, J.E., 2010, The DOE Used Fuel Disposition Campaign Features, Events, and Processes (FEP) Evaluation Report for Bentonite/Clay/Shale Systems, DOE Used Fuel Disposition Campaign, Lawrence Berkeley National Laboratory.
- Kim, H., T. Suk, S. Park, C. Lee, 1993, Diffusivities for ions through compacted Na bentonite with varying dry bulk density, *Waste Manag.* 13, p. 303–308.
- Kirby, B., 2010, *Micro- and nanoscale fluid mechanics, Transport in microfluidic devices*, Cambridge University Press, New York.
- Khan, S.A., 2002, Sorption of Long-Lived Radionuclides Cesium-134, Strontium-85 and Cobalt-60 on Bentonite, *Journal of Radionanalytical and Nuclear Chemistry*, Vol. 258, No. 1, p. 3-6.
- Lemmens, K., 2001, The Effect of Clay on the Dissolution of Nuclear Waste Glass”, *Journal of Nuclear Materials*, Vol. 298, p. 11-18.
- Leroy, P., A. Revil, 2004, A triple-layer model of the surface electrochemical properties of clay minerals, *Journal of Colloid and Interface Science* 270, p.371–380.
- Leroy, P., A. Revil, D. Coelho, 2006, Diffusion of ionic species in bentonite, *J. Colloid Interface Sci.* 296 (1), p. 248–255.
- Madsen, F.T., 1998, Clay mineralogical investigations related to nuclear waste disposal. *Clay Miner.* 33, 109-129.
- Muurinen A., 1994, Diffusion of anions and cations in compacted sodium bentonite. VTT Publication 168, Espoo Technical Centre, Finland.

- NAGRA, 2002, Project opalinus clay. Safety Report. Demonstration of disposal feasibility for spent fuel, vitrified high-level waste and long-lived intermediate-level waste (2002). TR 02-05.
- Nutt, M., 2010, Used Fuel Disposition Campaign International Activities Implementation Plan, (FCR&D-USED-2011-000016 REV 0), U.S. DOE Used Fuel Disposition Campaign.
- Nutt, M., 2011, Used Fuel Disposition Campaign Disposal Research and Development Roadmap (FCR&D-USED-2011-000065 REV 0), U.S. DOE Used Fuel Disposition Campaign.
- OECD, 2003, Engineering barrier systems and the safety of deep geological repositories (State-of-the-art Report), ISBN 92-64-18498-8.
- Ochs, M., B. Lothenbach, H. Wanner, H. Sato, M. Yui, 2001, An integrated sorption–diffusion model for the calculation of consistent distribution and diffusion coefficients in compacted bentonite, *J. Contam. Hydrol.* 47, p. 283–296.
- Pusch, R., 2001, The microstructure of MX-80 clay with respect to its bulk physical properties under different environmental conditions. SKB, TR-01-08, 111 pp.
- Sabodina, M.N., S.N. Kalmykov, Y.A. Sapozhnikov, E. V. Zakharova, 2006, Neptunium, Plutonium, and ¹³⁷Cs Sorption by Bentonite Clays and their Speciation in Pore Waters, *Journal of Radioanalytical and Nuclear Chemistry*, Vol. 270, No. 2, p. 349-355.
- Samper, J., C. Lu, L. Montenegro, 2008, Reactive Transport Model of Interactions of Corrosion Products and Bentonite, *Physics and Chemistry of the Earth* 33, p. S306–S316.
- Sondi, I., J. Biscan, V. Pravdic, 1996, Electrokinetics of pure clay minerals revisited, *Journal of Colloid and Interface Science* 178, p. 514–522C.
- Steeffel, C., Development of an explicit diffuse layer model for CrunchFlow, 2010.
- Steeffel, C., J. Rutqvist, C.F. Tsang, H.H. Liu, E. Sonnenthal, J. Houseworth, J. T. Birkholzer, Reactive Transport and Coupled THM Processes in Engineering Barrier Systems (EBS), Lawrence Berkeley National Laboratory (LBNL), Final Report of FY2010 Activities, Berkeley, August 2010.
- Van Genuchten, M.Th., 1980, A closed-form equation for predicting the hydraulic conductivity of unsaturated soils, *Soil Sci. Soc. Am. J.*, 44, p. 892-898.
- Van Loon, L., M. Glaus, W. Müller, 2007, Anion exclusion effects in compacted bentonites: Towards a better understanding of anion diffusion, *Applied Geochemistry* 22, p. 2536–2552.
- Wersin, P., E. Curti, C.A.J. Appelo, 2004, Modelling bentonite-water interactions at high solid/liquid ratios: swelling and diffuse double layer effects. *Appl. Clay Sci.* 26, p. 249-257.
- Zuidema, P., 2007, Advancements in Deep Geological Disposal of Radioactive Waste through International Cooperation: The Role of Underground Laboratories – Mont Terri Project, Proceedings of the 10 Year Anniversary Workshop, pp 69-71, Rep. Swiss Geol. Surv. 2.

**DISPOSAL SYSTEMS EVALUATION FRAMEWORK
(DSEF) VERSION 1.0 AND THERMAL ANALYSIS**

5. Disposal System Evaluation Framework (DSEF) and Thermal Analysis

5.1 DSEF Conceptual Abstraction

The Used Fuel Disposition (UFD) Campaign within the Department of Energy's Office of Nuclear Energy (DOE-NE) Fuel Cycle Technology (FCT) program has been tasked with investigating the disposal of the nation's high-level nuclear waste (HLW) for a range of potential waste forms and geologic environments.

The Disposal Systems Evaluation Framework (DSEF) is being developed at Lawrence Livermore National Laboratory to formalize the development and documentation of repository conceptual design options for each waste form and environment combination. This report summarizes current status and plans for the remainder of FY11 and for FY12.

This progress report defines the architecture and interface parameters of the DSEF *Excel* workbook, which contains worksheets that link to each other to provide input and document output from external codes such that concise comparisons between fuel cycles, disposal environments, repository designs and engineered barrier system materials can be performed. Collaborations between other Used Fuel Disposition Campaign work packages and US Department of Energy / Nuclear Energy campaigns are clearly identified. File naming and configuration management is recommended to allow automated abstraction of data from multiple DSEF runs.

Waste forms are examined with respect to three fuel cycles: open, modified open and closed. The resulting six waste types from each cycle are identified as examples with dimensions, mass, reactor burnup and properties. Seven disposal environments were initially identified, with the four key mined and saturated repositories (granite, salt, clay/shale and deep borehole) being part of the base case for DSEF evaluations. Together with six fuel types and pre-encapsulation aging times (short, moderate and extended), 24 base case models are proposed. Additionally, evaluation of the DSEF using tuff (Yucca Mountain) and salt (WIPP) will be used as validation test cases.

The DSEF interfaces with more sophisticated models for thermal analysis, and is capable of efficient calculations using simplified conceptual models. The DSEF will document the thermal calculations, but will not duplicate development or calculation results done by other UFD work packages. LLNL (as part of other UFD work packages) is also developing an interface to its sophisticated finite element thermal code that was developed outside of the UFD campaign. Thermal models have been identified and initially tested within the DSEF – analytic and finite element. Finite element modeling employs *TOPAZ3D* (Wemhoff et al, 2007) together with *TrueGrid* (Rainsberger 2006) to generate geometric shapes that represent waste packages. The analytic models use *Mathcad* (Mathcad 15.0). This tool will be available to all the UFD participants, including the Generic Disposal System Environments Performance Assessment development team, which currently does not incorporate a sophisticated thermal model.

In the performance assessment area, the DSEF documents the inputs going to, and the results coming from such GDSE performance assessment models, therefore documenting and integrating results rather than generating results directly. More importantly, DSEF is a knowledge management tool that creates a reference location for PA models to be documented and compared. Material properties to be used in the performance assessment portion of DSEF are identified and follow a *Features, Events and Processes* methodology for determination of relevance. Additionally, the impacts of DSEF on fuel cycle systems are explained. Cost analysis of each disposal environment is initially examined, with the goal of ultimately being able to derive rough

estimated costs of repository construction quickly from linked *Thermal, Materials Longevity* and PA worksheets within the DSEF.

5.2 DSEF Implementation

For each waste form and geologic environment combination, there are multiple options for a repository conceptual design. The Disposal Systems Evaluation Framework (DSEF) is being developed to formalize the development and documentation of options for each waste form and environment combination.

The DSEF is being implemented in two parts. One part is a *Microsoft Excel* workbook with multiple worksheets. This workbook is designed to be user friendly, such that anyone within the UFD campaign can use it as a guide to develop repository conceptual designs that respect thermal, geometric, and other constraints. The other part is a *Microsoft Access* relational database file that will be centrally maintained to document the ensemble of conceptual designs developed with individual implementations of the *Excel* workbook. At the present time, only the *Excel* portion of DSEF is under development, with the *Access* portion scheduled for development later in FY11 and FY12.

The DSEF *Access* relational database file will collect the key inputs, results, and interface parameters from each *Excel* workbook implementation. The power of a relational database will then be available to sort and organize groups of designs, and to answer queries about what evaluations have been done in the UFD campaign.

The DSEF *Excel* workbook includes worksheets for aspects of the repository design process, including waste form, environment, geometric constraints, engineered barrier system (EBS) design, thermal management, performance assessment (PA), materials longevity, cost, and fuel cycle system impacts. Each of these worksheets or sets of worksheets guides the user through the process of developing internally consistent design options, and documenting the thought process. The worksheets interact with each other to transfer information and identify inconsistencies to the user.

In some cases, the worksheets are stand-alone, and in other cases (such as PA), the worksheets refer the user to another tool, with the user being responsible to transfer summary results into the DSEF worksheet. For example, the DSEF PA worksheet will have only a minimal 1D analytic transport model, and will rely on the more sophisticated models such as those being developed by the Generic Disposal System Environment (GDSE) work packages in the UDF Campaign. Researchers at Sandia National Laboratories (SNL), Argonne National Laboratory (ANL) and Los Alamos National Laboratory (LANL) are developing Generic Disposal System Environment (GDSE) performance assessment models using the *GoldSim* software package (Goldsim 2009) for salt, clay, and granite repository environments, respectively (Wang and Lee 2010, Chu et al. 2011, Freeze and Lee 2011, Wang 2011, Lee et al. 2011, Nutt et al. 2011). The DSEF documents the inputs going to, and the results coming from such GDSE performance assessment models. LLNL and SNL have licenses for GoldSim and are able to execute the GDSE PA models directly. Other laboratories may request SNL or LLNL to execute the GDSE PA model. It should be noted that the GDSE model interfaces with an input spreadsheet and with a parameter database. The DSEF user will use those same tools for the GDSE calculation. The user will document in the DSEF the pertinent inputs and results from GDSE, as well as configuration management information (GDSE version and GDSE parameter database version) and GDSE files (input spreadsheet, and output files). In the PA area, the DSEF documents and integrates results, rather than generating the results directly.

A second example of DSEF interface with more sophisticated models is thermal analysis. As described in more detail in Section 5.8, the DSEF (or its auxiliary software) will be capable of efficient calculations using simplified conceptual models. LLNL (as part of the Thermal and EBS work packages) is also developing an interface to its sophisticated finite element thermal code that was developed (and is maintained) by the weapons program. This tool will be available to all the UFD participants, including the GDSE PA development team, which currently does not incorporate a sophisticated thermal model. The DSEF also will document results from the user's home organization thermal codes, should those be used. Again, the DSEF will document the thermal calculations, but will not duplicate development or calculation results done by other UFD work packages.

Finally, the DSEF includes several top-level worksheets, including inputs and results, interface parameters, and knowledge management (i.e. references to reports, models, and publications). These sheets enable the user to see the overall picture on only a few summary worksheets, while developing the design option systematically using the detailed worksheets.

5.2.1 Excel File Architecture

The DSEF *Excel* file architecture is designed for two types of users. Each realization or instance of the file corresponds to a single repository conceptual design. The developer of the realization (i.e., the *repository designer*) is led through a logical process to develop an internally consistent conceptual design for a given waste form and geologic environment, that respects known geometric and thermal constraints. This requires carefully crafted worksheets for each aspect of the repository design, as well as a substantial body of information taken from the literature and organized to assist the repository designer. The other type of user is someone seeking to understand the design (the *post-design user*). This type of user needs to quickly see the inputs, constraints, design decisions, and results (performance, cost, footprint, etc.). The post-design user needs well-organized high-level information suitable to enable comparison of multiple designs. The post-design user will be able to obtain the information from the top-level worksheets in an *Excel* file documenting a single realization, as well as from the *Access* database that collects the results from multiple realizations. To meet the goals of the two types of users, the DSEF *Excel* file is organized into top-level worksheets and detail worksheets as described in Section 5.2.2. Because use of the DSEF will occur during its development, well-documented revision control is essential, so that post-design users can determine if comparison of results from different versions of the DSEF are valid, or if early results need to be rerun before the comparison is valid. Revision control is described in Section 5.2.3.

5.2.2 Architecture

Figure 5-1 shows the high level structure of the DSEF. At the top level, there are two elements of the DSEF. The *Excel* workbook is a user-friendly interface for data entry, documentation of repository designer decisions, and the results (performance, cost, etc.). It is designed for use by both the repository designer (and thus contains substantial background material for the designer's use) and by those seeking to understand the design (post-design users). Each design corresponds to a single realization of the *Excel* workbook, and the workbooks will be collected and archived. The *Access* database collects the results from multiple realizations, and is an alternative to examining individual *Excel* files, for post-design users. The functionality of a relational database greatly expands the capabilities of the post-design users, allowing searches for combinations of input parameters or for combinations of results (e.g., find all designs that had a performance better than a specified standard, or rank all designs by cost).

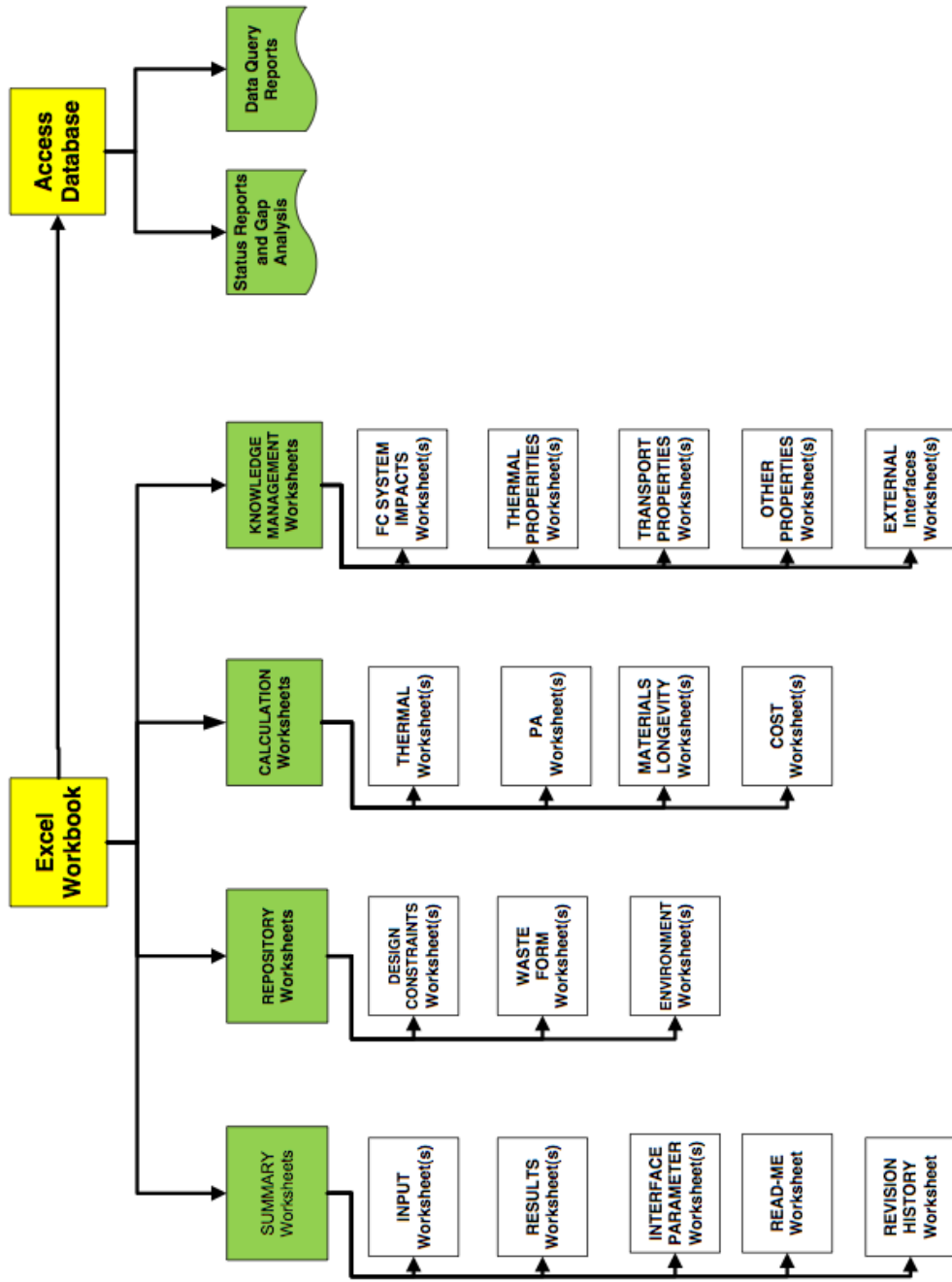


Figure 5-1. DSEF architecture schematic diagram.

For the *Excel* workbook, the worksheets are grouped into categories. The *Summary* category includes the *Input*, *Results*, and *Interface Parameter* worksheets. The *Input* worksheet guides the user through the input process and prompts the user to go to other worksheets during the design process. The *Results* worksheet documents the results of the design. The *Interface Parameter* worksheet documents all parameters that are passed from worksheet to worksheet, facilitating extraction of pertinent information to the *Access* database, and reducing the potential for hard-wired changes to mask differences between revisions of the DSEF. Finally, the *Read-me* and *Revision History* worksheets document the DSEF itself, and provide an entry point for users.

The *Repository* category of worksheets includes upper-level worksheets that show the *Design Constraints* (e.g., temperature limits), the *Waste Form* options, and the *Geologic Environments*. As the repository designer progresses through these worksheets, decisions will be made to accept pre-loaded information (e.g., the decay heat curve for a given waste form), or to use alternative information provided by the user. These decisions will be documented on both the individual worksheet and on at least one of the *Summary* category worksheets.

The *Calculation* category of worksheets documents the key aspects of the repository design. The *Thermal* worksheet uses the geometric decisions, along with the waste-form and environment properties, to determine if thermal design constraints are met. The user can iterate this process until an acceptable design is found. The *Results* worksheet will allow the user to capture the results of the failed thermal iterations, as well as the final iteration, to assist subsequent users (both post-design users and users developing alternative designs). The *Thermal* worksheet provides the user a number of options to calculate temperatures. These will include look-up tables of previous calculations, simple analytic models (located in separate files), more complex finite element models (located in separate files), or to documentation of calculations performed with the user's own model.

The *PA* worksheet uses the geometric decisions, the waste form, the environment, and the thermal results to estimate repository performance. The worksheet will include look-up tables of previous calculations, simple analytic models (located in separate files), and pointers to the Generic Disposal System Environment (GDSE) models available for use. The *PA* worksheet will document the *PA* calculation selected by the user, including inputs to GDSE models from the DSEF file. Results will also be documented on at least one of the *Summary* worksheets.

The *Materials Longevity* worksheet will document the engineered material chosen for the design, and will evaluate the viability of the selected materials in the repository environment.

The *Cost* worksheet uses unit costs (e.g., cost per unit length of a tunnel of a specified size in a specified geologic medium) taken from more detailed designs in the literature. The DSEF will prompt the user to develop the set of parameters needed to generate subsystem costs (tunnels, waste packages, etc.) for the design. Results will be documented on both the *Cost* worksheet and at least one of the *Summary* worksheets.

The *Knowledge Management* category of worksheets includes properties used by the other worksheets and interfaces of the design with other NE campaigns. The *Thermal Property* and *Transport Property* worksheets provide the property values to be used by the *Calculation* worksheets. Properties vary with environment type (e.g., clay vs. salt) and within an environment type (e.g., boom clay vs. Opalinus clay). Further, the literature often provides a range for a given property, due to material heterogeneity and measurement uncertainty. These worksheets show the user the options (including the ranges), and clearly document the user's choices, both on the

Property worksheet and at least one of the *Summary* worksheets. The *Property* worksheets (thermal and transport) include the upper level worksheet in which property values are selected, mid-level worksheets that show how the property ranges were developed, and reference-level worksheets that show or hyper-link to the underlying property data.

The *Fuel Cycle System Impacts* worksheet develops parameters to be provided to other NE campaigns, including the *Systems Analysis* and *Systems Engineering* campaigns. Figure 5-22 in Section 5.12 shows the relationship of the DSEF to the other fuel cycle models in the model pyramid. Finally, the External Interfaces worksheet shows information to be provided to (or taken from) other work packages within the *Used Fuel Disposition* Campaign. Section 5.3 shows more detail of the interaction among these worksheets.

5.2.3 Revision Control

Because DSEF inputs and outputs will change with each execution of the framework for differing scenarios, it is vital to clearly document revisions within the workbook itself. A *Revision Control* worksheet within the DSEF workbook will summarize (in text form) information on the system (clay, salt, granite etc), the waste form, and key inputs together with the date, time and *DSEF Developer* information. *Repository Design* users will also be required to enter notes documenting their usage of the file (date, time) on the *Input* worksheet, which will automatically be replicated on the *Revision Control* worksheet. This will provide a unique and transparent log of activities performed for each realization. The worksheet will also include a “to-do” list, in which the *Repository Design* user can identify previous realizations that need to be re-run with updated inputs. A “suggested improvement” list will allow any user to document their ideas for future runs.

The filename of the DSEF workbook includes characters that will be used to document revisions. The filename will be modified each time a revision is made such that traceability exists between current and previous workbooks, and such that no worksheets or results are overwritten. The filename will follow the following nomenclature:

DSEF-R#.#m-AA-NN-yyyymmdd-Run##.xlsx

where #.# are the revision numbers, and *m* is the minor revision letter for the DSEF version. For the run itself, AA is the 2-letter code for the users institution, NN is the user’s initials, yyyymmdd is the four digit year, 3 character month, and two digit day of the run, and Run## starts with 01 for the first run of the day by that user. A uniform filename structure will allow automated manipulation and abstraction of data from multiple DSEF workbooks, and logical sequencing of files in the DSEF archive of files.

Similar to the notations used within the NE Project Management system, AA should be replaced with AN for Argonne National Laboratory, IN for Idaho National Laboratory, LA for Los Alamos National Laboratory, LB for Lawrence Berkeley National Laboratory, LL for Lawrence Livermore National Laboratory, OR for Oak Ridge National Laboratory, PN for Pacific Northwest National Laboratory, SN for Sandia National Laboratories, etc. For example, the second model run of the day at LLNL by Harris Greenberg on April 1, 2012, using DSEF version 3.2a, would have file name:

DSEF-R3.2a-LL-HG-2012Apr01-Run02.xlsx

5.2.4 Configuration Management

Configuration management (CM) will be documented in a file stored on the LLNL GS Server, in path

“Programs – E/Nuclear Fuel Cycle/DSEF”

The CM file name is

“READ-ME-DSEF Configuration Management-R#.docx”

This file will be periodically updated as configuration management (CM) processes evolve. When that occurs, the CM file updater will increase the R# in the CM file name and move the prior version of the CM Read-me file to the

“Archive CM”

folder in the above path. The file updater will also add a line to the Revision History table (Table 5-1).

Table 5-1 Revision History

Revision	Updater	Date/time	Description of the Change
0	J. Blink	5/11/11	Initial file

The LLNL UFD-EBS work package manager will appoint a Responsible Individual and an Alternate Configuration Management of DSEF files. At the time of this deliverable report, Harris Greenberg is the Responsible Individual and James Blink is his Alternate.

The repository for DSEF files is the LLNL GS Server, in the above path. This server is regularly backed-up by LLNL-GS-IT staff. In addition, Harris Greenberg will maintain a duplicate set of folders on his PC.

LLNL staff with access to the GS Server can obtain DSEF software from the above path and write modified software files and DSEF realizations to the above path. Only Harris Greenberg or Jim Blink are allowed to delete files from the above path or to move them between folders. Staff (at LLNL or elsewhere) without access to the GS Server can obtain DSEF software from Harris Greenberg or Jim Blink, and can provide realization files to Harris or Jim Blink for storage in the above path. Once DSEF has matured, a user version may be placed on a UFD-accessible site such as the INL Portal or SNL SharePoint.

The following folders have been established in the above path. The purpose of each folder is listed after the folder name. For grouped files, see the note following the list of folders.

“Superseded CM READ-ME files” – This folder stores prior versions of this file.

“Current Software” – This folder stores the latest version of the DSEF *Excel* file (with version number #.#m in file name, which has the format

DSEF-R#.#m-AA-NN-yyyymmdd-Run##.xlsx,

where the first two fields are numbers and the third is a lower case letter). It also has the latest version of the DSEF *Access* file and the latest versions of auxiliary software files (such as *Mathcad* files)

“Superseded Software Versions” – This folder stores all prior versions of the DSEF *Excel*, *Access*, and auxiliary (such as *Mathcad*) files

“DSEF Realizations” – This folder stores completed realizations of the DSEF *Excel* and auxiliary files.

“Superseded DSEF Realizations” – This folder stores *DSEF Excel* and auxiliary files. The file name will be the original name, with “-superseded” inserted prior to the extension (e.g., prior to “.xlsx” for *Excel* files). In the “Input” worksheet of DSEF *Excel* files, and at or near the top of auxiliary files, the following will be placed: “superseded by file *name*”, where *name* is the file name of the superseding file.

A note on file grouping: In some cases, a DSEF realization will include the *Excel* file and one or more auxiliary files. These files will be placed in a subfolder in “DSEF Realizations” or “Superseded DSEF Realizations”. The subfolder will be named as if it were a standalone DSEF *Excel* file (with no extension), i.e.,

DSEF-R#. #m-AA-NN-yyyymmdd-Run##

The determination of when a series of minor revisions (the “m” in “#. #m”) is complete will be made by Harris Greenberg or Jim Blink. At that time, the final file will be archived in “Superseded Software Versions”. The same file will remain as the current file in “Current Software, with the second “#” being incremented, and the lower case letter changed to “a”. Similarly, when a series of revisions is complete and the next major release is due, the final file will be archived, and the current file (same content as the file being archived) will be named with the first # incremented and the second # and letter being “0a”. Thus, the first release of DSEF will have name “DSEF-R0.0a.xls”, and all realizations using that release will have names beginning with “DSEF-R0.0a”.

5.3 Inputs and Results

Figure 5-2 shows the flow of information through the DSEF *Excel* file. The remainder of this section discusses that information flow.

The *Inputs* worksheet is the starting point for the DSEF user (the repository concept developer). Upon entry to the worksheet, the user is asked to save the DSEF file with a name that meets the requirements of Section 5.2.4 (those requirements are repeated in the worksheet. Then, the user is asked to describe the repository concept being documented by this DSEF file. That description cell and the filename will be propagated to all the worksheets, so that printouts will be easily identifiable.

The *Inputs* worksheet then leads the user through a set of decision steps designed to elicit as much information as possible about the repository design being developed. The first step is to determine the geologic environment, the waste form, and the design and thermal constraints to be applied. This is done with a succession of list boxes. The choices made in early boxes tailor later boxes. For example, if the user selects a clay environment, there will be a subsequent list of types of clay (e.g. boom clay) to assist the user in selecting properties to be used in thermal and other analyses.

As the user further defines the repository design, opportunities are presented that allow choices among pre-loaded options. For example, if the user has selected boom clay, available thermal property values will be presented, including available minimum, maximum, and representative values from one or more references. In addition to having the option to select one of these numbers, the user is presented with the option to use their own number. The DSEF will clearly document, in the *Results* worksheet, the actual numbers used, as well descriptions of each number (e.g., *number provided by user with comment “_____”, or representative value from reference “author, date”*). After the *Inputs* worksheet has led the user through the choices available in the *Environments*, *Waste Forms*, and *Design Constraints* worksheets (supported by the *Thermal Properties* and *Transport Properties* worksheets, it will send the user to the *Thermal* worksheet, where the user will use internal DSEF tools or auxiliary software to develop temperature histories. The *Thermal* worksheet also leads the user to compare the temperatures to the design constraints and decide if the design (aging time, number of assemblies or canisters per waste package, waste package emplacement geometry, waste package spacing in boreholes/alcoves/drifts, and borehole/alcove/drift spacing) meets the constraints. If it does not, the user is prompted to enter the pertinent information in a table documenting iterations (which will be mirrored in the *Results* worksheet) and to modify the design parameters and run another iteration. When the user is satisfied that the constraints are met, the user is prompted to return to the *Inputs* worksheet.

The *Inputs* worksheet, after some clarification actions, sends the user to the *Materials Longevity* worksheet, which will address coupled processes and EBS materials performance. Again, iteration is permitted, including iteration back to the *Inputs* and *Thermal* worksheets.

When the *Materials Longevity* worksheet actions are complete, the user is sent to the *Inputs* worksheet and then on to the *PA* worksheet. The *PA* worksheet will function similarly to the *Thermal* worksheet, offering the user the opportunity to interpolate from prior results, to use a simple analytic transport model in auxiliary software, or to use the GDSE software being developed in other UFD work packages. Again, iteration is permitted, including iteration back to the *Inputs*, *Thermal*, and *Materials Longevity* worksheets.

When the *PA* worksheet actions are complete, the user is sent to the *Inputs* worksheet and then on to the *Cost* worksheet. A similar iterative process is followed there, and the user ends up back at the *Inputs* worksheet to finalize the DSEF realization. At this point, the *Results* worksheet has automatically pulled results in from the four *Calculation* worksheets (*Thermal*, *Materials Longevity*, *PA*, and *Cost*), and the *Interface Parameters* worksheet has recorded all information passed between among those four *Calculation* worksheets. As part of the finalization actions, the *Inputs* and *Results* worksheets provide information to the *FC Systems Impacts* and *External Interfaces* worksheets, where it will be recorded in the format requested by the external organizations.

The DSEF Access Database will draw information directly from the *Inputs* and *Results* worksheets, and if appropriate, from the *Interface Parameters* worksheet.

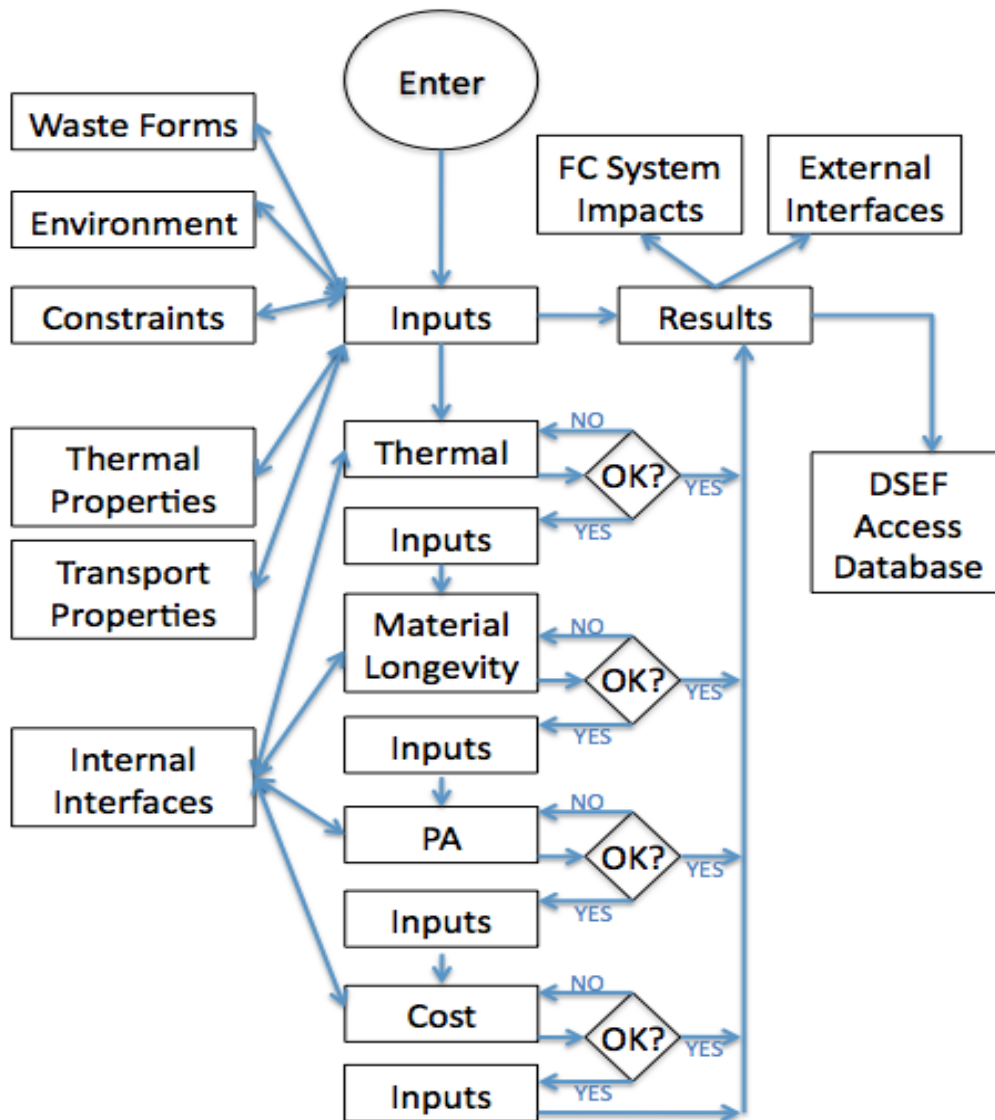


Figure 5-2. Information flow through DSEF Excel workbook.

5.4 Interface Parameters

As described in Section 5.2.2, the *Interface Parameter* worksheet documents all parameters that are passed from worksheet to worksheet (other than the *Inputs* and *Results* worksheets), facilitating extraction of pertinent information to the *Access* database, and reducing the potential for hard-wired changes to mask differences between revisions of the DSEF.

Interfaces between worksheets within DSEF are considered internal interfaces, and interfaces to other UFD work packages and to other DOE-NE campaigns are considered external interfaces.

5.4.1 Internal Interfaces

Calculation worksheets will require interface with information from a number of other worksheets. To ensure that these interfaces are easily understood and documented, the information passing between worksheets (other than the *Input* and *Results* worksheets) will pass through the *Interface*

Parameters worksheet. For example, a thermal property could pass to the *Input* and *Interface Parameters* worksheets and then be read by the *Thermal* worksheet.

Figure 5-3 is an Input-Process-Output diagram that provides an example of how the DSEF worksheets and external programs interface and work together to evaluated repository alternatives.

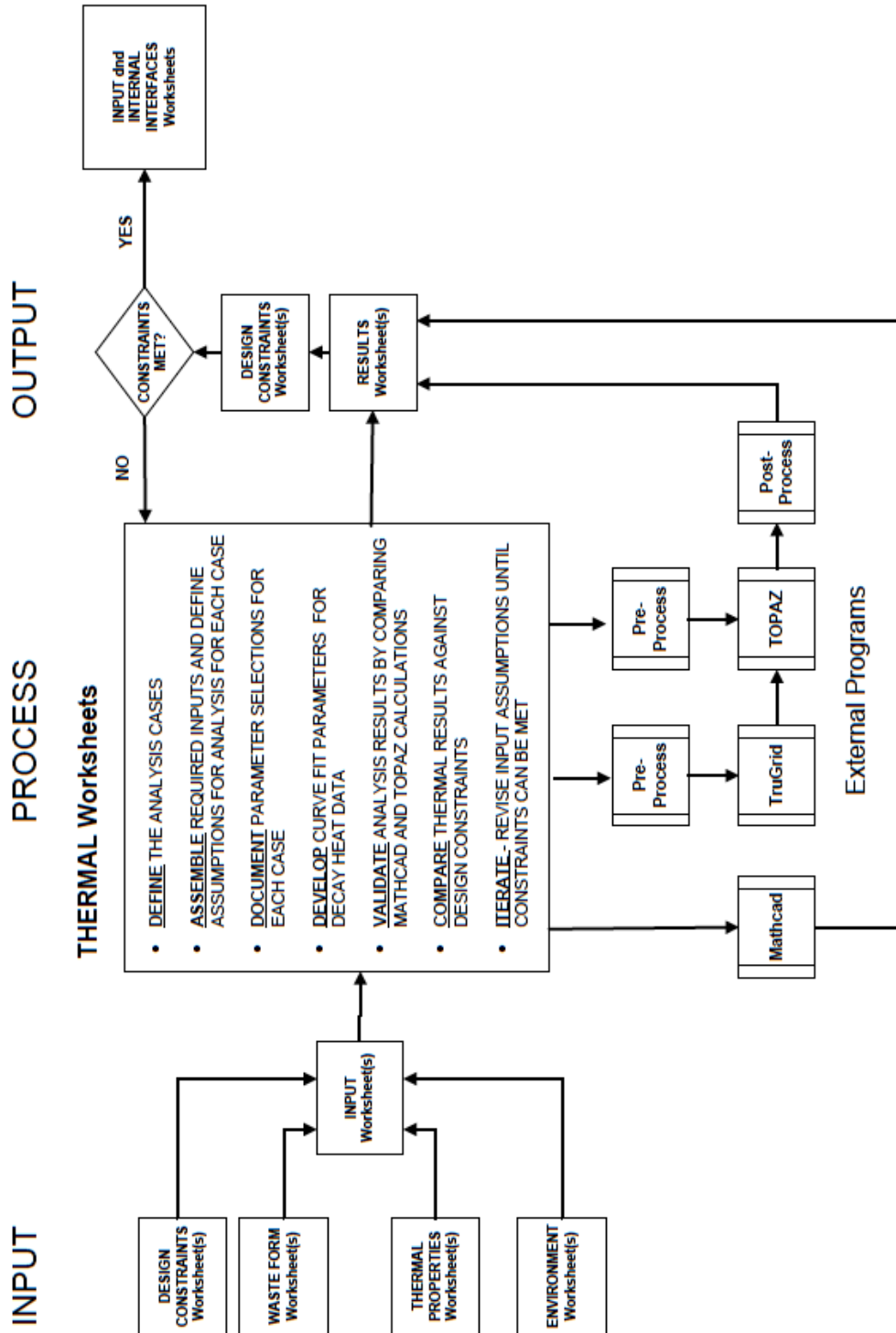


Figure 5-3. Interface Parameters – thermal worksheet input-process-output example.

On the left hand side of the figure several working-level worksheets feed information into the Inputs worksheet as follows:

Design Constraints:

- Repository Layout / Geometry
- Engineered Barrier Configuration / Materials
- Repository Environment Description
- Constraints – Thermal, Mechanical, Chemical, etc.

Waste Form:

- General Physical Description
- Radionuclide Inventory
- Decay Heat Data
- Canister Volume and Dimensions
- Thermal Properties:
- Host Rock Properties
- Engineered Barrier Material Properties
- Mean values, Ranges / Distributions
- QA Status / Confidence in Data
- Limitations / Assumptions

Environment:

- Host Rock Type
- Geologic Stratigraphy Assumed
- Porosity / Saturation Assumed
- Expected Chemical Environment

The central area of the figure shows the process steps addressed in the *Thermal* worksheet, and shows the external programs and interfaces where data are passed to *Mathcad* (Mathcad 15.0) and *TOPAZ3D* (Wemhoff et al, 2007), as described further in Section 5.8 of this report.

Mathcad has an *Excel* component that can read and write directly to the DSEF worksheets. However, pre-processing and post-processing interface programs are currently being developed to allow the DSEF user to set up and run *TOPAZ3D* (and its gridding pre-processor, *TrueGrid*) directly from the DSEF worksheets.

The *Thermal* worksheet will pass the following kinds of information to these external programs:

To Mathcad:

- Decay Heat
- Material Properties
- Other Problem Definition Data

To the *TrueGrid* grid generation tool (and its simplified interface being developed as part of DSEF):

- Geometry
- Mesh Spacing
- Material Zone Boundaries
- Boundary Conditions

To *TOPAZ3D* finite element code (and its simplified interface being developed as part of DSEF):

- Decay Heat
- Material Properties
- Other Problem Definition Data

The right-hand side of the figure shows the data passed from the external thermal analysis programs and the *Thermal* worksheet to the *Results* worksheet, and the operation of checking the results against the *Constraints*. If the results do not meet the constraints, then the design user modifies the input and performs additional iterations until the constraints are met. Once the constraints have been met, the successful combination of inputs and results are returned to the *Input* worksheet and passed to the *Interface Parameters* worksheet.

Data passed from the *Thermal* worksheet to *Results*:

- Definition of Cases Evaluated
- Waste Form and Canister Parameters
- Surface Storage Time
- Geologic Environment
- Repository Design Parameters

Data passed from the external analysis programs to *Results*:

- Peak and Transient Temperature Results for Each Analysis Case for
- Waste Form
- Canister Surface
- EBS Components
- Host Rock

5.4.2 External Interfaces

As described in Section 5.4.1, the *Interface Parameter* worksheets in DSEF will document information passing from one element of the DSEF to another element. This is similar function to that provided by the Information Exchange Documents (IED) on the Yucca Mountain Project, which tracked information passed between elements of the repository design and between the design and the performance assessment. The *Interface Parameter* worksheet provides a standard, common location to exchange information between the DSEF elements. Similarly, external interface worksheets are included to exchange information with other Work Packages in the Used Fuel Disposition Campaign and between the UFD Campaign and other DOE-NE Campaigns (Figure 5-3). The DSEF worksheets that will be specifically tailored for other organizations are the *FC System Impacts* worksheet (tailored for the Systems Analysis Campaign) and the *External Interfaces* worksheet.

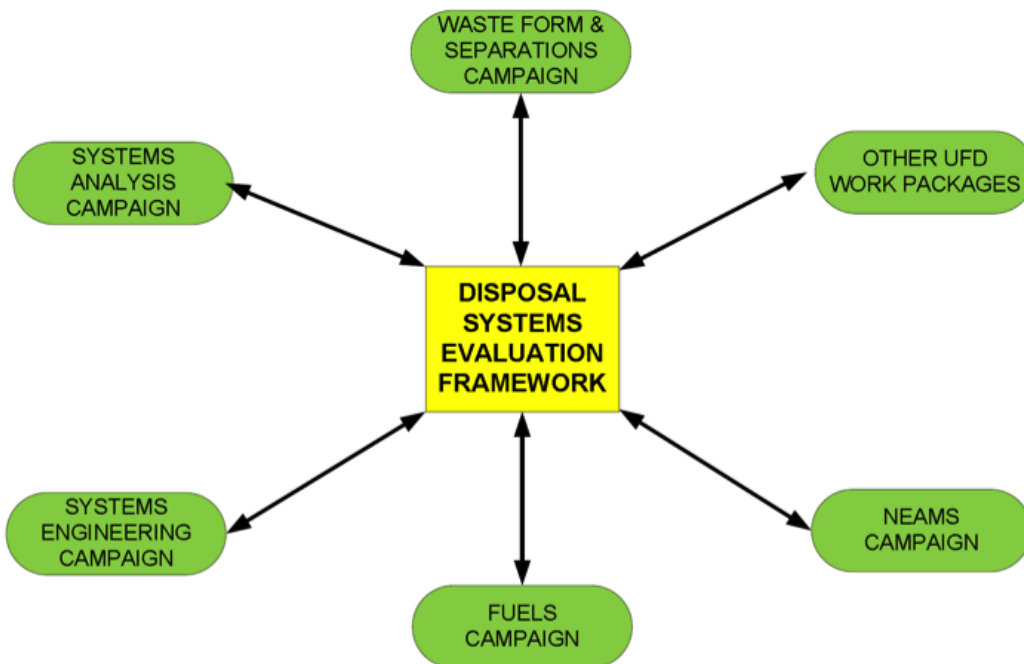


Figure 5-3. Schematic showing DSEF interfaces with other UFD campaigns.

5.5 Waste Forms

The DSEF began with a catalog (developed by the larger UFD Campaign team for Features, Events and Processes (FEPs) development and by other DOE-NE Campaigns) of potential waste forms (Freeze et al. 2010). These include the generic waste forms summarized in Table 5-2. More specific information on the radionuclide inventory within each of the waste form types can be found in (Carter and Luptak 2010).

The DSEF is integrated with the FEPs development and also with work in the thermal design work packages. The latter effort is integrated with the waste form work packages and has developed three base case fuel cycles with specific waste forms (Carter, et al., 2011), summarized in Table 5-2 and Table 5-3. Each fuel cycle consisting of light water reactors (LWRs), specifically pressurized water reactors (PWRs). The three fuel cycle options are shown in Figures 5-4, 5-5, and 5-6.

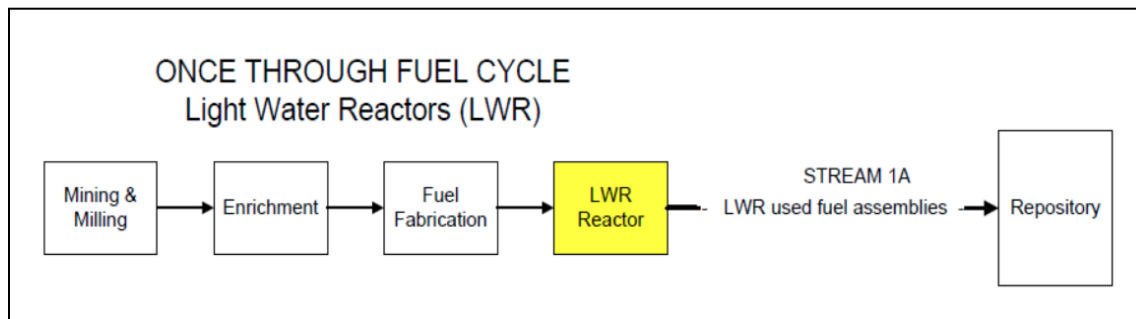


Figure 5-4. Once Through Fuel Cycle Waste Stream.

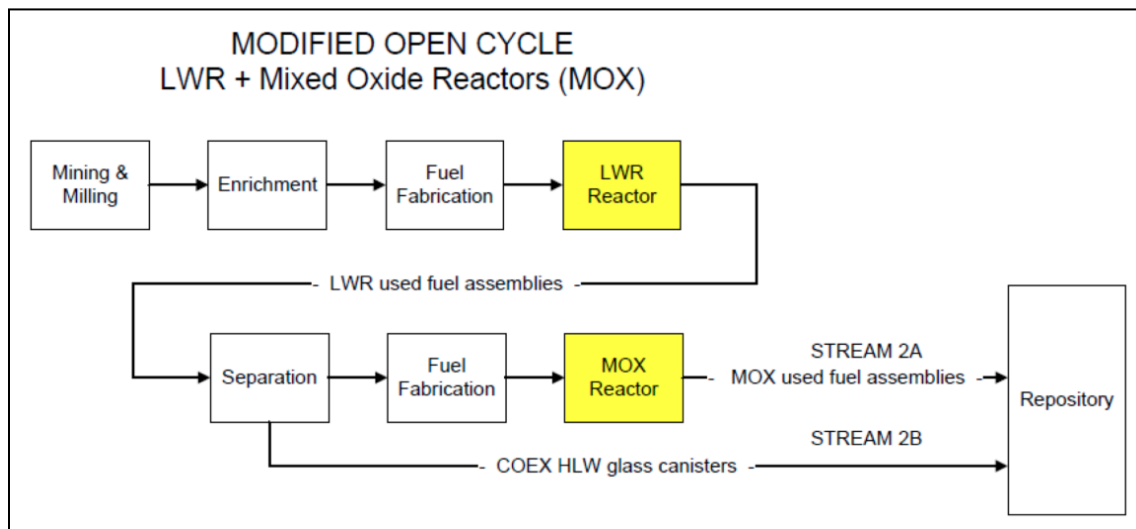


Figure 5-5. Modified Open Cycle Waste Streams.

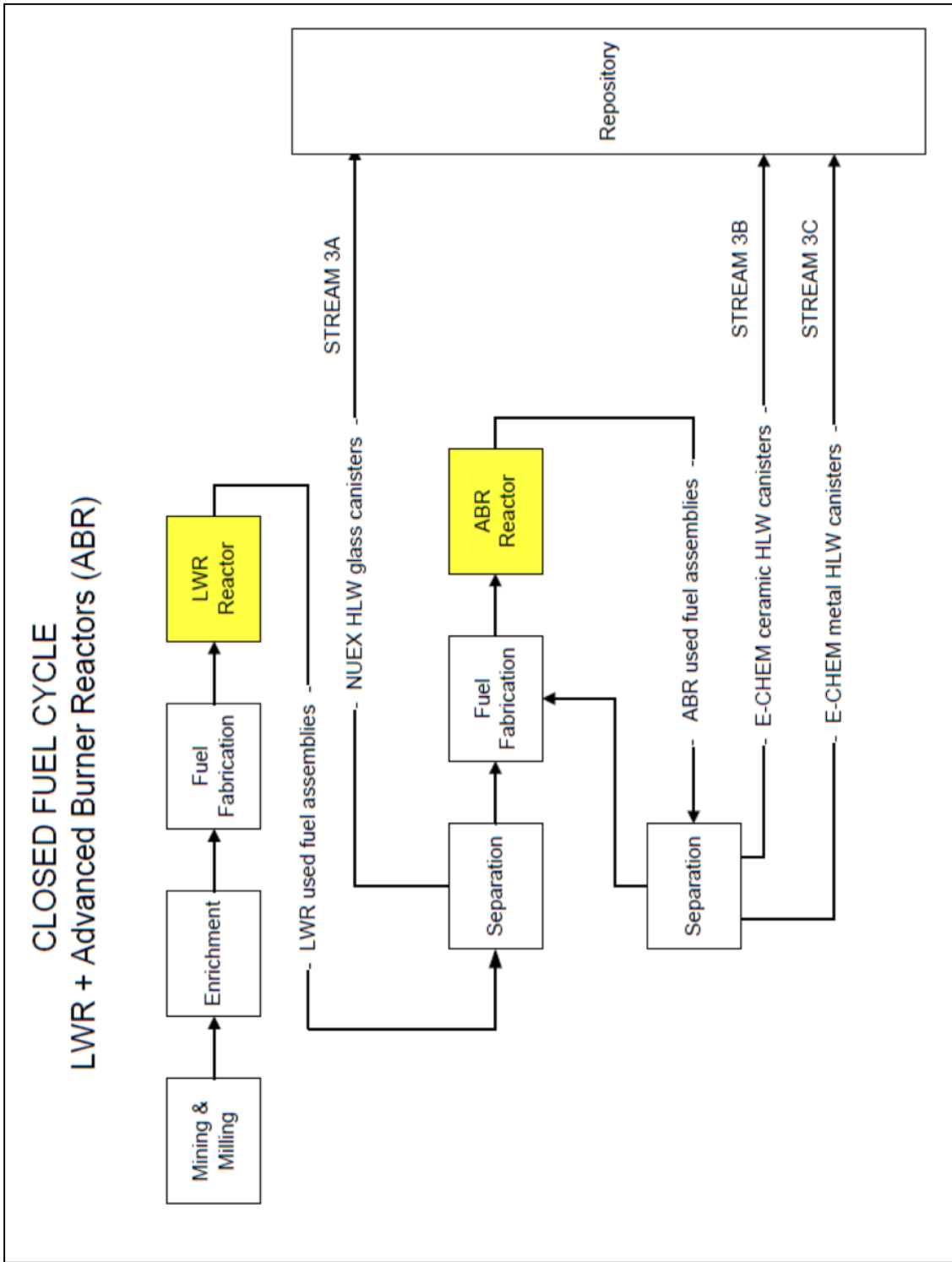


Figure 5-6. Closed Fuel Cycle Waste Streams.

An open fuel cycle consists of light water reactors (LWRs), specifically pressurized water reactors (PWRs), with all waste going to storage and disposal.

In the modified open cycle (MOC), the LWR used fuel is reprocessed with Co-Extraction (COEX) aqueous processing similar to the current generation of deployed technology (e.g., the Rokkasaho Reprocessing Facility). In COEX, uranium and plutonium are recovered together (no pure plutonium separation), producing 108.9 kg of mixed oxide fuel (MOX) for each metric ton (MT) of LWR fuel, based on an average plutonium enrichment of 10.74%. The principal fission product waste including the minor actinides are combined with the undissolved solids (UDS) and recovered technetium into a single COEX borosilicate glass waste form. The total burnup of the cycle, per MT of original LWR fuel, is $BU_{UOX} + BU_{MOX} * (MT_{MOX}/MT_{LWR}) = 56.4$ GWt-days/MT_{UOX}. The remaining waste stream from the MOC does not produce a significant amount of heat. Nevertheless, physical accommodation of that waste stream will be addressed in the DSEF, based on the information in Carter, et al. (2011), and repository concept development will consider co-disposal of that waste in the repository footprint.

For a closed fuel cycle (CFC), all used fuel is reprocessed with New-Extraction (NUEX) aqueous processing that recovers all transuranic (TRU) elements for reuse. According to Carter, et al. (2011), NUEX will include Transuranic Extraction (TRUEX) and the Trivalent Actinide Lanthanide Separation by Phosphorus-based Aqueous Komplexes [sic.] (TALSPEAK) process for complete TRU recovery. The principal fission product wastes are combined with the UDS and separated technetium into a single NUEX borosilicate glass waste form. In this base-case closed fuel cycle, the recovered transuranic elements from the LWR used fuel (0.6142 MT per MT of LWR fuel) will fuel Advanced Burner Reactors (ABRs) that are sodium cooled, produce 1 GW_t, use U-TRU-Zr metal alloy fuel, have a TRU conversion ratio of 0.75. The used fuel from the ABRs is reprocessed using an electro-chemical (EC) process that is a dry process using conductive molten salt baths to recover all TRU elements. In this process, the fission products are split between three waste streams. Elements more noble than uranium (e.g., cladding and noble metal fission products) remain as metals and are incorporated into a metal alloy waste form. Elements less noble than uranium are converted to chloride salts. The lanthanide elements are recovered from the salt by electrolysis and converted to a lanthanide glass. Excess salt is purged, and the chloride is absorbed by zeolite and bonded with glass to make the final waste form (termed EC-Ceramic in the DSEF). After a short period, the heat from the EC lanthanide glass is negligible, and thus only the NUEX glass, the EC-metal, and the EC-Ceramic waste forms are considered in the thermal aspects of the DSEF. The remaining waste streams from the NUEX reprocessing and the EC reprocessing do not produce a significant amount of heat. Nevertheless, that waste stream will be quantified in the DSEF, based on the information in Carter, et al. (2011), and repository concept development will consider co-disposal of that waste in the repository footprint.

Table 5-2 Base case waste forms for once-through, modified open and closed fuel cycles.

Cycle	WF type	Canisters per GW _e -yr cycle	Width diameter, m	Length, m	Mass, kg	Burnup GW _{td} /MT
OC	SNFA	39.2	0.22	4.07	470	60
MOC	COEX (UOX)	3.7	0.6096	4.572	2,900	51
	SNFA (MOX)	4.5	0.22	4.07	470	50
	Total	8.2	NA	NA	NA	56.4
CFC	NUEX	0.97	0.6096	4.572	2,900	51
	EC-Ceramic	4.9	0.6096	4.572	2,900	99.6
	EC-Metal	6.6	0.6096	3.048	3,600	
	Total	12.47	NA	NA	NA	112.2

The three fuel cycles described above produce the following waste forms that are considered in the thermal aspects of the DSEF.

The thermal decay curves from the six heat-producing waste forms (1 from the Open Cycle, 2 from the MOC, and 3 from the CFC) are shown in Figure 5-7. It is important to note that these curves are based on the time after the fuel is removed from the neutron flux in the reactor that produced it, rather than the time after reprocessing.

There are other modified open and closed fuel cycles that are similar to those above. The DSEF developers treat the above base cases as representative of those many possibilities, but will follow the progress in the DOE-NE Separations and Waste Forms Campaign and add options accordingly. In addition, there are more "exotic" waste forms that have historically been proposed. Many of these waste forms require spent nuclear fuel to be reprocessed and separated prior to encapsulating in a waste form. Examples include glass encapsulated silver zeolite, functionalized silica aerogels, chalcogenide aerogels, silicon carbide, iron phosphate glass, glass ceramics, cermets, epsilon metals and bentonite clay with copper. Some of these will be added to future DSEF versions.

The DSEF assembles summary information about waste form and waste package combinations. Waste form parameters include heat/volume ratio, heat/mass ratio, and heat/electrical-energy (from which the waste was derived) ratio, as well as the mass and half lives of the radionuclides in the waste. This information will interface with the FCT Systems Engineering Campaign fuel cycle catalog, the FCT Systems Analysis Campaign "VISION" model of nuclear fuel cycles and material flows, and the Separations and Waste Forms Campaign waste stream and waste form descriptions, as well as with the Waste Form, EBS, Natural Systems and FEPS work packages in the UFD Campaign.

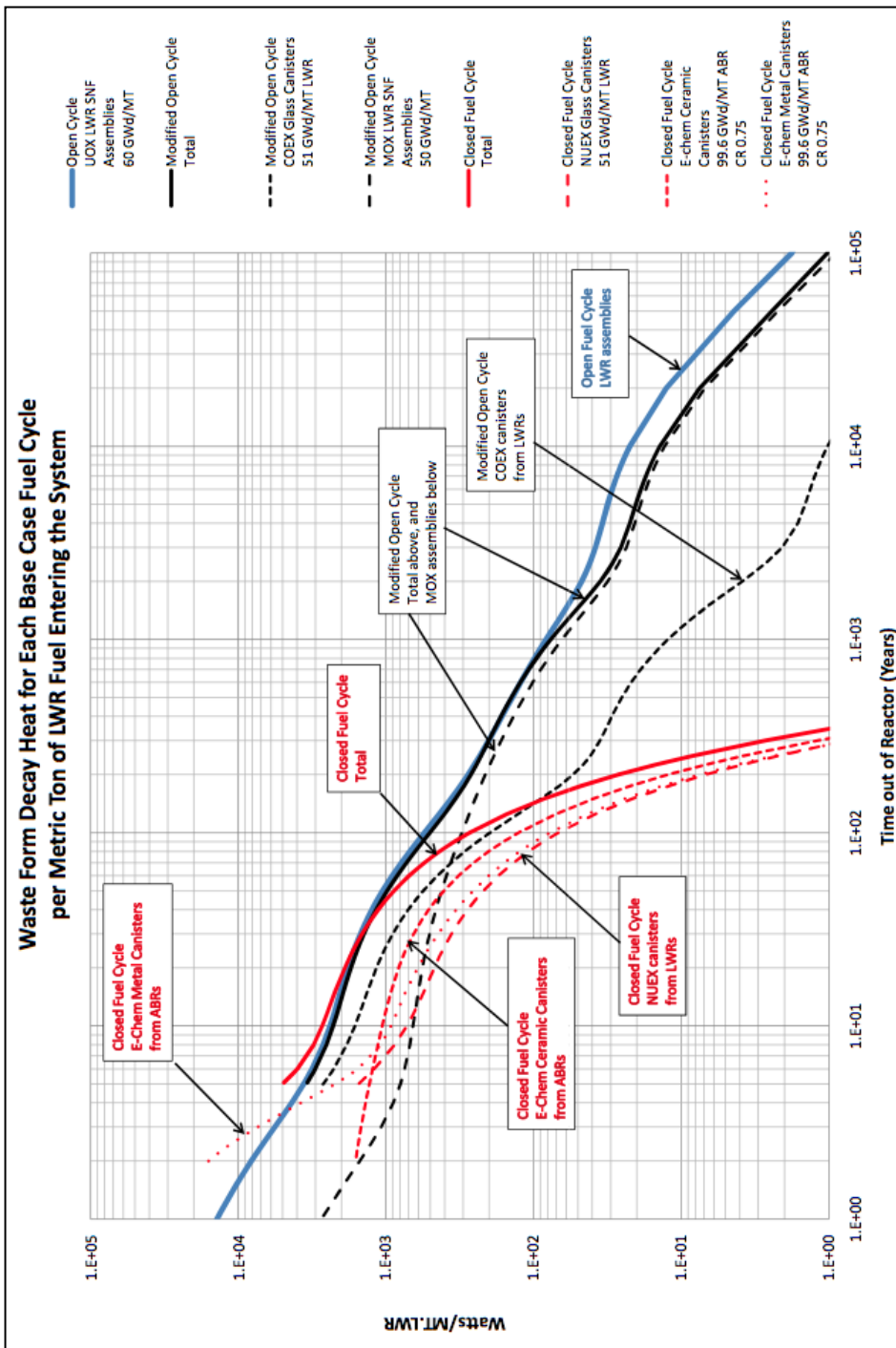


Figure 5-7. Thermal decay curves from the six heat-producing waste forms (OC, MOC, CFC).

Table 5-3 FEPs-identified waste forms.

Category	Sub-category
Used Nuclear Fuel (UNF)	Commercial Spent Nuclear Fuel (CSNF) with nominal burnup: Uranium (U) & mixed oxide (MOX) from Light Water Reactors (LWRs)
	CSNF with high burnup: U & MOX, >50% burnup without reprocessing, such as in some fusion-fission hybrids
	High Temperature Gas Reactor (HTGR) fuel using TRISO/graphite elements: Large volume, low volumetric heat, and higher burnup than LWRs
	DOE Spent Nuclear Fuel (DSNF): U metal from N-reactor, and carbides & oxides
High-Level Waste (HLW) Glass	Current borosilicate glass: Includes processing chemicals from original separations, with U/Pu removed, but minor actinides and Cs/Sr remaining
	Potential borosilicate glass: No minor actinides and/or no Cs-137/Sr-90. Mo may be removed to increase glass loading of radionuclides. This waste form has a lower volumetric heat rate
HLW Glass Ceramic / Ceramic	Glass-bonded sodalite from Echem processing of EBR-11, and from potential future Echem processing of oxide fuels
	An advanced waste form that includes iodine volatilized during chopping, which is then gettered during head-end processing of used fuels
HLW Metal Alloy	Metal alloy from Echem: Includes cladding as well as noble metals that did not dissolve in the Echem dissolution
	Metal alloy from aqueous reprocessing: Includes undissolved solids (UDS) and transition metal fission products
Lower Than HLW (LTHLW)	Includes Classes A, B, and C, as well as Greater Than Class C (GTCC)
Other	Molten salt, electro-chemical refining waste, new waste forms, and radionuclides removed from other waste forms (e.g. Cs/Sr, I-129, C-14, H-3 and Kr-85)

5.6 Disposal System Environment

Seven specific disposal environments have been identified (in the FEPs work packages) for further investigation (Freeze et al. 2010), in addition to other possible environments such as deep seabed, and carbonate rocks. These environments are summarized in Table 5-4. Historical perspectives on each of the disposal systems can be found in (Sutton et al. 2011). The first two of these (Surface Storage and Shallow Disposal) are being studied by the Storage and Transportation work packages in the UFD Campaign, and will be integrated into a future version of the DSEF. The third environment in Table 5-4 (Unsaturated Hard Rock) has been studied extensively for the Yucca Mountain Site. The results of those studies will be used to validate the architecture and algorithms for the DSEF, during its development. The thermal design work packages have identified the next

four environments in Table 5-4 for development of base cases for UFD. These are salt, clay, saturated hard rock, and deep boreholes.

Table 5-4 FEPs-identified disposal system environments.

Category	Description
Surface Storage	Long-term interim storage at reactors or at centralized sites
Shallow Disposal	Depths \leq 100 m (e.g., near-surface disposal, LTHLW sites)
Mined Geologic Disposal (Hard Rock, Unsaturated)	Unsaturated Zone (UZ): Granite/crystalline or tuff (Depths > 100 m)
Mined Geologic Disposal (Hard Rock, Saturated)	Saturated Zone (SZ): Granite/crystalline or tuff (Depths > 100 m)
Mined Geologic Disposal (Clay/Shale, Saturated)	SZ: Clay/shale (Depths > 100 m)
Mined Geologic Disposal (Salt, Saturated)	SZ: Bedded or domal salt (Depths > 100 m)
Deep Borehole Disposal	Granite/crystalline (Depths \sim 1000 m or deeper)
Other	Examples include deep seabed, and carbonates

Thermal design constraints for each of the disposal environments are discussed in Section 5.7 of this report, and material property requirements are discussed in Section 5.9.

5.7 Design Constraints

The three base-case fuel cycles described in Section 5.5 produce six total waste forms with sufficient heat output to significantly influence the repository design. The four base-case environments described in Section 5.6 result in 24 combinations of waste forms and environment. The thermal design for a repository is based on thermal power, which declines with aging time; hence, a range of aging times needs to be considered for each of these cases. Initially, the thermal design work packages planned to investigate three aging periods for each combination. A minimal aging period (5 yr), a medium aging period (50 yr), and a long aging period (100 yr) were initially selected for investigation. This would result in 72 combinations of waste form composition, environment, and aging time. The thermal design investigators (from SNL, ORNL, SRNL, and LLNL) decided that an adequate range of designs would result if some combinations were eliminated (i.e., minimal aging for very high initial power waste forms, and long aging periods for very low initial power waste forms). The result is shown in Table 5-5, which shows 24 combinations of waste form composition, environment, and aging time. These, in addition to the validation cases of YMP and WIPP, will be the base cases for the DSEF. The 24 fuel cycle cases and the 2 validation cases will be prioritized rather than being developed and executed in parallel.

Table 5-5 Fuel cycle, disposal environment, and aging time for 24 base case combinations.

Fuel Cycle	Hard Rock, Saturated	Clay/Shale, Saturated	Salt, Saturated	Borehole
Once Through (SNFA)	Moderate Aging Extended Aging	Moderate Aging Extended Aging	Moderate Aging Extended Aging	Moderate Aging Extended Aging
Modified Open Cycle (COEX from UOX and MOX SNFAs)	Short Aging Moderate Aging	Short Aging Moderate Aging	Short Aging Moderate Aging	Short Aging Moderate Aging
Closed Fuel Cycle (NUEX from UOX, and EC-Ceramic and EC-Metal from ABRs)	Short Aging Moderate Aging	Short Aging Moderate Aging	Short Aging Moderate Aging	Short Aging Moderate Aging

With a number of repository designs and environments being evaluated in countries across the world, data on proposed thermal constraints are available for many of the environments listed in Table 5-5.

For a repository in granite various limits have been proposed. The French designs have thermal limits of <100°C at the canister surface, to minimize the vaporization/condensation processes that could cause corrosive salts to deposit on the surface of the copper waste package. Packages are separated by 12-15 m and have a maximum heat output of 1.6 kW/can UOX and 1.1 kW/can MOX (ANDRA 2005b). In Finland, the maximum heat output in granite is limited to 1.7 kW/can (Posiva Oy 2010). Swedish repository designs at Forsmark and Laxemar in granite assume an initial thermal output of 1.7 kW/can and use a waste package separation of 7.4 m to limit the temperature on the surface of a waste package to <100°C. Additionally the buffer temperature should not exceed 100°C to minimize dehydration and chemical alteration (SKB 2006).

For clay repositories in France and Belgium, the maximum temperature is generally limited to less than 100°C based on mineral stability. Temperatures close to or above 100°C tend to dry out the clay and cause deformation cracks and subsequently fast pathways for potential radionuclide release to the biosphere. Thermal constraints in France are <100°C in argillite, with canisters spaced at 7.5 m parallel and 10.3 m perpendicular, and maximum heat outputs of 1.6 kW/can UOX and 1100 W/can MOX (ANDRA 2005a). In Belgium, canisters are spaced 3 m apart, and temperatures of HLW and SNF are limited to <400°C and <350°C respectively, with 188 W/can UOX and 905 W/can MOX (NIROND 2001). These values were chosen because HLW glass undergoes structural and mechanical changes at 500°C and to prevent excessive pressure buildup via He in fuel (NIROND 2001). In Switzerland thermal constraints are limited to 125°C in emplaced bentonite with canisters spaced 3 m apart with a maximum heat output of 1.5 kW/can (NAGRA 2002).

For engineered backfill, Swiss studies have demonstrated the dehydration and illitization of bentonite buffer EBS material above 120-150°C in wet conditions, although dry conditions require

higher temperatures (perhaps up to 350°C (P. Wersin, L.H. Johnson and I.G. McKinley, Performance of the bentonite barrier at temperatures beyond 100°C: A critical review, Physics and Chemistry of the Earth, Parts A/B/C, Volume 32, Issues 8-14, 2007, Pages 780-788). In Belgium, temperature constraints are limited to <100°C in the backfill to prevent physico-chemical alteration of the backfill and any significant disturbance of the local hydraulic system from buildup of interstitial pressures (NIROND 2001).

Studies of a conceptual salt repository in the US led to a waste package spacing of 7.5 m. The maximum glass temperature, cladding temperature and salt temperature were 500°C, 375°C and 250°C respectively, and the maximum heat output was 6.6 t kW/can containing 12 PWR assemblies (BMI 1985, DOE 1987). A more recent study found that maintaining waste package temperatures below 500°C and salt bed below 200°C would reduce the disposal concept's uncertainty (AFCI 2009). Salt tends to decrepitate above 200°C and melts above 800°C. Intact salt creep is exponentially related to temperature and creep occurs without forming fractures with salt deformation being dominated by plastic behavior at elevated temperatures (Hansen and Leigh 2011).

Thermal constraints also exist for waste package material. Long-range order transformations in Alloy C22 are not expected at 200°C over very long timescales (Turchi et al. 2007). Low temperature sensitization of some stainless steels occurs over long time periods above 400°C (Sutton et al. 2010, Farmer 1988). Copper alloys have been shown to remain stable up to at least 300°C (Sutton et al. 2010, Farmer 1988).

5.8 Thermal

There are two thermal model systems within the DSEF: analytic and finite element. There will also be tables of prior results (which will be updated in later versions based on realizations using the early versions); these tables can be used to interpolate results for new cases, if most of the input parameters are suitably similar.

As described in the subsections of Section 5.8.1, the analytic models in the DSEF will use a variety of source and environment geometries that have existing published analytic solutions. Source geometries (all in an infinite medium) include a point heat source, a finite line source, an infinite line source, an array of finite line sources, a finite plane source, a semi-infinite plane source, an infinite plane source, and an infinite cylinder source. These solutions can be extended (by superposition of reflected geometries) to a semi-infinite medium bounded by an isothermal surface and an infinite region bounded by two parallel isothermal surfaces. The analytic models can be executed in commercially available off-the-shelf (COTS) software such as *Microsoft Excel*, *Mathcad* (Mathcad 15.0 2010) or *Mathematica* (WRI 2010). These models use textbook empirical equations to solve heat flow in a variety of geometries and offer a simple and quick examination of a unit cell. For the DSEF, *Mathcad* models will be included as auxiliary software. These models can be run at the appropriate point in the development of the repository design, and documented in the *Thermal* worksheet of the DSEF.

The finite element models (Section 5.8.2) within DSEF evaluate heat flow within a more complex geometry using specifically designed thermal transport software such as *TOPAZ3D* and an input mesh that more accurately describes the waste package and unit cell (or repository region). These models are more complex than analytic models and require more effort to perform. During the remainder of FY11, the application of *TOPAZ3D* to address complexities not addressed by the analytic models will be tested.

Section 5.8.3 is a report of the initial comparison of analytic and finite element models. Section 5.8.4 concludes the thermal section with a description of the decay heat formulation to be input to these models.

5.8.1 Analytic Models

There are a number of analytical solutions that are potentially applicable as a basis for the planned UFD thermal design analyses. There are several basic references that document the analytical solutions for a wide class of conduction heat transfer problems, but the most widely cited is Carslaw and Jaeger (1959, Section 8.1.3).

Analytic solutions that were developed in *Mathcad*, and used on the Yucca Mountain Project have been used to some extent in developing the suite of analytical solutions documented below (Chipman et al. 2004).

The finite line and plane source solutions are derived from the transient solution for a continuous point source ($q(t)$) in an infinite homogeneous media (Carslaw and Jaeger 1959, Section 10.4, p261). In the following sections, the radial distance from the point source is r , and the initial temperature is zero.

5.8.1.1 Solution for a Point Source in an Infinite Medium

This solution is based on linear superposition in a conduction only heat transfer environment (Duhamel's theorem, Carslaw and Jaeger 1959, Section 1.14). The following equation is a convolution integral of a transient heat source $q(t)$.

$$T_p(t, r) = \frac{1}{8 \cdot \rho \cdot C \cdot (\pi \alpha)^2} \int_0^t \frac{q(\tau) \cdot e^{-\frac{r^2}{4 \cdot \alpha \cdot (t-\tau)}}}{(t-\tau)^2} d\tau$$

(Carslaw and Jaeger 1959, Section 10.4 equation (1))

If $q(t)$ is a constant = q_0 , then the result simplifies to:

$$T_{\text{point}}(t, r) = \frac{q_0}{4\pi \cdot (\rho \cdot C) \cdot \alpha \cdot r} \operatorname{erfc}\left(\frac{r}{\sqrt{4 \cdot \alpha \cdot t}}\right)$$

(Carslaw and Jaeger 1959, Section 10.4 equation (2)); where *erfc* is the complementary error function.

The conversion from the spherical coordinates of the solution to the Cartesian coordinates of the repository is:

$$r^2 = (x - x_0)^2 + (y - y_0)^2 + (z - z_0)^2$$

Where the source is located at (x_0, y_0, z_0) .

5.8.1.2 Solution for a Finite Line Source in an Infinite Medium

The line source solution is obtained by applying the differential transform:

$$q_L(t) \cdot dy_0 = q(t)$$

We then integrate y_0 over the length of the line source (with line length L). When the line source is centered at $y_0=0$, the line source solution becomes:

$$T_i(t, x, y, z) = \frac{1}{8\rho C (\pi\alpha)^2} \int_{-L/2}^{L/2} \frac{q_L(t_0)}{(t-t_0)^2} e^{-\frac{[(x-x_0)^2 + (z-z_0)^2]}{4\alpha(t-t_0)}} e^{-\frac{(y-y_0)^2}{4\alpha(t-t_0)}} dy_0$$

The definite integral over dy_0 is recognized as a form of the error function. The coordinate (x_0, z_0) is set to $(0, 0)$. The line source solution reduces to:

$$T_i(t, x, y, z) = \frac{1}{4\sqrt{\pi}} \int_0^t \frac{q_L(t_0)}{(t-t_0)^{3/2}} e^{-\frac{(x^2+z^2)}{4\alpha(t-t_0)}} \left[\operatorname{erf}\left(\frac{y+L/2}{\sqrt{4\alpha(t-t_0)}}\right) - \operatorname{erf}\left(\frac{y-L/2}{\sqrt{4\alpha(t-t_0)}}\right) \right] dt_0$$

5.8.1.3 Solution for an Infinite Line Source in an Infinite Medium

The solution for a constant heat flux infinite line source q_{0L} along the y -axis is:

$$T_i(t, x, z) = \frac{q_{0L}}{4\sqrt{\pi}} \left[\sqrt{\frac{t}{\alpha}} - \frac{x^2}{4\alpha t} \right] e^{-\frac{(x^2+z^2)}{4\alpha t}}$$

(Carslaw and Jaeger 1959, Section 10.3 equation (1));

The equivalent convolution integral solution for a time varying line source was applied on the Yucca Mountain Project (DOE 2008a, equation 6.1-2) and is defined as:

$$T_i(t, x, z) = \frac{1}{4\pi k i} \int_0^t \frac{q_L(t_0)}{(t-t_0)^{3/2}} e^{-\frac{(x^2+z^2)}{4\alpha(t-t_0)}} dt_0$$

5.8.1.4 Solution for Multiple Finite Line Sources in an Infinite Medium

The temperature field for multiple line sources is obtained by the linear addition of single line sources. In the equation below, it is assumed that we have one source at the coordinates ($z=0$, $x=0$) and that there is a plane of symmetry at $x=0$. The variable N_s is the number of additional line sources on one side of the plane of symmetry. Hence, $N_s = 0$ produces a single source, $N_s = 1$ produces 3 sources, $N_s = 2$ produces 5 sources, and so on.

$$T(t, x, y, z, N_s) = \sum_{n_s = -N_s}^{N_s} T_{\text{line}}(t, x - n_s \cdot L_{\text{offset}}, y, z)$$

$$T_{\text{line_mul}}(t, x, y, z, N_s) = \sum_{n_s = -N_s}^{N_s} T_{\text{line}}(t, x - n_s \cdot L_{\text{offset}}, y, z)$$

where

$$T(t, x, y, z, N_s) = \frac{1}{\alpha} \int_0^t \left[\sum_{n_s = -N_s}^{N_s} c_x(x, t_0) \right] \frac{e^{-\frac{z^2}{4\alpha(t-t_0)}}}{4\alpha(t-t_0)} dt_0$$

$$c_x(x, t_0) = \sum_{n_s = -N_s}^{N_s} e^{-\frac{[(x-n_s) \cdot L_{\text{offset}}]^2}{4\alpha \cdot (t-t_0)}}$$

5.8.1.5 Solution for a Finite Plane Source in an Infinite Medium

The plane source solution is obtained by applying a differential transform to the solution for a finite line (length L):

$$q_P(t) \cdot dx_0 = q_L(t)$$

and integrating x_0 over the width of the plane source (W_P). When the plane source is centered at $x=0$, the plane source solution becomes:

$$T_p(t, x_1, y, z) = \frac{1}{8\pi k} \int_0^t \frac{q_p(\tau) e^{-\frac{z^2}{4\alpha(t-\tau)}}}{\sqrt{t-\tau}} \left[\frac{1}{2} \left[\frac{y+L}{\alpha(t-\tau)} \right] e^{-\frac{(x-x_1)^2}{4\alpha(t-\tau)}} + \frac{1}{2} \left[\frac{y-L}{\alpha(t-\tau)} \right] e^{-\frac{(x-x_1)^2}{4\alpha(t-\tau)}} \right] d\tau \quad (5.8.1.5)$$

The definite integral over dx_0 is recognized as a form of the error function. When the plane is centered about $x=0$, the solution reduces to:

$$T_p(t, x, y, z) = \frac{\alpha}{8k\sqrt{\pi\alpha}} \int_0^t \frac{q_p(\tau) e^{-\frac{z^2}{4\alpha(t-\tau)}}}{\sqrt{t-\tau}} \left[\operatorname{erfc}\left(\frac{x}{\sqrt{4\alpha(t-\tau)}}\right) + \operatorname{erfc}\left(\frac{y}{\sqrt{4\alpha(t-\tau)}}\right) \right] d\tau \quad (5.8.1.6)$$

where

$$\operatorname{erfc}(x) = 1 - \operatorname{erf}(x) = \frac{2}{\sqrt{\pi}} \int_x^\infty e^{-\eta^2} d\eta$$

5.8.1.6 Solution for a Semi-Infinite Plane Source in an Infinite Medium

When the plane source is of infinite length, but finite width, the solution reduces to

$$T_s(t, x, z) = \frac{\alpha}{4k\sqrt{\pi\alpha}} \int_0^t \frac{q_s(\tau) e^{-\frac{z^2}{4\alpha(t-\tau)}}}{\sqrt{t-\tau}} \operatorname{erfc}\left(\frac{x}{\sqrt{4\alpha(t-\tau)}}\right) d\tau \quad (5.8.1.7)$$

where

$$\operatorname{erfc}(x) = 1 - \operatorname{erf}(x) = \frac{2}{\sqrt{\pi}} \int_x^\infty e^{-\eta^2} d\eta$$

5.8.1.7 Solution for an Infinite Plane Source in an Infinite Medium

The solution for an infinite plane source with a constant heat flux is given in Carslaw and Jaeger (1959, Section 10.3 equation (2)). The equivalent convolution integral solution for a time varying heat flux is:

$$T_i(t, z) = \frac{q_p}{2 \cdot k} \cdot \frac{\alpha}{\pi \cdot \alpha} \int_0^t q_p(t') \cdot e^{-\frac{z^2}{4 \cdot \alpha \cdot (t-t')}} dt'$$

5.8.1.8 Solution for an Infinite Medium Internally Bounded by a Cylinder

The thermal response of an infinite medium internally bounded by a cylinder (of radius a) subject to a constant flux Q (Carslaw and Jaeger 1959, Section 13.5, equation (17)) is defined as

$$T_{cylinder}(r, a, t) = \frac{-2}{(\pi \cdot k)} \int_0^t \int_0^\infty Q(t') \cdot [1 - e^{-\alpha \cdot u^2 \cdot (t-t')}] \cdot \left[\frac{(J_0(u \cdot r) \cdot Y_1(u \cdot a) - Y_0(u \cdot r) \cdot J_1(u \cdot a))}{u^2 \cdot (J_1(u \cdot a)^2 + Y_1(u \cdot a)^2)} \right] du dt'$$

The convolution integral for a time varying Q is therefore:

$$T_{cylinder}(r, a, t) = \frac{-2}{(\pi \cdot k)} \int_0^t \int_0^\infty Q(t') \cdot [1 - e^{-\alpha \cdot u^2 \cdot (t-t')}] \cdot \left[\frac{(J_0(u \cdot r) \cdot Y_1(u \cdot a) - Y_0(u \cdot r) \cdot J_1(u \cdot a))}{u^2 \cdot (J_1(u \cdot a)^2 + Y_1(u \cdot a)^2)} \right] du dt'$$

Where:

- J0 is the zero order Bessel function of the first kind
- J1 is the first order Bessel function of the first kind
- Y0 is the zero order Bessel function of the second kind
- Y1 is the first order Bessel function of the second kind.

This solution was applied on the Yucca Mountain Project (BSC 2004, Equation 6-57, page 6-25), where the equation was first put into dimensionless form, and evaluated at the drift wall (r = a) to predict the drift wall temperature transient. The drift wall temperature was subsequently used to evaluate the ventilation air stream, waste package surface, and cladding temperature transients.

For the Yucca Mountain case, the project simulated the convolution integral with a series summation of finite differences based on one-year time increments (BSC 2004). Section 6.4 of BSC 2004 describes the use of two ANSYS numerical models and the analytic solution model applied to calculate the ventilation system heat removal efficiency as well as the component temperatures. Section 6.6 of BSC 2004 presents the results of the two approaches and provides evidence of the effectiveness of the analytical solution in Table 6-7 on page 6-39. The ventilation system removal efficiency for a 600 m drift with 50 years of ventilation was calculated by the “ANSYS-LA-Coarse” model as 88.3% (documented in DTN: M00406MWDLACVD.001), and the same result was calculated by the “Analytical-LA-Coarse” model as 88.0% (documented in

DTN: M00406MWDAC8VD.001). The reference provides a similar comparison of results for an 800 m drift with the ANSYS and analytical model results of 85.8% and 86.0% respectively. The ANSYS model was then validated against a quarter-scale ventilation test as documented in the reference (Section 7 and Appendix XII). A pulse response to an assumed 1-year duration pulse was approximated by taking the solution above for a constant flux of Q , and subtracting a second solution for an assumed flux of $-Q$ shifted in time by one year. A convolution integral solution was then approximated by a series summation approach using an exponentially decaying heat source $Q(t)$ convolved with the “pulse” solution.

5.8.1.9 Extension of Analytic Solutions to a Semi-Infinite Domain Bounded by One Isothermal Surface

The analytic solutions for an infinite domain are extended to the case of a semi-infinite domain by the method of images (Carslaw and Jaeger 1959, Section 10.10, page 273). A sink of strength equal to the source is reflected across the isothermal plane at $z=Z_G$ (ground surface). The solution is based on the sum of the source and sink fields (superposition), shown in Figure 5-8.

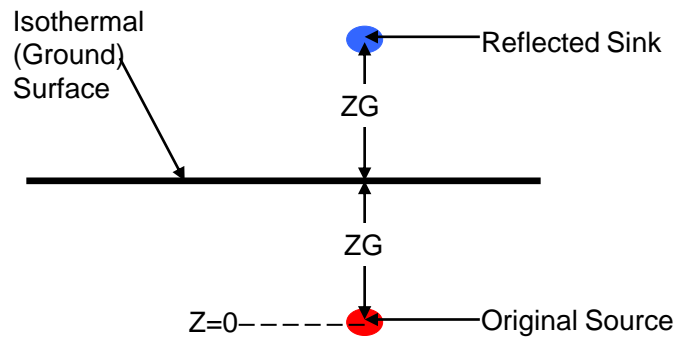


Figure 5-8. Application of the Method of Images for a Single Isothermal Surface.

The technique is applicable to all of the line and plane source solutions derived above. Hence,

$$T_{\text{line_1iso}}(t, x, y, z) = T_{\text{line}}(t, x, y, z) - T_{\text{line}}(t, x, y, z - 2 \cdot Z_G)$$

$$T_{\text{line_mult_1iso}}(t, x, y, z, N_s) = T_{\text{line_mul}}(t, x, y, z, N_s) - T_{\text{line_mul}}(t, x, y, z - 2 \cdot Z_G, N_s)$$

$$T_{\text{plane_1iso}}(t, x, y, z) = T_{\text{plane}}(t, x, y, z) - T_{\text{plane}}(t, x, y, z - 2 \cdot Z_G)$$

5.8.1.10 Extension of Analytic Solutions to a Semi-Infinite Domain Bounded by Two Parallel Isothermal Surfaces

The source/sink pair constructed above can then be reflected to create the lower (water table) isothermal condition. This, however, compromises the effectiveness of the first (ground) isothermal surface. The newly added sources and sinks are reflected about the plane $z=ZG$ to reestablish the first (ground) isothermal. This double reflection (first about $z=-ZW$ and then about $z=ZG$) is termed a "paired" reflection in this document, shown in Figure 5-9.

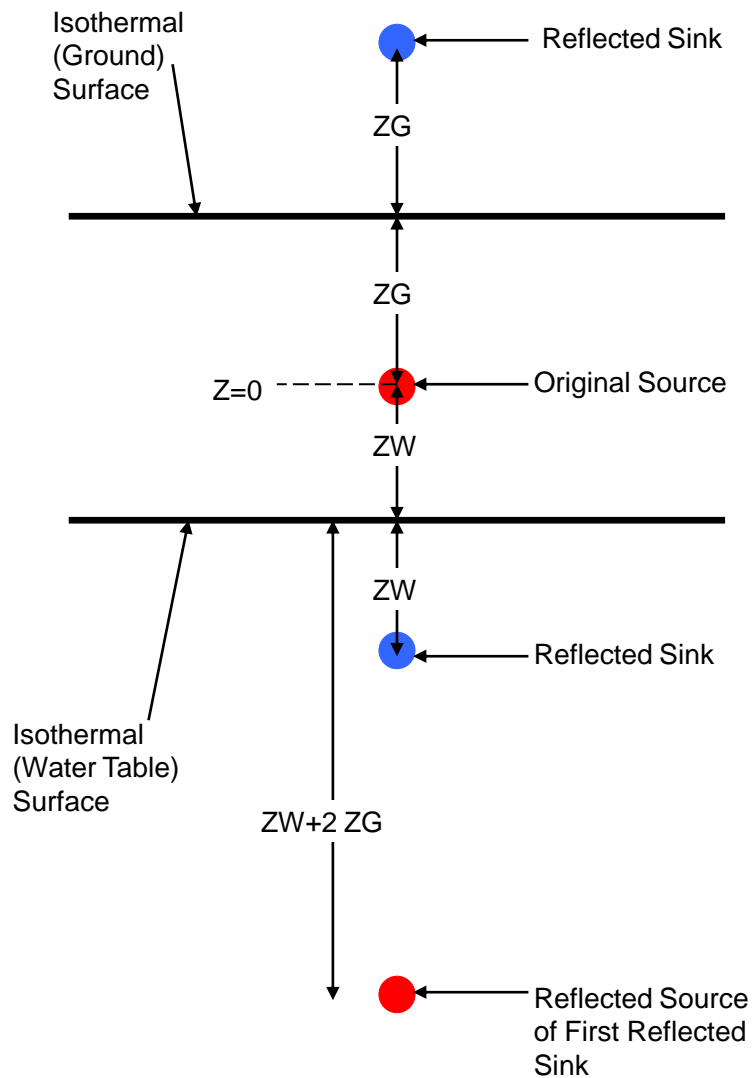


Figure 5-9. Application of the method of images to two isothermal surfaces (the ground and water table surfaces).

Continuation of the process produces an infinite series of sources and sinks. Because the series is convergent, a finite number of terms are used to approximate the solution. The series, derived by induction, always maintains the ground surface as a true isothermal surface. Increased numbers of paired reflections (N_r) produce successively closer approximations of an isothermal surface at the water table.

5.8.2 Finite Element Models

Among the capabilities of DSEF is the interface with the *TOPAZ3D* (Wemhoff 2007) finite element heat transfer code. *TOPAZ3D* solves for the steady state or transient temperature field on three-dimensional geometries and allows for temperature-dependent material properties, either isotropic or orthotropic. The code accepts a variety of time and temperature dependent boundary conditions, including temperature, flux, convection and radiation. Additional features include thermal contact resistance across an interface, bulk fluids, phase change and energy balances. The DSEF interface will read the required input data from a worksheet and translate them in the *TOPAZ3D* input format. Even for relatively simple geometries the setup of the mesh is a complex task; therefore, the DSEF interface will rely on the *TrueGrid* (Rainsberger 2006) mesh generator. This section illustrates the input data and the formatting required to generate a mesh using the *TrueGrid* code. In this preliminary stage, three representative geometries were selected: (1) multi-layered parallelepiped; (2) multi-layered parallelepiped with inclined layers; and (3) concentric cylinders. The geometries that DSEF will handle are expected to be a combination of the three selected.

5.8.2.1 Paralell Multi-Layer

The *block* command within the *TrueGrid* input file generates a rectangular mesh according to the input parameters. Its generic form is given as:

```
block i-list; j-list; k-list;  
      x-list; y-list; z-list;
```

The *i*-, *j*-, and *k*-list define boundary nodes in three directions, and *x*-, *y*-, and *z*-list define the corresponding boundary dimensions (the units are defined by the user; for clarity we will assume meter throughout).

This example illustrates the case of a stack of three layers of constant thickness. Each layer is made of a different material. The input file for *TrueGrid* is:

```
block 1 5; 1 7; 1 10 18 30;  
      0. 4.; 0. 5.5; 0. 4. 10. 15.;
```

Here, 5 equally spaced nodes and 4 elements are generated in the *x*-direction between 0 m and 4 m; 7 nodes and 6 elements in the *y*-direction between 0 m and 5.5 m; 10 nodes and 9 elements between 0 m and 4 m, 9 nodes and 8 elements between 4 m and 10 m, 13 nodes and 12 elements between 10 m and 15 m (total 30 nodes and 29 elements) in the *z*-direction. The lists also define partitions (*n*) with the block in the example above composed of one partition in the *x*- and *y*-direction, and three in the *z*-directions. Partitions can be referred to directly using the position of the boundary nodes in the block definition—reduced indices. For example, the second partition in the *z*-direction is bounded by node 10 and 18 that are in position 2 and 3 in the *k*-list; when a command requires a partition input, partition 2 in the *z* direction will be defined using reduced indices: 2 3.

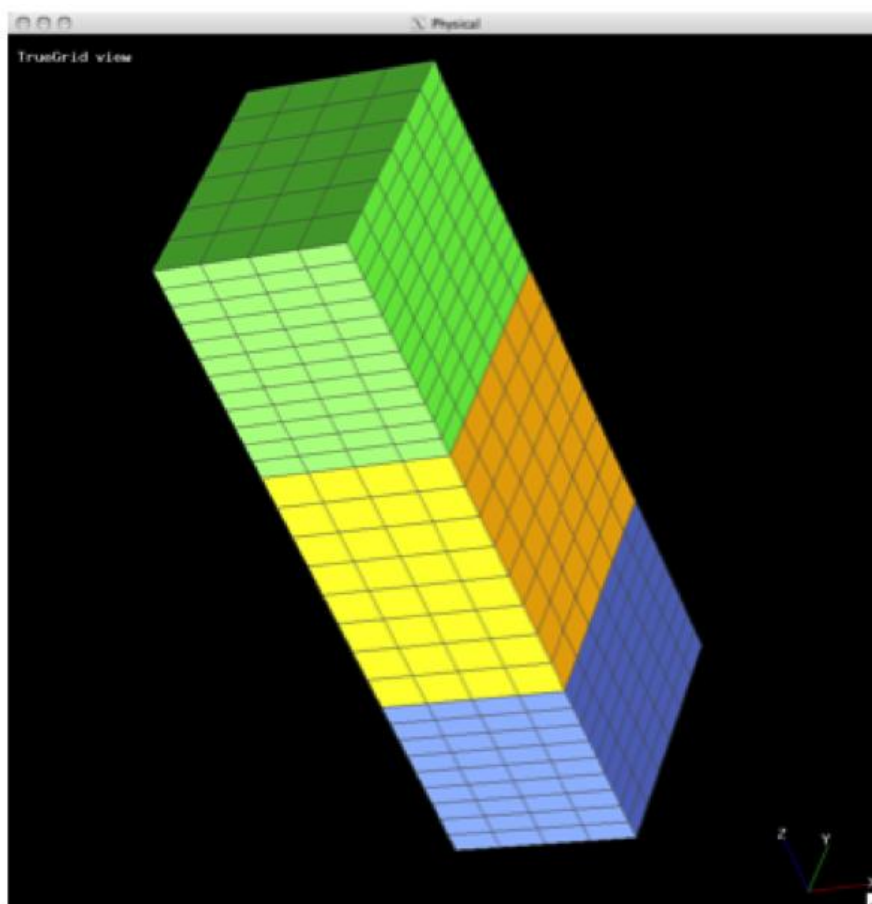


Figure 5-10. Example of a configuration with three parallel layers.

The mesh size is uniform within a partition, but can vary from a partition to another. The number of nodes within a partition can be modified without changing the partition indices using the *mseq* command.

The three partitions in the z-direction enable the possibility to assign a different material to each of them. Two options are available for specifying the material. The *mt* command uses the reduced indices of the boundary nodes to identify a partition and assign to it a material—this is called the “region” method:

```
mt 1 1 1 2 2 2 1
mt 1 1 2 2 2 3 2
mt 1 1 3 2 2 4 3
```

The first three integers are the minimum reduced indices in the three directions; the following three integers are the maximum reduced indices, and the last integer is the material number assigned to the partition.

The *mti* command, instead, uses the so-called “progression” method where a partition is still identified using reduced indices, but as follows:

```
mti 1 2; 1 2; 1 2; 1
mti 1 2; 1 2; 2 3; 2
mti 1 2; 1 2; 3 4; 3
```

The three pairs of integers separated by a semicolon identify the minimum and maximum reduced index of the partition in x-, y-, and z-direction, respectively. The last integer is the material number. The *mti* command allows assigning the same material to multiple zones in a single line.

Figure 5-10 shows the mesh structure as generated by *TrueGrid* for a parallelepiped with dimensions 4 x 5.5 x 15 m. Each color corresponds to a different material. Material properties will be defined at a later stage in the *TOPAZ3D* input.

All commands that identify a partition using the “region” method have a counterpart (same command with an *i* at the end) that uses the “progression” method. As the latter command allows a more compact syntax, it will be the preferred choice from this point on.

5.8.2.2 Inclined Multi-Layer

This second example refers also to a stratified configuration, but now with uneven layers. The input file for *TrueGrid* is the following:

```
block 1 5; 1 7; 1 10 18 30;
0. 4.; 0. 5.5; 0. 4. 10. 15.;
mbi -1; 1 2; -3; z 2.8
mbi -1; 1 2; -2; z -1.
mti 1 2; 1 2; 1 2; 1
mti 1 2; 1 2; 2 3; 2
mti 1 2; 1 2; 3 4; 3
```

The block definition is the same as in the previous example. The inclination is obtained by translating all the vertices on the edge of a partition using the *mbi* command. An edge, in the progression method, is identified by holding constant (negative sign) the reduced indices over two directions. Finally, the direction and size of the offset are provided. In this example the offset is in the z-direction and it is 2.8 m in the first case, negative 1 m in the second case. The resulting mesh structure is shown in Figure 5-11 for a parallelepiped with dimensions 4 x 5.5 x 15 m.

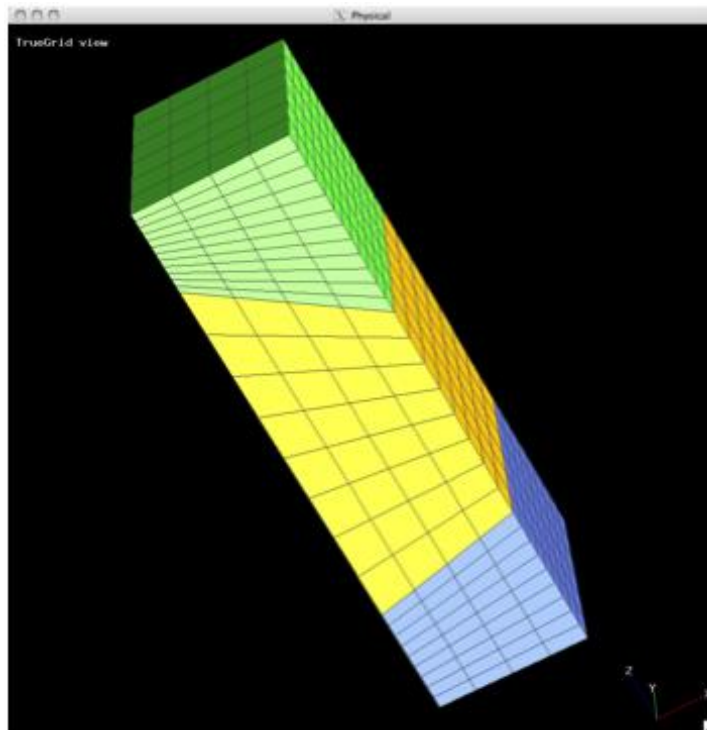


Figure 5-11. Example of a configuration with three non-parallel layers.

5.8.2.3 Concentric Cylinders

This example considers a configuration with two concentric cylinders. Two different approaches apply to this situation and are illustrated here. In the first approach the basic initial mesh structure is a simple block as for the examples above. The mesh is then deformed (or projected) on cylinders to resemble the desired geometry. The input file for *TrueGrid* is the following:

```
block 1 5 14 18; 1 5 14 18; 1 30;  
  0. 1. 3. 4.; 0. 1. 3. 4.; 0. 15.;  
sd 1 cyli 2. 2. 0. 0 0 1 2  
sd 2 cyli 2. 2. 0. 0 0 1 1  
sfi -1 -4; -1 -4; 1 2; sd 1  
sfi -2 -3; -2 -3; 1 2; sd 2  
mti 1 2 0 3 4; 1 2 0 3 4; 1 2; 1  
mti 2 3; 2 3; 1 2; 2
```

After the block is defined, two surfaces are introduced with the *sd* command. The first entry in this command is the surface number, followed by the surface type (cylinder). The next six entries are: three Cartesian coordinate of a point on the cylinder's axis; three coordinates of the directional unit vector parallel to the cylinder's axis (the z-axis in this case). The last entry is the cylinder radius. The *sfi* command deforms the mesh, projecting the boundary surfaces of a partition (selected using the progression method) onto one of the cylinders. The resulting mesh is illustrated in Figure 5-12, where the diameters of the inner and outer cylinders are 2 and 4 m respectively, and a length of 15 m.

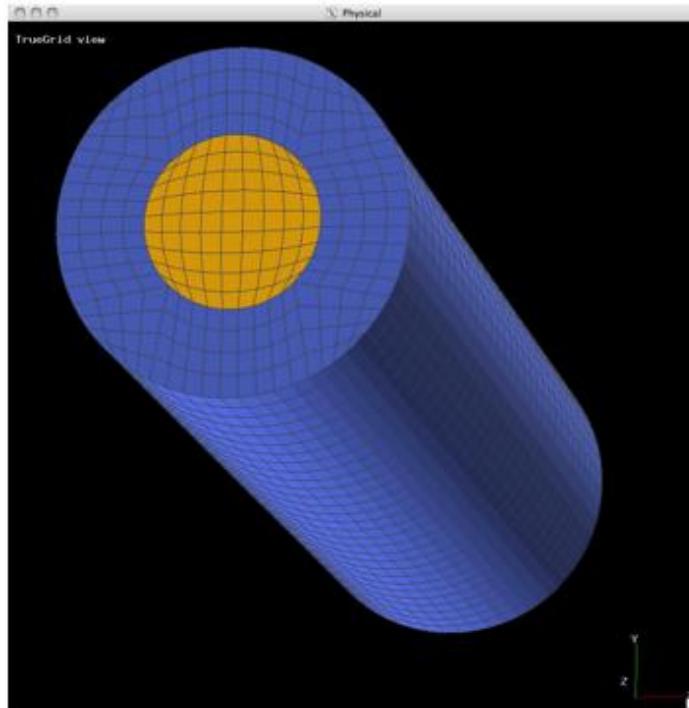


Figure 5-12. Example of a configuration with two concentric cylinders.

In the second approach the initial mesh structure is cylindrical rather than a block. The input file for *TrueGrid* is the following:

```

cylinder 1 10 19; 1 20; 1 30;
      0. 1. 2.; 0. 360.; 0. 15.;
mti 1 2; 1 2; 1 2; 2
mti 2 3; 1 2; 1 2; 1

```

The cylinder command is similar to the block command, but refers to a cylindrical coordinate system (r,θ,z) , where r is the radial coordinate, θ is the azimuthal coordinate and z is the height. The resulting mesh is illustrated in Figure 5-13. The mesh structure is regular with cylinder and irregular with block commands. In both cases the cylinders are approximated by quadrilateral elements (Figure 5-14). Cylinders in both Figure 5-13 and 5-14 have inner and outer diameters of 2 and 4 m respectively, and length of 15 m. Typically, even complex geometries are carved out of a single structure for which the block command is preferred.

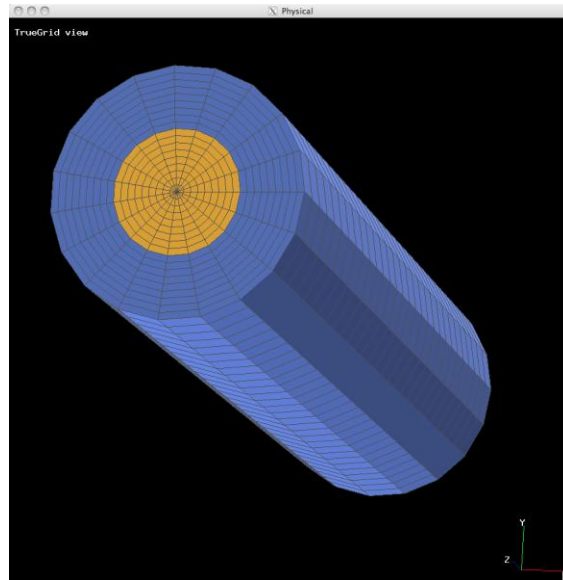


Figure 5-13. Example of a configuration with two concentric cylinders and cylindrical mesh.

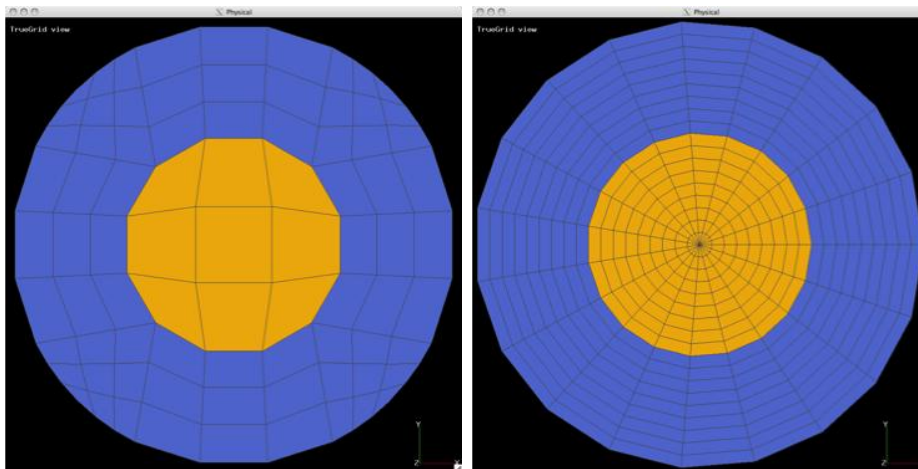


Figure 5-14. Mesh structure generated using the block (left) and the cylinder (right) structure.

5.8.3 Model Testing

Analytic models and finite element models were developed with a realistic thermal analysis case. Models were then prepared in *Mathcad* and *TOPAZ3D*. The model testing described below resulted in good agreements between both approaches.

5.8.3.1 Approach

To test the viability of the thermal modeling approach of using the thermal analyzer *TOPAZ3D* to check and extend thermal analyses using analytical models developed in *Mathcad*, a simple simulation of a temperature transient in a 3-dimensional solid parallelepiped was used.

Mathcad was used to prepare an analytical solution to a transient defined as follows:

Object analyzed – a solid parallelepiped of aluminum, measuring 2 cm x 2 cm x 8 cm

Initially at a constant temperature of 25°C

At time zero all exposed surfaces incur a step change to 100°C

Mathcad was used to predict the transient temperature at the centroid of the solid, and the transient average temperature of the solid.

A *TOPAZ3D* model was developed for the same scenario, and variations in gridding and other input variables were tested until agreement with the analytical solution was demonstrated.

5.8.3.2 Description of Mathcad Analysis

The solution for the temperature transient for a 1-dimensional case where a semi-infinite slab is exposed to a step change in temperature from T_0 to T_S is given in Carslaw and Jaeger (1959, Section 3.4, equation (4), page 100). An analysis using dimensionless parameters was used to duplicate Figure 11 in Carslaw and Jaeger to confirm the validity of the one-dimensional *Mathcad* model (see Figure 5-15). Using 10,000 series terms produced good agreement with the figure.

$$\Theta(t, x) := 1 - \frac{4}{\pi} \left[\sum_{n=0}^{10000} \left[\frac{(-1)^n}{2n+1} e^{-\frac{(2n+1)^2 \pi^2 Fo(t)}{4}} \cos\left(\frac{2n+1}{2} \pi \xi(x)\right) \right] \right]$$

where

$\Theta(t, x)$ was a dimensionless temperature change, such that the temperature

$$\text{Temp}(t, x) = T_0 + (T_S - T_0)\Theta(t, x)$$

T_0 initial temperature

T_S final surface temperature after time zero.

Fo dimensionless time = thermal diffusivity*t/(slab thickness)²

$\xi(x)$ dimensionless length = x/(slab thickness)

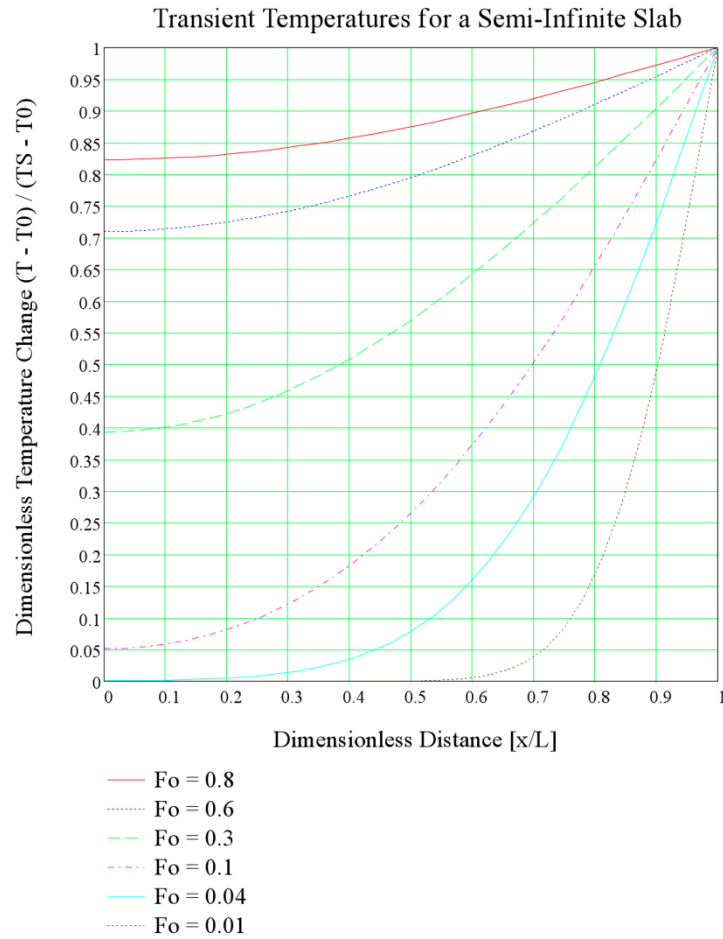


Figure 5-15. Mathcad model reproduction of Carslaw and Jaeger (1959, figure 11).

The equation for the average temperature of the slab at time t (Carslaw and Jaeger 1959, Section 3.3, equation (10), page 97) is given as:

$$\Theta_{\text{avg}}(t) := \frac{8}{\pi^2} \cdot \sum_{n=0}^{10000} \left[\frac{1}{(2n+1)^2} e^{-\frac{(2n+1)^2 \pi^2 \cdot \text{Fo}(t)}{4}} \right]$$

Both centroid and average dimensionless temperature transients were checked against Carslaw and Jaeger, Figure 12 as shown in Figure 5-16.

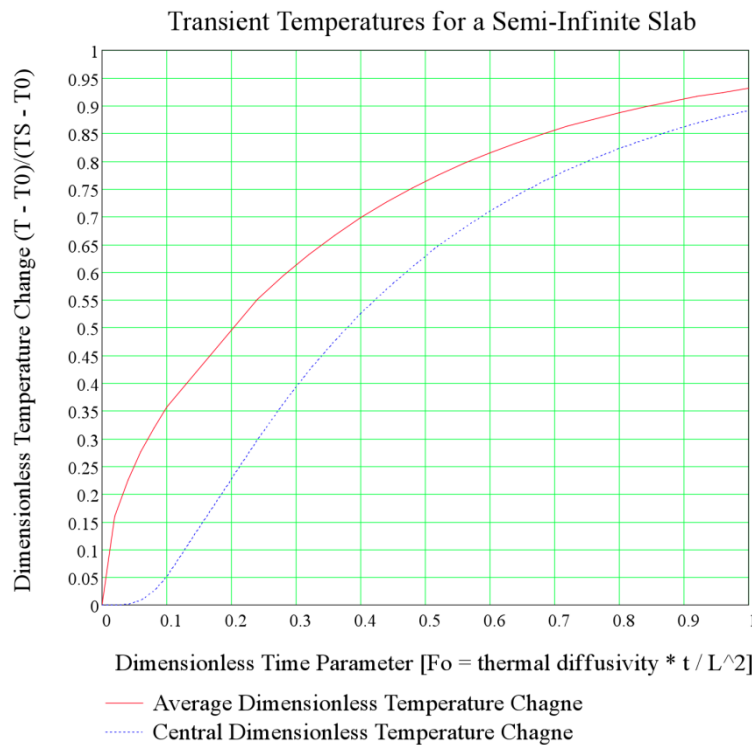


Figure 5-16. Mathcad model reproduction of Carslaw and Jaeger (1959, figure 12).

The 3-dimensional problem of the parallelepiped subjected to a step change in surface temperature at time zero is based on the Handbook of Heat Transfer, Second Edition (Rohsenow et al. 1998), page 4-87. The transient 3-dimensional solution for a number of solid geometry cases can be expressed in terms of the product of the one-dimensional slab solutions. The solution for various geometries is given in Rohsenow et al. (1998 Table 5 *Product Solutions for Internal and Central Temperatures in Solids with a Step Change in Surface Temperature*).

The temperature transients developed in this manner were compared against a *TOPAZ3D* model of the aluminum parallelepiped as described in Section 5.8.3.3.

5.8.3.3 Description of the *TOPAZ3D* Analysis

The temperature transients developed in the previous Section were compared against a *TOPAZ3D* model of the same aluminum parallelepiped. This model used material properties and assumptions coherent with the *Mathcad* model:

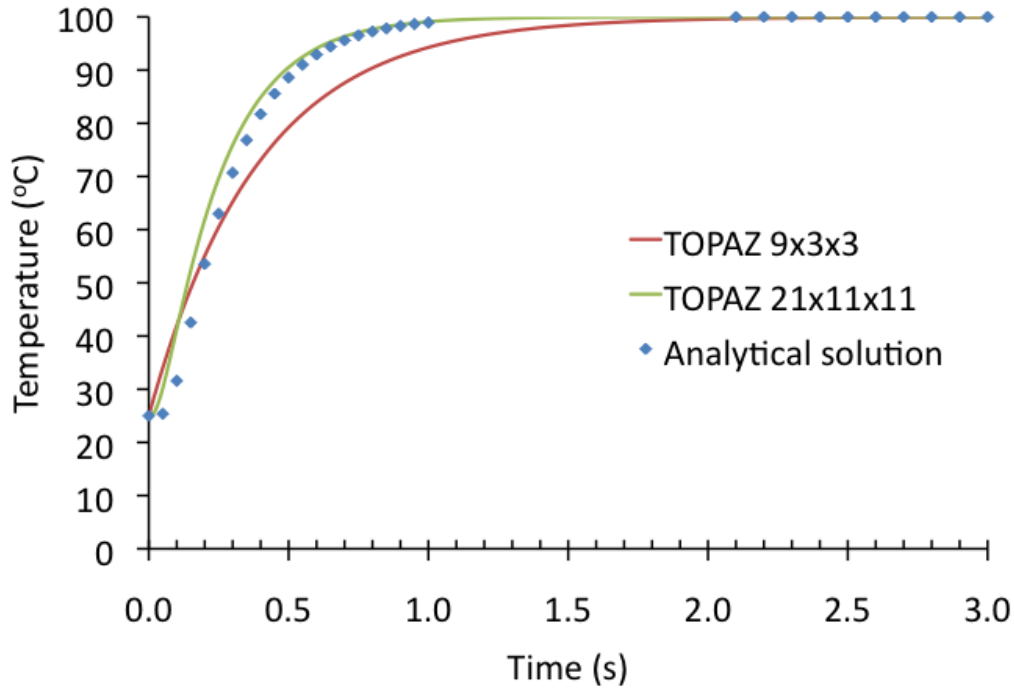
Density 2,700 kg/m³

Thermal conductivity 238.5 W/m-K

Specific heat 920.5 J/kg-K

Initially the sample is at a uniform temperature of 25°C; a step change is applied on the exposed surfaces (100°C) at time 0.

Figure 5-17 shows a comparison of the analytical solution and the *TOPAZ3D* solution for the temperature at the centerline of the parallelepiped as a function of time. The *TOPAZ3D* solution is very sensitive to the mesh size. The solution obtained applying a 21 x 11 x 11 nodes mesh is close to the analytical solution, whereas a coarser mesh (9 x 3 x 3 nodes) is inadequate for this problem. Further mesh refining was attempted, but led to a computational stall. That issue is currently under investigation. The time step size was optimized to guarantee a converged solution. Figure 5-18 shows the temperature distribution at the center of the parallelepiped of dimensions 2 x 2 x 8 cm



(see p.47) for selected time steps.

Figure 5-17. Comparison of the temperature at sample centerline as a function of time obtained with *TOPAZ3D* and dimensionless analysis.

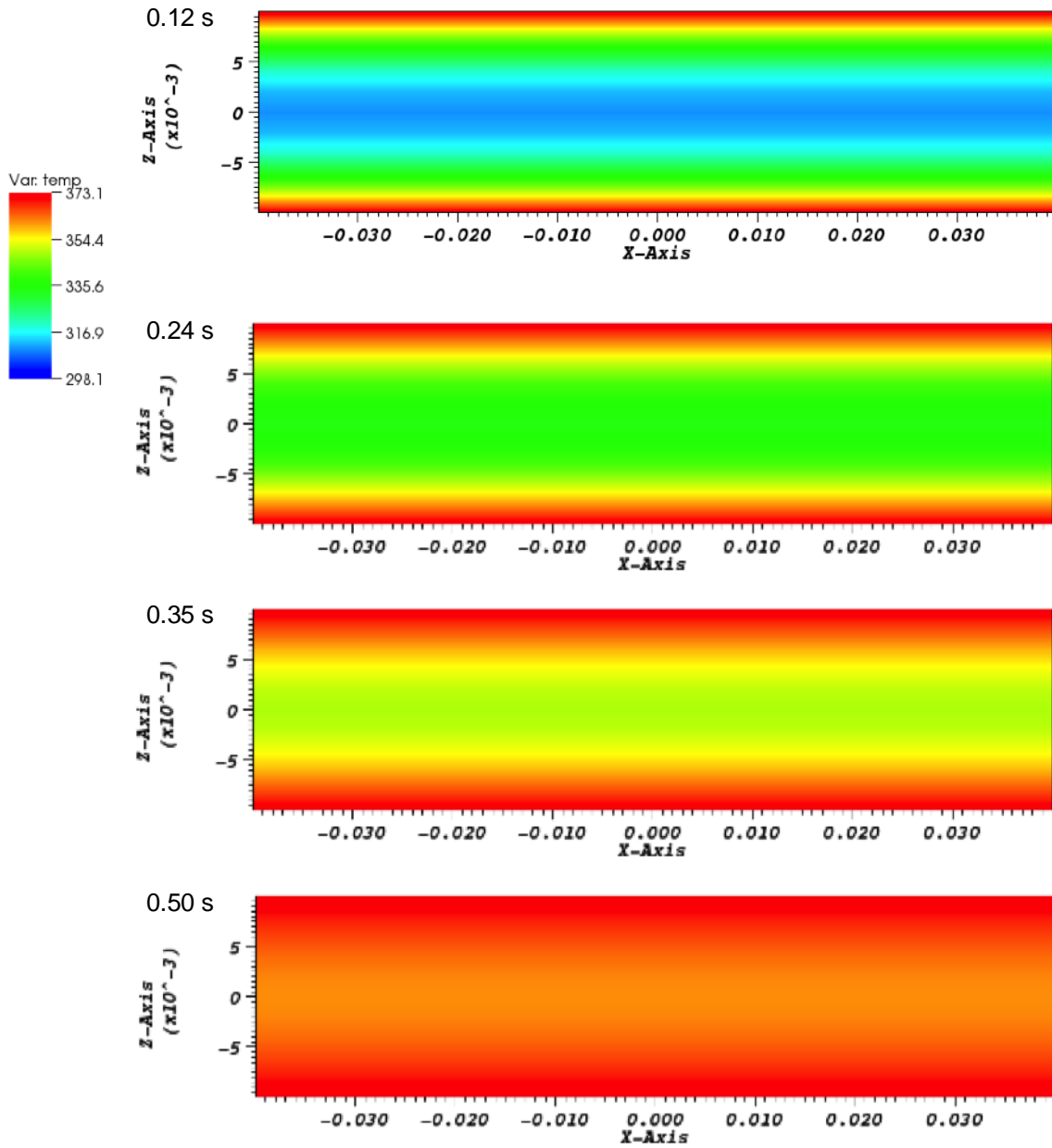


Figure 5-18. Fuel temperature distribution (K) for a central cross section of a 2 x 2 x 8 cm parallelepiped at selected time steps (x and z axis dimensions in meters).

5.8.4 Decay Heat

The decay heat data to be used in DSEF relies on data developed in Carter et al. 2011, which models specific radionuclide inventory data in each of the waste forms for the once-through (Figure 5-4), open-cycle (Figure 5-5), and closed-cycle (Figure 5-6) waste streams for various burnup and process time assumptions.

5.8.4.1 Approach

The approach used to model the decay heat data for used nuclear fuel on the Yucca Mountain Project DOE 2008a and BSC 2004 was to fit the detailed decay heat data (developed using ORIGEN or other codes that tracked radioisotope decay and in-growth for the specific waste streams) to a series of three or four exponential terms of the form:

$$Q_{\text{decay_heat}}(t) = A1 \cdot \exp(-B1 \cdot t) + A2 \cdot \exp(-B2 \cdot t) + A3 \cdot \exp(-B3 \cdot t) + A4 \cdot \exp(-B4 \cdot t)$$

In DOE 2008a and BSC 2004 the curve fit was performed by using the SOLVER Add-in in *Excel* to minimize the error based on the sum of the squares of the difference between the actual data and the curve fit equation. That approach worked well, but care was needed in selecting the initial guess for the process, to obtain convergence.

The approach taken here is to use the GENFIT function included in *Mathcad* to perform the curve fit operation. This approach was successfully tested against the decay heat data shown in the Yucca Mountain Repository License Application (DOE 2008b) Figure 1.5.1-6 *Thermal Power after Discharge: Comparison of Pressurized Water Reactor and Boiling Water Reactor*. The same issue of selecting an adequate initial guess in order to obtain convergence applies to the *Mathcad* approach as to the *Excel* SOLVER Add-in approach.

5.8.4.2 Waste Stream Decay Heat Data Development

The decay heat from all of the waste forms resulting from each of these potential fuel cycles is being addressed. The priority for running each waste form model is being evaluated based on input from the R&D Roadmap and related work packages such as Thermal and Waste Form.

Initial data provided in an *Excel* workbook by SRNL includes data based on assumed fuel cycle radionuclide inventory data and analysis using ORIGEN. The SRNL workbook's function is to determine the process wastes derived from reprocessing Used Nuclear Fuel and its properties especially the isotopic content of the products and wastes. The results of the workbook are documented in FCRD-USED-2010-00031 Rev 3. Alternate waste streams for potential future nuclear fuel cycles, including:

- Future Open Cycle - Light Water Reactor used nuclear fuels at higher burnup
- PWR used fuel data at 40, 51, 60, and 100 GWd of burnup
- BWR used fuel data at 30 and 50 GWd of burnup
- Partial Recycle – MOX fuel – at 50 GWd of burnup
- Full Recycle waste streams using different processes
- COEX glass and COEX BWR

- UREX glass and UREX BWR
- NUREX glass and NUREX BWR
- E-Chem – Glass, Zeolite (ceramic), and Metal

From the extensive set of possible fuel cycles and waste streams analyzed by SRNL, a subset of representative burnup, waste forms, and waste containers have been chosen to represent each of the proposed fuel cycles. Figures 5-19 and 5-20 shows the long-term and short-term decay heat, respectively, in units of W/canister or W/assembly to be utilized in modeling the repository design cases including:

- LWR fuel assemblies
- MOX fuel assemblies
- COEX glass HLW canisters
- NUREX glass HLW canisters
- E-CHEM ceramic HLW canisters
- E-CHEM metal HLW canisters

The *Excel* workbook includes the mass inventory of each of the radionuclide species as a function of time and develops decay heat data for each constituent and the total for all of the waste forms.

For analysis purposes curve fits will only be developed for the total decay heat for each of the waste streams analyzed.

Because of the wide variety of reactor types, fuel cycles and waste streams, for comparison purposes the data has been normalized to Megawatts Electric produced by the fuel. With this approach the waste volumes and decay heat generated by a given fuel cycle which produced an equivalent amount of electricity can be compared.

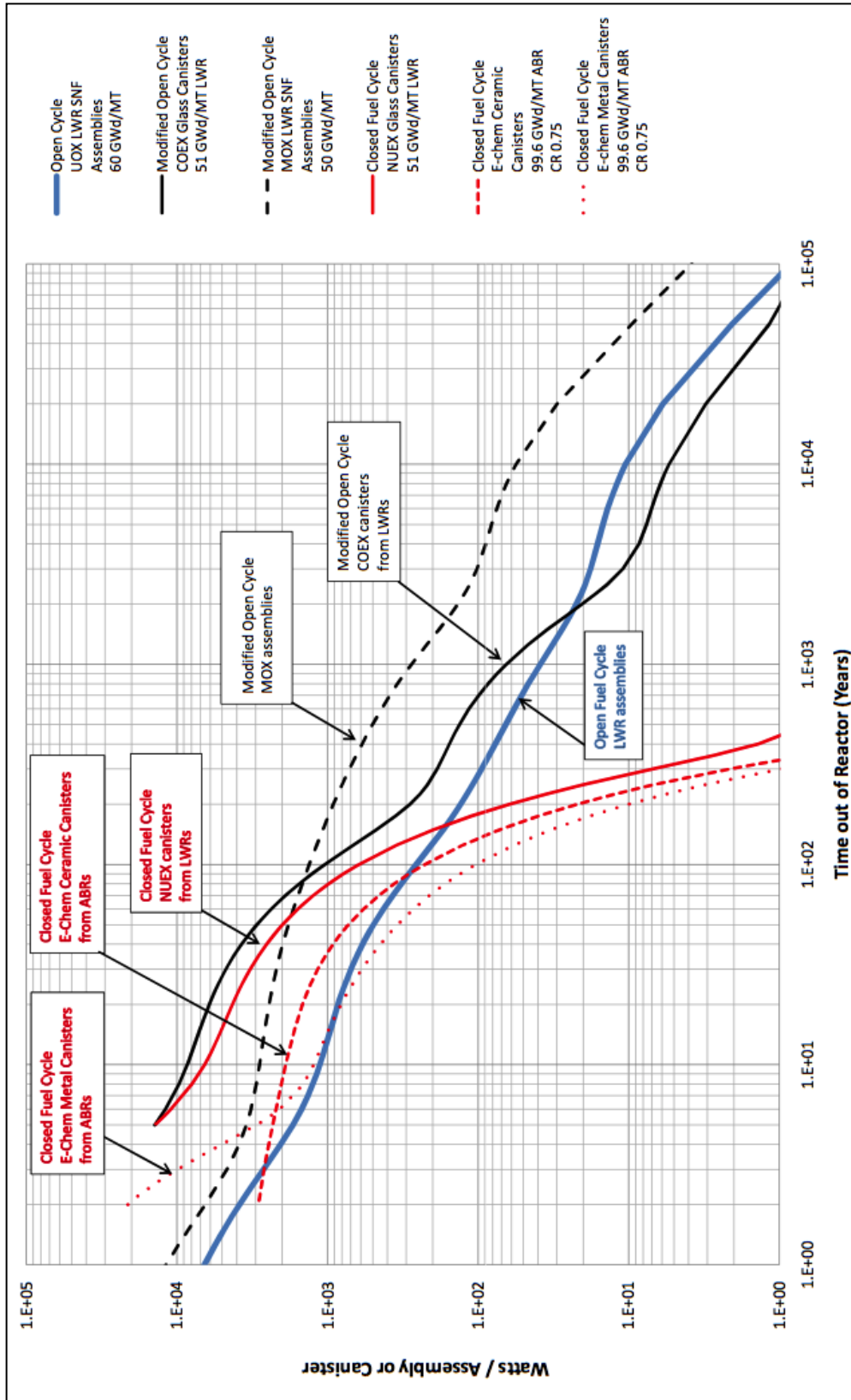


Figure 5-19. Long-term waste form decay heat for each base case fuel cycle per canister assembly or canister.

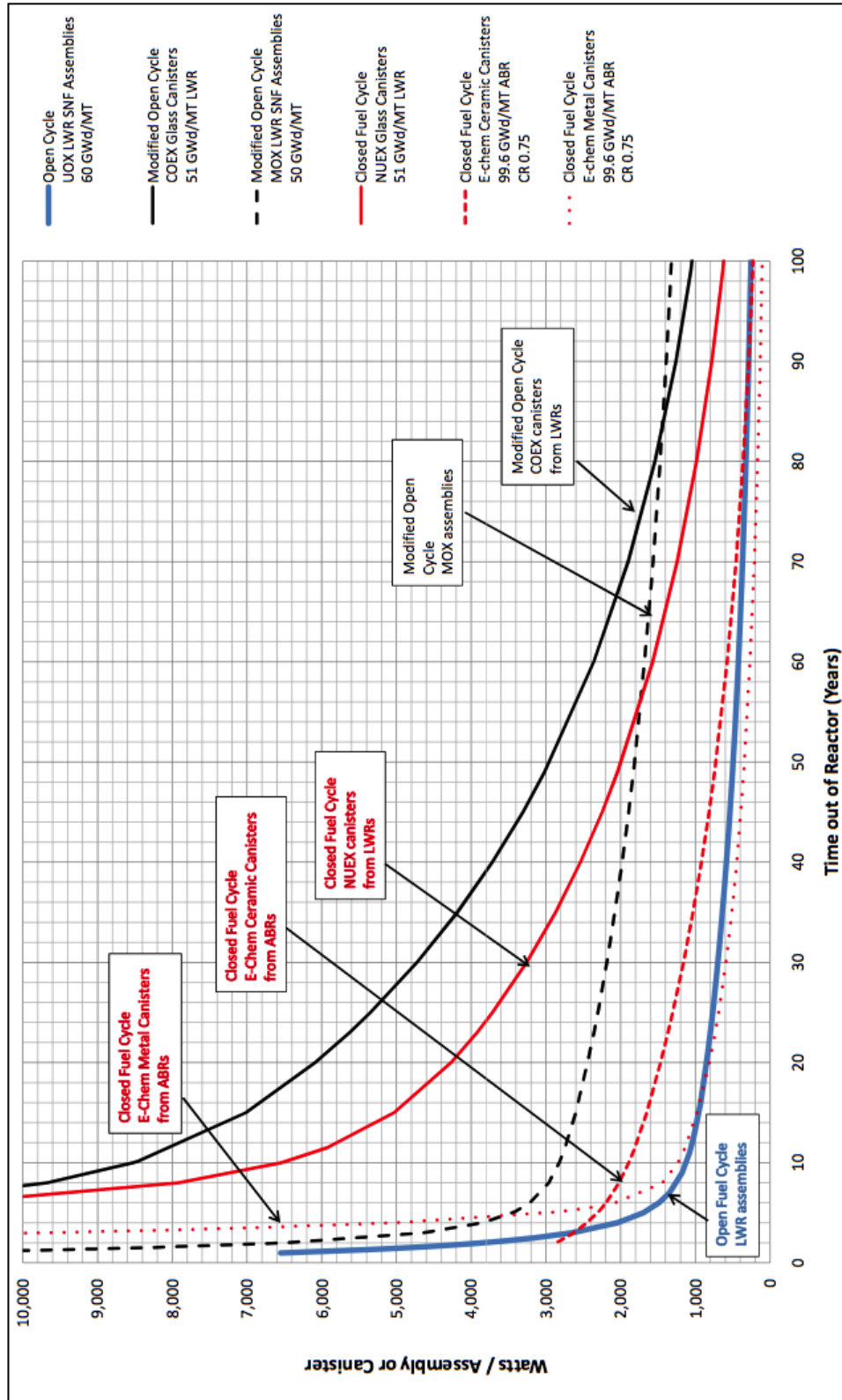


Figure 5-20. Short-term waste form decay heat for each base case fuel cycle per canister assembly or canister.

5.9 Material Properties

The material property data in the DSEF *Knowledge Management* worksheets (shown in Figure 5-1) include properties for both the natural environment (shown in Table 6-1 from Blink et al. (2011), Table 2) and the engineered barrier system components for the various repository options considered in by UFD, as shown in Table 5-6 (Blink et al. 2011, Table 3).

Table 5-6 Engineered Barrier System (EBS) concepts and components.

Category	Sub-category
EBS Emplacement Options	Large waste packages in drifts
	Horizontal or vertical borehole emplacement from drifts
	Deep boreholes
EBS Barrier Options	Waste form
	Cladding
	Barriers internal to the waste package
	The waste package itself
	Drip shields
	Backfill
	Buffer materials
	Sorptive materials
	Seals above deep boreholes
EBS Reactive Properties	Material porosity, tortuosity, bulk density and saturation
	Infiltrating and conditioned water chemistries
	Radionuclide solubilities
	Radionuclide sorption distribution coefficients, k_d
	Radionuclide diffusion
	Groundwater pore velocity

5.9.1 Example Structure and Data Included in the Thermal and Transport Property Worksheets

The *Thermal Property* data worksheets are structured as follows:

- Rows
 - Sections of groups of rows
 - Host Rock, Engineered Materials (includes buffers, plugs, liners for now)
 - Groups of rows for media types
 - Clay, Salt, Granite, Basalt, Limestone, Sandstone, Subseabed, Tuff
 - Cementitious Buffer, Stainless Steel Liner, Cementitious Backfill, Concrete Lining, Compacted Clay Backfill, Sand, Soil
 - Rows for specific media (e.g. Opalinus clay, Boom clay, etc.)
- Each row includes:
 - Overall reference information for the medium

- Property mean and ranges (in columns)
- Comments and citations (for each property)
- Properties in the columns
 - Bulk thermal conductivity, dry thermal conductivity, wet thermal conductivity, matrix porosity, total porosity, saturation, volume % water, bulk density, dry density, wet density, specific heat, volumetric heat capacity, thermal diffusivity (usually calculated)

In addition to the primary data worksheet, the *Thermal Properties* worksheets (some of which may be stored in an auxiliary file) include other worksheets as follows:

- References (full list of those cited on the sheets)
- Material sheets (key tables and figures from the cited references, sometimes equations and critical discussion sections)
 - Clay
 - Salt
 - Granite
 - Basalt
 - Tuff
 - Subseabed
 - EBS Materials
 - General

It should be noted that the tuff environment has been well covered by the Yucca Mountain Project and is included in the DSEF for validation purposes. Basalt and granite are two examples of hard rock (Table 5-5). Subseabed is not being considered in the DSEF but the properties were available in compilations reviewed and hence were captured for completeness.

The *Transport Property* worksheets utilize the same basic organization and structure as the *Thermal Property* worksheets, but address the following material properties: Permeability, Hydraulic Conductivity, Porosity, Effective Porosity, Coefficient of Molecular Diffusion, Longitudinal Hydrodynamic Dispersion

5.9.2 Data Evaluation and Selection of Input Values to Use as Representative Data for Analysis

The Material (*Thermal and Transport Property* worksheets provide a central assemblage of relevant material references and source data. However, before the information can be used in a thermal or radionuclide transport model calculation, the wide range of raw data needs to be evaluated to develop representative properties for use in the calculations.

Depending on the extent of the data available it may be treated differently, for example

- Very limited data – a bounding value may be assumed, with justification provided
- Small sample of data – a mean value and an uncertainty band may be developed for use
- Extensive data – a mean value with uncertainty band, or a parameter distribution function may be appropriate

This evaluation will be performed in the *Thermal* worksheets and the representative material properties for the selected natural environment and engineered barrier components will be summarized in the *Input* and/or *Interface Parameters* worksheets for potential reference in other worksheets within DSEF and in the *External Interface* and *FC System Impacts* worksheets for external organizations (see Figures 5-1 and 5-3).

5.9.3 Materials Longevity

The Material (*Thermal and Transport Properties* and *Materials Longevity* worksheets will pull data from the *Knowledge Management* worksheets based on the selections made by the DSEF user and will feed waste form degradation and waste package degradation data to the *PA* worksheet. Information from historical degradation mode surveys (e.g. Farmer 1988, Sutton 2010) together with more recent publications and data will be maintained such that the user can select the most appropriate container material for the repository environment and can determine the maximum corrosion rate. The rate of dissolution of waste form and waste package for a given repository environment is typically modeled using yearly fractional degradation rates.

The near-field volume is the volume of potentially saturated space inside the repository footprint that would be available for radionuclides to dissolve into. The bulk volume is defined as the repository footprint multiplied by the height. A reasonable assumption is that the near-field volume is comprised of 3 “compartments” (a) void space in the repository tunnels, (b) available pore space in the degraded EBS (including waste form, waste package, backfill), and (c) available pore space in the host rock. The near-field volume available for dissolved radionuclides to mix with is then defined as the porosity of each compartment multiplied by the available volume of each compartment. In some cases (e.g. salt repositories), the space between the waste package and the tunnel walls will be negligible, since the salt walls creep towards the waste package. For salt repositories, the tunnel height is assumed to be the diameter of a waste package, while for granite and clay the height is assumed to be twice the diameter of the waste package (Wang and Lee 2010). The data on area, height and porosity of EBS materials and host rock is fed to the *PA* worksheet from the Material (*Thermal and Transport*) *Properties* worksheets based on the selection of the repository design, waste package material and waste form within the DSEF workbook.

5.10 Performance Assessment

The Performance Assessment (*PA*) worksheet within DSEF will allow users to document and in some cases calculate various portions of the PA process. Factors that will be accounted for in the PA process will follow the FEPs process and should include:

- Waste package material and waste form degradation (corrosion rates in appropriate chemical and temperature environment)
- Near-field volume
- Radionuclide solubility and transport through the EBS (with defined EBS conditions and radionuclide solubility and sorption calculations, THCMRB processes)
- Radionuclide solubility and transport through the geosphere (ambient chemical far-field conditions, THCMRB processes)
- Radionuclide transport and uptake in the biosphere, and dose assessment.

Relevant data and worksheets within the Material (*Thermal and Transport*) *Properties* and *Materials Longevity* worksheets will feed the *PA* worksheet based on the selections for repository environment, repository design and thermal requirements made by the DSEF user for both the EBS and geosphere media.

The DSEF contains a simple, high-level 1-D transport code, and a dose calculation worksheet. Radionuclide concentration exiting the EBS will be transferred to a model predicting radionuclide concentration in the geosphere, subsequently the biosphere and dose calculations can be performed using either an undisturbed or human intrusion assumption. However, the *PA* worksheet will encourage the user to use more complex PA models in *GDSE*, which uses the *GoldSim* software package (Goldsim 2009).

Whether a high-level simple PA is calculated inside DSEF or a more complex PA is developed in an external code such as *GDSE* or *GoldSim*, the inputs, constraints, outputs and discussion of each run will be documented in DSEF. This will allow consistent comparison between many different scenarios for each base case model.

Initially, the PA portion of DSEF will evaluate and compare the 24 base case systems shown in Table 5-5 for six waste forms, 4 repository environments and two aging times. Initially, the baseline cases comparable to YMP and WIPP will be evaluated to provide confidence in the models. Subsequently, to provide maximum benefit to the UFD Campaign and decision-makers, the priority in which the remaining cases would be evaluated will then be decided based on the immediate needs of the Campaign. Beyond those base cases, users will continue to build a library of PA outputs that can be drawn upon to improve the repository design. It is expected that in FY12, DSEF will prove a useful capability in performing site-selection work.

5.11 Cost

The *Cost* worksheet will develop a rough estimate of the repository cost based on published unit costs developed by repository programs from around the world. It is recognized that cost models are relatively easy to develop, but are nearly impossible to validate. For that reason, the cost models will be most useful in comparing design options for a given waste form and environment, and less accurate in comparing design options for different waste forms and environments. Results of these high level cost models should not be used to try to establish the actual cost for use in developing an actual facility; detailed cost models should be developed specifically for such a facility.

Two of the DSEF team members followed the Yucca Mountain life cycle cost exercises over the years. In 2008, one of the DSEF team members obtained a more detailed cost breakout for Yucca Mountain and used it to develop a costing algorithm for a repository designed to dispose of ultra-high-burnup waste from laser fusion-fission hybrid reactors. That algorithm will be extended for the DSEF during the remainder of FY11.

Costs, at a high level, have been obtained for the WIPP repository, and more detailed costs area being sought. The international literature will also be surveyed to obtain other cost data for various repository media. Published cost comparisons will be most valuable, because they will enable linkage of multiple studies and a determination of whether unit cost estimates should be increased or decreased from a particular reference.

The cost algorithm will be based on unit costs for waste packages of a specified size and material, drilling costs, etc. In some cases, published unit costs are available, and in other cases, they will be estimated using raw material costs and/or material properties. This approach was implemented in the hybrid reactor study noted above.

The other three *Calculation* worksheets in the DSEF (*Thermal*, *Materials Longevity*, and *PA*) can complete their calculations based on a unit cell approach. The *Cost* worksheet will need to go beyond a single unit cell to estimate the repository footprint for a specified repository capacity. To facilitate cost comparisons, a reference capacity will be chosen to represent a fleet of reactors producing a specified amount of power for a specified period of time. A fuel cycle with higher burnup and less waste volume and/or heat will then be comparable to other fuel cycles on an even basis. The DSEF will clearly record the unit costs used as inputs to the cost calculations, to allow updating of estimates if additional cost data become available.

5.12 Knowledge Management

Section 4.2.4 of the UFD R&D Roadmap (FCR&D, 2011) describes Knowledge Management as applied to UFD as follows:

The collection, categorization, and dissemination of information regarding disposal system performance is essential as the U.S. embarks on the investigation of a variety of potential geologic media and repository concepts for the disposal of SNF and HLW that could be generated under advanced fuel cycles.

This applies to the U.S. program in that both a range of geologic environments and also a range of potential future nuclear fuel cycles and associated waste streams are being investigated.

In this chapter, we discuss the various levels of knowledge management within DOE-NE/UFD, and provide information on what role a LLNL knowledge management system has with respect to DSEF.

5.12.1 Levels of Knowledge Management

There is a hierarchy of knowledge management systems. At the highest level, the DOE-NE knowledge management system (which was discussed at the October 2010 PI meeting) is still being developed, and will subsequently be populated. The team at LLNL is supportive of this NE-wide repository of information.

Below the NE-wide knowledge management system is the INL document management system. Here, controlled documents, records and a library are available for the various Fuel Cycle Technology (FCT) campaigns. The INL system was created (and is maintained) in accordance with the DOE-NE-FCT QA program.

The UFD campaign-specific knowledge management system is SharePoint, managed by SNL. This resource is very similar to the YMP SharePoint created by SNL for sharing program documents, results and records. While useful, this system requires the researcher to be on-line and logged in with a secure account. The structure and population of the SNL UFD SharePoint system are still under development. The SNL UFD SharePoint knowledge management system is related (but not identical) to the UFD-Natural Barrier System knowledge management system, which is currently proposed by the NBS team within UFD and which may be more of a database than a collection of documents.

Each individual National Laboratory participant houses a reference collection, which contain archived material, journal articles, books, notebooks, reports etc. There is a certain degree of overlap between each Laboratory's libraries, but the material is available without a network connection and without log-in credentials, day and night. The material is also readily shared between National Laboratory partners. In some cases the material is electronic, in other cases it is a hard copy. This is where the DSEF knowledge management tool fits within the framework. Similar to the UFDC specific level, the YMP had a formal system of documents and records, and their system is still available to some degree through the DOE office of legacy management, where we have successfully obtained source files of DTNs and files from AMRs for use, in addition to highly valuable lessons learned material.

5.12.2 LLNL DSEF-Specific Knowledge Management

The DSEF is designed to be a flexible systematic analysis and knowledge-management framework for evaluation of disposal system options for a wide range of potential future nuclear fuel cycles and used fuel disposition alternatives (see Figure 5-22 taken from Blink et al. 2011, and the DSEF Architecture diagram, Figure 5-1). The *Excel* worksheets serve as a user-friendly data entry and retrieval system, and the *Access* database is used for generation of status reports and gap analyses. The *Access* database also serves as a query tool for data mining and extraction of specific technical information stored within DSEF.

This knowledge-management framework also serves as a valuable communication tool for the community of producers and users of knowledge. Figure 5-1, the DSEF Interface Architecture diagram shows how other Office of Fuel Cycle Technology (OFCT) campaigns interface with DSEF in its knowledge-management role.

The DSEF will: (1) facilitate integration of UFDC process and system models and data, (2) enhance the UFDC interface with other OFCT elements (see Figure 12-2 taken from Blink et al. 2011), and (3) provide rapid response capability to address information requests from DOE or other organizations. The DSEF will establish a UFDC knowledge management system to organize high-level information, data, and assumptions, thereby facilitating consistency in high-level system simulation and economic analyses.

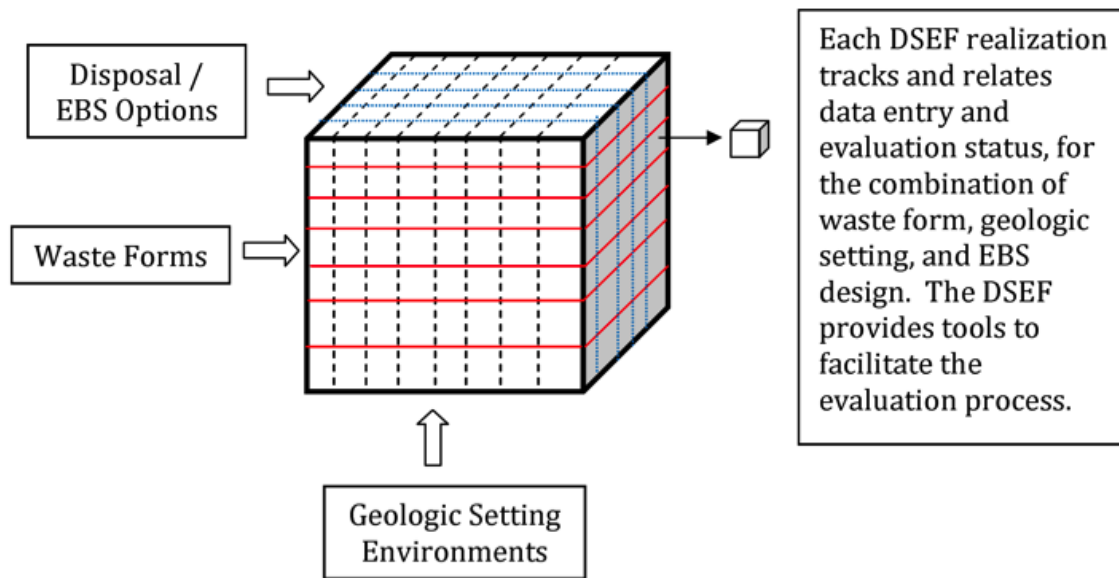


Figure 5-21. The DSEF addresses combinations of waste form, geologic setting, and repository design.

The material properties assembled to define the geologic settings shown in Figure 5-21 were described in Section 5.11. The knowledge management aspect of that data assemblage provides for the traceability of the data and references used to populate the *Excel* worksheets containing those material properties.

Specifically, where a reference provides a table of properties, which is then cited as a primary reference, where possible that reference will be readily accessible, and hyperlinked to the worksheet if it is available in electronic form. If the primary reference assembled the data and cited secondary references as the original source of the data, the full citation to the secondary reference will also be included in the DSEF worksheets. In this manner the traceability of the numbers used in analysis can be clearly tied to the original sources of the data.

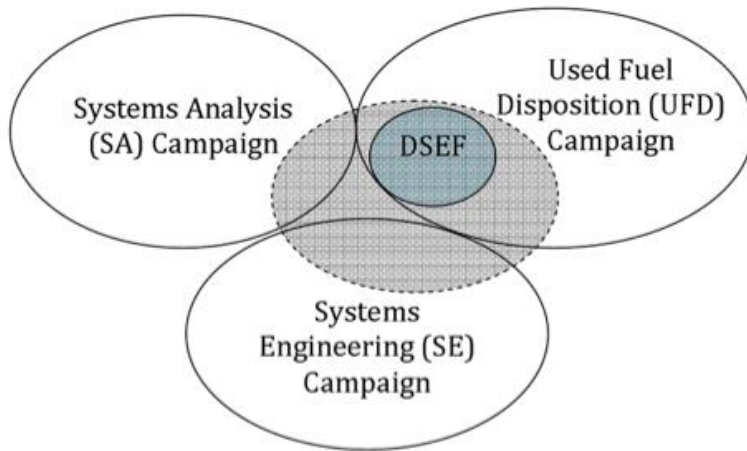


Figure 5-22. The relationship between DSEF and the SA, SE, and UFD campaigns.

5.13 Fuel Cycle System Impacts

As a framework for integrating the technical behavior of waste streams in differing disposal pathways, the DSEF is designed to serve as part of the waste management interface with the rest of the fuel cycle. In this role, it is intended to make the DSEF compatible with the information flows and the other models used in other parts of fuel cycle analysis, and to enable iterative analysis between disposal impacts and the rest of the nuclear fuel cycle.

The FCT Systems Analysis campaign serves the function of integrating models and analyses across the entire fuel cycle, and maintains interfaces with the various technical parts that comprise a complete fuel cycle, and builds and utilizes fuel cycle system models. Systems Analysis employs a “model hierarchy” as shown in Figure 5-23. In this hierarchy, fundamental process models form the base layers and are owned, developed and used by the technology R&D campaigns. In UFD, these would include process models such disposal environment thermal-hydrology, corrosion, waste form dissolution, radionuclide migration, etc. The middle portion of the hierarchy contains models for fuel cycle wide material flows (FIT) and dynamic nuclear energy facility evolution (VISION), and energy supply and demand models are at the top.

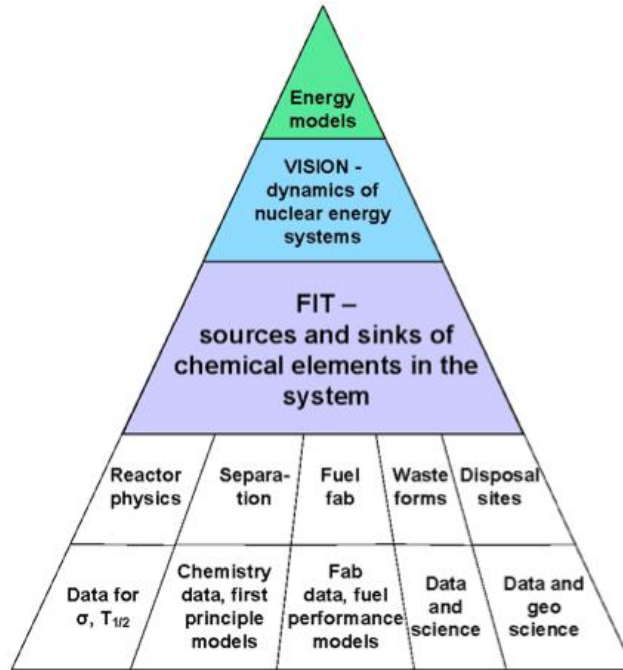


Figure 5-23. Hierarchy of nuclear fuel cycle models.

The role of the DSEF in this hierarchy includes integration of certain process models within the UFD campaign at the ‘lower-right’ corner of the hierarchy, connection to waste form models from the Waste Form and Separations campaign, and connection to the material flow models at the ‘middle-right’ edge.

Another interface for the DSEF development is with FCT Systems Engineering, where there is an ongoing activity to build a catalog of potential fuel cycles and their characteristics. Eventually, this catalog could be both a source of waste stream information and a place for DSEF to feed back disposal consequences to the rest of the nuclear energy enterprise. An example fuel cycle summary flows being developed for this catalog is shown in Figure 5-24 for the LWR once-through fuel cycle. The DSEF should be able to continue this flow into specific disposal pathways for the waste stream, and provide feedback on disposal implication.

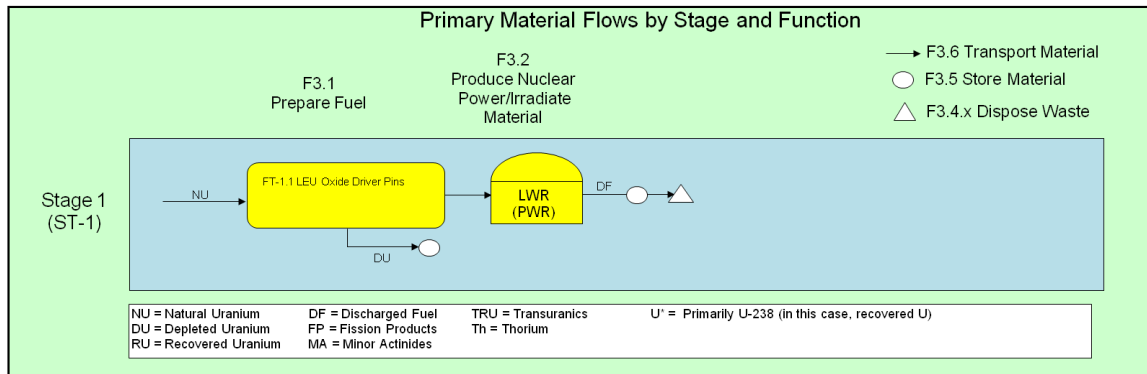


Figure 5-24. Systems Engineering Catalog - Fuel Cycle O-T/R.1 PWR UOX – Once-through.

Also, in the recently completed Systems Engineering “Initial Screening of Fuel Cycle Options” [Sevougian et al. 2011], the disposal aspects of the fuel cycle were represented parametrically, without specific disposal pathways being considered or technologies evaluated. In future screenings, it is desired to be able to include more specific disposal behaviors tied to waste streams and disposal alternatives. This could be enabled through DSEF analysis.

5.14 Summary of Current Status and Look Ahead

DSEF work is expected to continue through FY11 into FY12.

5.14.1 Current Status

At the present time, significant progress has been made in the thermal modeling of materials of various geometries. The structure of DSEF, the flow of information within worksheets of the DSEF workbook, and the flow of information in and out of DSEF have been designed and evaluated. Information on waste form properties (including heat) have been gathered and analyzed, and design constraints are being evaluated.

5.14.2 Looking Ahead in FY11 and FY12

In the remainder of FY11, we plan to:

- Complete DSEF structure and prepare initial prototype of DSEF *Excel* workbook(s)
- Talk to potential users and define requirements for *Access* database
- Finish populating *Thermal Properties* worksheets and develop representative repository thermal parameters for use in thermal calculations
- Run initial realizations for thermal analyses of repository design, waste form, and decay/storage option cases coordinating with the Repository Science / Thermal Load Management / Design Concepts work packages

For FY12, we plan to:

- Continue to assemble and populate realizations of DSEF worksheets for different evaluations
- Update DSEF *Excel* worksheet operation and capabilities based on user feedback and capability requests
- Develop specification for and prototype of the DSEF *Access* database
- In a deliverable report, document the validation of the DSEF software model using YMP and WIPP data and compare to other work package results, e.g., GDSE, THMC, Thermal Management, etc.

Run realizations utilizing priority configurations from the R&D Roadmap.

5.15 Recommended Areas of International Collaboration and Participation

At a level more comprehensive than the EBS work package, LLNL has provided the UFD International Collaboration Coordinator (Jens Birkholzer) with information pertaining to current LLNL international collaborations in the nuclear waste area and a suggested new collaboration. This area will be developed for the September 2011 LLNL deliverable in the EBS work package. Particular emphasis will be placed on identifying potential collaborations in the areas of thermal performance and stability and longevity of engineered components including canisters and buffer materials. See Section 1.3 of this report for detailed descriptions of areas of international collaboration.

5.16 References

- AFCI 2009, 3-D Thermal Analyses of High-Level Waste Emplaced in a Generic Salt Repository, Daniel J. Clayton and Carl W. Gable, AFCI-WAST-PMO-MI-DV-2009-000002 (February 2009).
- ANDRA 2005a, Argile -Architecture And Management Of A Geological Disposal System, ANDRA Report, France (December 2005).
- ANDRA 2005b, Granite – Safety Analysis Of A Geological Repository, ANDRA Report, France, (December 2005).
- Blink et al. 2011, The Disposal Systems Evaluation Framework for DOE-NE, J.A. Blink, H.R. Greenberg, W.G. Halsey, C.F. Jové-Colón, W.M. Nutt and M. Sutton, presented at the International High-Level Radioactive Waste Management (IHLRWM) Conference, Albuquerque, New Mexico (April 2011).
- BMI 1985, Waste Package/Repository Impact Study Final Report, Conceptual Design of a High-Level Nuclear Waste Repository in Salt, Battelle Memorial Institute Report BMI/ONWI/C-312 (September 1985).
- BSC 2004, Ventilation Model and Analysis Report. ANL-EBS-MD-000030 Rev 04, October 2004, (Yucca Mountain Project ACC: DOC.20041025.0002), Bechtel SAIC.
- Carslaw and Jaeger 1959, Conduction of Heat in Solids. H.S. Carslaw and J.C. Jaeger, 2nd Edition, Clarendon Press, Oxford (1959).
- Carter and Luptak 2010, Fuel Cycle Potential Waste Inventory for Disposition, Carter, J. T., and Luptak, A. J., FCR&D U.S. DOE, Report FCR&D-USED-2010-000031 (January 2010).
- Carter et al. 2011. Generic Repository Study, Draft 0a, in review (April 2011).
- Chipman et al. 2004, Yucca Mountain Project Preclosure Ventilation Heat Transfer Analysis: Solution Method and Results V. Chipman, Kersting, B. and Case, J., Proceedings of HT-FED04, 2004 ASME Heat Transfer/Fluids Engineering Summer Conference, Charlotte, NC (July 11-15, 2004).
- Chu et al. 2011, Monte Carlo Simulations for Generic Granite Repository Studies S. Chu, J.H. Lee and Y. Wang, presented at the International High-Level Radioactive Waste Management (IHLRWM) Conference, Albuquerque, New Mexico (April 2011).

DOE 1987, Site Characterization Plan Conceptual Design Report for a High-Level Nuclear Waste Repository in Salt, Vertical Emplacement Mode US DOE Report, DOE/CH/46656-15 (December 1987).

DOE 2008a, Postclosure Analysis of the Range of Design Thermal Loadings, US DOE Report ANL-NBS-HS-000057 Rev 00, (Yucca Mountain Project ACC: DOC.20080121.0002) (January 2008).

DOE 2008b, Yucca Mountain Repository License Application Safety Analysis Report US-DOE Report DOE/RW-0573 Update 1, (November 2008).

Farmer 1988, Survey of Degradation Modes of candidate Materials for High-Level Radioactive-Waste Disposal Containers- Vol. 3 Overview, J.C. Farmer, R.D. McCright, J.N. Kass, Lawrence Livermore National Laboratory Report UCID-21362 Overview (June 1988).

FCR&D 2011, Mark et al. Used Fuel Disposition Campaign Disposal Research and Development Roadmap, FCR&D-USED-2011-000065 REV 0, March 2011

Freeze et al. 2010, Used Fuel Disposition Campaign Features, Events, and Processes (FEPs): FY10 Progress Report G. Freeze, P. Mariner, J.E. Houseworth, J.C. Cunnane and F.A. Caporuscio, DOE FCR&D Report (August 2010).

Freeze and Lee 2011, A Simplified Performance Assessment Model for Radioactive Waste Disposal Alternatives G. Freeze and J.H. Lee, presented at the International High-Level Radioactive Waste Management (IHLRWM) Conference, Albuquerque, New Mexico (April 2011).

Goldsim 2009, Users Guide, GoldSim Probabilistic Simulation Environment, Version 10.0, Goldsim Technology Group (2009).

Hansen and Leigh 2011, Salt Disposal of Heat-Generating Nuclear Waste F.D. Hansen and C.D. Leigh, Sandia National Laboratory Report SAND2011-0161, Albuquerque NM (January 2011)

Lee et al. 2011, A Performance Assessment Model for Generic Repository in Salt Formation J.H. Lee, M. Siegel, C.F. Jove-Colon and Y. Wang, presented at the International High-Level Radioactive Waste Management (IHLRWM) Conference, Albuquerque, New Mexico (April 2011).

Mathcad 15.0 online Help, Copyright © 2010, Parametric Technology Corporation.

NAGRA 2002, Project Opalinus Clay Safety Report, NAGRA Report, Switzerland, (December 2002).

NIROND 2001, Technical overview of the SAFIR 2 report NIROND Report NIROND- 2001-05 E, Belgium (December 2001).

Nutt et al. 2011, Development of an Integrated Clay Generic Disposal System Environment Modeling Capability W.M. Nutt, E.E. Morris, T.H. Bauer and N. Dosev, presented at the International High-Level Radioactive Waste Management (IHLRWM) Conference, Albuquerque, New Mexico (April 2011).

Posiva Oy 2010, Interim Summary Report Of The Safety Case 2009, Posiva Oy Report POSIVA-2010-02, Finland (March 2010).

Rainsberger 2006, TrueGrid® User's Manual—A Guide and a Reference, Rainsberger, R. XYZ Scientific Applications, Inc. (2006).

Rohsenow et al. 1998, Conduction and Thermal Contact Resistances (Conductances), Chapter 3 in Handbook of Heat Transfer, 3rd Edition, W.M. Rohsenow, Hartnett, J.P. and Cho, Y.I. (eds), McGraw Hill (1998).

Sevougian et al. 2011, Initial Screening of Fuel Cycle Options, S. D. Sevougian et al, FCRD-SYSE-2011-000040, Rev. 0 (March, 2011).

SKB 2006, Long-term safety for KBS-3 repositories at Forsmark and Laxemar – a first evaluation SKB Report, Sweden (October 2006).

Sutton et al. 2010, FY10 Report on EBS Evaluations - Level 4 Milestone (M4): M4508042504 M. Sutton, J.A. Blink, W.G. Halsey and M.A. Serrano de Caro, Lawrence Livermore National Laboratory Report LLNL-TR-451253 (August 2010)

Sutton et al. 2011, Report on the Basis for Selection of Disposal Options: Level 3 Milestone: M31UF032801, M. Sutton, J.A. Blink, W.G. Halsey, Lawrence Livermore National Laboratory Report LLNL-TR-471858 (February 2011).

Turchi et al. 2007, Modeling of Ni-Cr-Mo Based Alloys: Part II - Kinetics, P.E.A. Turchi, L. Kaufman, Z-K Liu, Computer Coupling of Phase Diagrams and Thermochemistry 31 (2007) 237.

Wang and Lee 2010, Generic Disposal System Environment Modeling – Fiscal Year 2010 Progress Report Y. Wang and J.H. Lee (eds), Sandia National Laboratories report, September 2010).

Wemhoff et al. 2007, TOPAZ3D Users Manual – A 3 dimensional Finite Element Heat Transfer Code, Wemhoff, A.P., M. A. Havstad, A. B. Shapiro, Lawrence Livermore National Laboratory Report UCRL-SM-234673 (2007).

Wersin et al. 2007, Performance of the bentonite barrier at temperatures beyond 100°C: A critical review, P. Wersin, L.H. Johnson and I.G. McKinley, Physics and Chemistry of the Earth, Parts A/B/C, Volume 32, Issues 8-14, pp 780-788 (2007).

WRI 2010, Mathematica, Version 8.0, Wolfram Research, Inc., Champaign, IL (2010).